Simple Numerical modelling on Urban Heat Island in Hong Kong

Au Chun Bun Henry

DOCTOR OF PHILOSOPHY

Cardiff University

August 2019

ABSTRACT

Urbanization, including land use changes, building developments, emission of heat and human activities, has a significant impact to our environment and would also contributions to urban heat island (UHI) effect. UHI effect means the cooling rates in the urban space is slower than rural space. Provision of greenery, water feature, ventilation and high albedo material could reduce UHI effect and improve the thermal comfort of the outdoor environment. However, the lack of quantitative understanding about the UHI effect has prevented us systematically implement mitgrtion strategy during urban planning in Hong Kong.

Traditional computational fluid dynamics (CFD) approach is often used to study the microclimate of a small-scale area. The large domain size of the UHI modelling would induce problem of high computational power, long simulation time and complex setting. Therefore, traditional CFD approach is rarely used to study the UHI phenomenon. This research has developed a simplified CFD approach to quantify the UHI effect. The new approach used volume averaging approach on the Navies-Stoke equation and developed sets of sub-models for simplification. The new approach is able to simulate the thermal effect through radiation, conduction, convection, evaporation and etc, to re-create the thermal flow effect within the urban space under coarse grid model.

Hong Kong local weather data has been analysed to understand the impact of the urban characteristic to the thermal environment. Based on the analysis, Ta Kwu Ling is selected for the reference rural weather station for calculating UHI Intensity. A database has been created using GIS data, which stored the local urban characteristic of Hong Kong, including the greenery area, road area, construction area, building area, sea area, average building and terrain height.

The new approach has reduced the input requirement, modelling complexly, simulation time and computational power for simulating UHI effect in an urban space. The Tsim Sha Tsui Case study has shown the new approach can reduce the number of required grid cells 4000 times and reduce the required CPU time from 50,000 hours (CPU × 1) to 0.1 hour (CPU × 1) as compared with the traditional CFD approach. Thus, the new UHI modelling approach is more practical to be applied during the urban planning process as compared to the traditional. This thesis lays a foundation to predict the outdoor thermal environment and the UHI impact and to guide a sustainable urban design and planning through a performance-based approach.

ACKNOWLEDGMENTS

Foremost, I would like to express my sincere gratitude to my advisor Prof. Phil Jones for the continuous support of my Ph.D. study and related research. His guidance helped me in developing research and writing of this thesis. I could not have imagined having a better advisor and mentor for my Ph.D. study.

Besides my advisor, I would like to thank the rest of my thesis committee: Prof. Shiu-Keung, Tang, Prof. Daniel Chan and Dr. Sui-Hang, Yan for their insightful comments, but also for the hard question which help me to widen my research from different perspectives.

My sincere thanks also go to Dr. Vincent Cheng and Dr. Ngan-Tung, Lam Tony who provided me encouragement and support me to apply funding for the measurement, GIS data and weather data. Without their precious support it would not be possible to conduct this research. Also, I thank my friends Mr. Ka-Chun, Yeun Gary who gave me full supports on the field measurement works during the hot summer days.

A very special gratitude goes out to all down at the Hong Kong Polytechnic University and Community Weather Network for access to the labouratory and research facilities as well as providing the weather data for the research.

Finally, I thank my parents and my wife, Pinga Chan for supporting me throughout all my studies and for providing a comfortable home in which to complete my writing up.

TABLE OF CONTENTS

LIST OF TABLES

LIST OF FIGURES

GLOSSARY OF TERMS

$T_a(t)$	*predicted air temperature, ºC*
T_b	*base temperature, ºC*
$\Delta T_{sol}(t)$	*net air temperature changes due to radiation at given time t, ºC*
$\Delta T_{lw}(t)$	*net air temperature changes due to evaporation effect at given time t, ºC*
$\Delta T_{u-r(max)}$	*maximum air temperature different between the urban area and rural area, ºC*
$T_{deep\ ground}(t)$	*predicted underground (3m below ground) temperature at different time, ºC*
T_{sky}	*sky temperature, ºC*
T_s	*averaged ground surface temperature, ºC*
ST	*averaged ground surface temperature, ºC*
ϕ	*dependent variable that are expressed as functions of time and space*
ϕ_k	*dependent variable of individual phase*
Vol	*volume or total volume of the control volume, m^3*
Vol_k	*total volume in the control volume of an individual phase, m^3*
v_o	*Reference volume, m^3*
l_o	*reference length scale, m*
H	*control volume height or street canyon height, m*
W	*street canyon width, m*
GA	*ground area of the control volume, m^2*
WA	*building wall area of the control volume, m^2*
z_c	*canopy height, m*

Δz	*height between control volume and canopy, m*
ε_k	*porosity or void fraction or ratio of the volume of the respected phase, %*
t	*Time, s*
ρ	*density, kg/m^3*
P	*pressure, Pa*
Pop	*population*
T	*temperature, ºC*
h	*Enthalpy, J*
$\bar{v}$	*velocity magnitude, m/s*
u, v, w	*x, y, z component velocity respectively, m/s*
μ	*viscosity, m^2/s*
k	*thermal conductivity, W/(m.K)*
f	*drag force, N*
C_v	*specific heat capacity, J/(m^3.K)*
u_I	*velocity vector, m/s*
n_k	*flow direction of the dependent variable*
A	*Area, m^2*
A_k	*Area of an individual phase, m^2*
A_o	*Reference area, m^2*
A_{green}	*Area of greenery in control volume, m^2*
A_{road}	*Area of road in control volume, m^2*

A_{water}	*Area of water in control volume, m^2*
A_{plaza}	*Area of plaza in control volume, m^2*
S	*source term*
Q^*	*net radiation flux, W/m^2*
Q_F	*anthropogenic heat flux, W/m^2*
Q_H	*sensible heat flux, W/m^2*
Q_E	*latent heat flux, W/m^2*
Q_S	*thermal storage, W/m^2*
ΔQ_A	*advective flux from other space, W/m^2*
K^*	*Net shortwave radiation, W/m^2*
L^*	*Net longwave radiation, W/m^2*
$K\downarrow$	*shortwave radiation downward flux, W/m^2*
$K\uparrow$	*shortwave radiation upward flux, W/m^2*
$L\downarrow$	*longwave radiation downward flux, W/m^2*
$L\uparrow$	*longwave radiation upward flux, W/m^2*
$\Delta L_{lw}(t)$	*net outgoing longwave radiation flux at the given time t, W/m^2*
$L(t)$	*Latent Heat of Vaporization, kJ/kg*
$I_{lat}(t)$	*latent heat exchange flux at the given time t, W/m^2*
x	*soil depth, m*
n	*number of day*
SVF_w	*Sky View Factor of the wall or façade of building, %*

SVF_g	*Sky View Factor of ground surface, %*
m	*evaporation rate of different land type, mm/day*
ε_s	*surface emissivity of different land type, %*
a, b, c, d	*coefficient*
A1, A2	*SVF coefficient*
C_f, C_D	*Drag force coefficient, %*
δ	*constant (10^{-4})*
g	*gravity constant (-9.81m/s^2)*
k	*the phase, which could be either non-permeable phase or permeable phase*
n	*non-permeable phase (i.e. building, topography)*
p	*permeable phase (i.e. air)*
σ_{bolt}	*Stefan-Boltzmann coefficient (ε = 5.6x10-8 Wm-2K-4)*
hc	*surface heat transfer coefficient for convection heat transfer, W/(m^{2}K)*
γ_k	*area-weighted percentage of k type of land surface, %*
σ	*surface averaged absorptivity of the different land type, %*
$I_{SR}(t)$	*net solar radiation on the surface at time t, W/m^2*
$I_{dir}(t)$	*direct solar radiation on the surface at time t, W/m^2*
$I_{dif}(t)$	*diffuse solar radiation on the surface at time t, W/m^2*
ζ	*tree penetration coefficient, %*
c_{tree}	*specific heat capacity of tree, J/(kg·K)*
$\langle\phi\rangle$	*volume averaging of a variable*

$\langle \phi_k \rangle$	*extrinsic phase average of a variable*
$\langle \phi_k \rangle^k$	*intrinsic phase average of a variable*
grad	*gradient*
div	*divergence*
$\sim$	*spatial variation*
$-$	*average*
$\sum m_{jk}$	*sum of mass transfer between permeable phase and non-permeable phase, (kg/(m^{2}s)*
$\langle F_{jk} \rangle$	*Interactive momentum force, N*
$\langle q_{jk} \rangle$	*sum of heat transfer between non-permeable phase (topography or building) and permeable phase (air), W*

Chapter 1 Introduction

This Chapter will introduce the concept of Urban Heat Island (UHI) Effect and the general cause of the effect. Then it will discuss the impact of the UHI effect in Hong Kong. It will further discuss number of concerns from the Hong Kong government and citizens associated with the environmental deterioration due to the UHI effect. Then the chapter will discuss the mitigation measures and identify the challenges faced in implementing mitigation measures. And then it will discuss the Research Objectives of this thesis, which is to develop new simplified UHI modelling method to help to implement mitigation measures to reduce the UHI effect. Finally, it will discuss the use of Volume Averaging Approach and Urban Density Database that has been developed in this thesis to overcome the challenges in UHI Modelling.

1. 1 Background

UHI effect is a complex physical phenomenon. Figure C1. 1 shows the UHI effect impacts. According to M. Roth (2013), the urban climate is a combination of a dynamic process based on different scales. The urban climate also affected by nature of cities and atmospheres. UHI formation is a highly complicated thermodynamics process that happened at both microscopic and macroscopic level. For example, human metabolism is small-scale processes and atmospheric force is a mesoscale interaction (P. A. Mirzaei (2010)), thermal heat gain and loss and storage at building and ground surface and etc. It requires high computational power, complex boundary setup and long simulation time to model UHI effect precisely. In the early urban planning stage, the available information is often very simple, such as population, general building height and plot ratio. The information would be insufficient to model UHI effect using traditional CFD approach. Moreover, it is adequate to know the zone average UHI intensity for urban planning design, rather than the spatial UHI intensity distribution.

Thus, it is not necessary and impractical to model the UHI effect using a precise approach for urban planning design. This thesis aims to develop a simplified approach to model the UHI effect, by given up less important information.

This thesis demonstrates using Volume Averaging Approach to model the UHI effect and the Urban Density Database development using pixel analysis technique on the GIS data. A measurement has been carried out at July 2015 at 3 different locations of Tsim Sha Tsui Area. A high R^2 value ranging from 0.622 to 0.793 was observed between simulated and measured air temperature data, with the two datasets showing good agreement in both amplitude and trend. The results suggest that the new UHI modelling approach can well predict the UHI condition of the area. The newly developed Urban Density Database can generate the 3D geometry and grid cell automatically from the GIS data. The case study shows the new approach has reduced the number of grid cell 4,000 times and reduces the CPU time from 50,000 hours (CPU × 1) to 0.1 hour (CPU × 1) as compared with the traditional CFD approach. The new approach shows a significant improvement in computational power, simulation speed and reduces the boundary setup complexly.

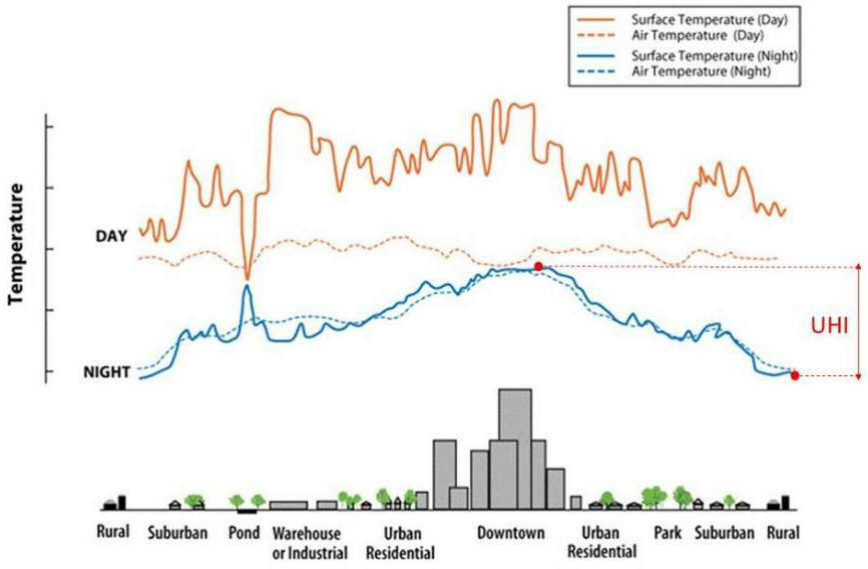

Figure C1. 1 Impacts of UHI effect (source: U.S. Environmental Protection Agency. 2008. "Urban Heat Island Basics." In: Reducing Urban Heat Islands: Compendium of Strategies)

1. 2 History of Urban Heat Island Effect

Urbanization involves quick changes of land use, reduce of greenery, heat emission from transportation and buildings and etc. It changes the local climate of a city and creates a unique microclimate environment. These changes induce significant impacts to the air temperature within the urban space, so called “Heat-island” effect. These changes have inevitably worsened the living environment as well as deterioration of our health, comfort and energy demand.

In 1958, Manley first introduced the concept of "urban heat island". Subsequently, many researchers (Chandler (1961), Oke and East (1971), Landsberg (1981)) have conducted studies on urban heat island effect interactions. The urban heat island (UHI) is a phenomenon refers to urban areas is significantly warmer than its surrounding undeveloped areas. Oke (1982) has referred the UHI to the relative warmth of air temperature near the ground (canopy layer). UHI occur in the air due to a difference in cooling between urban and rural areas. The UHI is clearly evident in numerous statistical studies of surface air temperatures over the years (Woolum (1964) and Critchfield (1983)), as shown in Figure C1. 2.

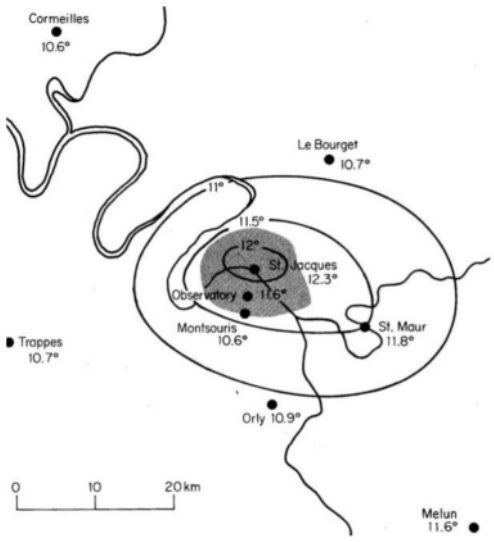

Figure C1. 2 Mean annual surface temperatures for Paris and Surroundings (Crtitchfield 1983)

UHI effect is caused by the cumulative impact arising from urbanization. For examples, reduce in the green area would also reduce surface evapotranspiration capacity and reducing the evaporative cooling effect; increase of buildings would also increase the heat capacity and allow more solar radiation energy to be absorbed and stored in the city areas; buildings in urban areas would induce wind blockage effect to reduce the amount of wind into the city; ventilation is less effective in urban than in rural, as the heat stagnation would reduce wind flow in the urban areas; decrease of surface albedo and sky view factor (SVF) are also contributing factors to UHI effect since the high-density building prevents the heat released into the high altitude.

1. 3 UHI Effect in Hong Kong

Hong Kong is highly urbanized with approximately 7 million people living in an area of roughly 1,100 km^2. The demand for a land far outweighs the amount of available space. Over past years, the citizens have witnessed the intensive urban development that magnifies the UHI effect of the city. According to research from J.E. Nichol (2009), the temperature in an urban center (Mongkok) can be up to 12℃ higher than that in rural areas. A report[1] from Hong Kong Observatory (HKO) also indicates that the urban area has been warming up at a rate of 0.4℃ per decade more than the rural area. The HKO report also shows that the UHI effect increase "the number of very hot nights" dramatically. The number of hot nights per year increased from 0 nights in 1950 to 37 nights in 2015 and predicts to further increase to over 45 nights in 2030. E. Y. Chan (2012) has studied the relationship of the air temperature and the mortality rates in Hong Kong. The statistical results show that an increase in 1°C daily mean temperature above 28.2°C is associated with 1.8% increase in mortality rates. Thus, Hong Kong government and citizens illustrate a variety of concerns associated with the

[1] Hong Kong Observatory. http://www.hko.gov.hk/climate_change/proj_hk_info_e.htm#temp

environmental deterioration caused by UHI effect.

1. 4 UHI Effect Mitigations Measures

The increase of ventilation, evaporation, reduce solar radiation can reduce UHI effect. Golany (1996), Wienert and Kuttler (2005) have suggested preserving wind corridors can enhance ventilation in the urban space and reduce the thermal load by carrying away the excessive heat of the city and replaces with cooler ambient air.

Mohamed F. Yassin (2011), A. C. Flowe & A. Kumar (2000), Hajra (2012), Zhao-Lin Gu (2011) have suggested that the street canyon design has a huge impact on the wind flow. These studies show how the buildings area ratio, the shape of the building, building width and height, sky view factor and building height to street width ratios related to the wind velocity.

Xiaomin Xie (2005), Fabio Murena (2009) and J. Gallagher (2012) have shown the pollutant dispersion within street canyon is depended on the wind velocity. These studies investigate the street design to improve wind velocity, including street aspect ratio, street patterns and orientations. Wang and McNamara (2007) investigate the air flow within the canopy by changing approaching wind angles.

Jian Hang & Yuguo Li (2011) has studies the wind flow through high-rise square building arrays as the approaching rural wind is parallel to the main streets in different aspect ratio. These studies prove that the wind velocity within a street canyon depends strongly on aspect ratio and street orientation.

The cooling effect of green areas in cities has been confirmed by many studies (Gomez (1998), Limor Shashua-Bar and Milo E. Hoffman (2000 & 2003), Dimoudi and Nikolopoulou (2003). Therefore, provision of greenery in a city has been considered as a

potential measure in mitigating the urban heat island effect. Nyuk Hiem Wong (2016) has investigated the greenery effect in Singapore – one of the most density megacities in Asia. The study shows that there is a strong correlation between the decrease of temperature and the greenery ratio. Areas have large greenery were obtained with lower temperature as compared to places with less greenery. Among the greenery, trees would be the most effective way to reduce the pedestrian temperature by to provide an opportunity to maximize shade in summer.

Shinji Yoshida (2006) has simulated the effect of the planted tree to the outdoor thermal environment in the canopy layer. The results show that the increase of the plants in the canopy layer improves the thermal environment during the hot summer season. However, over planting and/or excessive density of the planting causes would reduce the air flow inside the canopy, hence rise the thermal discomfort in the outdoor space.

M. Roth (2013) has stated that urban planning has an important role in regulating thermal comfort, reducing heat-related mortality, and the development of more sustainable cities. Analysing the climate data and built environment condition can help to achieve better urban planning and design in a climate responsive way.

1. 5 Research Motivation – lack of quantitative method for UHI effect in planning

UHI impact can be reduced through difference design measures such as enhance building layout, provide greenery area and use high albedo material to reflect solar radiation. And the design measures should be planned and implemented at the early urban planning stage. Yet, Hong Kong is still struggling to implement design strategies to mitigate UHI effect in the urban planning process (Green Power (2012)).

One major reason is that the urban planner is commonly lack of ability to predict the UHI

effects induced by the proposed urban design. It is challenging for planner to adopt effective design strategies. Consequently, urban planner will need a simple and practical method to evaluate the UHI impacts of the urban design. An efficient and quantitative method is, therefore, required to model the UHI effects.

1. 6 Research Objectives – Development of a new UHI modelling method

Currently, computational fluid dynamics (CFD) software is commonly used in early stages of planning to analyse the microclimate of a small development area in Hong Kong, such as the Air Ventilation Assessment (AVA), Environmental Microclimate Study and etc. However, there is no comprehensive UHI assessment has been conducted for urban planning in Hong Kong. It is mainly because traditional CFD approach requires detailed input data, intensive computational power and long simulation time. The key objective of this research is to develop a simple, low computational power numerical approach to model the urban heat island effect for the urban planning process.

1. 7 Challenges in UHI Modelling

There are challenges in UHI Modelling using traditional CFD approach:

- Extensive modelling area (up to 10km) creates huge domain area
- Huge domain area requires large number of grid cells
- large number of grid cells need huge computational power (number of RAM) and huge simulation time (CPU time)

Number of grid cells for UHI Modelling

Using traditional CFD approach, user requires to create three-dimensional geometry (including building, topography and etc). The three-dimensional space is then divided into

grid cells, which the simulation flow is solved. André Bakker (2006) has pointed out the grid cells of CFD has significant impact on rate of convergence, solution accuracy and CPU time required. In this thesis, the objective is not to improve the rate of convergence and solution accuracy, but to reduce the CPU time. Figure C1. 3 shows the predicted CPU time (hours) related to the number of grid cells from André Bakker (assuming CPU speed doubles every 1.3 years and estimated the simulation time in 2018).

Since grid cell size relates to CFD's rate of convergence and solution accuracy. Green Mark has set up a grid cell size requirement for outdoor wind CFD simulation. Referring Green Mark NRB (2015) the recommended grid cell size is around 0.1m to 5m for modelling building environment. The recommended grid cell size for each aspect is given in Table C1. 1. On the other hand, Oke (2009) has recommended the physical domain size need up to a city scale (10km) to fully capture the UHI phenomenon. For example, T. S. Saitoh (1996) has modelled the UHI effect of Tokyo the using Mesoscale Model with domain size of 40 × 40 km in the horizontal with 3 km in vertical height.

Refers to Green Mark NRB (2015), Oke (2009) and T. S. Saitoh (1996), using traditional CFD approach to model UHI effect would require a simulating domain of $10km^2$. For example, the physical domain in x, y, z directions could be 10,000m (H) × 10,000m (W) × 3,000m (H). The estimated minimum numbers of grid cells along x, y, z directions would be 4000 (x-axis), 4000 (y-axis) and 1200 (z-axis), respectively. The total number of grid cells in the physical domain would be 4000 × 4000 × 1200 = 2,400,000,000 grid cells using maximum 5m grid resolution, as recommended in Green Mark (2015). According to André Bakker (2006)'s prediction (given in Figure C1. 3), the simulation time (CPU hours) requires over 4,000,000 hours (under 1 × CPU) or approximately 24 hours (under 180,000 × CPU) for simulating 2,400,000,000 grid cells. Thus, using traditional CFD approach in UHI study requires huge computational power, input and simulation time, which is not a practical

approach for urban planning process in Hong Kong.

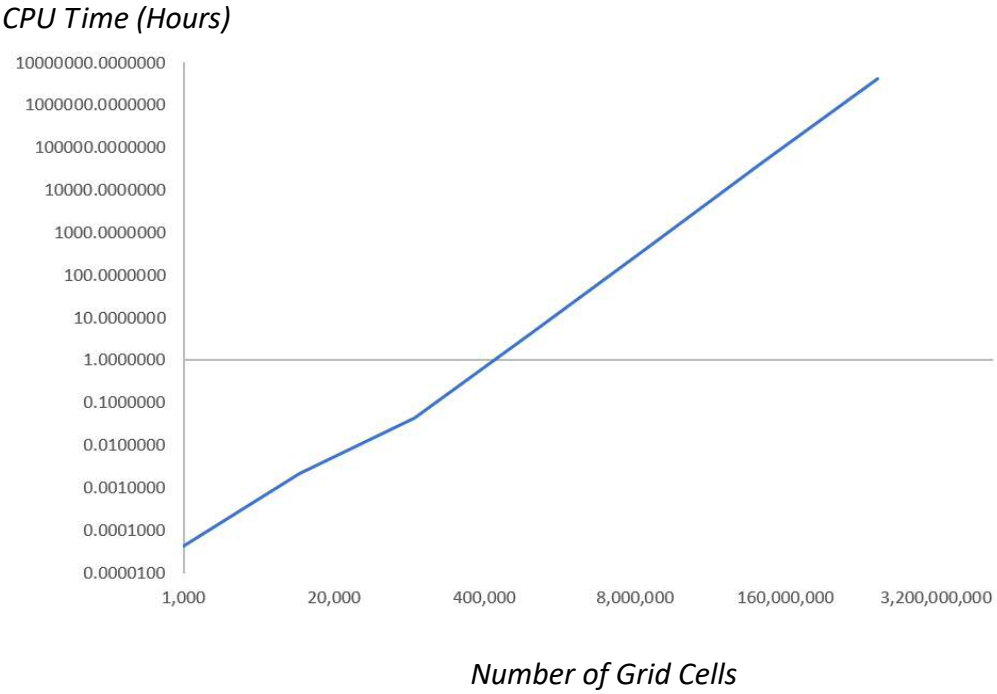

Figure C1. 3 Predicted CPU time (hours) v.s. number of grid cells (source: André Bakker (2006))

Table C1. 1 Recommended grid size setting in Green Mark (2015) for building environment CFD simulation

Location	Grid Size (m)
Within the functional spaces of interest	0.1-0.5
Building of interest	0.5-1.0
Surrounding building	1.0-5.0
From ground surface to 10m height in vertical direction	0.5-1.0
From 10m height to H_{max} height in vertical direction, (H_{max} is the height of the tallest building among the group of buildings modelled explicitly	1.0-5.0

1. 8 An Application Approach for UHI Modelling - Volume Averaging Approach

Jim Thom (2009) has pointed out that CPU time in simulation grows exponentially with number of cells. To reduce the number of grid cells, this thesis applies Volume Averaging Approach as an upscaling method to upscale the fine grid model to coarse grid model. Figure

C1. 4 shows an example of fine grid model and coarse grid model from V. L. Hauge (2014) for reservoir simulation.

Volume Averaging Approach has been well developed for solving two-phase / multiphase system which can be found in textbook of The Method of Volume Averaging by S. Whitaker (1995) and Advanced Heat and Mass Transfer by Amir Faghri (2009) and many other literatures. This approach is able to define the average properties for the two-phase or multiphase system and obtain solvable governing equations that can be used to predict the macroscopic properties of the system. However, this approach is mainly applied for reservoir simulation, solute transport in porous media simulation (Sergey Chaynikov (2013), reservoir engineering simulation (M. J. King (1998)) or other such as oil or gas flow simulation, geotechnical analysis and etc. In this thesis, Volume Averaging Approach is applied to set of governing equations to model the mean velocity and temperature profile for UHI effect.

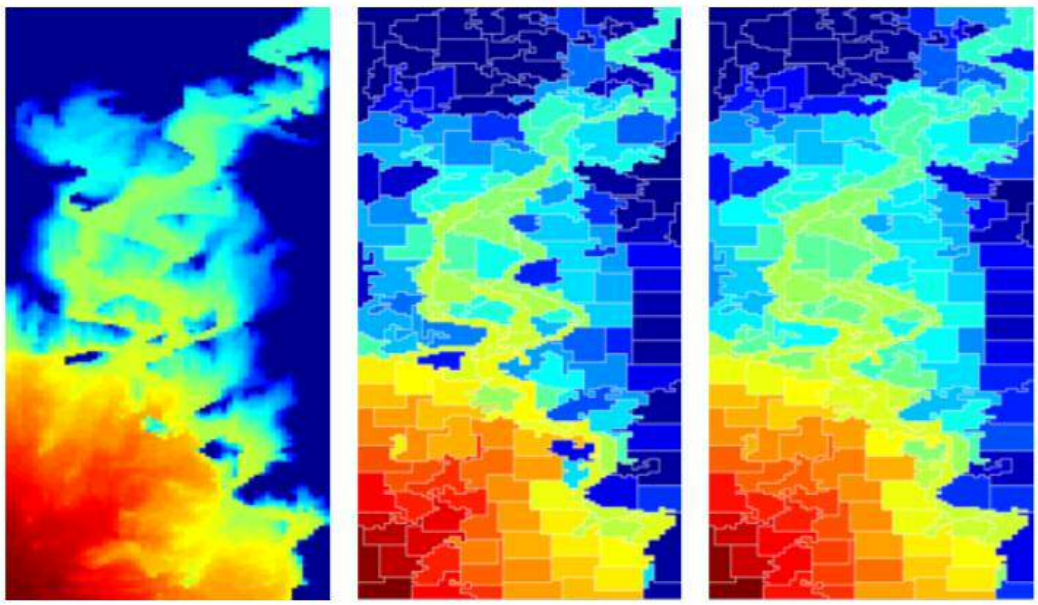

Figure C1. 4 Comparison of results for different grid scale – fine grid model (left), coarse grid model 1 (middle), coarse grid model 2 (right) in reservoir engineering simulation (Source: V. L. Hauge (2014))

The grid cells under traditional CFD approach and the newly UHI model (using Volume Averaging Approach) is showing at Figure C1. 5. Volume Averaging Approach allows to

model the fluid flow in the system in a larger grid-cell diameter.

Traditional CFD Approach | **Volume Averaging Approach**

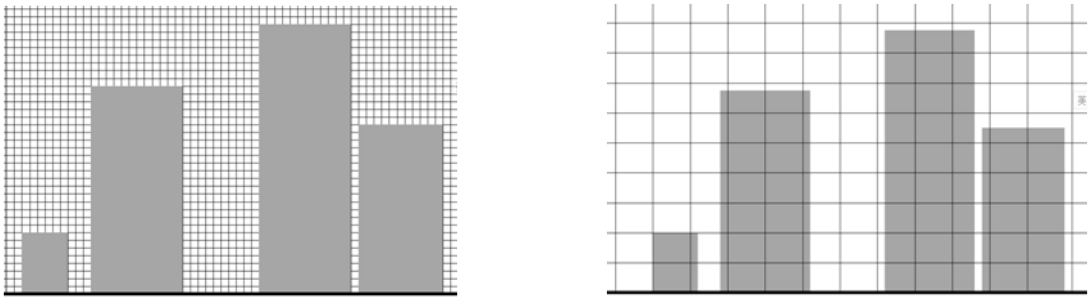

Each grid represents local spatial average of velocity

Numerically, each grid corresponds to representing the averaged velocity at a point as the average of all velocities within the

Figure C1. 5 Grid for Traditional CFD Approach (left) and Volume Averaging Approach (right) in our study

However, Volume Averaging Approach upscales the grid cells from fine grid model to coarse grid model and will cause information loss (Dasheng Qi (2000), Amir Faghri (2010), Hui Liu (2017)). The detail of the information loss during volume averaging is given in Chapter 2.10. Therefore, additional terms and equations, namely "Sub-Model", are created during the volume averaging process. For example, an interactive momentum force term, F_{jk} , is added to the volume averaged momentum equation during the volume averaging process, as shown in Equation C3. 23. The additional interactive momentum force term represents the fluid force of the physical structure within the cell or drag force of urban canopy. The interactive momentum force term adopted the urban canopy drag force model proposed by Maruyama (1992). Maruyama has correlated the fluid force per volume to porosity and permeability of the control volume. The volume averaging approach is discussed in Chapter 3.1 to 3.8 and the Sub-Modelling approach is discussed in Chapter 3.9 to 3.15.

This thesis has also applied the Volume Averaging Approach to energy conservation

principles. The detail of volume averaging process on Energy Equation is given in Chapter 3.8. Set of Sub-Models is created to link up with the volume averaged Energy Equation (Equation C3. 31) that could consider the effect of short wave and long wave radiation heat transfer, evaporation heat transfer, conduction and convection heat transfer and etc. The heat transfer of the Sub-Model is strongly depended on the building height, the topography elevation, the amount of different type of areas, such as greenery, sea, road, building and etc. However, to input the area data into the traditional CFD bounadary condition is also time consuming and labour intensive. There is a need to create a simplified approach to input the data into the UHI model.

1. 9 Creation of Urban Density Database

Even through the UHI Model has been largely simplified by the Volume Averaging Approach, the model still requires detail input at the boundary condition, such as building height, the topography elevation, the amount of different type of areas. For example, the model need the information of porosity and permeability (in x, y, z-direction) of each control volume to simulation the general flow field. The model also needs the area of greenery, road, building, water features and etc within each control volume to solve the heat transfer of energy equation with the Sub-Model.

An Urban Density Database has been developed in this thesis to simplify the UHI model input process. Urban Density Database is a self-developed computational code to transform the GIS image and data, such as, digital maps, digital orthophotos, and 3D spatial data into urban density parameters in respect to a xy coordination system. The xy coordination system is using Hong Kong 1980 Grid Coordination System. The urban density parameters includes, the spatial average of building area, road area, water area, greenery area, building height and terrain height. The grid resolution of the urban density database is 10m $\times$ 10m.

1. 10 Measurement v.s. Case Study

An on-site measurement had been carried out at 3 locations in Hong Kong during June 2015. The measurement data is used to compare with the simulated data from a case study to validate the UHI model. 3 measurement points were at Tsim Sha Tsui Area, including Kowloon Park, HKO Headquarter Station and the Hong Kong Polytechnic University (PolyU), respectively. The measurement stations were located at the same district with around 500m distance from one to other. Each station is surrounded with a different type of built environment. For example, (1) Kowloon Park has the largest urban park in Hong Kong that consist of significant amount of greenery; (2) HKO Headquarter Station represents a typical high-density and high-rise built environment of Hong Kong; (3) PolyU has one of the largest building density in Hong Kong that consist of significant amount of building mass. A simulation study using the UHI model has been carried out for Tsim Sha Tsui Area. The domain size is approximate 2640m(D) $\times$ 2640m(W) $\times$ 2640m(H) with grid cells of 33 $\times$ 33 $\times$ 33 in xyz coordination. The simulated results are compared with the measurement data for from 11 Jun 2015 to 14 Jun 2015. The comparison shows that the UHI model predictions are in good agreement with the measurement data with high R^2 value ranging from 0.622 to 0.793. The results suggest that the UHI model can well predict the UHI effect in a complex urban space.

1. 11 New UHI Model – Significant Improvement

UHI model has shown a significant improvement on the grid cells number reduction and simulation time (CPU time) in modelling Tsim Sha Tsui Area. Refers to the Green Mark NRB (2015) recommended grid cells size of max. 5m, the new UHI model can reduce the number of grid cells for 4,000 times and simulation time (CPU time) for 500,000 times (50,000 hours (CPU $\times$ 1) to 0.1 hour (CPU $\times$ 1)). The detail is summarized in Chapter 7.4.

1. 12 Summary

Urbanization has significant impact on a climate of a city. One of the most well-known consequences is the Urban Heat Island (UHI) effect, which develops when the urban cooling rates are slower than the rural ones. The changes of land use, the densely urban infrastructure and anthropogenic heat cause the lower cooling effect in built-up areas, resulting in large temperature difference.

Implement of mitigation measures – a new UHI Prediction Model

UHI impact can be reduced through different design strategies. A UHI Prediction Model can helps to implement the design strategies at the early urban planning stage to effectively reduce the UHI impact. However, there are technical difficulties and limitations that prevent using traditional Computer fluid dynamics (CFD) approach to predict the UHI results. Thus, a new prediction model is needed for UHI prediction.

Limitation of traditional simulation method - CFD

Computer fluid dynamics (CFD) software is commonly used to analyse the microclimate of a small area. However, it is not practical to use traditional CFD approach to carry out UHI Study in Hong Kong, since it requires large amount of grid cells to model the heavily built-up areas. Large amount of grid cells would induce problem of large computational power, long simulation time and complex data input. For example, refers to Andre Bakker (2006) findings, traditional CFD may requires approximately 4,000,000 hours (1 CPU) or 1 hour (180,000 CPU) to simulate 10 km^2 area.

Develop Volume Averaging Approach for simplification

In order to reduce the amount of required grid cells, this thesis has applied Volume

Averaging Approach as an upscaling method to upscale the fine grid model to coarse grid model. An Urban Density Database is developed to allow the GIS data transforms to the UHI model input data. The Urban Density Database has stored geometrical information of greenery, road, building, water features in a 10m × 10m grid cell resolution.

Validation Works

A comparison study has been carried out in Tsim Sha Tsui Area. The simulated air temperature has been compared with the measurement data from 11 Jun 2015 to 14 Jun 2015. The simulation results show in a good agreement with the measurement results, suggesting that the new UHI model can well predict the UHI effect of complex urban space. The case study also demonstrates the significant improvement on the grid cells and simulation time (CPU time) reduction as compared to the traditional CFD approach.

Thesis Outline

This thesis contributes to the theoretical and numerical UHI Modelling in the followings area

- Developed a practical approach on Volume Averaging Approach on UHI Modelling. The background and equation of the Volume Averaging Approach for the literature and textbook are presented in Chapter 2 - Literature Review of the thesis;

- The derivation of the governing equations for Volume Averaging the UHI model is presented in Chapter 3 - Urban Heat Island Modelling. Both microscopic and macroscopic effects are also modelled and represented clearly in Chapter 3;

- The Development of Urban Density Database for UHI Modelling based on GIS data and the methodology is presented in Chapter 4. The database allows the GIS

data transform to UHI model input using pixel analysis. Thus, the time required for 3D geometry modelling, grid meshing and boundary condition setting is reduced;

- Generic numerical techniques for solving the Volume Averaging equations and Sub-Models are introduced in Chapter 5. The finite volume method is used for the discretization progress. The procedure for the coding and for solving the field variables as well as the connection between Volume Averaging equations and Sub-Models are illustrated in Chapter 5;

- Weather data from 9 weather stations have been collected and further analysed using Urban Density Database in Chapter 6;

- A model validation of the new UHI modelling approach are preformed and compared with the measurement data in Tsim Sha Tsui Area during 11 Jun 2015 to 14 Jun 2015. The simulation results are in a good agreement with the measurement results, suggesting that the new UHI model can well predict the UHI effect of a complex urban space. The new UHI model also demonstrates a significant grid cells number and simulation time reduction as compared with using traditional CFD approach. The information is illustrated in Chapter 7.

Chapter 2 Literature Review

This chapter presents the literature review of existing urban heat island study, including the measurement and simulation methodology, summarize the key findings and etc. Firstly, the chapter discusses the proposed UHI modelling domain size from Oke (2009). Oke has suggested the modelling domain size should be at least 10km to capture the full UHI phenomenon and it would significantly enlarge the required amount of grid cells. The chapter also discusses the methodology of UHI measurement and modelling approach, including statistical model, urban climate, urban energy balance model and numerical model approach. The chapter then discusses the Volume Averaging Approach including, the concept of "upscaling", the advantage and disadvantage, development and application in engineering industry. Finally, the thesis introduces the general equation of Volume Averaging Approach by referring the works of Amir Faghri (2010).

2. 1 Urban Heat Island Domain Size

The CFD domain size affects the heat transfer process between near ground layer and upper layer and creational of heat island effect. Therefore, the domain size is an important consideration in UHI study. Oke (2009) has proposed different domain size for different type of studies. For UHI study, Oke has suggested the scale should be up to a city scale (10km) to capture the phenomenon. Table C2. 1 listed the recommended scale for different environmental studies proposed by Oke.

Traditional CFD approach is commonly used in Hong Kong urban planning to analyse the microclimate of a small area. Figure C2. 1 shows the scale different between a typical microclimate model and the proposed UHI domain size by Oke (2009). However, there is around 2,400,000,000 grid cells (under max. 5m grid resolution) is required to cover the

10km Physical Range, as suggested in Chapter 1 Section 1.11, while the large amount of grid cells requires large computational power and long simulation time. The key objective of this thesis is to overcome the grid limitation by developing a simple, low computational power numerical approach to model the urban heat island effect for the urban planning process.

Table C2. 1 Recommended scale for different environmental studies proposed by Oke (2009)

Study	**Scale**	**Physical Range**
Building design	Street	Up to 500m
Pollution dispersion	Building / Neighbourhood / City	Up to 1,000m
Urban energy balance	Building / Neighbourhood / City	Up to 10,000m
Urban heat island	Neighbourhood / City	100m to 10,000m
Weather forecast	City / Regional	At least 1000m

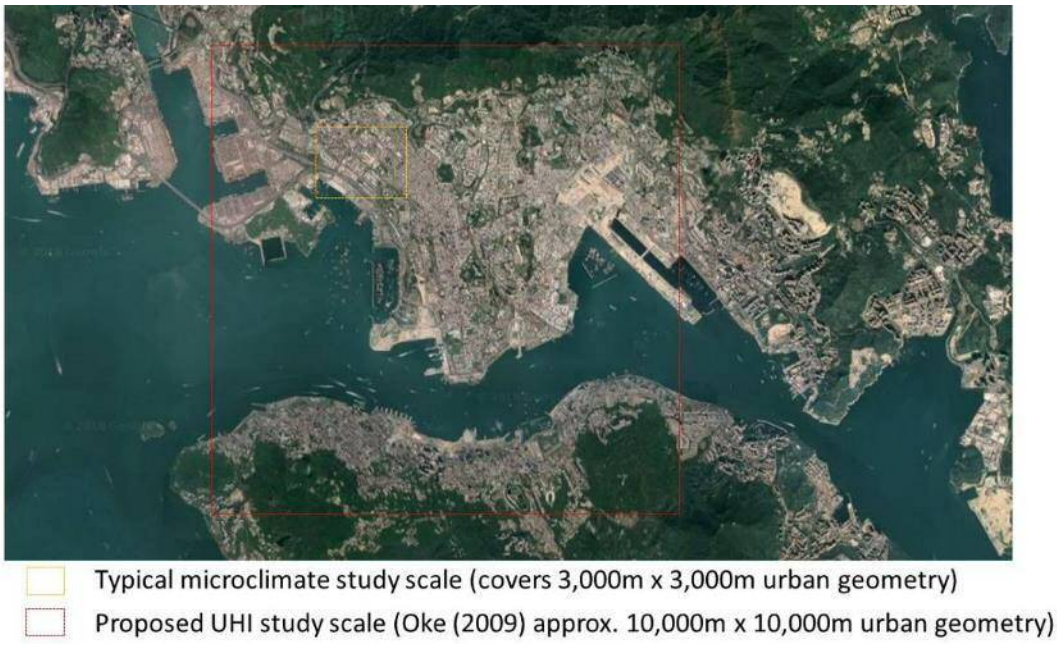

Figure C2. 1 Scale of a typical microclimate study area (yellow line) and Oke's proposed scale for UHI study (red line)

2. 2 UHI Study Measurement

There are several measurement approaches to study urban heat island effect. There are mainly 3 most common approaches, including (1) air temperature measurement by fix local weather station, (2) surface temperature by remote sensing data, (3) air temperature by mobile transverse measurement.

Air temperature measurement by fix local weather station – this approach measurement the air temperature in a space and analyse the temperature changes against time to study the characteristics of urban heat island. Since this approach measures the air temperature directly, the data is reliable. However, the disadvantage of using this approach is that the record data would be single point data. Thus, the spatial air temperature resolution is quite low and the complete spatial distribution of air temperature is not known.

Surface temperature by remote sensing data – this approach is based on remote sensing data from satellite thermal image to capture the surface temperature. This approach can capture the instantaneous condition of a large area and resolves the low-resolution problem of air temperature measurement. However, the problem of this approach is that it can only provide short duration information. Thus, this approach cannot capture the thermal delay during the day or seasonal air temperature changes. Also, cloudy, high air pollutant or humid weather conditions could block the view of the satellite sensors and affects the accuracy of surface temperature results.

Air temperature by mobile transverse measurement – this approach is to measure the air temperature using mobile transverse tools, such as bicycle, vehicle. However, Fung Wing Yee (2009) has suggested that the coverage of the measured areas is often restricted by Hong Kong's road layout and could weaken to the accuracy of measurement.

Even through the measurement approach is one of the most common methods to study UHI effect, the approach is mainly used for validation or quantify the current environmental condition rather than predict the UHI intensity urban planning design. Thus, the measurement data is not useful for the developing the UHI model. In this thesis, the air temperature measurement by fix weather stations is used to provide validation data for the UHI model. A field measurement has been carried out in 11 Jun 2015 to 14 Jun 2015 in Tsim Sha Tsui Area. The measurement data is used for validating the UHI model, as given in Chapter 7.

2. 3 Existing Urban Heat Island Modelling Approach

Wong Nyuk Hien (2016) has suggested UHI modelling could be used to better understand the UHI effect. It is particularly important to understand the effectiveness of mitigation measures that change the climatic condition and urban morphology.

Measurement data or statistical UHI models are not useful to predict the UHI effect during urban planning. In recent years, the development of using computer technology to predict and analyse the thermal environment or micro-climate study has made great progress. Numerical models offer better capabilities and reliabilities that allow to consider interact of atmosphere with the urban context and provides detail results in the 3D spatial environment. At present, the simulation model for micro-climate study is mainly composed of urban canopy model, computational fluid dynamics, ENVI-met and so on.

However, the current simulation tools have limitation that makes them not useful or not practical to be applied in the Hong Kong urban planning design. As the results, there is still no a comprehensive UHI assessment has been conducted for Hong Kong urban planning.

2. 4 Statistical UHI Models

Many researchers (Arnfield (2003), Santamouris (2007), M. Santamouris and C. Georgakis (2003) Santamouris (2001) and R. Giridharan (2004)) have carried out measurements to investigate the heat island effect by different cities that have different size and climatic characteristics. Using the measured data, researchers have developed statistical models to predict the UHI effect.

For example, Oke (1973) has proposed a model that describes the maximum heat island intensity related to population.

$$\Delta T_{u-r(max)} = a \times \log(Pop) + b \qquad \text{(Equation C2. 1)}$$

Here a & b denotes the coefficient of the equation, Pop denotes the population, $\Delta T_{u-r(max)}$ (ºC) denotes the maximum air temperature different between the urban area and rural area. Oke (1981) had also described the maximum heat island intensity related to street canyon geometry.

$$\Delta T_{u-r(max)} = 7.45 + 3.97 \times \ln\left(\frac{H}{W}\right) \qquad \text{(Equation C2. 2)}$$

Here H denotes the street canyon height, W denotes the street canyon width and $\Delta T_{u-r(max)}$ (ºC) denotes the maximum air temperature different between the urban area and rural area.

However, the of the statistical UHI models is limited in urban planning design since the model only work well for specific location. For example, Fung Wing Yee (2009) has proved that the measured maximum UHII is not highly correlated with population for Hong Kong.

2. 5 Urban Climatic Map

Matzarakis (1992) has proposed a concept of a climate-mapping system for planning purposes through a statistical approach. This concept is further developed by Scherer (1999), Matzarakis (2005) to an urban climatic map (UCMap). It is a two-dimensional spatial map contains urban climatic factors and town planning considerations. E. Ng (2009) has produced a UCMap for Hong Kong that combined the information of surface temperature, wind velocity, topographic, land use to produce an urban climate recommendation maps with planning instruction. Figure C2. 2 shows the UCMap developed by E. Ng (2009).

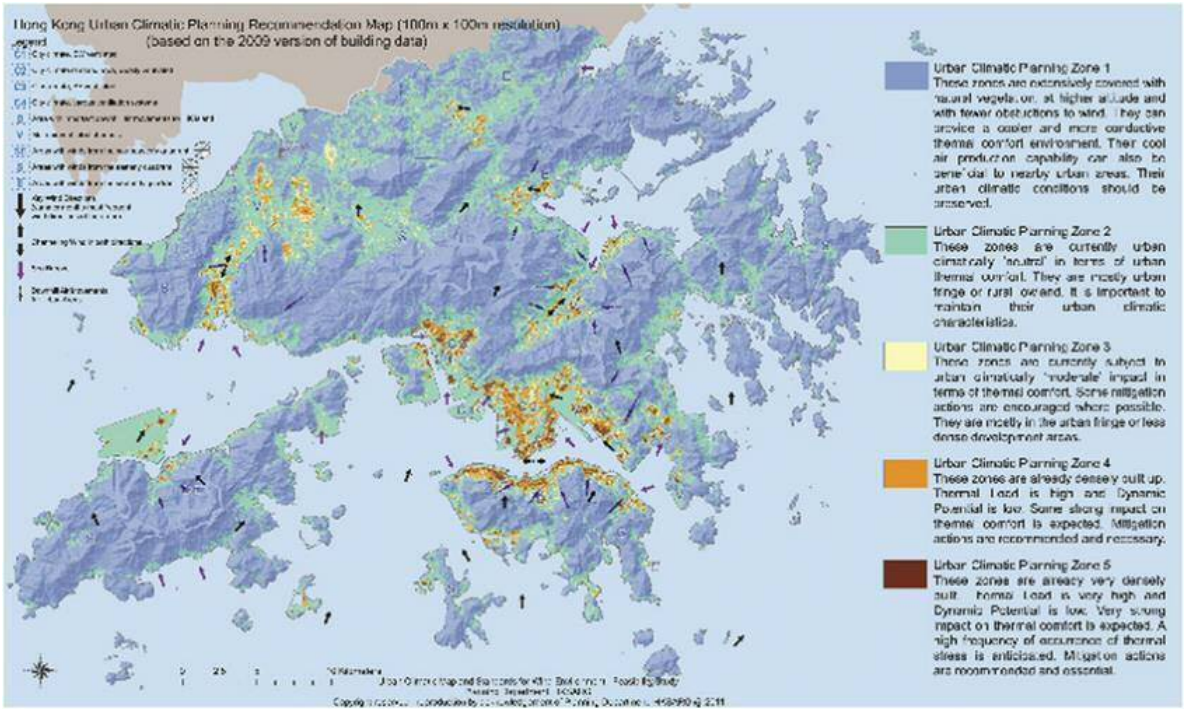

Figure C2. 2 Urban Climatic Map of Hong Kong (source: E. Ng (2009))

The UCMap is developed by correlate the existing environmental data, remote sensing data and measurement data and related to human thermal comfort. The map also classifies areas into different thermal zone. Thus, the UCMap is particularly useful for policymakers to exam the district-level planning strategies.

However, the disadvantage of UCMap is that it developed based on the existing condition

and it is not able to predict the air temperature changes of a completely new town planning. Furthermore, the correlation is purely statistical approach and there is no relationship between grids. For example, the thermal affect or ventilation affect from adjacent zone through district wind corridor, building separation alignment, urban park could not be obtained through UCMap. Thus, this approach could not give sufficient flexibilities for designing urban context and not particularly useful for optimizing the urban planning design.

2. 6 Urban Energy Balance

Oke (1988) has developed an urban energy balance equation to study the energy at any location by considering the heat transfer of net radiation flux, sensible and latent heat fluxes, energy change by thermal mass, advective heat flux and anthropogenic heat flux. The general form of the energy balance equation can be described by:

$$Q^* + Q_F = Q_H + Q_E + Q_S + \Delta Q_A \qquad \text{(Equation C2. 3)}$$

Here Q^* denotes the net radiation flux (w/m^2), Q_F denotes the anthropogenic heat flux (w/m^2), Q_H denotes the sensible heat flux (w/m^2), Q_E denotes the latent heat flux (w/m^2), Q_S denotes the thermal storage (w/m^2), ΔQ_A denotes the advective flux from other space (w/m^2).

Oke (1988) has also pointed the available energy at any location to heat the air or ground or evaporate water depends on the radiation balance as shown below:

$$Q^* = K^* + L^* = K\downarrow - K\uparrow + L\downarrow - L\uparrow \qquad \text{(Equation C2. 4)}$$

Here Q^* denotes the net radiation (w/m^2), K^* denotes the net shortwave radiation (w/m^2), L^* denotes the net longwave radiation (w/m^2), $\downarrow$denotes the downward flux and $\uparrow$ denotes the upward flux.

The urban energy balance equation from Oke (1988) is a concept of how the heat transfer occurs in the urban canopy. It could not be used directly to assessment the UHI effect. Thus, the urban energy balance equation is further developed by many researches to study the UHI effect. According to Harman (2004), there are four most well-known urban energy balance model which can be used to predict the UHI Intensity, including (1) Slab canopy model, (2) Volumetric averaging model, (3) Urban street canyon - single layer models and (4) Urban street canyon - multi-layer models.

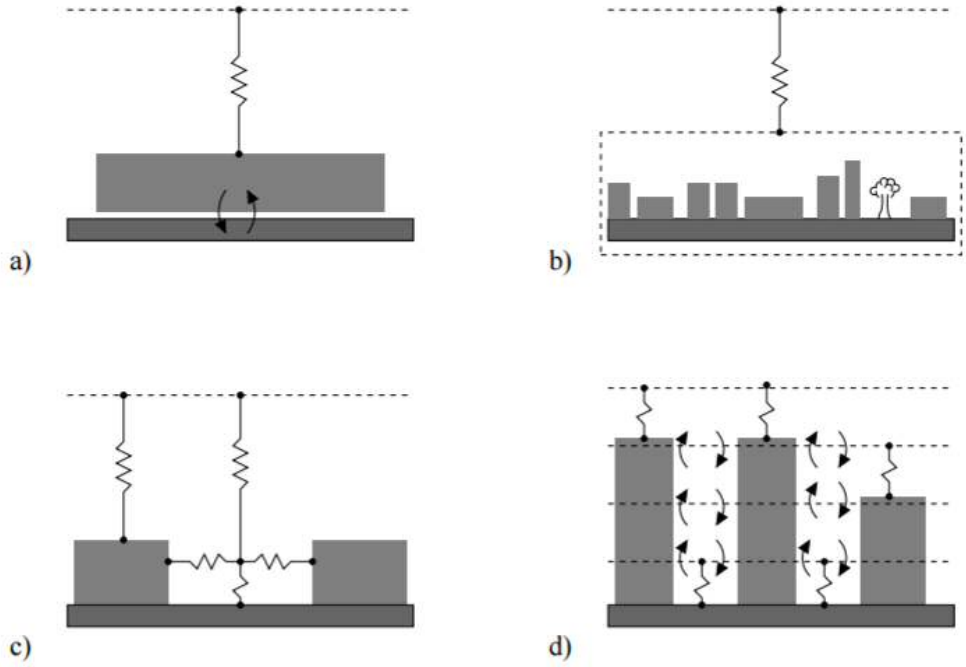

Figure C2. 3 Different approach to model urban energy balance (Source: from Harman (2004)) (a) canopy models (e.g. Best (1998)); (b) volumetric averaging models (e.g. Grimmond (1991)); (c) urban street canyon - single layer models (e.g. Masson (2000)); (d) urban street canyon - multi-layer models (e.g. Martilli (2002)).

Slab canopy model

Figure C2. 3(a) shows the schematic of slab canopy model from Best (1998). The model approximates the urban surface as one slab or one surface with weighted average surface characteristics of different urban areas.

However, the disadvantage of slab canopy model is that it only considers the whole urban space as one temperature and interacts to the sky and ground through heat transfer. The approach is too simplified for the highly complex urban content of Hong Kong and not particularly useful for optimizing the urban planning design.

Volumetric averaging model

Figure C2. 3(b) shows the schematic of energy balance model using the volumetric averaging technique on a large urban space that developed by Grimmond (1991). This approach requires to implement statistical coefficients into the model to determine the net radiative, storage effect of different surface morphology.

Compare with the slab canopy model, resultant urban temperature of volumetric averaging model can determine the more complicate heat transfer of the space through statistical coefficients, such as the net radiative effect and storage effect.

However, the disadvantage of volumetric averaging model is still considered the whole urban surface as one temperature and interacts with the sky and ground temperature. Furthermore, the statistical coefficients is based on statistical data that may requires fine-tuning before applying to Hong Kong environment. Fung Wing Yee (2009) has also pointed out statistical model usually not working well in Hong Kong due to the highly complex built environment natural. Thus, this approach is also too simplified for the highly complex urban content of Hong Kong and not particularly useful for optimizing the urban planning design

Urban street canyon - single layer models

Figure C2. 3(c) shows the schematic of urban street canyon - single layer models and linking with numerical weather prediction (NWP) models by Masson (2000). Unlike the slab canopy model and volumetric averaging model, the NWP model provides a more accurate boundary condition for urban street canyon - single layer models to predict the urban energy and UHI intensity. The slab canopy model then considers the average energy balance of individual building façade and the entire urban energy balance is explicitly incorporated in the formulation of the terms of the energy balance.

However, the disadvantage of this approach is that grid resolution from NWP is very large. The true velocity and wind direction due to different building disposition or urban layout cannot be reflected under this approach. The NWP is particularly inaccurate for modelling high-rise and high density building region. Since the outdoor wind has a huge impact on the accuracy of heat transfer of the air temperature from advection heat transfer and convection heat transfer from the building façade and topography. Thus, this approach is not recommended in for modelling UHI effect in Hong Kong.

Urban street canyon - multi-layer model

Figure C2. 3(d) shows the schematic of urban street canyon - multi-layer models by Martilli (2002). This approach considers the different types of urban surface and allows each surface to have thermal interaction with different atmospheric levels. Compare with the other energy balance models, multi-layer model has the advantage of considering heat transfer more realistic way, as the heat transfer has extended from 1-dimensional to 2-dimensional.

This multi-layer model considers the properties of the urban surface using the average properties on a spatial scale appropriate to the resolution of the mesoscale model. According

to HKO website[2], the resolution of the mesoscale model can be ranging from 2km x 2km grid to 100km x 100km grid. The disadvantage of the multi-layer model is that using the energy balance model alone is not sufficient to capture the fine detail of the urban surface. Thus, the multi-layer model is too simplified for the highly complex urban content of Hong Kong and not particularly useful to consider the buildings disposition effect to the wind flow.

An improved version of multi-layer model is adopted in this thesis to develop the "Ground Energy Balance Model" and "Building Energy Balance Model" in Chapter 5.4 and 5.5, respectively.

Cluster thermal time constant (CTTC) analytical model

Swaid and Hoffman (1990a) has combined the energy balance model with analytical model to develop a cluster thermal time constant (CTTC) analytical model. It used to predict the air temperature and UHI intensity variations in the urban canopy. The CTTC model considers the thermal inertia of the urban landscapes, evaporation of greenery, net radiation heat transfer effect using the volumetric averaging technique. The study of Swaid and Hoffman shows the modelling results are in a good agreement with the measured air temperature in Jerusalem. Swaid and Hoffman have proposed that the urban air temperature can be expressed as the sum of the contributions in energy balance, which can be described as:

$$T_a(t) = T_b + \Delta T_{sol}(t) - \Delta T_{lw}(t) \qquad \text{(Equation C2. 5)}$$

Here $T_a(t)$ denotes the predicted air temperature (°C) of a location, T_b denotes base temperature (°C), $\Delta T_{sol}(t)$ denotes the net air temperature (°C) change due to radiation at given time t, $\Delta T_{lw}(t)$ denotes the net air temperature (°C) change due to evaporation effect at given time t.

[2] HKO, Mesoscale Model, https://www.hko.gov.hk/nhm/mesomodel_e.htm

Limor Shashua-Bara and Milo E. Hoffman (2002) have further developed the CTTC model to consider the effect of plant transpiration and shade on temperature changes. The proposed CTTC model can assess the impact of green distribution on the thermal environment of the neighbourhood, but the model emphasizes the impact on the near-surface thermal environment only.

However, the disadvantage of the CTTC model is that it does not consider advection effect. Furthermore, the CTTC mode is not valid under wind speed above 1m/s. As the results, this model is not able to consider the cooling effect from adjacent zone, such as sea breeze, land breeze, urban greenery. Thus, it is also not particularly useful to consider the wind enhance strategies for urban planning design.

2. 7 Numerical UHI Modelling

ENVI-met

The ENVI-met model is 3 a dimensional CFD model to simulate the heat transfer between surface-vegetation-air-structures in urban environments. ENVI-met has been widely used for simulates the local changes in urban planning. ENVI-met model is particularly useful for carry out small scale micro-climate environment simulation such as the interaction of wind, heat, wet environment and solar radiation.

However, the disadvantage of using Envi-met is that it has been designed for micro-scale projects only. For example, the largest amount of grid cells in Envi-met (v.3.1) is 250 (x-axis) × 250(y-axis) × 30(z-axis). Refers to Green Mark (2015) Table C1. 1 of maximum allowable grid cell size of 5m, the maximum domain size would be only 1250m × 1250m × 150m. This indicates that Envi-met is only allows to perform microclimate size study rather than large area simulations, such as UHI Study. Thus, Envi-met is not able to perform a

large scale UHI study and not practical to apply in the Hong Kong urban planning design.

Integrated Environmental Solutions (IES)

Similar to *ENVI-met,* the IES model uses 3 dimensional CFD approach. Rajagopalan (2014) has used IES to simulate the urban flow to study the UHI effect in Muar, Malaysia. However, the disadvantage of the IES model is the domain size has only approximately 600m × 450 m, which the size is also insufficient to carrying out UHI study.

Mesoscale Modelling

Mesoscale Model is commonly used for creating weather forecasts and climate projections. It is able to carry out the complex heat transfer and air flow simulation. B. Bass and E.S. Krayenhoff (2002) have used Metamorphic Model MC2 (Mesoscale Compressible Community Model) to simulate the Canadian green roof of Toronto. The findings show that if 5% of the building applied green roof, the temperature of the city of Toronto will drop 0.5℃. Thus, Mesoscale Model can be a useful tool to assess the greenery design strategies in the urban planning design.

However, the disadvantage of Mesoscale Model is that the resolution of the model is quite low. The horizontal resolution of the model is typical around 1 ~ 10 km^3. Also, the wind flow based on surface roughness is only a rough estimation and difficult to estimate and apply during the urban planning design. Thus, Mesoscale Model is rarely used to study the UHI effect.

Computational Fluid Dynamic (CFD)

Many researchers have applied CFD techniques to simulate the wind flow in an urban canopy

[3] HKO - Mesoscale Model: https://www.hko.gov.hk/nhm/mesomodel_e.htm

layer. Honjo (1990) used two-dimensional k-ε two-way turbulence model to study the cooling effect of the green roof. Dimoudi and M. Nikolopoulou (2003) have applied simplified plant models with CFD to simulate the microclimate effect of urban green space to show that urban green space can reduce the urban air temperature about 0.8 K for 10% increase of forest. Kristóf (2009) has applied CFD with user defined function package to create the coriolis force effects and urban heat island circulation effect.

However, the simulation studies of Honjo (1990), Dimoudi and M. Nikolopoulou (2003) and Kristóf (2009) were all carried out at a small area only. For example, Kristóf (2009) case study maximum domain size is only 70m long. Miklós Balogh (2009) has pointed out that the detailed numerical simulation requires complex geometries and that makes CFD unrealizable to apply for large domains study. CFD is particularly difficult to apply for urban heat island study, which the domain size may requires around 10km to capture all of the heat island phenomena as suggested by Oke (2009). For example, T. S. Saitoh (1996) modelled Tokyo UHI effect using a domain size of 40 x 40 km in the horizontal with 3 km in vertical height using Mesoscale Model. For applying traditional CFD approach for 40 x 40 km domain size, the estimated required grid cell number can reach up to 38,400,000,000 in three-dimensional cases (using max. allowable 5m grid cell size from Green Mark (2015) in Table C1. 1). Thus, tradational CFD approach is not a practical for urban planning design due to the huge computational power and time.

2. 8 Volume Averaging Approach

History of "up-scaling" concept and Volume Averaging Approach

Due to the lack of computational power in the old day, the "up-scaling" concept has developed as early as 1967 to reduce the computational requirement. Anderson and Jackson (1967) has introduced "up-scaling" concept with a set of derivations in fluidized beds study.

Slattery (1967) and S. Whitaker (1967) has used a similar approach to study viscoelastic fluids flow and fluids flow in porous media. S. Whitaker (1967) has proposed spatial distribution of the fluids flow rate could be expressed by a resultant of the local averaged fluids flow rate and the spatial deviation term. After nearly a decade of development, Whitaker (1977) has shown the method to model drying in a porous media using Volume Averaging Approach.

Current "up-scaling" approach application

Currently, the "up-scaling" approach is still a popular simulation approach and has been further developed to a wider application, such as hydrology, solute transport, reservoir engineering, oil or gas flow simulation, geotechnical analysis and etc. For examples, H. Eichel (2004) has used the "up-scaling" approach to model the porous media in hydrology, Sergey Chaynikov (2013) has used the "up-scaling" approach to model solute transport in porous media, M. J. King (1998) has used the "up-scaling" to study the reservoir condition.

The reason for "up-scaling" approach is still a popular simulation approach is mainly due to the technical problem arise from high computation power, long simulation time, complexity of geometry and grid generation. For example, Hartmut Eichel (2004) has pointed out that the intrinsic heterogeneities in the Porous Media influence the multi-phase flow behavior of a dense non-aqueous phase liquids (DNAPL) infiltrating into a natural soil. However, it is not possible to model the heterogeneities in the Porous Media due to small size, irregular form and complex structure. Figure C2. 4 to Figure C2. 6 shows "up-scaling" simulation model of a reservoir simulation. Hong Kong urban content is also highly irregular, complex and covers large areas. Thus, "up-scaling" approach is required for simulating UHI Study in Hong Kong to address the problems.

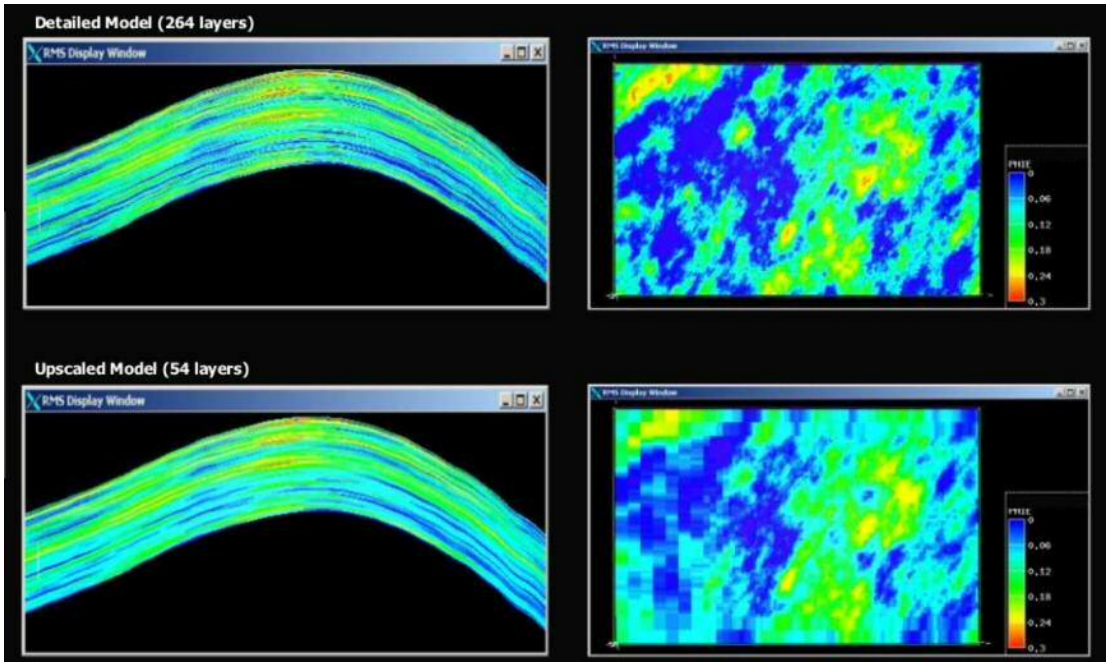

Figure C2. 4 Upscaling simulation model sample – Grid Size 100x100m^2 (top) and Grid Size 1600x1600m^2 (Bottom) (Source: Reservoir Characterization Study – Upscaling & Simulation Model Initialization)

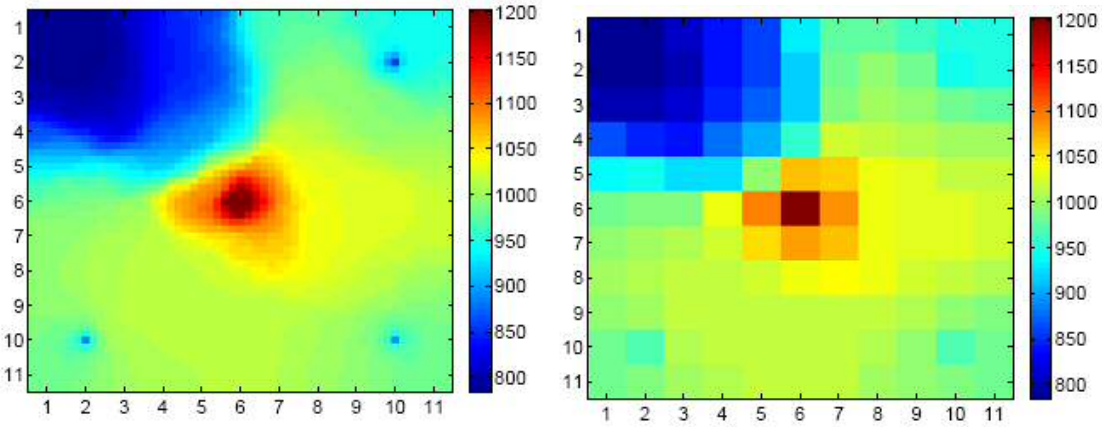

Figure C2. 5 Fine-scale model (left) and Upscaled model (right) (Source: Hangyu Li, Global upscaling for compositional flow simulation)

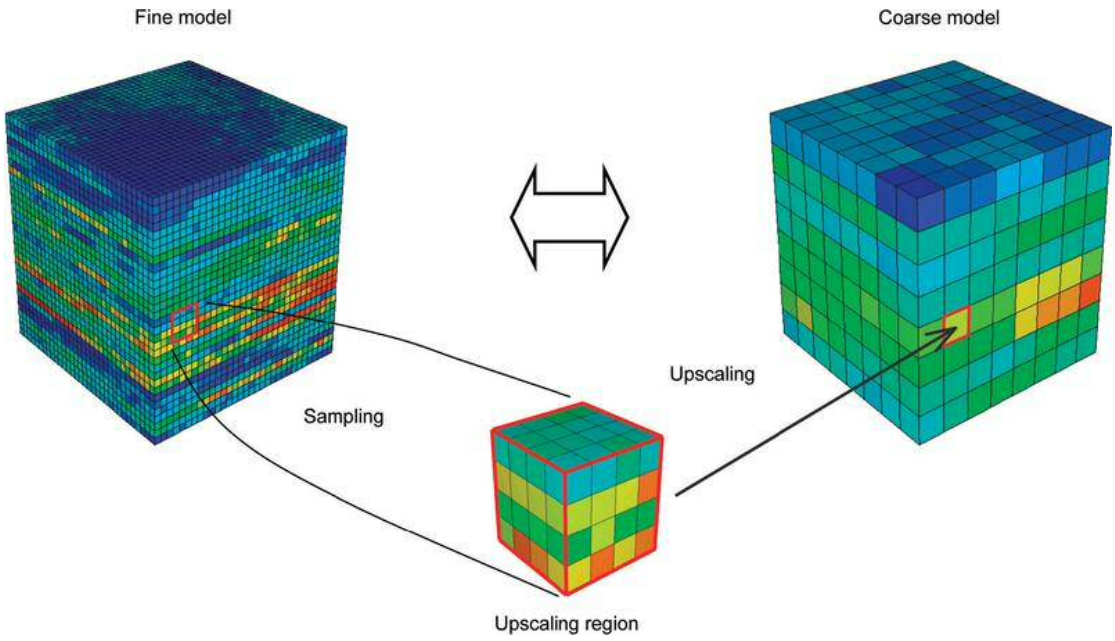

Figure C2. 6 Example of up-scale the modelling space in 3D (Source: PetroWiki - Upscaling of grid properties in reservoir simulation [4])

Concept of Volume Averaging Approach

The process of up-scaling governing differential equations from one length scale to another has been widely applied in many engineering disciplines to reduce the computation power, complexity of geometry and grid generation. The Volume Averaging Approach is one of most commonly used approach for the "up-scaling" process. I. J. Losada (2016) has indicated that the traditional CFD approach requires fine grid model to solve the Reynolds averaged Naiver-Stokes equation. By applying the Volume Averaging Approach to the Reynolds averaged Naiver-Stokes equation, a set of fine CFD grid (with heterogeneous condition), as shown in Representative Elementary Volume (REV) at Figure C2. 7 (left), could be up-scaled to a coarse grid model or Representative Elementary Volume (REV) (refers to the red dotted square in Representative Elementary Volume (REV).

[4] PetroWiki: Upscaling of grid properties in reservoir simulation, https://petrowiki.org/Upscaling_of_grid_properties_in_reservoir_simulation

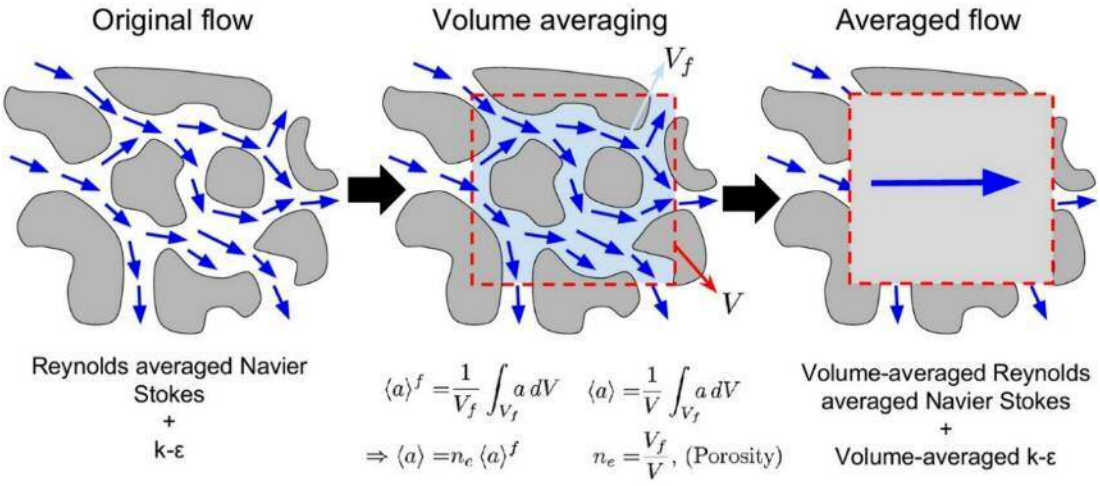

Representative Elementary Volume (REV)

Figure C2. 7 Diagram of Volume Averaging Approach: Traditional CFD Approach requires fine grid model (left), Process of Volume Averaging Reynold averaged Naiver Stoke equation (middle), Volume Averaged Approach requires less fine grid or coarse grid model (right) (Source: I. J. Losada (2016))

Figure C2. 7 (left) shows that the fine grid model has a heterogeneous condition, which allows the spatial distribution of variables such as velocity / temperature / pressure could be different across the field. By Appling the Volume Averaging Approach to the Reynolds averaged Navier-Stokes equation, the spatial distribution of variables such as velocity / temperature / pressure inside the REV (within the red dotted square in Figure C2. 7 (middle and right)) would be averaged out to obtain a homogeneous condition with the grid cell "up-scaling" to become a REV. Moreover, as the spatial distribution of variables inside the REV has become homogeneous condition (Figure C2. 7 (right)), there are no spatial variation information of the variables within the REV. Thus, Amir Faghri (2010) refers this condition as "information loss". The lost information and treatment in this UHI Model will be discussed in more detail in Section 2.10.

UHI Study is suitable to apply Volume Averaging Approach

The importance of the lost information would determine whether Volume Averaging Approach is a suitable approach or not. Oke (1987) has proposed to quantify the urban heat

island impact by using urban heat island intensity (UHII) (refers to Equation C6. 1). It generally defined as regional temperature difference between the urban and rural spaces. The fine detail of spatial detailed distribution of temperature / velocity / pressure are not the interest of the UHI study. Thus, the Volume Averaging Approach is suitable to be used for UHI Study.

Microscopic and Macroscopic Level

P.A. Mirzaei (2010) has pointed out that the UHI formation is a highly complicated thermodynamics process at both microscopic and macroscopic level. For example, heat transfer would interact between small-scale processes like human metabolism (microscopic level) and mesoscale interactions like outdoor wind flow (macroscopic level). As discussed in Chapter 1, the major problem of simulating both microscopic (small) and macroscopic (large) level information in one model requires massive number of grid cells.

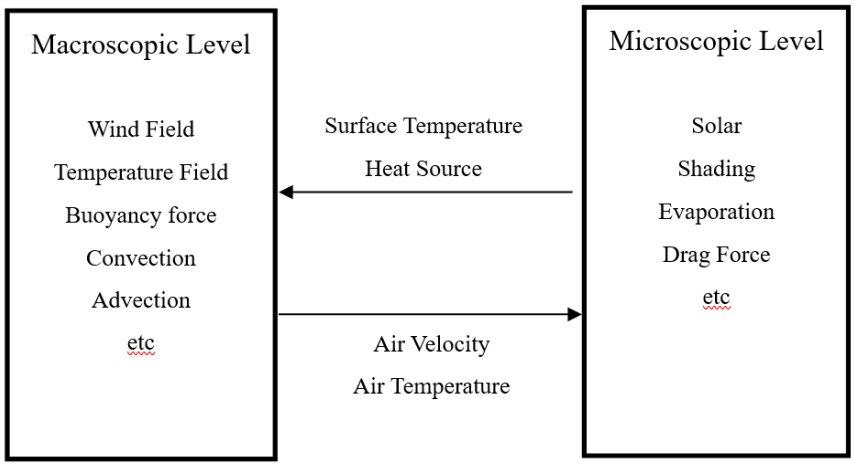

Figure C2. 8 Schematic of the interfacing for the macroscopic level and microscopic level in the UHI Model

In this thesis, the Volume Averaging Approach is used for "up-scaling" the grid cell in UHI Modelling. The mesoscale interactions like outdoor wind flow, gravity force, buoyancy effect, advection effect is considered in macroscopic level model, while the small-scale processes like solar radiation on topography and building, evaporation effect of greenery and water

feature are considered in microscopic level model. Figure C2. 8 shows the schematic of the interfacing for the macroscopic level and microscopic level in the UHI Model. This approach can greatly reduce the grid cells requirement for modelling urban flow or UHI effect in CFD and allows numerical analysis able to a model domain size of exceeding 10km.

2. 9 Macroscopic Governing Equations

The macroscopic governing equations for the fluid flow in a permeable space can be derived by averaging the microscopic continuity and momentum equations over a volume (Liang Wang, 2015). Many researchers had developed these theorems forming the basis of the Volume Averaging Approach. For example, Whitaker (1967) and Slattery (1967) has studied the flow inside the porous media. It determined that local quantities in space (e.g. spatial variation of variable such as temperature, velocity, pressure, chemical and etc) could be averaged within the Representative Elementary Volume (REV) based on the point conservation law. The momentum, heat and mass transfer at the macroscopic level will be modelled by sets of averaged local quantities (e.g. averaged spatial variation of variable such as averaged spatial temperature, averaged spatial velocity, averaged spatial pressure, averaged spatial chemical within the REV, as shown in Figure C2 .7) are represented, while the microscopic information will be represented by interfacial integrals.

Amir Faghri (2010) has described Eulerian averaging methods in detail. The Eulerian averaging defined the changes of dependent variables, ϕ (velocity, temperature, and pressure), as functions of time and space coordinates, which are independent variables. Eulerian volumetric averaging is performed over a volume element, Vol (m^3), around a point (x,y,z) in the flow.

In this thesis, a volume consists of two different phases only.

1. **non-permeable phase - building structure, topography and water feature element**

2. **permeable phase – air element**

This thesis applied Volume Avenging Approach for the UHI Model development. Thus, it is important to first understand the concept of the Volume in traditional CFD and Volume Avenging Approach.

In Chapter 1 and 2, it is understood that CFD requires to generate grid cells for simulation. These grid cells are also known as “control volume”. CFD commonly use finite-volume method at grid node to transforms the partial differential equations representing conservation laws over differential volumes into discrete algebraic equations over finite volumes.

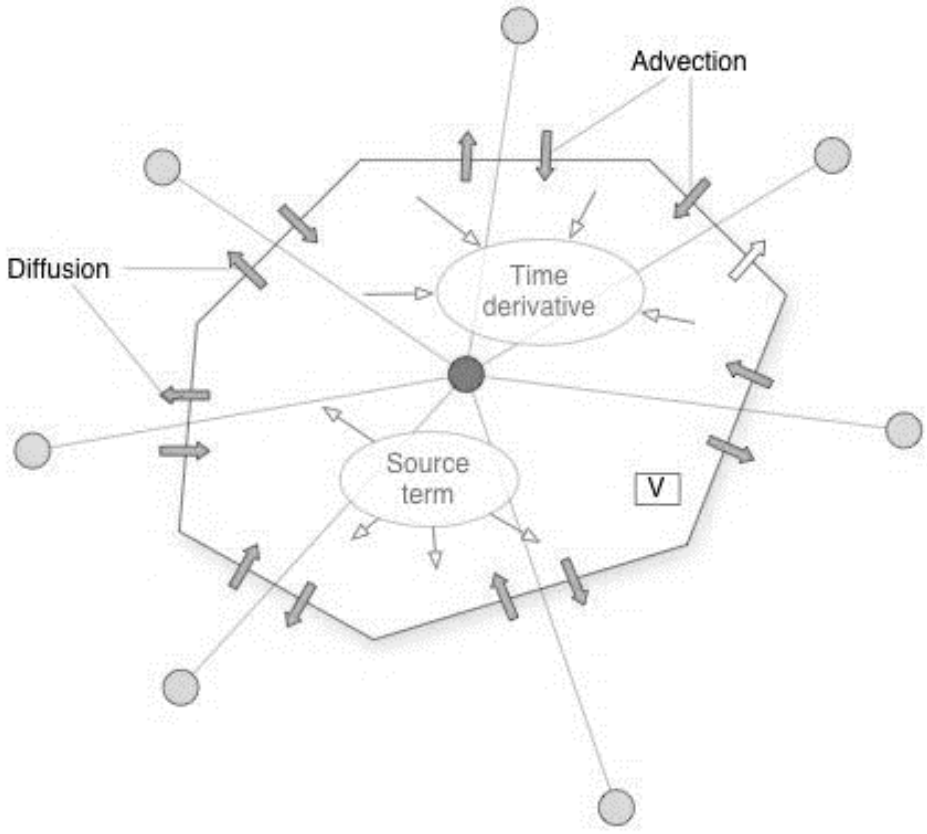

Figure C2. 9 Diagram of control volume in CFD (Source: CFD@AUB research group)

Thus, the total volume of the control volume can be denoted as:

$$\text{Total volume of the control volume} = \text{Vol} \qquad \text{(Equation C2. 6)}$$

In Volume Avenging Approach, the total volume of the control volume can be also denoted as Vol (m^3). And the volume can be also equals the summation of the individual phase (which is non-permeable phase and/or permeable phase) volume that can be described as:

$$\text{Vol} = \sum_{k} \text{Vol}_k \qquad \text{(Equation C2. 7)}$$

Here Vol denotes the total volume (m^3) of the whole control volume, Vol_k (m^3) denotes the total volume in the control volume of an individual phase, k denotes the phase that could be either non-permeable phase or permeable phase. Figure C2. 10 shows an example of ratio of the volume of the respected phase.

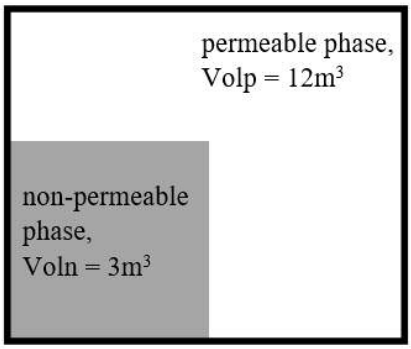

$$\varepsilon_n = \frac{3}{(12+3)} = 20\% \qquad \varepsilon_p = \frac{12}{(12+3)} = 80\%$$

Figure C2. 10 Diagram of ratio of the volume of the respected phase

The ratio of the volume of the respected phase is also important in the study. It is also known as **Porosity or void fraction**. Porosity is a measure of the void (i.e. "empty") spaces in a material and is a fraction of the volume of voids over the total volume, between 0 and 1. Figure C2. 11 shows an example of porosity at different level.

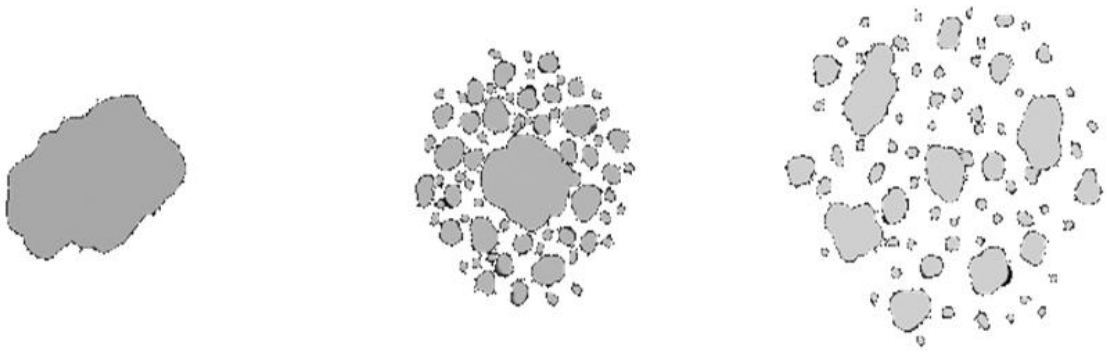

Figure C2. 11 Diagram of porosity sample

The ratio of the volume of the respected phase, ε_k, to the total volume can be described as:

$$\varepsilon_k = \frac{\mathrm{Vol}_k}{\mathrm{Vol}} \qquad \text{(Equation C2. 8)}$$

Here ε_k denotes the ratio of the volume of the respected phase Vol_k denotes the total volume (m^3) in the control volume of an individual phase and Vol denotes the total volume (m^3) of the whole control volume.

Since the control volume only consist of non-permeable phase and permeable phase, summation of the volume fraction of non-permeable phase and permeable phase must equal to 1.

$$\sum_{k} \varepsilon_k = 1 \qquad \text{(Equation C2. 9)}$$

Now that apply Volume Averging over a dependent variable, ϕ, that are expressed as functions of time and space. In this thesis, the dependent variable is velocity, pressure or temperature.

$$\phi = \phi(x, y, z, t) \qquad \text{(Equation C2. 10)}$$

Here ϕ denotes dependent variable that is expressed as functions of time and space.

Refers to Amir Faghri (2010) Volume Averging equation of a dependent variable can be expressed as:

$$\langle \phi \rangle = \frac{1}{V} \sum_{k=1}^{\Pi} \int_{V_k} \phi_k(x, y, z, t)\, dVol \qquad \text{(Equation C2. 11)}$$

Here ϕ denotes the average dependent variable for all phases, ϕ_k denotes the dependent variable of the individual phase k. Figure C2. 12 shows an example of average dependent variable for all phases.

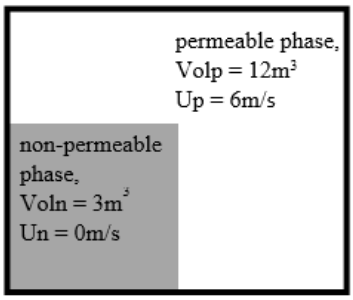

Volume averaging of velocity

in permeable phase

$$\langle U \rangle = \frac{1}{(12+5)}\, x\, [(6\, x\, 12) + (0\, x\, 3)]$$

$$= 4.8 \text{m/s}$$

Figure C2. 12 example of average dependent variable for all phases

There are also two important expressions need to be introduced for Volume Averging to describe phase averaging the value of a variable, which is intrinsic phase average and extrinsic phase average.

Intrinsic phase average is describing the averaging of a variable for that individual phase only.

$$\langle \phi_k \rangle^k = \frac{1}{\text{Vol}_k} \int_{\text{Vol}_k} \phi_k \, d\text{Vol} \qquad \text{(Equation C2. 12)}$$

Here $\langle \phi_k \rangle^k$ denotes intrinsic phase averaging of a variable ϕ_k of the individual phase k, Vol_k denotes the total volume (m^3) in the control volume of an individual phase.

Extrinsic phase average is describing the averaging of a variable for all phases.

$$\langle \phi_k \rangle = \frac{1}{Vol} \int_{Vol_k} \phi_k \, dVol \qquad \text{(Equation C2. 13)}$$

Here $\langle \phi_k \rangle$ denotes extrinsic phase averaging of a variable ϕ_k of the individual phase k, Vol denotes the total volume (m3) of the whole control volume.

Figure C2. 13 gives an example of intrinsic phase average and extrinsic phase average on a dependent variable.

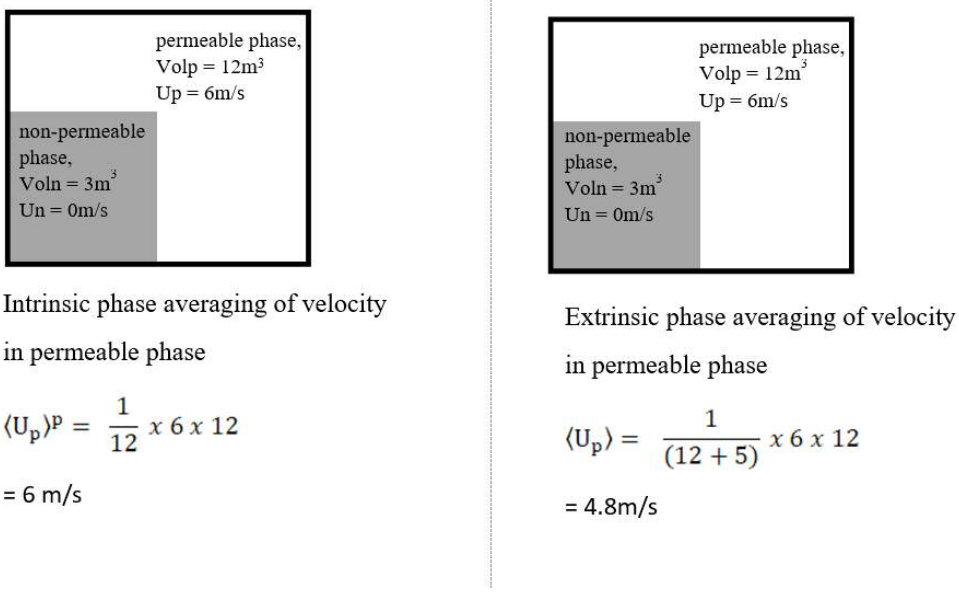

Figure C2. 13 example of intrinsic phase average and extrinsic phase average

Refers to Amir Faghri (2010), both intrinsic and extrinsic phase average can be related by the ratio of the volume of the respected phase.

$$\langle \phi_k \rangle = \varepsilon_k \langle \phi_k \rangle^k \qquad \text{(Equation C2. 14)}$$

Here ε_k denotes the ratio of the volume of the respected phase.

And both intrinsic and extrinsic phase average can be related to the whole volume by:

$$\langle \phi \rangle = \sum_{k=1}^{\Pi} \langle \phi_k \rangle = \sum_{k=1}^{\Pi} \varepsilon_k \langle \phi_k \rangle^k \qquad \text{(Equation C2. 15)}$$

Here ϕ denotes the average dependent variable for all phases, $\langle \phi_k \rangle$ denotes extrinsic phase averaging of a variable ϕ_k of the individual phase k and ε_k denotes the ratio of the volume of the respected phase.

For the control volume, Vol, the volume averaging of the partial derivate with respect to time based on general transport theorem can be described as:

$$\langle \frac{\partial \phi_k}{\partial t} \rangle = \frac{\partial \langle \phi_k \rangle}{\partial t} + \frac{1}{\mathrm{Vol}} \int_{A_k} \phi_k u_I . n_k dA_k \qquad \text{(Equation C2. 16)}$$

The left side represents the extrinsic phase average of the rate of change of dependent variable ϕ_k. The right side represent the rate of change of extrinsic phase average of dependent variable ϕ_k in control volume + the net flow of dependent variable ϕ_k–through between non-permeable phase and permeable phase. Here ϕ_k denotes the dependent variable of individual phase, u_I denotes the velocity vector, n_k denotes the flow direction of the dependent variable.

Amir Faghri (2010) further discussed some expression that would apply to Volume Averaging the governing equation. For example, the volume averaging of gradient for any dependent variable ϕ_k can be described as:

$$\langle \mathrm{grad}\, \phi_k \rangle = \mathrm{grad}\, \langle \phi_k \rangle - \frac{1}{\mathrm{Vol}} \int_{A_k} \phi_k n_k dA_k \qquad \text{(Equation C2. 17)}$$

Here $\mathrm{grad}\, \phi_k$ denotes the gradient of any dependent variable. For example, the 2nd term at

the right-hand side of the momentum equation – (μ grad V) would need to apply this expression during the Volume Averaging. V denotes the fluid velocity (m/s). $\langle \text{grad}\, \phi_k \rangle$ denotes the volume averaging of a gradient of any dependent variable, $\text{grad}\, \langle \phi_k \rangle$ denotes the gradient of the intrinsic phase averaging of a variable ϕ_k, the last term at the right hand side of Equation C2.17 denotes the net resultant particular process of dependent variable ϕ_k through between non-permeable phase and permeable phase. Using (μ grad V) term as an example, it would mean the net of rate of increase of directional momentum force per unit volume of the individual phase.

Another expression would be the volume averaging of a divergence of any dependent variable ϕ_k can be described as:

$$\langle \text{div}\, \phi_k \rangle = \text{div}\, \langle \phi_k \rangle - \frac{1}{\text{Vol}} \int_{A_k} \phi_k \,.\, n_k \, dA_k \qquad \text{(Equation C2. 18)}$$

Here $\text{div}\, \phi_k$ denotes the divergence of any dependent variable. For example, the 2nd term at the left-hand side of the momentum equation – (div ρV) would need to apply this expression during the Volume Averaging. It is noted that the V denotes the fluid velocity (m/s) and ρ denotes the fluid density (kg/m^3).

The last term at the right hand side of Equation C2.18 denotes the net flow of dependent variable ϕ_k through between non-permeable phase and permeable phase during that particular process.

Amir Faghri (2010) also discussed some mathematics treatment during Volume Averaging, such as the products of two averaged variable can be described as:

$$\langle \phi_k \psi_k \rangle^k = \langle \phi_k \rangle^k \langle \psi_k \rangle^k + \langle \widetilde{\phi_k} \widetilde{\psi_k} \rangle^k \qquad \text{(Equation C2. 19)}$$

$$\langle \phi_k \psi_k \rangle = \varepsilon_k \langle \phi_k \rangle^k \langle \psi_k \rangle^k + \langle \widetilde{\phi_k} \widetilde{\psi_k} \rangle^k \qquad \text{(Equation C2. 20)}$$

Here ϕ_k or ψ_k denotes the any dependent variable of the respected phase, $\widetilde{\phi_k}$ denotes the spatial variation of the dependent variable of the respected phase, ε_k denotes the ratio of the volume of the respected phase.

Interactive Force Term

Geometry effect or force induced by any non-permeable structure is presented by the net rate of increase of surface force per unit volume of a fluid particle (here within after "interactive force term"). However, once the Volume Averaging Approach is applied to momentum equation, the geometry information within the REV would be lost. Thus, it is difficult to determine the interactive force as it related to the geometry information, such as volume, shape, and permeability of the subject. In this thesis, an additional Sub-Model is created to represent the interactive force within the REV in the momentum equation.

Many researchers used experimental data to develop an empirical model to represent the interactive force, namely drag force equation. Burke & Plummer (1982) has carried out an experiment that considered a porous medium consisting of sand or some porous rock or glass beads or cotton cloth contained in a pipe.

Plummer (1982) has identified that the fluid force on any bluff body or drag force can be described with the drag coefficient C_D and reference area A_o as:

$$f = -\frac{1}{2}\rho C_D A_o |\tilde{u}|\tilde{u} \quad \text{(Equation C2. 21)}$$

$$f = -\frac{1}{2}\rho C_f \frac{1}{l_o} l_o |\bar{u_1}|\bar{u_1} \text{ , whereas} \quad \text{(Equation C2. 22)}$$

$$C_f = \frac{C_D}{(1-\epsilon_o)^2} \quad \text{(Equation C2. 23)}$$

$$l_o = \frac{V_o}{A_o} \quad \text{(Equation C2. 24)}$$

Here f denotes the drag force (N), ρ denotes the fluid density (kg/m^3), C_f & C_D denotes the drag coefficient from measurement, V_o denotes the reference volume (m^3), A_o denotes the reference area (m^2), l_o denotes the reference length scale (m), $\bar{u_1}$ denotes the average air velocity (m/s), ϵ_o is limited from 0 to $1-\delta$ to increase the numerical stability. δ is a constant value of 10^{-4}.

Maruyama (1992) has also proposed a model to describe the fluid force in urban canopy, in which the drag force, f can be described as:

$$f = -\frac{1}{2}\rho C_D \frac{A_o}{Vol} |\bar{u_1}|\bar{u_1} \quad \text{(Equation C2. 25)}$$

Maruyama (1992) has further carried out a set of wind tunnel test for building models with different density and obtained the drag coefficient, C_D.

Based on the measurements, the drag coefficient C_D of the urban canopy can be described as:

$$C_D = \min\left(\frac{1.53}{(1-\epsilon_o)}, 2.75(1-\epsilon_o)\right) \quad \text{(Equation C2. 26)}$$

Value ϵ_o is limited from 0 to $1-\delta$ to increase the numerical stability. δ is a constant value of 10^{-4}. Coirier and Kim (2006) have suggested the method to simplify the drag coefficient C_D. It was calculated as a function of the volumetric porosity of the obstacle array.

$$C_D = \begin{cases} \dfrac{\min(\Delta z, H - z_c + 0.5\,\Delta z)}{[1-\epsilon_f]\Delta z}, & \text{if } z_c - 0.5\Delta z \le H, \\ 0, & \text{if } z_c - 0.5\Delta z > H, \end{cases} \quad \text{(Equation C2. 27)}$$

Here H denotes the control volume height (m), z_c denotes the canopy height (m), Δz denotes the height between control volume and canopy (m).

Miklos Balogh (2009) has suggested that the drag term of the momentum equation is composed of the viscous and drag force, while the value of the viscous component is much lower than the drag force component. Therefore, the viscous force could be neglected. With this simplification, the drag force of the urban canopy can be described as the source terms of the momentum equation without viscous component:

$$S = -\rho C_D A u_i \bar{u} \quad \text{(Equation C2. 28)}$$

Here S denotes the source term of momentum force (N), C_D denotes the drag coefficient, ρ denotes the density (kg/m^3), A denotes the reference area (m^2), u_i denotes the velocity vector (m/s), $\bar{u}$ denotes the average velocity (m/s),

Some researcher has also successfully to implement drag force equation to carry out large scale wind flow simulation. For example, Liu Huizhi (2002) has investigated the flow field in urban canopy layer of Beijing. The modelling area is 700m × 700m. Porous (%) of the control volume is used present the permeability of the space to calculate the buildings drag force influence on the flow field. Figure C2. 14 shows the distribution of porous (%) value of the simulated area. Porous (%) is used to replace geometric shape of the building, thus, no detail geometric shape of the building is required to be input into the simulation. The results show that the wind velocity profile obtained from the model has a good agreement with the measurement data.

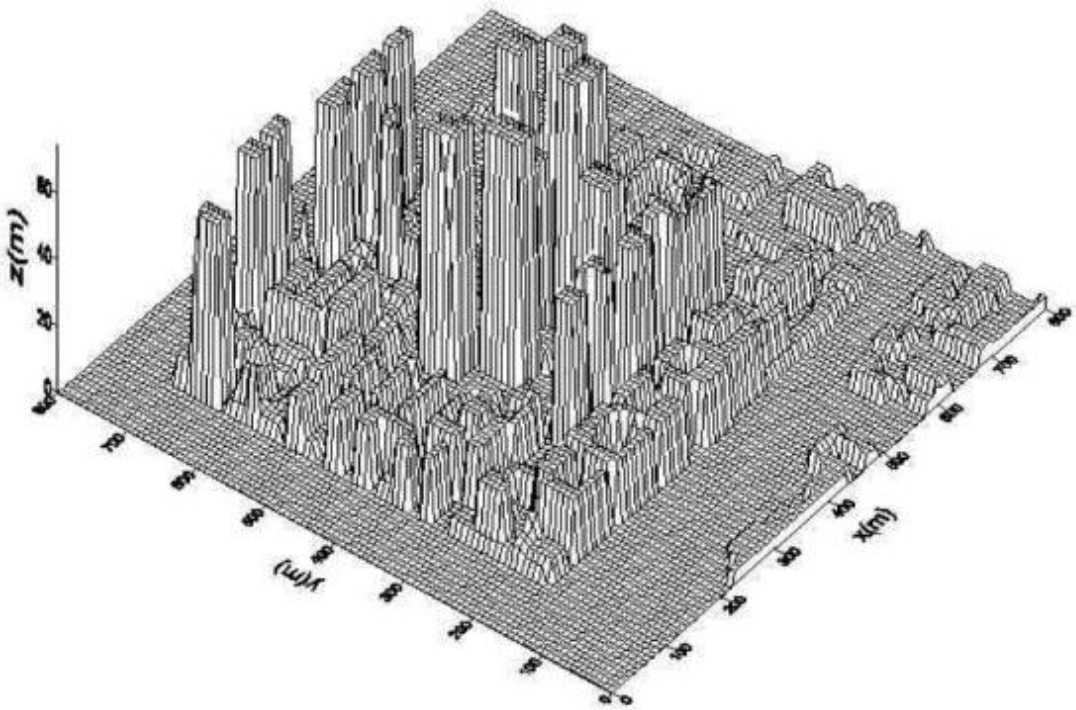

Figure C2. 14 The distribution of porous (%) of Liu Huizhi (2002) study

Atsushi Yamaguchi (2009) has developed a fluid force model to represent the drag force of vegetation and building. A scale down model is used for the wind tunnel test of the scale model verify the proposed fluid force model. The results show that the fluid force model is in

a good agreement with the measurement data and possible to replace the real physical model.

However, the fluid force model / drag force model from Liu Huizhi (2002) and Atsushi Yamaguchi (2009) did not consider the interaction of the flow field and thermal effect, such as buoyancy force that could affect the wind pattern. In this thesis, the fluid flow would consider many factors, including interactive force and buoyancy force. The interactive force term (refers equation C3. 24) and boussinesq equation (refers equation C5. 36) is linked to the volume averaged momentum equation in the UHI model.

2. 10 Volume Averaging - Information Loss

In traditional CFD approach, the spatial variation of variable such as temperature, velocity, pressure, chemical and etc can be easily obatined due to a fine grid condition. For example, the geometrical effect, such as building wall would divert the wind flow in other directions can be created by boundary condition setting in Continuity Equation and Momentum Equation.

As discussed in Section 2.8, I. J. Losada (2016) has pointed out the major different between traditional CFD approach and Volume Averaging Approach. In traditional CFD approach, the spatial nature is heterogeneous due to the fine grid model, while the under the Volume Averaging Approach the spatial nature is homogeneous under the coarse grid model. Figure C2. 15 shows fine grid model has heterogeneous condition (left) and coarse grid model has homogeneous condition within the REV. Hui Liu (2017) presented the schematic description of the heterogeneous unit and equivalent homogeneous unit in Figure C2. 16

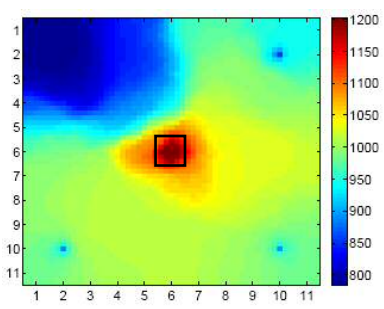

Every value condition within the □space is heterogeneous. The spatial variation information is known.

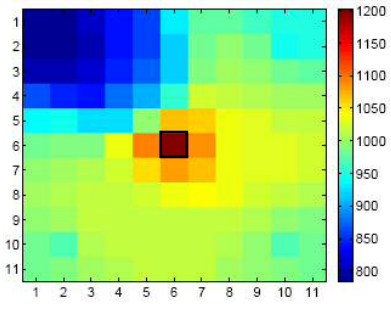

Every value condition within the □ space is homogeneous. The spatial variation information is lost.

Figure C2. 15 Heterogeneous Condition (left) and Homogeneous Condition (right) (Source: H. Li[5])

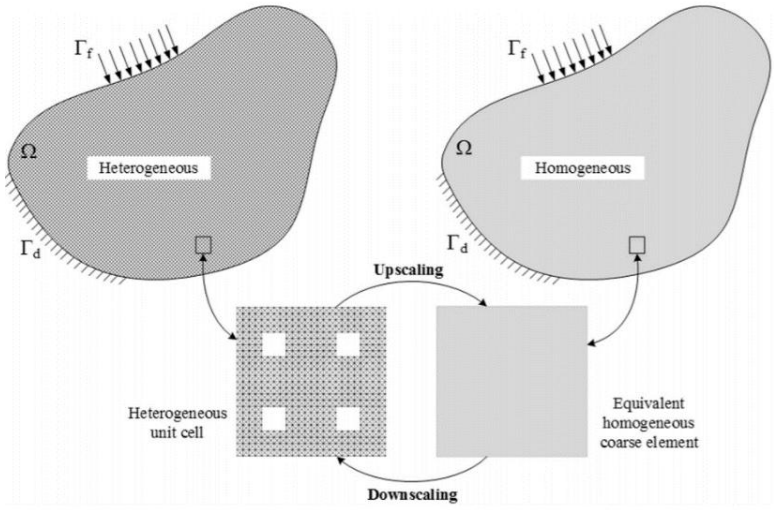

Figure C2. 16 Schematic description of the heterogeneous unit and equivalent homogeneous unit (Source: Hui Liu (2017))

Dasheng Qi (2000) study has further explained the essence of Volume Averaging Approach.

The essence of upscaling is to replace a heterogeneous unit with an equivalent homogeneous one, such that the fluid behavior in the two systems is similar.

Dasheng Qi (2000) also pointed out that the Volume Averaging Approach is changing the grid from fine grid model to coarse grid model and also changing some local explicit heterogeneity to implicit heterogeneity. Thus, information loss during the Volume Averaging

[5] H. Li, Global upscaling for compositional flow simulation: https://supri-b.stanford.edu/research/hangyu-li-1

Approach is inevitable.

For example, the UHI Model use coarse grid model to simulation macroscopic level interaction such as outdoor wind flow. However, the coarse grid model could not model the drag force due to the geometry information is lost in the REV and thus the geometrical effect cannot appear in the Volume Averaged Continuity and Momentum Equations. Additional Sub-Model is required to homogenization the permeability and porosity information within the grid from the building geometry information to model the drag force effect.

In this thesis, the UHI Model has two level of modelling.

1. **Macroscopic level (Volume averaged governing equations)**

2. **Microscopic level (Sub Models)**

Macroscopic level contains the volume averaged governing equations using REV. The main purpose is to obtain the information of fluid motion and thermal impact occur in macroscopic level, including air velocity field, air temperature field, pressure field, buoyancy force and etc. The converged volume averaged velocity and air temperature would be passed from Macroscopic level to Microscopic level model. Microscopic level contains sets of Sub-Model to approximate the lost information in the macroscopic level, such as geometrical effect, solar radiation, greenery evaporation effect etc. The converged surface temperature and heat source would be passed from Microscopic level back to Macroscopic level model. Table C2. 2 discuss the lost information treatement in UHI Model. After performing volume averaging on the microscopic governing equation to obtain the volume averaged form of the macroscopic equation, some of the additional terms will generate. For example, volume averaged momentum equation will generate two additional terms such as momentum exchange between phases and the interactive force term. In this study, we can simply assume there is no

mass and momentum exchange between the phases for reducing the complexity of the equation since the amount of mass transfer between non-permeable phase (building) and permeable phase (air) is not significant.

Table C2. 2 Lost information treatment in UHI Model

Heterogeneous Unit (Traditional CFD Approach)	**Homogeneous Unit**	
	Macroscopic level (Volume Averaging Approach)	**Microscopic level (Additional Terms Required)**
Information		
Building Geometry	No information	Building geometry approx. by Interactive Force Term [equation C3. 24] (require porosity & directional permeability of control volume from urban density database)
Topo Geometry	○ Surface Averaging Value of Topo Geometry ○ Lost spatial variation of Topo Geometry*	N/A
Greenery Surface	No information	Surface Averaging Greenery Surface, Area $_{greenery}$ from urban density database
Water Surface	No information	Surface Averaging Water Surface, Area $_{water}$ from urban density database
Road Surface	No information	Surface Averaging Road Surface, Area $_{road}$ from urban density database
Construction Site Surface	No information	Surface Averaging Construction Site, Area $_{construction}$ from urban density database
Air Velocity Vector, u	○ Volume Averaging Air Velocity, [equation C3. 23] ○ Lost spatial variation of air velocity*	Average Near Ground Air Velocity [equation C3. 41]
Air Temperature, T	○ Volume Averaging Air Temperature, [equation C3. 31] ○ Lost spatial variation of air temperature*	N/A

Heterogeneous Unit (Traditional CFD Approach)	Homogeneous Unit	
	Macroscopic level (Volume Averaging Approach)	**Microscopic level (Additional Terms Required)**
Surface Temperature, ST	○ Surface Averaging Surface Temperature [boundary condition of equation C3. 31] (Surface averaging surface temperature are obtained by macroscopic level convection, diffusion effect and resultant surface temperature of in microscopic level) ○ Lost spatial variation of Surface Temperature*	○ Surface Averaging of Surface Temperature, [equation C3. 32] (Surface averaging surface temperature are obtained by microscopic level net radiation, shading, evaporation, thermal storage effect and macroscopic level convection effect)
Net Radiation Load, I_{SR}	No information	Surface Averaging Net Radiation, I_{SR} & I_{LW} [equation C3. 35 & C3. 42]
Evaporation Load, I_{lat}	No information	Surface Averaging Evaporation, I_{lat} [equation C3. 47]
Ground Layer Temperature, T_{ground}	No information	Surface Averaging Surface Temperature by Thermal Storage, T_{ground} [equation C3. 32]
Ground Temperature, T_{deep}	No information	Surface Averaging Temperature by deep ground temperature, T_{deep} [equation C3. 52]
Shading Area, γ_{shade}	No information	○ Surface Averaging tree shading area, γ_{tree} from urban density database [equation C3. 35] ○ Average Sky View Factor, SVF_g & SVF_w [equation C3. 50 & C3. 51]
Simulating Fluid Motion / Heat Transfer Effect		
Mass Conservation	Volume Averaging Continuity Equation [equation C3. 16]	N/A
Advective flow of momentum except Geometrical effect	Volume Averaging Momentum Equation [equation C3. 23]	N/A
Geometrical effect	Lost all information	Drag force equation by Porosity & directional Permeability of Control Volume [equation C3. 24]
Surface Force	Lost all information	Drag force equation by Porosity & directional Permeability of Control Volume [equation C3. 24]

Heterogeneous Unit (Traditional CFD Approach)	Homogeneous Unit	
	Macroscopic level (Volume Averaging Approach)	Microscopic level (Additional Terms Required)
Body Force	Volume Averaging Momentum Equation [equation C3. 22]	N/A
Buoyancy force	Volume Averaging Momentum Equation of the boussinesq approximation term [equation C5. 36]	N/A
Advective heat transfer	Volume Averaging Energy Equation [equation C3. 28]	N/A
Convection Heat transfer	Volume Averaging Energy Equation [equation C3. 29]	N/A
Diffusive heat transfer	Volume Averaging Energy Equation [equation C3. 29]	N/A
Radiative Heat Transfer – Shortwave, longwave, shading effect	No information	SVF Sub Model [equation C3. 50 & C3. 51] Net Radiation Sub Model [equation C3. 35, C3. 38 & C3. 46]
Evaporative Heat Transfer – water feature, ocean, greenery	No information	Evaporation Sub Model [equation C3. 47]
Thermal Storage Heat Transfer – Ground material, deep ground temperature	No information	Ground layer Sub Model [equation C3. 32] Deep ground surface Sub Model [equation C3. 52]

2. 11 Summary

UHI study domain size

This chapter summarizes the findings of the Literature Review on Urban Heat Island Study and Volume Averaging Approach. This chapter first discusses the study domain area for urban heat island study shall covers up to 10km to fully capture the processes affecting and creating UHI effect (Oke (2009)). However, using traditional CFD approach for UHI study would require huge amount of grid cells to cover the 10km domain area, which induces technical problems of high computational power and long simulation time. Thus, traditional CFD approach is not practical approach for carrying out UHI Study.

Existing UHI Study

Next section discusses the advantage and disadvantage of current UHI study approach, including (1) UHI Study Measurement, (2) Urban Heat Island Modelling, (3) Statistical UHI Models, (4) Urban Climatic Map, (5) Urban Energy Balance and (6) Numerical UHI Modelling.

There are several measurement approaches to study urban heat island effect, including (1) air temperature measurement by fix local weather station, (2) surface temperature by remote sensing data, (3) air temperature by mobile transverse measurement. However, the measurement approach is mainly used for validation or quantify the current environmental condition rather than predict the UHI intensity urban planning design. Thus, the measurement data is not useful for the developing the UHI model. In this thesis, the air temperature measurement by fix weather stations is used to provide validation data for the UHI model only.

Oke (1971) has proposed several statistical modelling to study UHI effect. For example, Oke

has described the maximum heat island intensity (UHII) related to population or related to street canyon geometry. However, the statistical modelling is location dependent and requires fine-tuning to be applied in different places. Fung Wing Yee (2009) has also proved that the statistical approach may not be suitable for Hong Kong due to the high-density and high-rise built environment.

E. Ng (2009) has developed a UCMap for Hong Kong. UCMap is quite useful for policymakers to exam the district-level planning strategies. However, the UCMap is developed by correlate the existing environmental data, remote sensing data and measurement data. Since UCMap is developed based on the existing condition and it is not able to predict the air temperature changes of a completely new town planning. Thus, this approach could not give sufficient flexibilities for designing urban context and not particularly useful for optimizing the urban planning design.

Oke (1987) has also developed an urban energy balance equation to study the urban energy. Best (1998), Myrup (1969), Carlson and Boland (1978), Grimmond (1991), Masson (2000), Martilli (2002) and other researchers has further developed the urban energy balance equation to another more comprehensive model, including (1) Slab canopy model, (2) Volumetric averaging model, (3) Urban street canyon - single layer models and (4) Urban street canyon - multi-layer models. However, these models are often too simplified and often adopted large grid size. Therefore, these models could not capture the fine detail of the surface and the application in urban planning design is also limited without modification.

Swaid and Hoffman (1990a) had further used the energy balance model to develop a cluster thermal time constant (CTTC) analytical model. Swaid and Hoffman also shows the modelling results are in a good agreement with the measured air temperature in Jerusalem. However, the CTTC model does not consider the advection effect and is not valid under wind

speed above 1m/s. Thus, the CTTC model is also not particularly useful to consider the wind enhance strategies for urban planning design, which is important impact in UHI Study.

Both Envi-met and Integrated Environmental Solutions (IES) use traditional CFD approach to study the thermal and air flow pattern of an area. However, the maximum allowable grid number of both simulation tools is quite small and insufficient to covers UHI study area. These tools are only suitable to simulate micro-scale projects not UHI study.

Krayenhoff (2002) has proved Mesoscale Modelling can be a useful tool to assess the greenery design strategies through his study in Toronto. However, resolution of the Mesoscale Modelling is quite low. The wind flow based on surface roughness is only a rough estimation and difficult to estimate and apply during the urban planning design. Thus, Mesoscale Model is rarely used to study the UHI effect.

Volume Averaging Approach - modelling the heterogeneities conditions

The second part of this chapter discusses the concept of Volume Averaging Approach for "up-scaling" the grid cells. The concept of "up-scaling" approach is proposed in 1967 by Anderson and Jackson. The approach resolves the technical difficulties arise from modelling the heterogeneities in the porous media due to small size, irregular form, highly complex environment which resulting high computation power and long simulation time. Hong Kong urban content is also highly irregular, complex and covers large areas. Thus, Volume Averaging Approach is required for simulating UHI Study in Hong Kong to address the problems.

Volume Averaging Approach - concept and general equations

The general equations of Volume Averaging Approach are introduced by referring the works of Amir Faghri (2010) in Section 2.9. The concept and equations of porosity, intrinsic phase

average, extrinsic phase averaging has also discussed. Volume Averaging Approach has two levels, i.e. Microscopic and Macroscopic Level. Macroscopic level contains the volume averaged governing equations using REV to solve macroscopic information, such as air velocity field, air temperature field, pressure field, buoyancy force and etc. Microscopic level contains sets of Sub-Model to approximate the lost information in the macroscopic level, such as geometrical effect, solar radiation, greenery evaporation effect etc. The information loss occurs during the process of Volume Averaging Approach as it is changing the grid from fine grid model to coarse grid model. Table C2. 2 listed the lost information in the macroscopic level and the Sub-Model / additional terms on the microscopic level. The equation of the additional terms and the connection between macroscopic level and microscopic level will be further discussed in Chapter 3.

Volume Averaging Approach to reduce the computational requirement has been widely applied in hydrology, solute transport, reservoir engineering, oil or gas flow simulation, geotechnical analysis and etc. This thesis applied the same principle for modelling Hong Kong urban content, which is also highly irregular, complex and covers large areas, i.e. heterogeneities condition. Currently, there is still no research applied Volume Averaging Approach to model UHI.

Chapter 3 Urban Heat Island Modelling

In this Chapter, the thesis introduces process of volume averaging on governing equations and sets of Sub-Models. This Chapter shows how the macroscopic governing equations for the fluid flow in a space can be derived by averaging the microscopic governing equations over a volume. This Chapter discusses (1) the microscopic governing equations, (2) apply Volume Averaging Approach on the microscopic governing equations and transform into (3) macroscopic governing equations as well as the (4) additional terms generated during the process and (5) the sub-model to resolve the additional terms.

3. 1 Microscopic Governing Equations

The microscopic governing equations of fluid represents mathematical statements of the conservation laws of physics (1) The mass of a fluid is conserved, (2) the rate of change of momentum equals the sum of the forces on a fluid particle (Newton's second law) and (3) the rate of change of energy equals to the sum of the rate of heat addition to and the rate of work done on a fluid particle.

Here, divergence operator is introduced for generalization of terms in the equation. It usually denoted by the symbol div. This can be regarded as a vector whose components in the three principle directions of a Cartesian coordinate system are partial differentiations with respect to those three directions.

$$Net\ efflux\ per\ unit\ volume = \frac{\partial \mathrm{J}_x}{\partial \mathrm{x}} + \frac{\partial \mathrm{J}_y}{\partial \mathrm{y}} + \frac{\partial \mathrm{J}_z}{\partial \mathrm{z}} = \mathrm{div}\,\mathrm{J} \qquad \text{(Equation C3. 1)}$$

where div denotes the divergence operator, J denotes a flux influencing a typical dependent variable $\emptyset$.

3. 2 Continuity Equation

A continuity equation in physics is an equation that describes the transport of some quantity, say influencing a typical dependent variable $\emptyset$. It also indicates the conservation of mass in three dimensions.

Rate of increase $\emptyset$ of fluid element + Net rate of $\emptyset$ flow out of fluid element = Rate of increase of $\emptyset$ for a fluid particle

Refers to the literature of Versteeg and Malalasekera (1995), the net rate of flow of mass into a three dimensions fluid element can be written as

$$\frac{\partial \rho}{\partial t} + \frac{\partial \rho u}{\partial x} + \frac{\partial \rho v}{\partial y} + \frac{\partial \rho w}{\partial z} = 0 \qquad \text{(Equation C3. 2)}$$

$$\frac{\partial \rho}{\partial t} + \text{div } \rho V = 0 \qquad \text{(Equation C3. 3)}$$

where the ρ denotes the density (kg/m^3), t denotes the time (s), div ρV denotes divergence of density (kg/m^3) and velocity (m/s), denotes the u, v, w denotes the x, y, z component velocity (m/s), respectively. The first term on the left hand side describes the change in fluid density over time, and the second term describes the transport of the fluid.

3. 3 Momentum Equation

Newton's second law states that the rate of change of momentum of a fluid particle equals to the sum of the forces on the particle.

Rate of increase of momentum of fluid particle = Sum of forces on fluid particle

Again, refers to the works of Versteeg and Malalasekera (1995), the momentum equation can be written as:

X-Momentum

$$\frac{\partial \rho u}{\partial t} + \frac{\partial \rho uu}{\partial x} + \frac{\partial \rho vu}{\partial y} + \frac{\partial \rho wu}{\partial z} = -\frac{\partial P}{\partial x} + \frac{\partial}{\partial x}\left(\mu \frac{\partial u}{\partial x}\right) + \frac{\partial}{\partial y}\left(\mu \frac{\partial u}{\partial y}\right) + \frac{\partial}{\partial z}\left(\mu \frac{\partial u}{\partial z}\right) + \rho g_x + S_x \quad \text{(Equation C3. 4)}$$

Y-Momentum

$$\frac{\partial \rho v}{\partial t} + \frac{\partial \rho uv}{\partial x} + \frac{\partial \rho vv}{\partial y} + \frac{\partial \rho wv}{\partial z} = -\frac{\partial P}{\partial y} + \frac{\partial}{\partial x}\left(\mu \frac{\partial v}{\partial x}\right) + \frac{\partial}{\partial y}\left(\mu \frac{\partial v}{\partial y}\right) + \frac{\partial}{\partial z}\left(\mu \frac{\partial y}{\partial z}\right) + \rho g_y + S_y \quad \text{(Equation C3. 5)}$$

Z-Momentum

$$\frac{\partial \rho w}{\partial t} + \frac{\partial \rho uw}{\partial x} + \frac{\partial \rho vw}{\partial y} + \frac{\partial \rho ww}{\partial z} = -\frac{\partial P}{\partial z} + \frac{\partial}{\partial x}\left(\mu \frac{\partial w}{\partial x}\right) + \frac{\partial}{\partial y}\left(\mu \frac{\partial w}{\partial y}\right) + \frac{\partial}{\partial z}\left(\mu \frac{\partial w}{\partial z}\right) + \rho g_z + S_z \quad \text{(Equation C3. 6)}$$

where the ρ denotes the density (kg/m^3), t denotes the time (s), P denotes pressure (Pa), μ denotes viscosity (m^2/s), g denotes the gravity (m/s^2), S denotes the source term (N/m^3) and u, v, w denotes the x, y, z component velocity (m/s) respectively. And the generalization of

terms in the momentum equation can by written as:

$$\frac{\partial \rho u}{\partial t} + \text{div}\, \rho u V = -\text{div}\, P + \text{div}(\mu\, \text{grad}\, V) + \rho g + S \qquad \text{(Equation C3. 7)}$$

3. 4 Energy Equation

Again, refers to the works of Versteeg and Malalasekera (1995), Energy equation with neglecting pressure work, viscous work and work done by concentration gradient can be written as:

$$\frac{\partial \rho C_v T}{\partial t} + \frac{\partial \rho u C_v T}{\partial x} + \frac{\partial \rho v C_v T}{\partial y} + \frac{\partial \rho w C_v T}{\partial z} = -\left(\frac{\partial}{\partial x}\left(k\frac{\partial T}{\partial x}\right) + \frac{\partial}{\partial y}\left(k\frac{\partial T}{\partial y}\right) + \frac{\partial}{\partial z}\left(k\frac{\partial T}{\partial z}\right)\right) + S \qquad \text{(Equation C3. 8)}$$

where the ρ denotes the density (kg/m^3), t denotes the time (s), k denotes the thermal conductivity (W/(m.K)), T denotes the temperature (ºC), C_v denotes the specific heat capacity (J/(m^3.K)), S denotes the source term (W/m^3) and u, v, w denotes the x, y, z component velocity (m/s) respectively.

And the generalization of terms in the energy equation can by written as:

$$\frac{\partial \rho h}{\partial t} + \text{div}\, \rho h = -\text{div}\, (k\, \text{grad}\, T) + S \qquad \text{(Equation C3. 9)}$$

Here h denotes the enthalpy (J) and $h = C_v T$, T denotes the temperature (ºC), C_v denotes

the specific heat capacity (J/kg), S denotes the source term (W/m^3).

3. 5 Macroscopic governing equations

Chapter 2 had already introduced the basic principles of Volume Averaging Approach. It also pointed out that the information loss occurs during the volume averaging process on the governing equations. Additional terms / Sub-Models are required to provide information for the lost information, which has been listed in Table C2. 2.

In this thesis, the UHI Model has divided into two parts, (1) macroscopic level model, which consists of the volume averaged governing equations (from Equation C3.10 to Equation C3.31), (2) microscopic level model (which is the sub-model of Macroscopic level model), which consist of all the additional terms to generate the lost information in Macroscopic level model. Using the above method, the local quantities (such as temperature / air velocity and etc) can be expressed in a macroscopic point of view and without losing major microscopic information.

In the below section, it would first discuss the Macroscopic level model - volume averaged governing equations, while the Microscopic level model would be presented in later section. Also, recap in Chapter 2 Section 2.9, this thesis only consists of two different phases, i.e. (1) **non-permeable phase**, **n** and (2) **permeable phase, p**. Thus, for any dependent variable ϕ, under **non-permeable phase is denotes as** ϕ_n, under **non-permeable phase is denotes as** ϕ_p.

3. 6 Continuity Equation

By applying extrinsic phase averaging (refers to equation C2. 13)) to the Continuity Equation (equation C3. 10), the averaged forms of k phase on continuity equation can be written as:

$$\langle \frac{\partial \rho_k}{\partial t} \rangle + \langle \mathrm{div}\,(\rho_k V_k) \rangle = 0 \qquad \text{(Equation C3. 10)}$$

Here $\langle \quad \rangle$ denotes the extrinsic phase averaging of any variable, ρ_k denotes the density (kg/m^3), V_k denotes the velocity (m/s).

The 1st terms on the left-hand side can be obtained by using equation C2. 16.

1st term:

$$\langle \frac{\partial \rho_k}{\partial t} \rangle = \frac{\partial \langle \rho_k \rangle}{\partial t} + \frac{1}{\mathrm{Vol}} \int_{A_k} \rho_k u_I . n_k dA_k \qquad \text{(Equation C3. 11)}$$

Here $\langle \quad \rangle$ denotes the extrinsic phase averaging of any variable, $\langle \rho_k \rangle$ denotes the extrinsic phase averaged density (kg/m^3), Vol denotes the volume of the control volume (m^3), u_I denotes the velocity vector, n_k denotes the flow direction of the dependent variable, A_k denotes the area of the control volume (m^2).

The 2nd terms on the left-hand side can be obtained by using equation C2. 18.

2nd term:

$$\langle \mathrm{div}\,(\rho_k V_k) \rangle = \mathrm{div}\,\langle \rho_k V_k \rangle - \frac{1}{\mathrm{Vol}} \int_{A_k} \rho_k V_k . n_k dA_k \qquad \text{(Equation C3. 12)}$$

Here $\langle \quad \rangle$ denotes the extrinsic phase averaging, $\langle \rho_k V_k \rangle$ denotes the extrinsic phase averaged density (kg/m^3) and velocity (m/s) of the individual phase k, Vol denotes the volume of the control volume, V_k denotes the velocity (m/s) of the individual phase k, n_k

denotes the flow direction of the dependent variable, A_k denotes the area of the control volume (m^2).

Substituting the above expression back into the volume averaged continuity equation will generate an additional term on the left-hand side of the equation. The new term represented the mass transfer between phases due to phase change (Amir Faghri (2010), Whitaker (1967) and Slattery (1967)). As discussed in the previous chapter, since the ventilation exchange between the buildings (non-permeable phases) and air (permeable phase) are not significant, thus we simply assume there is no mass exchange between phases and therefore the additional term is equal to zero.

$$-\frac{1}{V}\int_{A_k} \rho_k(u_k - u_I).\, n_k dA_k = \sum m_{jk} = 0 \qquad \text{(Equation C3. 13)}$$

Here $\sum m_{jk}$ denotes the sum of mass transfer (kg/s) between permeable phase (e.g. air) and non-permeable phase (e.g. building). Therefore, the volume averaged continuity equation can be described as:

$$\frac{\partial\langle\rho_k\rangle}{\partial t} + \operatorname{div}\langle\rho_k u_k\rangle = 0 \qquad \text{(Equation C3. 14)}$$

Apply equation (15) to equation (34), we can relate the extrinsic phase averaged density and velocity to the intrinsic phase averaged density and velocity. Furthermore, refers to the equation (20), using the expression of products from two averaged variables $\langle\rho_k u_k\rangle$, the volume averaged continuity equation becomes:

$$\frac{\partial\varepsilon_k\langle\rho_k\rangle^k}{\partial t} + \operatorname{div}\left(\varepsilon_k\langle\rho_k\rangle^k\langle u_k\rangle^k\right) + \langle\widetilde{\rho_k}\widetilde{u_k}\rangle^k = 0 \qquad \text{(Equation C3. 15)}$$

Here ε_k denotes the ratio of the volume of the respected phase, $\langle u_k\rangle^k$ denotes the intrinsic

phase averaged velocity (m/s), $\langle \rho_k \rangle^k$ denotes the intrinsic phase averaged density (kg/m^3), $\langle \widetilde{\rho_k} \widetilde{u_k} \rangle^k$ denotes the spatial variation of the density (kg/m^3) and velocity (m/s).

According to the works of Whitaker (1967) and Amir Faghri (2010), the dispersion term $\langle \widehat{\rho_k} \widehat{u_k} \rangle^k$ is very small and can be neglected. For this UHI study, the spatial variation of the density and velocity is not an important factor, whereas our main objective is to calculate an averaged air velocity and temperature of a space. Thus, the treatment of spatial variation of the density and velocity $\langle \widetilde{\rho_k} \widetilde{u_k} \rangle^k$ can be neglected in this UHI model and according to Section 2.10 and spatial variation of density and velocity is lost and no sub-model would be provided. Finally, the intrinsic phase averaging form of Continuity Equation can be written as

$$\underbrace{\frac{\partial(\varepsilon_k \langle \rho_k \rangle^k)}{\partial t} + \operatorname{div}(\varepsilon_k \langle \rho_k \rangle^k \langle u_k \rangle^k) = 0}_{\text{Macroscopic Level}} \qquad \text{(Equation C3. 16)}$$

Here ε_k denotes the ratio of the volume of the respected phase, $\langle u_k \rangle^k$ denotes the intrinsic phase averaged velocity (m/s), $\langle \rho_k \rangle^k$ denotes the intrinsic phase averaged density (kg/m^3).

3. 7 Momentum Equation

By applying extrinsic phase averaging (equation C2. 13) to the Momentum Equation (equation C3. 17), the averaged forms of k phase on Momentum equation can be written as

$$\left\langle \frac{\partial \rho_k u_k}{\partial t} \right\rangle + \langle \text{div}\,(\rho_k u_k V_k) \rangle = \langle -\text{div}\, P_k \rangle + \langle \text{div}\, \mu_k \,\text{grad}\, V_k \rangle \qquad \text{(Equation C3. 17)}$$

$$+ \langle \rho_k g \rangle + S$$

Here $\langle \quad \rangle$ denotes the extrinsic phase averaging of any variable, ρ_k denotes the density (kg/m^3), V_k denotes the velocity (m/s), P_k denotes the pressure (Pa), μ_k denotes the viscosity (m^2/s), g denotes the gravity (m/s^2), S denotes the source term (N/m^3).

The 1st terms on the left-hand side can be obtained by using equation C2. 16.

1st term:

$$\left\langle \frac{\partial \rho_k u_k}{\partial t} \right\rangle = \frac{\partial \langle \rho_k u_k \rangle}{\partial t} + \frac{1}{\text{Vol}} \int_{A_k} \rho_k u_k u_I \,.\, n_k \, dA_k \qquad \text{(Equation C3. 18)}$$

Here $\langle \quad \rangle$ denotes the extrinsic phase averaging of any variable, $\langle \rho_k \rangle$ denotes the extrinsic phase averaged density (kg/m^3), $\langle u_k \rangle$ denotes the extrinsic phase averaged velocity (m/s), Vol denotes the volume of the control volume (m^3), u_I denotes the velocity vector, n_k denotes the flow direction of the dependent variable, A_k denotes the area of the control volume (m^2).

The 2nd terms on the left-hand side can be obtained by using equation C2. 18.

2nd term:

$$\langle \mathrm{div}\, \rho_k u_k V_k \rangle = \mathrm{div}\, \langle \rho_k u_k V_k \rangle - \frac{1}{\mathrm{Vol}} \int_{A_k} \rho_k u_k V_k \,.\, n_k dA_k \qquad \text{(Equation C3. 19)}$$

Here $\langle \quad \rangle$ denotes the extrinsic phase averaging of any variable, $\langle \rho_k \rangle$ denotes the extrinsic phase averaged density (kg/m^3), $\langle u_k \rangle$ denotes the extrinsic phase averaged velocity (m/s) at given direction, $\langle V_k \rangle$ denotes the extrinsic phase averaged velocity magnitude (m/s), Vol denotes the volume of the control volume (m^3), n_k denotes the flow direction of the dependent variable, A_k denotes the area of the control volume (m^2).

3rd term:

$$\langle \mathrm{div}\, P_k \rangle = \mathrm{div}\, \langle P_k \rangle - \frac{1}{\mathrm{Vol}} \int_{A_k} P \,.\, n_k dA_k \qquad \text{(Equation C3. 20)}$$

Here $\langle \quad \rangle$ denotes the extrinsic phase averaging of any variable, $\langle P_k \rangle$ denotes the extrinsic phase averaged pressure (Pa), n_k denotes the flow direction of the dependent variable, A_k denotes the area of the control volume (m^2).

4th term:

$$\langle \mathrm{div}\, \mu_k \,\mathrm{grad}\, V_k \rangle = \mathrm{div}\, \langle \mu_k \,\mathrm{grad}\, V_k \rangle$$

(Equation C3. 21)

$$- \frac{1}{\mathrm{Vol}} \int_{A_k} \mu_{\gamma k} \,\mathrm{grad}\, V_k \,.\, n_k dA_k$$

Here μ_k denotes the intrinsic phase averaged viscosity (m^2/s), $\langle V_k \rangle$ denotes the extrinsic

phase averaged velocity magnitude (m/s), n_k denotes the flow direction of the dependent variable, A_k denotes the area of the control volume (m^2).

For the 5th terms on equation, since g is the gravity constant. Thus, the equation can be described as

5th term:

$$\langle \rho_k g \rangle = \langle \rho_k \rangle g \qquad \text{(Equation C3. 22)}$$

Here $\langle \rho_k \rangle$ denotes the extrinsic phase averaged density (kg/m^3), g denotes the gravity constant (m/s^2).

By applying the same approach used in Continuity Equation the intrinsic phase averaging form of Momentum equation can be written as:

$$\frac{\partial \varepsilon_k \langle \rho_k \rangle^k \langle u_k \rangle^k}{\partial t} + \operatorname{div}\left(\varepsilon_k \langle \rho_k \rangle^k \langle u_k V_k \rangle^k\right) = -\operatorname{div} \varepsilon_k \langle P_k \rangle^k + \varepsilon_k \langle \rho_k \rangle^k g + \operatorname{div} \langle \mu_k \operatorname{grad} \varepsilon_k \langle u_k \rangle^k \rangle + \langle F_{jk} \rangle \qquad \text{(Equation C3. 23)}$$

Macroscopic Level

Microscopic Level
(momentum force from sub-model)

Here $\langle F_{jk} \rangle$ denotes the Interactive momentum force (N/m^3), $\langle u_k \rangle^k$ denotes the intrinsic phase averaged velocity vector (m/s) at given direction, $\langle V_k \rangle^k$ denotes the intrinsic phase averaged velocity magnitude (m/s), μ_k denotes the intrinsic phase averaged viscosity (m^2/s), ε_k denotes the intrinsic phase averaged porosity, $\langle P_k \rangle^k$ denotes the intrinsic phase averaged pressure (Pa).

Additional terms - Interactive momentum force

The term, $\langle F_{jk} \rangle$ denotes interactive force (N/m^3) between two phases (Amir Faghi, 2010). In this study, the interactive force mainly induced by the geometrical effect. For example, the change of momentum force as wind passing through a group of buildings. Maruyama (1992) has carried out a set of wind tunnel test in terms of different urban canopy layout, and proposed a model to describe the momentum change due to the geometrical effect. The fluid force per unit volume can be described as in volume averaged form:

$$\langle F_k \rangle = -\frac{1}{2}\varepsilon_k \langle \rho_k \rangle^k C_D \frac{dA}{\varepsilon_k Vol} \left| \langle V_k \rangle^k \right| \langle u_k \rangle^k \qquad \text{(Equation C3. 24)}$$

Here C_D denotes the drag coefficient due to the geometrical effect, ε_k denotes the porosity of the control volume, $\langle \rho_k \rangle^k$ intrinsic phase averaged density (kg/m^3), $\langle u_k \rangle^k$ denotes the intrinsic phase averaged velocity vector (m/s) at given direction, $\langle V_k \rangle^k$ denotes the intrinsic phase averaged velocity magnitude (m/s). The drag coefficient can be described as

$$C_D = \min\left(\frac{1.53}{\varepsilon_k}, 2.75\varepsilon_k\right) \qquad \text{(Equation C3. 25)}$$

ε_k is the porosity of the control volume and it is limited from 0 to $1 - \delta$ to increase the numerical stability. δ is a constant value of 10^{-4}.

3. 8 Energy Equation

By applying extrinsic phase averaging (equation C2. 13)) to the Energy Equation (equation C3. 26), the averaged forms of k phase on Energy Equation can be written as:

$$\left\langle \frac{\partial \rho_k C_v T_k}{\partial t} \right\rangle + \langle \text{div}\, \rho_k u_k C_v T_k \rangle = -\langle \text{div}\, (k\, \text{grad}\, T_k) \rangle + S \qquad \text{(Equation C3. 26)}$$

Here h denotes the enthalpy (J) (where $h_k = C_v T_k$), ρ denotes the density (kg/m^3), t denotes the time (s), k denotes the thermal conductivity (W/(m.K)), T denotes the Temperature (ºC), C_v denotes the specific heat capacity (J/(m^3.K)), S denotes the source term (W/m^3) and u, v, w denotes the x, y, z component velocity (m/s) respectively. And the generalization of terms in the energy equation can by written as**:**

The 1st terms on the left-hand side and rest of the terms can be obtained by using equation C2. 16:

1st term:

$$\left\langle \frac{\partial}{\partial t} \rho_k h_k \right\rangle = \frac{\partial}{\partial t} \langle \rho_k h_k \rangle + \frac{1}{V} \int_{A_k} \rho_k h_k u_I \,.\, n_k \, dA_k \qquad \text{(Equation C3. 27)}$$

Here $\langle \quad \rangle$ denotes the extrinsic phase averaging of any variable, $\langle \rho_k \rangle$ denotes the extrinsic phase averaged density (kg/m^3), $\langle h_k \rangle$ denotes the extrinsic phase averaged enthalpy (J), V denotes the volume of the control volume (m^3), u_I denotes the velocity vector (m/s), n_k denotes the flow direction of the dependent variable, A_k denotes the area of the control volume (m^2).

The 2nd terms on the left-hand side and rest of the terms can be obtained by using equation C2. 18:

2nd term:

$$\langle \mathrm{div}\,(\rho_k u_k h_k)\rangle = \mathrm{div}\,\langle \rho_k u_k h_k\rangle - \frac{1}{\mathrm{Vol}}\int_{A_k} \rho_k u_k h_k \,.\, n_k dA_k \qquad \text{(Equation C3. 28)}$$

Here $\langle \quad \rangle$ denotes the extrinsic phase averaging of any variable, $\langle \rho_k \rangle$ denotes the extrinsic phase averaged density (kg/m^3), $\langle u_k \rangle$ denotes the extrinsic phase averaged velocity (m/s), $\langle h_k \rangle$ denotes the extrinsic phase averaged enthalpy (J), Vol denotes the volume of the control volume (m^3), u_I denotes the velocity vector (m/s), n_k denotes the flow direction of the dependent variable, A_k denotes the area of the control volume (m^2).

3rd term:

$$\langle -\mathrm{div}\,(k\ \mathrm{grad}\ T_k)\rangle = -\mathrm{div}\,\langle k\ \mathrm{grad}\ T_k\rangle - \frac{1}{\mathrm{Vol}}\int_{A_k} k\ \mathrm{grad}\ T_k \,.\, n_k dA_k \qquad \text{(Equation C3. 29)}$$

Here $\langle \quad \rangle$ denotes the extrinsic phase averaging of any variable, $\langle k \rangle$ denotes the extrinsic phase averaged thermal conductivity (W/(m.K)), $\langle T_k \rangle$ denotes the extrinsic phase averaged temperature (ºC), n_k denotes the flow direction of the dependent variable, A_k denotes the area of the control volume (m^2).

The terms $\frac{1}{V}\int_{A_k} \rho_k u_k h_k \,.\, n_k dA_k$ and $\frac{1}{V}\int_{A_k} k\ \mathrm{grad}\ T_k \,.\, n_k dA$ represents the convective and diffusive heat transfer between the non-permeable phase (topography and building) and permeable phase (e.g. air).

$$-\frac{1}{V}\int_{A_k}(\ \rho_k u_k h_k - k\ \mathrm{grad}\ T_k).\ n_k dA_k = \langle q_{jk}\rangle^k \qquad \text{(Equation C3. 30)}$$

Here $\langle q_{jk}\rangle$ denotes the sum of heat transfer (W) between non-permeable phase (topography or building) and permeable phase (e.g. air).

The resultant heat transfer would be closely related to the amount of solar radiation, long wave radiation, evaporation of the area. It will be further discussed in the next section. By applying the same approach used in Continuity Equation the intrinsic phase averaging form of Energy equation can be written as

$$\underbrace{\frac{\partial \varepsilon_k \langle \rho_k\rangle^k \langle h_k\rangle^k}{\partial t} + \mathrm{div}\ \varepsilon_k \langle \rho_k\rangle^k \langle u_k h_k\rangle^k = -\ \mathrm{div}\ \langle k\ \mathrm{grad}\ T_k\rangle^k}_{\text{Macroscopic Level}} + \underbrace{\langle q_{jk}\rangle}_{\text{Microscopic Level (heat transfer from sub-model)}} \qquad \text{(Equation C3. 31)}$$

Here $\langle\ \ \rangle$ denotes the extrinsic phase averaging of any variable, $\langle \rho_k\rangle^k$ denotes the intrinsic phase averaged density (kg/m^3), $\langle u_k\rangle^k$ denotes the intrinsic phase averaged velocity (m/s), $\langle h_k\rangle^k$ denotes the extrinsic phase averaged enthalpy (J), ε_k denotes the porosity, $\langle q_{jk}\rangle$ denotes sum of heat transfer (W) between non-permeable phase (topography or building) and permeable phase (e.g. air).

3. 9 Sub Model - Energy Balance Model

The UHI model also needs to consider the balance of the incoming and outgoing energy flows as refers to Oke (1987). The amount of surface energy is directly depended on the urban surface characteristics, and the differences would affect the amount of heat generation and transfer, which lead to different surface and air temperatures between spaces. The model

could descript the heat transfer process in the urban space by (1) thermal inertia effects from difference material types, (2) convective heat transfer and (3) diffusive heat transfer, (4) heat gain or release due to shortwave and long-wave radiation from solar, (5) evaporation effect from greenery and sea and (6) advective effect from neighbourhood. One of the major difficulties is these heat generation processes mainly occurs at the microscopic level, whereas our main interest in the present study is the resultant air temperature and wind flow variation in macroscopic point of view. A set of sub model is introduced in this section to obtain the resultant air temperature from the energy balance of urban canopy at the microscopic level and heat exchange between microscopic and macroscopic level. The intensity of the heat exchange between the microscopic and macroscopic equation can be related by using convection and diffusive heat transfer between the average surface temperature of the ground/building and air. In order to resolve the resultant air temperature without model the environment at the microscopic level in detail, averaging point energy conservation equations with the sub-modelling approach are introduced in this section. The heat transfer of the Ground/Building Energy Balance Model can be further developed based on one-dimensional transient conduction / convection-conduction heat transfer equation, as shown in Figure C3. 1.

Return to Macroscopic Level

From Macroscopic Level

$$\rho c \frac{\partial T}{\partial t} = \frac{}{\partial z}\left(k \frac{\partial T}{\partial z}\right) + hc \frac{\partial (ST - \langle T_p \rangle^p)}{\partial z} + S \qquad \text{(Equation C3. 32)}$$

where for Ground Energy Balance Model

$$S = I_{SR}(t)dA_{ground} + \Delta L_{lw}(t)dA_{ground} + I_{lat}(t)dA_{green} \qquad \text{(Equation C3. 33)}$$

where for Building Energy Balance Model

$$S = I_{SR}(t)dA_{wall} + \Delta L_{lw}(t)dA_{wall} \qquad \text{(Equation C3. 34)}$$

Here hc denotes the convective heat transfer coefficient W/(m^{2}K), k denotes the thermal conductivity (W/(m.K)), ST denotes the ground surface temperature (ºC), $\langle T_p \rangle^p$ denotes the air temperature (ºC) (from Macroscopic Level), C_v denotes the specific heat capacity (J/(m^3.K)), S denotes the source (W/m^2), z denotes the ground layer thickness (m). For $I_{SR}(t), \Delta L_{lw}(t), I_{lat}(t)$ denotes the shortwave radiation (W/m^2), longwave radiation (W/m^2) and latent heat transfer (W/m^2) respectively, which will be discussed in more detail in below.

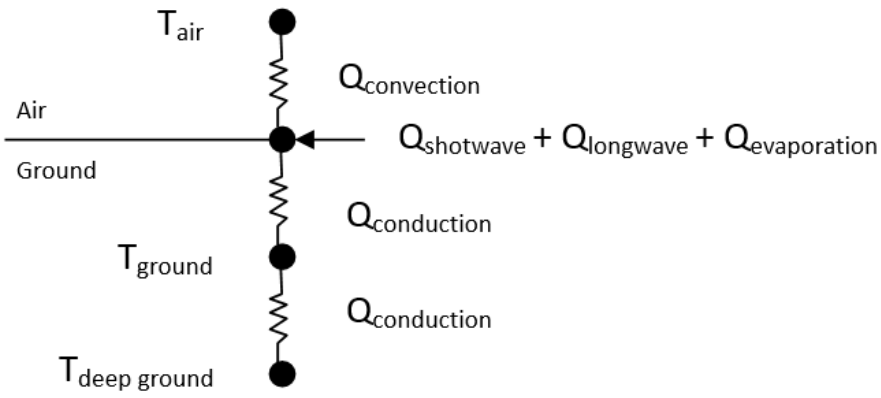

Figure C3. 1 Thermal circuits for ground Energy Balance Model

3. 10 Net Shortwave Solar Radiation Model

Solar radiation is radiant energy emitted by the sun and absorbed by the atmosphere and the heat emitted by the earth increase the air temperature. The time-dependent contribution of the solar radiation (direct + diffuse) to air temperature can be calculated by $I_{SR}(t)$ (W/m^2).

In Ground Energy Balance Model, $I_{SR}(t)$ consider the thermal effect of the direct and diffuses solar radiation on the horizontal surface and includes the effect of shading effect from the buildings/trees. Figure C3. 2 shows the solar radiation consideration on ground and under tree.

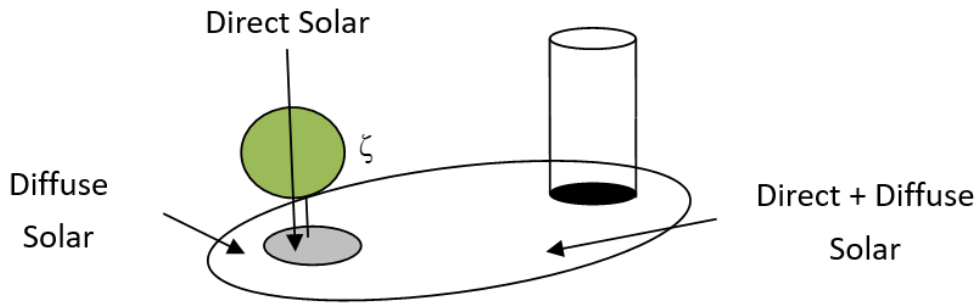

Figure C3. 2 Example of solar radiation consideration on ground

Tree shading effect on ground

The thermal effect of the shade trees is estimated by the effect of solar radiation penetration through the tree canopy and by the intensity of evapotranspiration. Bo-rong Lin (2004) had correlated the Leaf Area Index (LAI) to the amount of solar radiation penetration through the tree crown and suggested tree penetration coefficient, ζ, and specific heat capacity of the tree crown, c_{tree}, from different tree type and time. Leaf Area Index (LAI) is a dimensionless quantity that characterizes plant canopies. It is defined as the one-sided green leaf area per unit ground surface area (LAI = leaf area / ground area, m^2 / m^2). The tree penetration coefficient and specific heat capacity are summarized in Table C3. 1.

Table C3. 1 Tree penetration coefficient and specific heat capacity (Source: Bo-rong Lin (2004))

Condition	ζ (Summer)	ζ (Winter)	C
No direct sunlight reaches the ground through tree crown	0.1	0.7	0.7
Direct sunlight reaches the ground through tree crown no more than 50% area	0.3	0.75	
Direct sunlight reaches the ground through tree crown over 50% but no more than 70% area	0.5	0.8	
Direct sunlight reaches the ground through tree crown over 70% area	0.8	0.85	

Building shading effect on ground

Shading effect from the building structure cannot be obtained directly, since the UHI model do not contains the building geometrical information. The Average Sky View Factor (SVF) of area within the control volume is used to approximate the building shading effect on ground. More detail will be discussed in Section 3.14. Thus, the average total solar radiation can be described as:

$$I_{SR}(t) = I_{dir}(t)\left[\left(1-\gamma_{tree}{}'-\gamma_{building}{}'\right)SVF_g\right] + I_{dir}(t)\left[\gamma_{tree}{}'(1-\zeta)(1-c_{tree})\right]S + I_{dif}(t)\left[1-\gamma_{building}{}'\right]SVF_g \quad \text{(Equation C3. 35)}$$

$$\gamma_{tree}{}' = \frac{A_{tree}}{A_{total}} \quad \text{(Equation C3. 36)}$$

$$\gamma_{building}{}' = \frac{A_{building}}{A_{total}} \quad \text{(Equation C3. 37)}$$

Here $I_{SR}(t)$ denotes the net solar radiation (W/m^2) on the surface at time t within the control volume, $I_{dir}(t)$ denotes the direct solar radiation (W/m^2) on the surface at time t within the

control volume, $I_{dif}(t)$ denotes the diffuse solar radiation (W/m^2) on the surface at time t within the control volume, ζ denotes the tree penetration coefficient, c_{tree} denotes the specific heat capacity. A_{tree} denotes the total area (m^2) of tree crown within the control volume, $A_{building}$ denotes the total area of building within the control volume, γ_{tree}' denotes the ratio of tree area and total control volume area at z direction. $\gamma_{building}'$ denotes the ratio of tree area and total control volume area at z direction, SVF_g denotes the average Sky View Factor of ground within the control volume.

Building shading effect on building

The building shading effect on the building surface is also considered using SVF. The $I_{SR}(t)$ can be described simply as:

$$I_{SR}(t) = [I_{dir}(t) + I_{dif}(t)]SVF_w \quad \text{(Equation C3. 38)}$$

Here $I_{SR}(t)$ denotes the net solar radiation (W/m^2) on the surface at time t within the control volume, $I_{dir}(t)$ denotes the direct solar radiation (W/m^2) on the surface at time t within the control volume, $I_{dif}(t)$ denotes the diffuse solar radiation (W/m^2) on the surface at time t within the control volume, SVF_g denotes the average Sky View Factor of wall surface within the control volume.

The absorptive of the surface σ, is the relative ability of its surface to absorb energy by radiation, usually from the solar. For an area with more than one land use type, the absorptive shall be obtained by area-weighted average absorptive of the surface to solar radiation.

$$\sigma = \sum_{k} \gamma_k \sigma_k \qquad \text{(Equation C3. 39)}$$

Here σ denotes the surface averaged absorptivity of the different land type, γ_k is the area-weighted percentage of k type of land surface, including greenery, sea, building and etc. The area-weighted average of the surface could be obtained through the urban density database.

3. 11 Surface Convective Heat Transfer Model

Surface convective heat transfer coefficient is used to estimate the amount of heat transfer between the canopy air temperature and the canopy surface temperature through convective heat transfer. Bo-rong Lin (2004) related the surface convective heat transfer coefficient, hc, with the mean velocity of the urban canopy. Mean velocity is obtained from the macroscopic flow field.

$$hc = 10.9 + 4.1 \langle V_p \rangle^p \qquad \text{(Equation C3. 40)}$$

whereas

$$\langle V_p \rangle^p = \sqrt{\langle u_p \rangle^{p\,2} + \langle v_p \rangle^{p\,2} + \langle w_p \rangle^{p\,2}} \qquad \text{(Equation C3. 41)}$$

Here hc denotes the surface heat transfer coefficient ($W/(m^2K)$) for convection heat transfer, $\langle V_p \rangle^p$ denotes the intrinsic phase average velocity (m/s) of the permeable phase (i.e. air) within the control volume.

3. 12 Net Longwave Radiation Model

The basic equation for most of the longwave radiation models is the Stefan-Boltzmann Law. The equation suggested that the amount of longwave radiation is related to the absolute temperature and the emissivity of the emitting object, whereas the Stefan-Boltzmann coefficient is $5.6\text{x}10^{-8}$ $Wm^{-2}K^{-4}$.

$$I_{LW}(t) = \varepsilon\sigma_{bolt}T^4 \qquad \text{(Equation C3. 42)}$$

Here $I_{LW}(t)$ denotes the amount of longwave radiation, ε denotes the material emissivity, σ_{bolt} denotes the Stefan-Boltzmann coefficient ($\varepsilon = 5.6\text{x}10^{-8}$ $Wm^{-2}K^{-4}$), T denotes the temperature (ºC).

The incoming longwave radiation is expressed by equations C3. 43, while the outgoing longwave radiation can be simply expressed by equation C3. 45.

$$I_{LW\_1}(t) = \sigma_{bolt}T_{sky}(t)\varepsilon_{sky} \qquad \text{(Equation C3. 43)}$$

$$\varepsilon_{sky} = 0.920\text{x}10^{-5}[\langle T_p \rangle^p + 273]^4 SVF_g \qquad \text{(Equation C3. 44)}$$

$$I_{LW\_2}(t) = -\varepsilon_s\sigma_{bolt}T_s(t)^4 \qquad \text{(Equation C3. 45)}$$

Here $I_{LW}(t)$ denotes the incoming or outgoing longwave radiation (W/m^2), T_{sky} denotes the sky temperature (ºC), ε_s denotes the surface emissivity of different land type, σ_{bolt} denotes the Stefan-Boltzmann coefficient ($\sigma_{bolt} = 5.6\text{x}10^{-8}$ $Wm^{-2}K^{-4}$), T_s denotes the averaged ground surface temperature (ºC).

The contribution of the net outgoing longwave radiation flux, $\Delta L_{lw}(t)$, to air cooling is expressed by the net of incoming and outgoing longwave radiation.

$$\Delta L_{lw}(t) = I_{LW\_1}(t) - I_{LW\_2}(t) \quad \text{(Equation C3. 46)}$$

Here $\Delta L_{lw}(t)$ denotes the net outgoing longwave radiation flux (W/m^2) at the given time t.

3. 13 Latent Heat Transfer Model

Greenery and water features can reduce temperatures through evapotranspiration, which is the sum of evaporation and plant transpiration from the land surface to atmosphere.

For latent heat exchange, $I_{lat}(t)$, it would be calculated by:

$$I_{lat}(t) = g_h L(t)/3.6 \quad \text{(Equation C3. 47)}$$

$$g_h = A_{green} m_{green} + A_{road} m_{road} + A_{water} m_{water} + A_{plaza} m_{plaza} \quad \text{(Equation C3. 48)}$$

$$L(t) = 2491.146 - 2.302\langle T_p \rangle^p(t) \quad \text{(Equation C3. 49)}$$

Here $I_{lat}(t)$ denotes the latent heat exchange flux (W/m^2) at the given time t, A denotes the area (m^2) of different land type, m denotes the evaporation rate (mm/day) of different land type, $L(t)$ denotes the Latent Heat of Vaporization (kJ/kg), $\langle T_p \rangle^p$ denotes the intrinsic phase average temperature (ºC) of the permeable phase (i.e. air) within the control volume.

3. 14 Shading Model

Sky view factors (SVF) defined as the ratio between radiation received by a planar surface and that from the entire hemispheric radiating environment by Oke (1981). According to Andrew Marsh (2007), checking if any object is in shade at a particular time is simply a matter of determining if the Sun in it's current position is obstructed by any other surrounding objects. The SVF presented the amount of unobstructed area ratio and can be used to assess the shading effect of the surface. Figure C3. 3 shows a diagram of the relationship of the

unobstructed area and the sunlight on the particular surface.

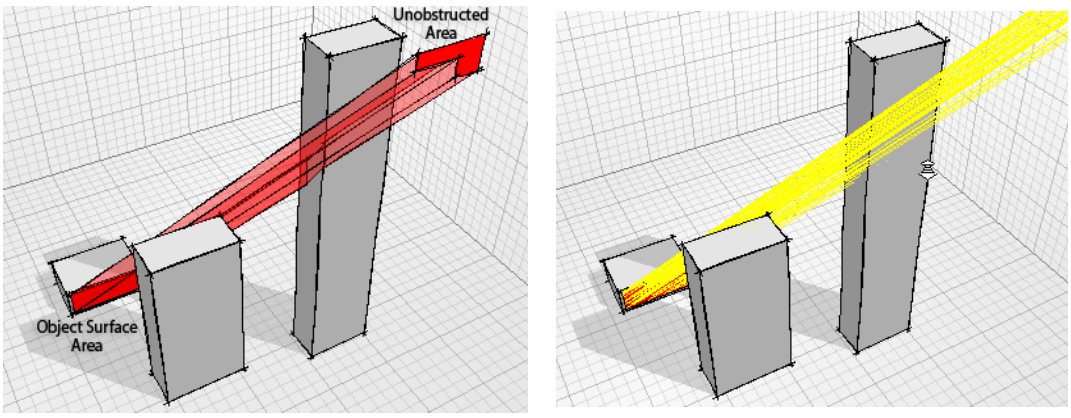

Figure C3. 3 Diagram SVF used to calculate percentage shading at a time on a surface building analysis tools. Using SVF (left) and ray-tracing techniques (right)

For example, the entire sky is blocked from view by obstacles (i.e. totally shaded), the SVF = 0. On the other hand, if there is an obstacle blocking parts of the sky view, the SVF will be greater than 0. SVF is one of the possible approximations to consider the shading effect in the urban content, such as Ariane Middel (2018) study the Sky View Factor at San Francisco, Paris, New York and Singapore for urban climate modelling. Figure C3. 4 show the some SVF samples of difference areas.

Figure C3. 4 Example of difference SVF (Source: Ariane Middel (2018))

Oke (1987) also suggested that an area with high SVF could allow radiant cooling of urban surfaces under the dark sky at night which beneficial to mitigating nocturnal urban heat island effect. Kam Shing Leung (2008) has developed a method to calculate the average sky view factor at ground and building facades, while applicable to complex urban forms. The ground sky view factor, SVF_g, can be obtained by the ratio of ratio of ground area to building exterior wall area using Equation C3.50. A1 is the coefficients of the equations for SVF_g. Kam Shing Leung (2008) suggested the coefficient shall be 1.342.

$$SVF_g = A1\left(\frac{GA}{GA + WA}\right) \qquad \text{(Equation C3. 50)}$$

Here SVF_g denotes the Sky View Factor of ground surface, GA denotes the ground area (m^2) of the control volume, the WA denotes the building wall area (m^2) of the control volume and $A1$ denotes the coefficient given by Kam Shing Leung (2008).

The wall surface sky view factor, SVF_w, can be obtained similar approach using equation C3. 51. A2 is the coefficients of the equations for SVF_w. Kam Shing Leung (2008) suggested the coefficient shall be depended on the built form and ranging from 1.231 to 1.437.

$$SVF_w = \frac{GA}{WA} \text{ x } (1 - \frac{A2 \text{ x } GA}{GA + WA}) \qquad \text{(Equation C3. 51)}$$

Here SVF_w denotes the Sky View Factor of the wall or façade of building, GA denotes the ground area (m^2) of the control volume, the WA denotes the building wall area (m^2) of the control volume and $A2$ denotes the coefficient given by Kam Shing Leung (2008).

3. 15 Deep Ground Temperature Model

The deep ground temperature, T_{deep}, is used for the boundary condition of the ground energy balance model. The temperature is modelled using a research from T.T. Chow (2011). He

carried out a correlation study of the ground temperatures up to a soil depth of 3m with the weather parameters has been performed making use of the observed data in the 4-year period 2006–2009. The corresponding coefficients are shown in Table C3. 2.

$$T_{deep\ ground}(\mathrm{t}) = a_1 \exp(-a_2 x)\langle \mathrm{T_p}\rangle^{\mathrm{p}}(t) + b_1 \exp(-b_2 x)\sin\left(\frac{2\pi}{365}n + b_3 x + b_4\right) + c_1\left(-\frac{2}{\pi}\right)\tan^{-1}(c_2 x) + d_1 \quad \text{(Equation C3. 52)}$$

Here $T_{deep\ ground}(\mathrm{t})$ denotes the predicted underground (3m below ground) temperature (ºC) at different time (s), $\langle \mathrm{T_p}\rangle^{\mathrm{p}}$ denotes the intrinsic phase average temperature (ºC) at permeable phase (i.e. air), x denotes the soil depth (m), n denotes the number of day. Equation C3.52 shows the coefficients of the deep ground temperature model given by T.T. Chow (2011).

Table C3. 2 Numerical coefficients for the refined model based on the equation

a_1	a_2	b_1	b_2	b_3	b_4	c_1	c_2	d_1
0.4041	1.4284	4.687	0.2223	−0.3465	−2.0866	15.3297	−2.7204	11.4603

3. 16 Summary

General governing equations (Microscopic Level)

In this chapter, the general governing equations for CFD has been recapped. They represent mathematical statements of the conservation laws of physics (1) The mass of a fluid is conserved, (2) the rate of change of momentum equals the sum of the forces on a fluid particle (Newton's second law) and (3) the rate of change of energy equals to the sum of the rate of heat addition to and the rate of work done on a fluid particle in Microscopic Level. The following general governing equations (Microscopic Level) has been discussed step by

step:

- Continuity Equation [equation C3. 2 to C3. 3]
- Momentum Equation [equation C3. 4 to C3. 7]
- Energy Equation [equation C3. 8 to C3. 9]

Volume averaging governing equations (Macroscopic level)

The thesis applied the Volume Averaging Approach to develop the general governing equations (Microscopic Level) to volume averaging governing equations (Macroscopic level) for the UHI Model. The Volume Averaging Approach equation has been discussed in Chapter 2. The following volume averaging governing equations (Macroscopic level) has been discussed step by step:

- Volume Averaging Continuity Equation [equation C3. 10 to C3. 16]
- Volume Averaging Momentum Equation [equation C3. 17 to C3. 23]
- Volume Averaging Energy Equation [equation C3. 26 to C3. 31]

Lost information and sub-modelling

As discussed in Chapter 2, microscopic information would be lost during the Volume Averaging process on the governing equations, such as Building Geometry information, spatial variation of Air Temperature, Air Velocity, Surface Temperature and etc. As the results, some of the thermal fluid dynamic process cannot be generated in the macroscopic level simulation, such as the geometrical effect on the wind flow, the heat transfers between air and ground/building and etc. Thus, sets of sub-models have been developed for microscopic level simulation and to provide essential information to the macroscopic

equations. The following sub-models has been discussed step by step:

- Interactive Momentum Force Model [equation C3. 24 to C3. 25]

  Interactive Momentum Force Model would recreate the geometrical effect induced by building geometry. The volume averaged form of Maruyama (1992) model has applied in this study to form the Interactive Momentum Force term in the at the Volume Averaging Momentum Equation [equation C3. 23]

- Ground / Building Energy Balance Model [equation C3. 32 to C3. 34]

  Ground / Building Energy Balance Model calculates the resultant air temperature from the energy balance of urban canopy at the microscopic level and heat exchange between microscopic and macroscopic level. It calculates the heat exchange between the microscopic and macroscopic equation can be related by using convection and diffusive heat transfer between the average surface temperature of the ground/building and air.

- Net Shortwave Solar Radiation Model [equation C3. 35 to C3. 39]

  Net Shortwave Solar Radiation Model calculates the time-dependent contribution of the solar radiation (direct + diffuse) to air temperature based on the hourly solar radiation, tree density, tree penetration, surface absorptive and sky view factor (openness to sky).

- Surface Convective Heat Transfer Model [equation C3. 40 to C3. 41]

  Mean velocity is obtained from the macroscopic flow field to calculate the surface convective heat transfer between the air temperature and surface ground / building temperature. This study applied Bo-rong Lin (2004) model (Equation C3.40) to obtained the surface convective heat transfer coefficient.

- Net Longwave Radiation Model [equation C3. 42 to C3. 46]

  Stefan Boltzmann Law is adopted to calculate the net longwave radiation heat transfer.

- Latent Heat Transfer Model [equation C3. 47 to C3. 49]

  Latent Heat Transfer Model calculates the evaporation and plant transpiration from the greenery and water features.

- Shading Model [equation C3. 50 to C3. 51]

  Surface sky view factor model developed by Kam Shing Leung (2008) is used to estimate the shading effect of the building on ground or building wall.

- Deep Ground Temperature Model [equation C3. 52]

  T.T. Chow (2011) has recorded the deep ground temperature of Hong Kong and developed a Deep Ground Temperature Model. This model is used for the boundary condition of the ground energy balance model.

Chapter 4 Urban Density Database

This chapter discuss the development of Urban Density Database for the new UHI Model. This chapter introduce the GIS data format that collected from Hong Kong Lands Department, such as 3D Spatial Data, Digital Orthophoto DOP5000 and Digital Topographic Map iB5000. The Urban Density Database use pixel analysis to directly read the image generated by GIS data. Thus, it indicated that the Urban Density Database can apply anywhere across the world. Then the chapter discuss the method of using pixel analysis to obtain the road, water body, building, sea and tree area and coordination information.

In Chapter 3, the governing equation has been “upscaled” using Volume Averaging Approach to become volume averaged governing equation. These equations are used to model the macroscopic level environment such as the volume averaged velocity and volume temperature. However, the volume averaged governing equation cannot model the microscopic level environment and the microscopic level information is modelled by several sub-model, such as (1) the Interactive Force Model, (2) building heat balance model and (3) ground heat balance model. As discussed in Chapter 3, these sub-models require unique input information and the purpose of the Urban Density Database is to general the input information directly from the GIS data.

The new approach does not require to model the 3D geometry, such as building, tree or water features and etc. It also does not require to input the thermal and material properties of each feature. The geometrical information is simplified and represented by porosity (%) and permeability (%) per unit control volume, while other urban features such as a tree, river, lake are represented by greenery, road, building, construction, plaza in area weighted percentage (%) per control volume. A computational code has been developed using Python to transfer the Hong Kong GIS data to modelling input and created an Urban Density Database. Thus,

the UHI model allows to extract the information from the database while model anywhere in Hong Kong. Of course, this method can also apply to other areas GIS data, thus, it makes the UHI model able to apply at anywhere in the world. The Python computational code and results and example of the Urban Density Database are given in Appendix A and Appendix C, respectively.

4. 1 GIS data

The UHI Model requires the area information of urban environment. An urban density database of Hong Kong is developed based on the GIS data. It analyses the GIS data and transform into different layer, such as the area of greenery, road, building, construction, plaza, sea and the terrain elevation and building height which calculated from the GIS data. Figure C4. 1 shows the concept of the urban density database and Figure C4. 2 show the screen capture of Urban Density Database. The data is extracted from the GIS maps that purchase from Hong Kong Lands Department (LandsD). These GIS maps are Digital Topographic Map iB5000 (scale 1:5000) in FGDB format and the Digital Orthophoto DOP5000 (Scale 1:5000) respectively.

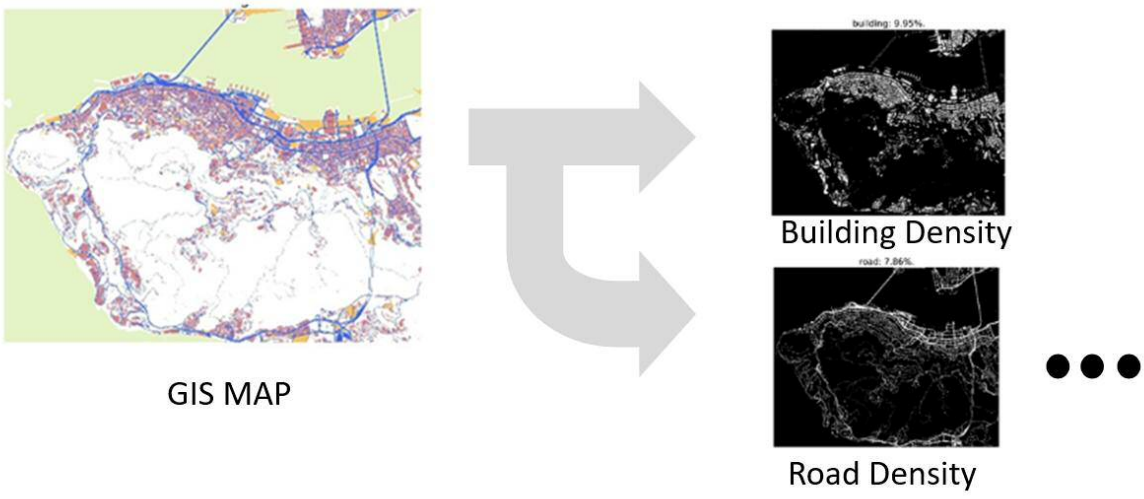

Figure C4. 1 Analyse GIS data and transform into different layer

Ground Elevation (m)

Building Height (m)

Building Area (m^2)

Road Area (m)

Greenery Area (m)

Water Feature Area (m^2)

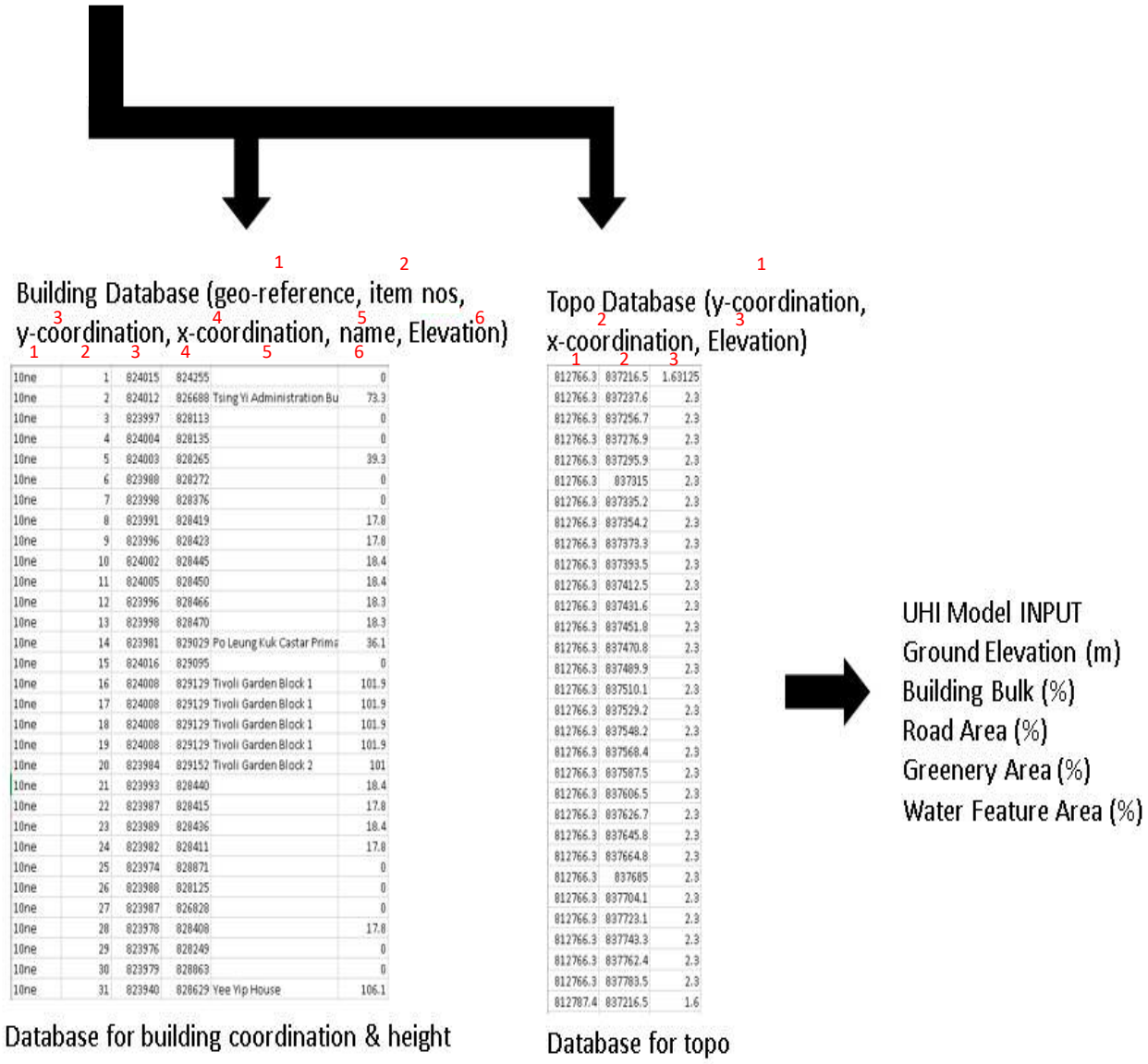

Figure C4. 2 Calculate GIS data and transform to database

4. 2 Digital Topographic Map iB5000

Refers to Lands Department, Tthe Digital map detail is represented as single coordinated points or lines of multiple coordinated points. Coordinates of the Digital Map are in Hong Kong 1980 Grid, and heights are in meters above the Hong Kong Principal Datum. It provides variable information such as building area, road area, waterfront line, open space and etc. However, the building height and greenery information are not included in the maps. Figure C4. 3 shows an example of iB5000 Digital Topographic Map.

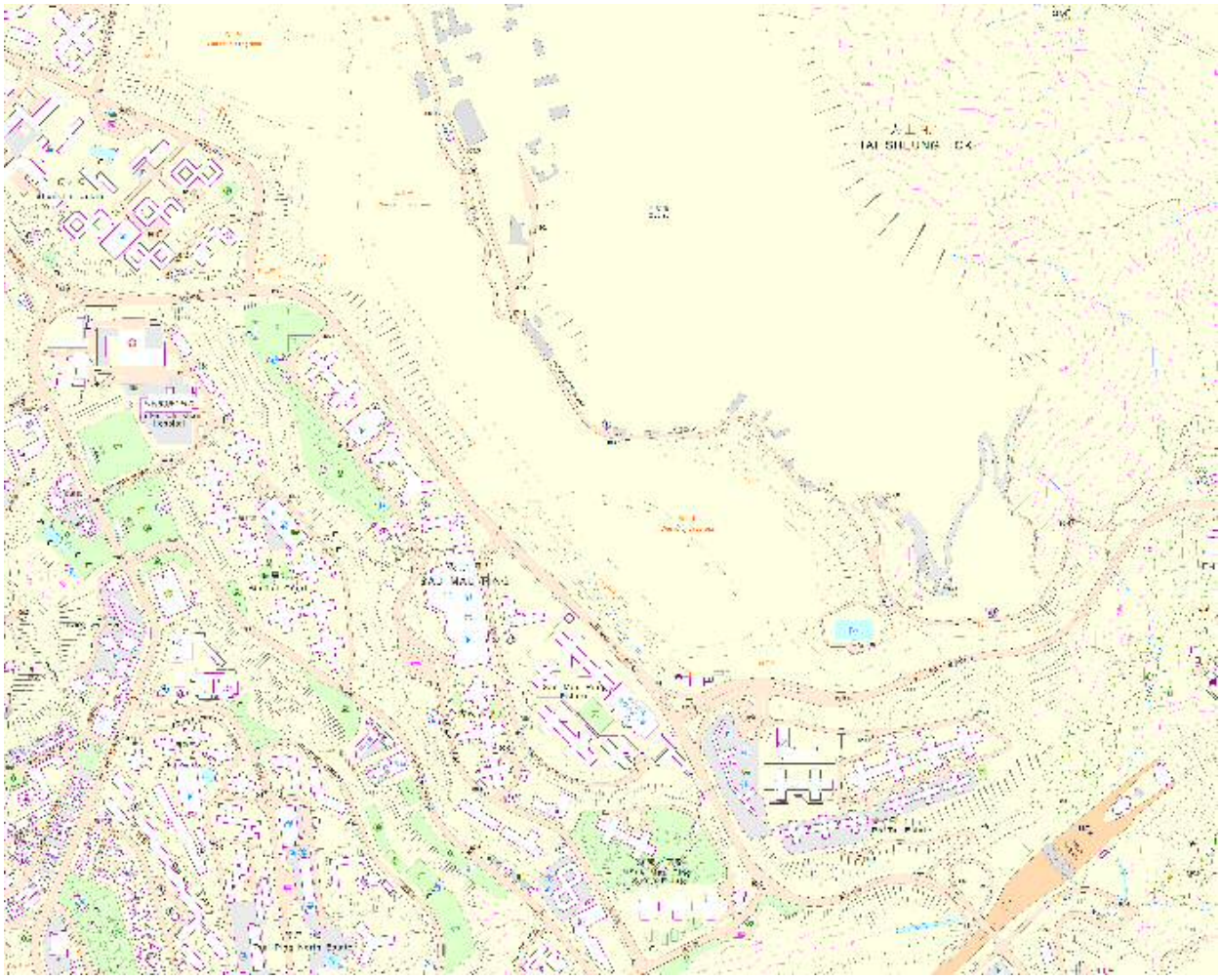

Figure C4. 3 Sample of Digital Topographic Map iB5000

4. 3 Digital Orthophoto DOP5000

According to Lands Department, an orthophoto is derived from aerial photos in which image displacement caused by relief and camera tilts has been rectified. Orthophoto maintains the pictorial information of the original aerial photos and has a uniform scale. Digital Orthophoto DOP5000 series is produced from the aerial photos taken mainly at a flying height of 2,400m and supplemented by 3600m and/or 6000m flying height aerial photos. Distortions of photographic images caused by tilting of aerial camera and relief are rectified except those of the building structures. True ortho-rectification has also been applied to elevated roads and bridges. DOP5000 series consists of 190 grid covering all the land area of Hong Kong Special Administrative Region. It is provided in Tiff format on tile basis including a world file with geo-referencing data in Hong Kong 1980 Grid. Digital Orthophoto DOP5000 is used to evaluate the amount of greenery in a particular area. Figure C4. 4 shows an example of Digital Orthophoto.

Figure C4. 4 Sample of Digital Orthophoto

4. 4 3D Spatial Data (Series: 3D-BIT00)

3D Spatial Data is a set of territory-wide digital 3D model data created to represent the shape, appearance, and position of different types of ground features including building, infrastructure and terrain, as illustrated in Figure C4. 5. The 3D Spatial Data is used to evaluate the building and terrain height. Totals of around 60,000 building height have been stored in the database.

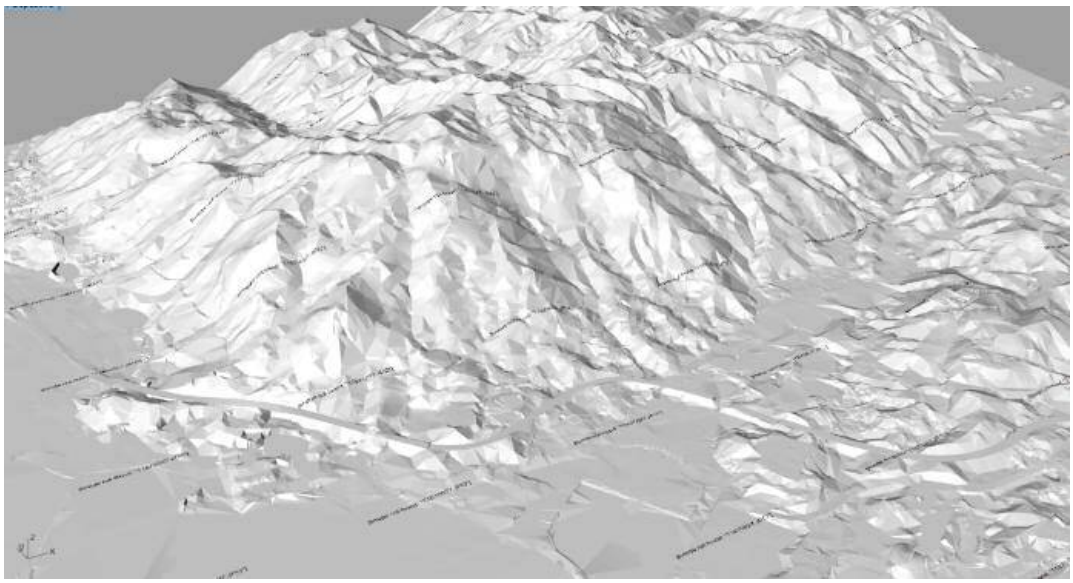

Figure C4. 5 Sample of 3D Spatial Data

Since the data is in 2D or 3D format. In order to extract the density information in respect of 10m x 10m grid, a computational code is further developed to transform the information for the UHI Model input.

4. 5 Pixel Analysis

The GIS information requires additional works in order to transform into the UHI model input information. A computational code is developed to analyse the RGB of each pixel in the digital map and to evaluate the percentage of Greenery area, Building area, Sea area, Open Space area and Road Area per grid. Figure C4. 6 shows an example of Pixel based image analysis transform information from digital map to numerical data.

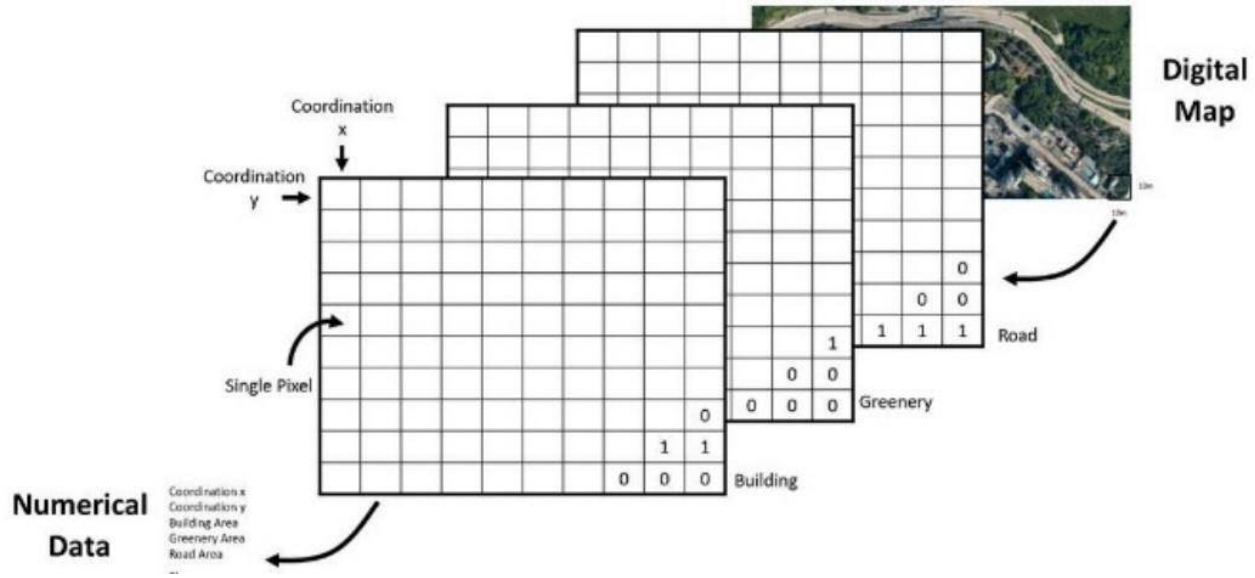

Figure C4. 6 Pixel based image analysis transform information from digital map to numerical data

Step 1: Colouring

In the first step, it is required to highlight the area of building, road, construction and sea on the Digital Topographic Map iB5000. By doing so, it is required to redefine the GIS into specific RGB value based on the land type, so that to allow the program to calculate the amount of pre-defined pixel in the later stage, as shown in Figure C4. 7. Finally, the digital map is saved in jpeg file format with fix resolution to further carry out a pixel analysis.

Land Types	RGB Value			Colour
	R	G	B	
Building	214	133	137	
Road	64	101	235	
Sea	230	243	200	
Construction	246	197	103	

Figure C4. 7 Colour definition for Pixel Analysis

For example, the GIS is divided into 4 types of areas in this stage, i.e. (1) Building, (2) Road, (3) Construction and (4) Sea at Figure C4. 8.

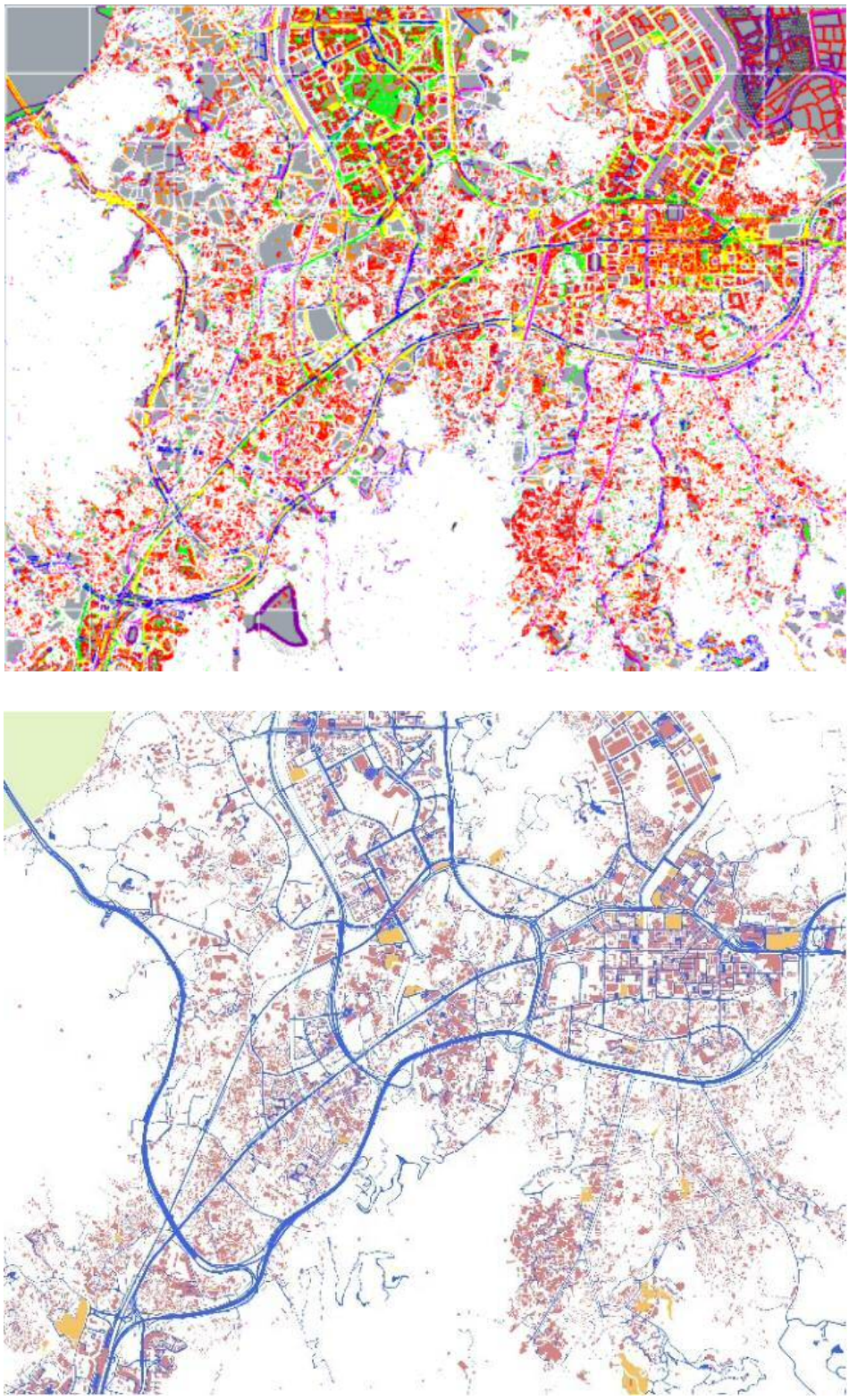

Figure C4. 8 Example of colouring the GIS data. (Top) Original GIS Map, (Bottom) GIS Map after colouring.

Step 2: Overlaying

The next step is to overlay the highlight Building, Road, Construction and Sea areas into the Digital Orthophoto DOP5000 at the exact location and combined into a single image, as shown in Figure C4. 9.

Figure C4. 9 Example of Overlaying the GIS data. (Top) Digital Orthophoto DOP5000 Map, (Bottom) Digital Orthophoto DOP5000 overlaid with the (1) Building, (2) Road, (3) Construction and (4) Sea data.

Step 3: Pixel Analysis

The combined image now contains information of greenery, building, road, construction and sea. The information of individual land type is extracted and then divided into a smaller grid size. The grid size can be ranged from a large size of 500m × 500m to a small size of 10m × 10m. The amount of area density of certain land types in each grid is calculated through the number of white pixel (for example, the white pixel is the road area at the road density map) and the total number of pixel in each pixel. The coordination and the amount of area is store into a database. Figure C4. 10 shows an calculation of the road density from the urban density database.

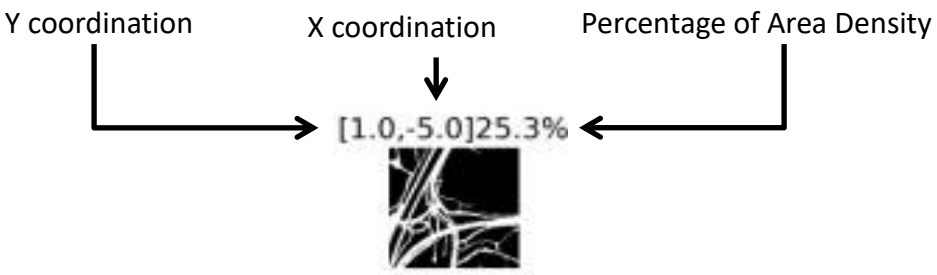

Figure C4. 10 Example of Pixel Analysis. (top) Road Density Map in 10m × 10m, (bottom) Road Density Map in 500m × 500m

4. 6 Calculate Building Height and Terrain Height

For Building Height and Terrain Height information, it can be obtained from the GIS 3D data.

1. Input the 3D Spatial Data into Rhino.

2. Using Grasshopper to place a set of control points in 10m separation and projected on to the building or terrain surface. The XYZ coordinate of each test point is then extracted and stored in the database.

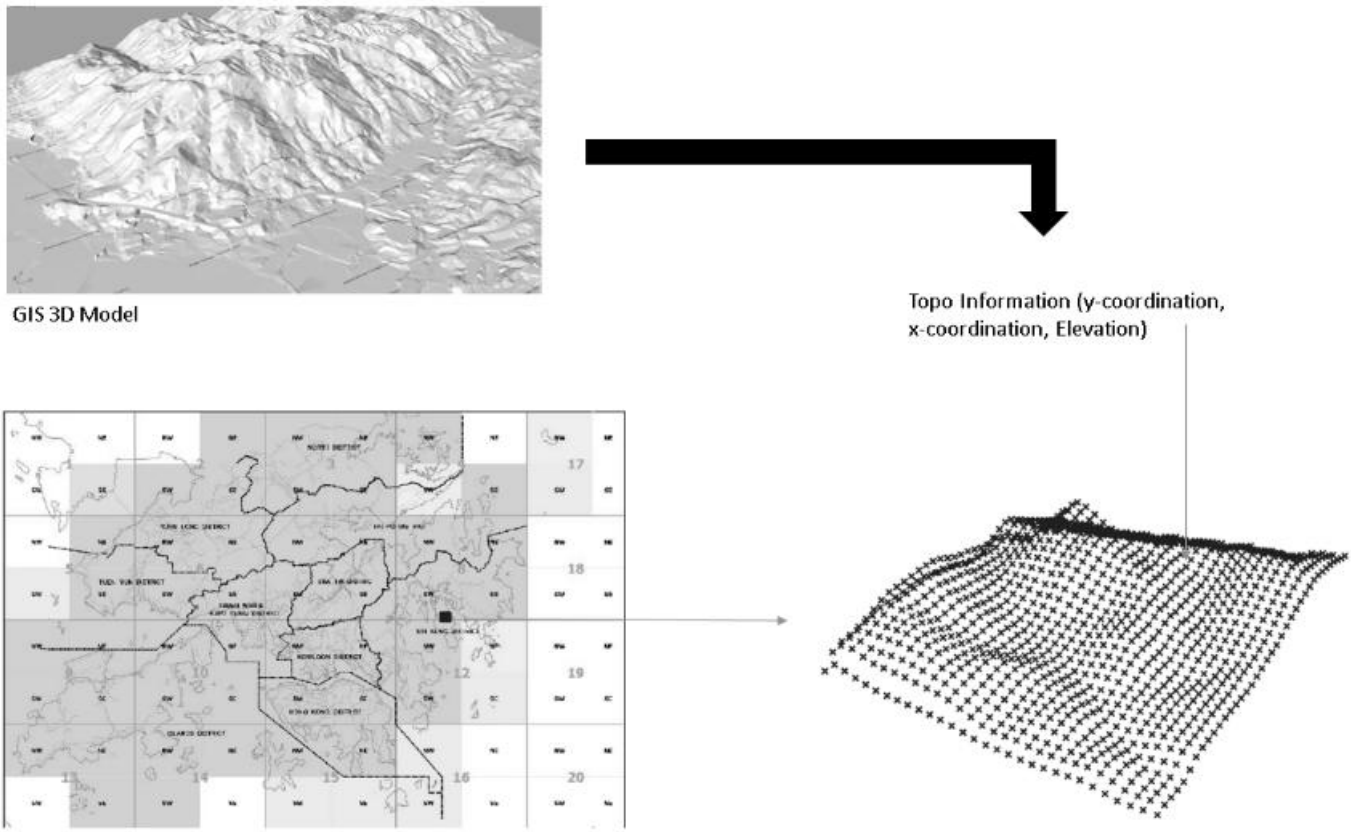

Figure C4. 11 Calculate the average terrain elevation using 3D Spatial Data

4. 7 Summary

The Urban Density Database is an essential for the UHI Model. In UHI Model simulation, the model required to read the urban area data from the database to calculate the area, height, porosity and permeability within the computational grid.

The GIS-based analysis tool extracts GIS data from Digital Topographic Map iB5000 (scale 1:5000), Digital Orthophoto DOP5000 (Scale 1:5000) and 3D spatial data into images (available from the Lands Department). Table C4. 1 summarized the overview of GIS Data to create the database. The images are scanned and divided into a 10m x 10m grid from 2,500 numbers of maps covering 60,000m x 50,000m area.

Pixel-based image analysis is carried out to analyses the corresponding coordination and area information in each grid of the digital map, evaluate the areas of building, greenery, marine, open space, and road area per each grid and capture the geometry and boundary information. The results are then stored in a database for the geometry and boundary setup for simulation. Figure C4. 12 shows a database sample created using GIS data from Lands Department.

To assess UHI effects, the user is only required to input the location and the size of the simulation area. The GIS-based analysis tool uses the location and size information to extract the geometry information from the database, input to the CFD model and automatically generates the spatial mesh and setup the boundary condition at the urban geometry.

The new digital tool greatly reduces the amount of time, work and modelling complexity required to analyses a large area. It can thus provide a quick tool for planners and architects to carry out UHI assessment at an early stage of planning, enable a more streamlined and efficient workflow so that strategies to mitigate the impacts of UHI can be incorporated to achieve a more sustainable urban design.

An urban density map of Hong Kong is given in Appendix C from Figure A9 to Figure A12. Figure C4. 12 and Table C4. 1 summarized the overview of GIS Data to create the database. The database created based on Python and the program code is given in Appendix B.

Table C4. 1 Overview of GIS Data for the Urban Density Map

Parameter in Urban Density Database	GIS Data
Building Area	Digital Map iB1000
Road Area	Digital Map iB1000
Sea / Water Area	Digital Map iB1000
Greenery Area	Digital Orthophoto DOP5000
Construction Area	Digital Map iB1000
Building Height	3D Spatial Data 3D-BIT00
Terrain Height	3D Spatial Data 3D-BIT00

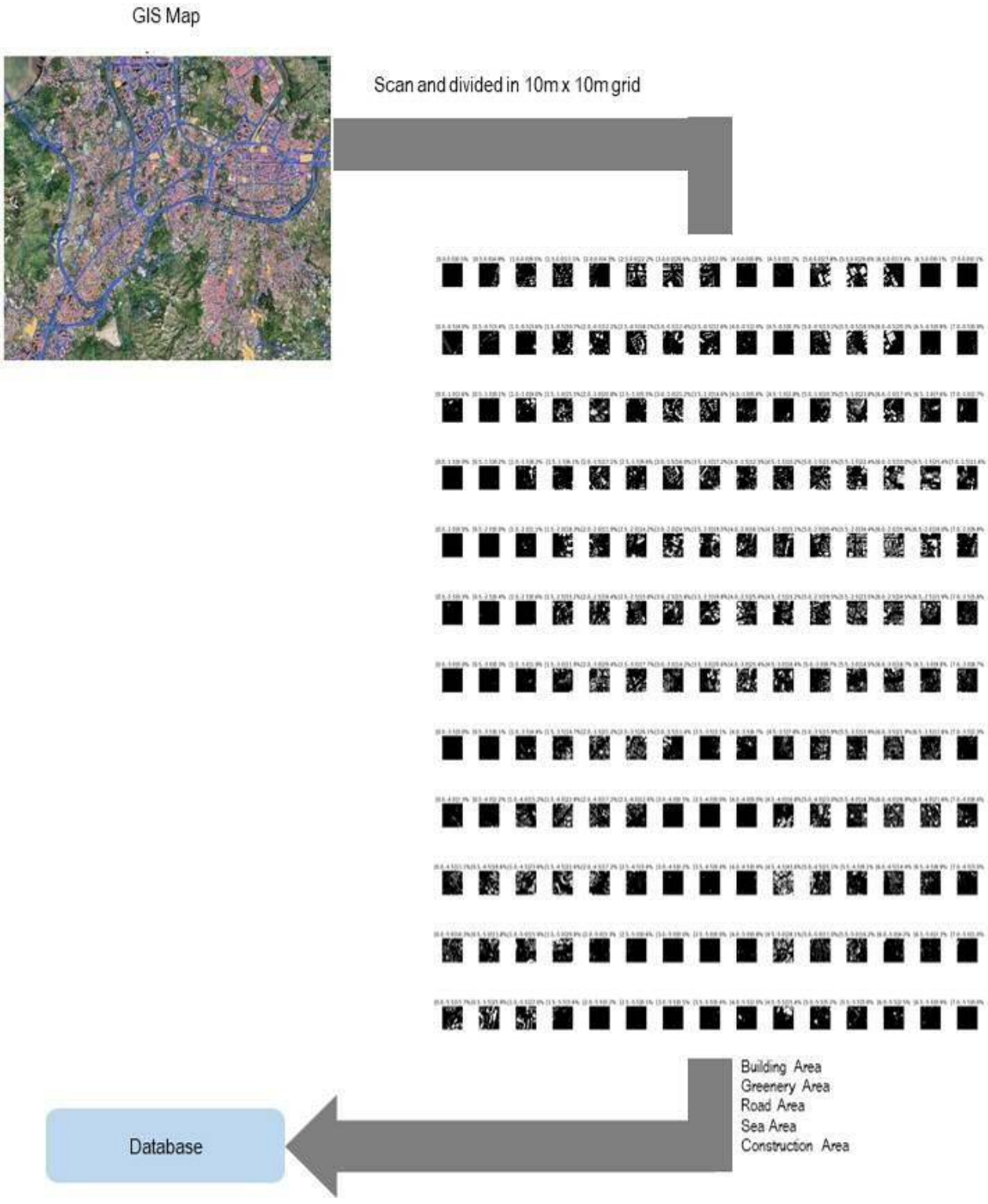

Figure C4. 12 Work example of transformation from GIS data to database

Chapter 5 Numerical Approach for UHI Model

This chapter discusses the discretization of the volume averaged governing equation developed in Chapter 4. This chapter also discusses the reason of selecting cartesian grids for the UHI model computational grid and introduce the differencing schemes for momentum equation, energy equation, ground energy balance model and building energy balance model. Unlike traditional CFD approach program, this new UHI model requires to connect to Urban Density Database and three sub-models, i.e. (1) the Interactive Force Model, (2) building heat balance model and (3) ground heat balance model. Therefore, this chapter also discusses the flow diagram for UHI model and connection between the governing equation, database and the sub-models.

It is well known that the Navier-Stokes equations cannot be solved using an analytical approach. One of the most common approaches is to use discretization method to solve the equations numerically under certain assumptions. It means to reformulate the equations under certain assumptions and to solve the solution using numerical approach. There are many discretization methods has been developed, such as finite difference method (FDM), finite element method (FEM), finite volume method (FVM) and etc. FVM can be used to approximate a system of the partial differential equations (PDE) by an algebraic equation. This approach is well documented in the textbook such as Suhas V. Patankar (1980) and H. K. Versteeg and W. Malalasekera (1995). And this study adopted FVM approach to solving the momentum and energy equation.

5. 1 Computational Grid

Before using the discretization method to solve the system of governing equation the first step is to generate the computational grid. The computational grid can be generated by

partitioning a physical domain into a set of discrete volumes. There are many methods to generate a computational grid, such as structured and unstructured approaches. The unstructured approach could reduce the numerical error and has the highest flexibility by allowing the user to define the grid size at a specific location. However, the generation of unstructured grids would require complicated algorithms and increase the complexity of the UHI model.

Since the UHI model does not require to create physical geometry (which would be replaced by the porosity and permeability) and therefore the model does not need to define different of grid size at specific locations. Thus, this model does not need to use unstructured grids approach. It can simply apply Cartesian grids method. This method allows a simple and flexible grid generation and an easy discretization of the solved PDE. The grid generation further applied linear transfinite interpolation (TFI) method to allow higher resolution of the grid to be generated at the higher resolution of the grid or urban canopy to reduce numerical error. Figure C5. 1 shows the 70 × 70 × 70 Cartesian grids generated by the UHI Model.

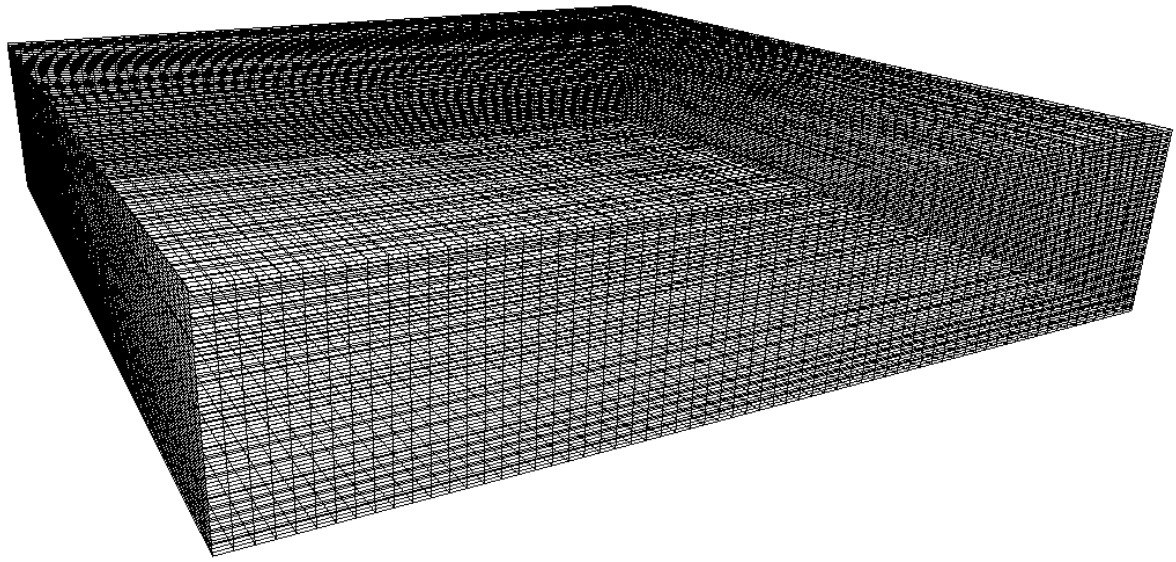

Figure C5. 1 70 × 70 × 70 Cartesian grids

Numerical solution schemes can be mainly classified into explicit approach or implicit approach. For using explicit approach, the dependent variables are determined based on known quantities. Since the governing equations in the study are generally nonlinear with a range of unknown variables, Fully Implicit Scheme would often extra stability and allows large time step in solving the PDE.

There are many different types of differencing schemes to approximate the governing equation. Patankar (1980) has listed out several mathematical approaches such as Upwind Differencing Scheme, Central Differencing Scheme, Hybrid Differencing Scheme and etc for different of consideration. In this study, the UHI model is generally applied Hybrid Differencing Scheme. The function of A(P) for different schemes (Patankar 1980).

$$A(|P|) = \max(0, 1 - 0.5|P|) \qquad \text{(Equation C5. 1)}$$

where Peclet number, P is to be taken as the ratio of F and D.

5. 2 Differencing Schemes - Momentum Equation

The discretization process for the momentum equation set will be illustrated here. The averaged forms of gas phase on momentum equation have been discussed and given in Chapter 3. The general differential equation under the Cartesian coordination with uniform grid spacing can be written as:

$$\begin{aligned}\frac{\partial \varepsilon_k \langle \rho_k \rangle^k \langle u_k \rangle^k}{\partial t} &+ \operatorname{div}\left(\varepsilon_k \langle \rho_k \rangle^k \langle u_k V_k \rangle^k\right) \\ &= -\operatorname{div} \varepsilon_k \langle P_k \rangle^k + \varepsilon_k \langle \rho_k \rangle^k g \\ &+ \operatorname{div} \langle \mu_k \operatorname{grad} \varepsilon_k \langle u_k \rangle^k \rangle + \langle F_{jk} \rangle\end{aligned} \qquad \text{(Equation C5. 2)}$$

Here $\langle\ \ \rangle$ denotes the extrinsic phase averaging of any variable, $\langle F_{jk} \rangle$ denotes the

Interactive momentum force (N/m^3), $\langle u_k \rangle^k$ denotes the intrinsic phase averaged velocity vector (m/s) at given direction, $\langle V_k \rangle^k$ denotes the intrinsic phase averaged velocity magnitude (m/s), μ_k denotes the intrinsic phase averaged viscosity (m^2/s), ε_k denotes the intrinsic phase averaged porosity, $\langle P_k \rangle^k$ denotes the intrinsic phase averaged pressure (Pa). The differential equation can be turned into the discretization equation by applying Hybrid Differencing Scheme according to Patankar (1980).

$$a_p T_P = a_E T_E + a_W T_W + a_N T_N + a_S T_S + a_T T_T + a_S T_S + b \quad \text{(Equation C5. 3)}$$

where

$$a_E = D_e A(|P_s|) + \max[-F_e, 0] \quad \text{(Equation C5. 4)}$$

$$a_W = D_w A(|P_w|) + \max[-F_w, 0] \quad \text{(Equation C5. 5)}$$

$$a_N = D_n A(|P_n|) + \max[-F_n, 0] \quad \text{(Equation C5. 6)}$$

$$a_S = D_s A(|P_s|) + \max[-F_s, 0] \quad \text{(Equation C5. 7)}$$

$$a_T = D_t A(|P_t|) + \max[-F_t, 0] \quad \text{(Equation C5. 8)}$$

$$a_B = D_b A(|P_b|) + \max[-F_b, 0] \quad \text{(Equation C5. 9)}$$

$$S_c = \varepsilon_k \Delta P + \varepsilon_k \left(\langle \rho \rangle^k - \langle \rho \rangle^k_{ref} \right) g + \mu \varepsilon_k \frac{\langle u_k \rangle^k}{\varepsilon_k} + \varepsilon_k \frac{\langle \rho \rangle^k{}_{old} \langle u_k \rangle^k{}_{old}}{\Delta t} \quad \text{(Equation C5. 10)}$$

$$b = S_c \, \Delta x \Delta y \Delta z + a_P^0 \langle u_k \rangle^k{}_{old} \quad \text{(Equation C5. 11)}$$

$$S_p = \langle F_{jk} \rangle \quad \text{(Equation C5. 12)}$$

$$a_P^0 = \frac{\langle \rho \rangle^k{}_{old} \Delta x \Delta y \Delta z}{\Delta t} \quad \text{(Equation C5. 13)}$$

Here $\langle u_k \rangle^k{}_{old}$ denotes the intrinsic phase averaged velocity (m/s) at last time step, $\langle \rho_k \rangle^k{}_{old}$

denotes the intrinsic phase averaged density (kg/m^3) at last time step.

The strength of the convection *F* and the diffusion *D* can be defined as:

$$D_e = \frac{k_e \, \Delta y \Delta z}{(\Delta x)_e} \qquad F_e = (\rho u)_e \Delta y \Delta z \qquad \text{(Equation C5. 14)}$$

$$D_w = \frac{k_w \, \Delta y \Delta z}{(\Delta x)_w} \qquad F_w = (\rho u)_w \Delta y \Delta z \qquad \text{(Equation C5. 15)}$$

$$D_n = \frac{k_n \, \Delta z \Delta x}{(\Delta y)_n} \qquad F_n = (\rho v)_n \Delta z \Delta x \qquad \text{(Equation C5. 16)}$$

$$D_s = \frac{k_s \, \Delta z \Delta x}{(\Delta y)_s} \qquad F_s = (\rho v)_s \Delta z \Delta x \qquad \text{(Equation C5. 17)}$$

$$D_t = \frac{k_t \, \Delta x \Delta y}{(\Delta z)_t} \qquad F_t = (\rho w)_t \Delta x \Delta y \qquad \text{(Equation C5. 18)}$$

$$D_b = \frac{k_b \, \Delta x \Delta y}{(\Delta z)_b} \qquad F_b = (\rho u)_b \Delta x \Delta y \qquad \text{(Equation C5. 19)}$$

5. 3 Differencing Schemes - Energy Equations

The discretization process for the Energy equation set will be illustrated here. The averaged forms of gas phase on Energy equation has been discussed and given in In Chapter 3. The general differential equation under the Cartesian coordination with uniform grid spacing can be written as:

$$\frac{\partial \varepsilon_k \langle \rho_k \rangle^k \langle h_k \rangle^k}{\partial t} + \text{div}\, \varepsilon_k \langle \rho_k \rangle^k \langle u_k h_k \rangle^k = -\,\text{div}\, \langle k \,\text{grad}\, T_k \rangle^k + \langle q_{jk} \rangle \qquad \text{(Equation C5. 20)}$$

Here $\langle \quad \rangle$ denotes the extrinsic phase averaging of any variable, $\langle \rho_k \rangle^k$ denotes the intrinsic phase averaged density (kg/m^3), $\langle u_k \rangle^k$ denotes the intrinsic phase averaged velocity (m/s),

$\langle h_k \rangle^k$ denotes the extrinsic phase averaged enthalpy (J), ε_k denotes the porosity, $\langle q_{jk} \rangle$ denotes sum of heat transfer (W) between non-permeable phase (topography or building) and permeable phase (e.g. air).

The differential equation can be turned into the discretization equation by applying Hybrid Differencing Scheme according to Suhas V. Patankar (1980) as listed in Equation C5.3.

$$a_E = D_e A(|P_s)| + \max[-F_e, 0] \quad \text{(Equation C5. 21)}$$

$$a_W = D_w A(|P_w)| + \max[-F_w, 0] \quad \text{(Equation C5. 22)}$$

$$a_N = D_n A(|P_n)| + \max[-F_n, 0] \quad \text{(Equation C5. 23)}$$

$$a_S = D_s A(|P_s)| + \max[-F_s, 0] \quad \text{(Equation C5. 24)}$$

$$a_T = D_t A(|P_t)| + \max[-F_t, 0] \quad \text{(Equation C5. 25)}$$

$$a_B = D_b A(|P_b)| + \max[-F_b, 0] \quad \text{(Equation C5. 26)}$$

$$S_c = \langle q_{jk} \rangle = h_c T_s A_b \quad \text{(Equation C5. 27)}$$

$$b = S_c \Delta x \Delta y \Delta z + a_P^0 \langle T_k \rangle^k{}_{old} \quad \text{(Equation C5. 28)}$$

$$a_P^0 = \frac{\langle \rho_k \rangle^k{}_{old} \Delta x \Delta y \Delta z}{\Delta t} \quad \text{(Equation C5. 29)}$$

Here S_c or $\langle q_{jk} \rangle$ denotes sum of heat transfer (W) between non-permeable phase (topography or building) and permeable phase (e.g. air), hc denotes the convective heat transfer coefficient (W/(m^{2}K)), T_s denotes the surface temperature from the Ground Energy Balance Model and Building Energy Balance Model, A_b denotes the surface area from the Ground Energy Balance Model and Building Energy Balance Model, $\langle T_k \rangle^k{}_{old}$ denotes the

intrinsic phase averaged air temperature (°C) at last time step, $\langle \rho_k \rangle^k{}_{old}$ denotes the intrinsic phase averaged density (kg/m^3) at last time step.

The heat transfer of the convection *F* and the conduction *D* can be defined as:

$$D_e = \frac{k_e \, \Delta y \Delta z}{(\Delta x)_e} \qquad F_e = (\rho c T)_e \Delta y \Delta z \qquad \text{(Equation C5. 30)}$$

$$D_w = \frac{k_w \, \Delta y \Delta z}{(\Delta x)_w} \qquad F_w = (\rho c T)_w \Delta y \Delta z \qquad \text{(Equation C5. 31)}$$

$$D_n = \frac{k_n \, \Delta z \Delta x}{(\Delta y)_n} \qquad F_n = (\rho c T)_n \Delta z \Delta x \qquad \text{(Equation C5. 32)}$$

$$D_s = \frac{k_s \, \Delta z \Delta x}{(\Delta y)_s} \qquad F_s = (\rho c T)_s \Delta z \Delta x \qquad \text{(Equation C5. 33)}$$

$$D_t = \frac{k_t \, \Delta x \Delta y}{(\Delta z)_t} \qquad F_t = (\rho c T)_t \Delta x \Delta y \qquad \text{(Equation C5. 34)}$$

$$D_b = \frac{k_b \, \Delta x \Delta y}{(\Delta z)_b} \qquad F_b = (\rho c T)_b \Delta x \Delta y \qquad \text{(Equation C5. 35)}$$

k represents the conductivity of the surface and can be calculated by interpolating the material conductivity from two neighbouring nodal points. Buoyancy force is an upward force exerted by a fluid that opposes the weight of an immersed object.

The buoyancy term is added in momentum equation as a source term.

$$b = \varepsilon_k \left(\langle \rho \rangle^k - \langle \rho \rangle^k_{ref} \right) g \qquad \text{(Equation C5. 36)}$$

Here $\langle \rho \rangle^k$ denotes the intrinsic phase averaged density (kg/m^3), $\langle \rho \rangle^k_{ref}$ denotes the intrinsic phase averaged reference density (kg/m^3).

5. 4 Differencing Schemes - Ground Energy Balance Model

The Ground Energy Balance Model is assumed to be unsteady 1D conduction and convection heat transfer process. Thus, unlike the discretization process for the momentum and energy equations, the Ground Energy Balance Model would use FDM (Explicit) to approximate. The general differential equation under the Cartesian coordination with uniform grid spacing can be written as equation C5. 37 and the discretization equation can be written as below:

$$\frac{\partial T}{\partial t} + \frac{\partial \rho c \bar{u} T}{\partial z} = \frac{\partial}{\partial z}\left(k \frac{\partial T}{\partial z}\right) + b \qquad \text{(Equation C5. 37)}$$

$$T_i^{n+1} = T_i^n + \frac{1}{a_P^0}\left(h_c A_t (T_{i+1}^n - T_i^n + \frac{k}{\Delta z} A_t (T_{i-1}^n - T_i^n) + b_1\right) \qquad \text{(Equation C5. 38)}$$

$$T_i^{n+1} = T_i^n + \frac{1}{a_P^0}\left(\frac{k}{\Delta z} A_t (T_{i+1}^n - T_i^n + \frac{k}{\Delta z} A_t (T_{i-1}^n - T_i^n)\right) \qquad \text{(Equation C5. 39)}$$

$$T_i^{n+1} = T_i^n + \frac{1}{a_P^0}\left(\frac{k}{\Delta z} A_t (T_{i+1}^n - T_i^n + \frac{k}{\Delta z} A_t (T_{DG}(t) - T_i^n)\right) \qquad \text{(Equation C5. 40)}$$

$$a_P^0 = \frac{\rho c \Delta x \Delta y \Delta z}{\Delta t} \qquad \text{(Equation C5. 41)}$$

$$b_1 = I_{SR}(t) + \Delta I_{LW}(t) + I_{Lat}(t) \qquad \text{(Equation C5. 42)}$$

Here T_i^n denotes the ground temperature at layer n, $I_{SR}(t)$ denotes the net solar radiation (W/m^2) on the surface at time t within the control volume, $\Delta L_{lw}(t)$ denotes the net outgoing longwave radiation flux (W/m^2) at the given time t, $I_{lat}(t)$ denotes the latent heat exchange flux (W/m^2) at the given time t.

5. 5 Differencing Schemes - Building Energy Balance Model

Similarly, The Building Energy Balance Model is also assumed to be unsteady 1D conduction and convection heat transfer process, and the discretization equation can be written as below:

$$\frac{\partial T}{\partial t} + \frac{\partial \rho c \bar{u} T}{\partial z} = \frac{\partial}{\partial z}\left(k \frac{\partial T}{\partial z}\right) + b \qquad \text{(Equation C5. 43)}$$

$$T_i^{n+1} = T_i^n + \frac{1}{a_P^0}\left(h_c A(T_{i+1}^n - T_i^n + \frac{k}{\Delta z} A(T_{i-1}^n - T_i^n) + b_1\right) \qquad \text{(Equation C5. 44)}$$

$$T_i^{n+1} = T_i^n + \frac{1}{a_P^0}\left(\frac{k}{\Delta z} A(T_{i+1}^n - T_i^n + \frac{k}{\Delta z} A(T_{i-1}^n - T_i^n)\right) \qquad \text{(Equation C5. 45)}$$

$$T_i^{n+1} = T_i^n + \frac{1}{a_P^0}\left(\frac{k}{\Delta z} A(T_{i+1}^n - T_i^n + \frac{k}{\Delta z} A(T_{core}(t) - T_i^n)\right) \qquad \text{(Equation C5. 46)}$$

$$a_P^0 = \frac{\rho c \Delta x \Delta y \Delta z}{\Delta t} \qquad \text{(Equation C5. 47)}$$

$$b_1 = I_{SR}(t) + \Delta I_{LW}(t) \qquad \text{(Equation C5. 48)}$$

Here T_i^n denotes the building temperature at layer n, $I_{SR}(t)$ denotes the net solar radiation (W/m^2) on the surface at time t within the control volume, $\Delta L_{lw}(t)$ denotes the net outgoing longwave radiation flux (W/m^2) at the given time t, $I_{lat}(t)$ denotes the latent heat exchange flux (W/m^2) at the given time t.

Under-relaxation term is applied in the momentum, energy, and pressure correction equation as suggested by Suhas V. Patanker (1980). The under-relaxation factor is introduced by:

$$\frac{a_p}{\alpha_u}\emptyset_p = \sum a_{nb}\emptyset_{nb} + b + (1 - \alpha_u)\frac{a_p}{\alpha_u}\emptyset_p^* \qquad \text{(Equation C5. 49)}$$

5. 6 Computational Code Procedure

A computational code has been written for the UHI model in this study using Excel VBA. The core of the program is given in Appendix B. However, unlike traditional CFD approach program, this new UHI model requires to connect to Urban Density Database and three sub-model, i.e. **(1) the Interactive Force Model, (2) building heat balance model and (3) ground heat balance model**. Therefore, as part of the thesis development it is requires to develop the flow and connection between the governing equation, database and the sub-models.

In the main program, the computational code main controls the flow of the calculation. It starts up by calling the control setting, defines the variable, prepares and calculates the constant parameter. Figure C5. 2 shows the flow of the main program.

At the beginning, the user is required to provide the input data to the computational code, such as location in HK 1980 Grid Coordinates, domain size, the number of a grid point. Based on the user input data, computation code would create control volume using Cartesian grid method. It would also call out the urban density database and obtains the density parameters, such as greenery area, building area, the road area as well as building height and terrain level for each computational grid and calculate the porosity and permeability value. The user is also required to input the boundary conditions, such as boundary, temperature, pressure and wind profile. The chart of Urban Density Database is shown in Figure C5. 3

At the beginning of the outer iteration, the initial condition of temperature and velocity field will be applied. Then the computational code will solve momentum equation, pressure correction equation, sub-models, and energy equation in order. The simulation will go to next stage either the convergence target or the maximum step is reached. The procedures are repeated until the target is reached and more to next time step.

The Momentum Equation would be the first set of the equation to be solved. At the beginning, the density of the air will be updated based on the pressure correction and temperature. Then, the convective and diffusive coefficients are calculated based on the face velocity and density, and together with the source term, to form a new algebraic equation. Using the new algebraic equation for u,v,w momentum components, the velocity for u,v,w components is solved by using Stone's Method individually and the constant parameters are feed to pressure correction equation for next stage. The flow chart of Momentum Equation is given in Figure C5. 4.

In the Pressure Correction Equation, the mass conservation will be first calculated and followed with pressure coefficients and source terms based on the predicted velocity at the momentum equation in the previous procedure. The algebraic equation will be further updated based on the boundary condition and then solved using Stone's Method. Velocity and the pressure field are updated at the end based on the computed pressure correction field. The flow chart of Pressure Correction Equation is given in Figure C5. 6.

The Energy Equation will be linked to two sub-model i.e. Ground Energy Balance and Building Energy Balance Model in two different ways. Since the Ground Energy Balance Model controls the near ground surface temperature, the sub model would mainly update the boundary value of the Energy Equation based on the resultant surface temperature. On the other hand, the Building Energy Balance Model would form as one of the source terms in the Energy Equation. While the remaining steps are similar to momentum and pressure correction equation and the temperatures are solved successively until a stable solution is reached.

The Ground Energy Balance Model will solve the surface ground temperature for each grid representing the terrain surface temperature. At the beginning of solving Ground Energy Balance Model, it first read the density distribution based on the HK 1980 Grid Coordinates,

the size of the grid from the Urban Density Database. The computational code runs through the sub-model of net short wave solar radiation, longwave radiant exchanges and latent heat exchange to calculate the net energy source on the near ground. The temperature at present iteration step is solved based on the air temperature and velocity at the previous step, ground material properties, and deep ground temperature. It is assuming the air temperature and velocity is constant at present iteration, while the variation of deep ground temperature is only depended on time. The flow chart of Ground Energy Balance Model is given in Figure C5. 7.

Similar to the Ground Energy Balance Model, the Building Energy Balance Model will solve the surface building temperature for each grid. At the beginning, it first read the density distribution based on the HK 1980 Grid Coordinates, the size of the grid from the Urban Density Database. The computational code estimated the vertical building surface area and runs through the sub-model of net short wave solar radiation and longwave radiant exchanges to calculate the net energy source with the urban canopy. The temperature at present iteration step is solved based on the air temperature and velocity at the previous step and building material properties. It is assuming the air temperature and velocity is constant at present iteration, while the variation of deep ground temperature is only depended on time. The flow chart of Building Energy Balance Model is given in Figure C5. 8.

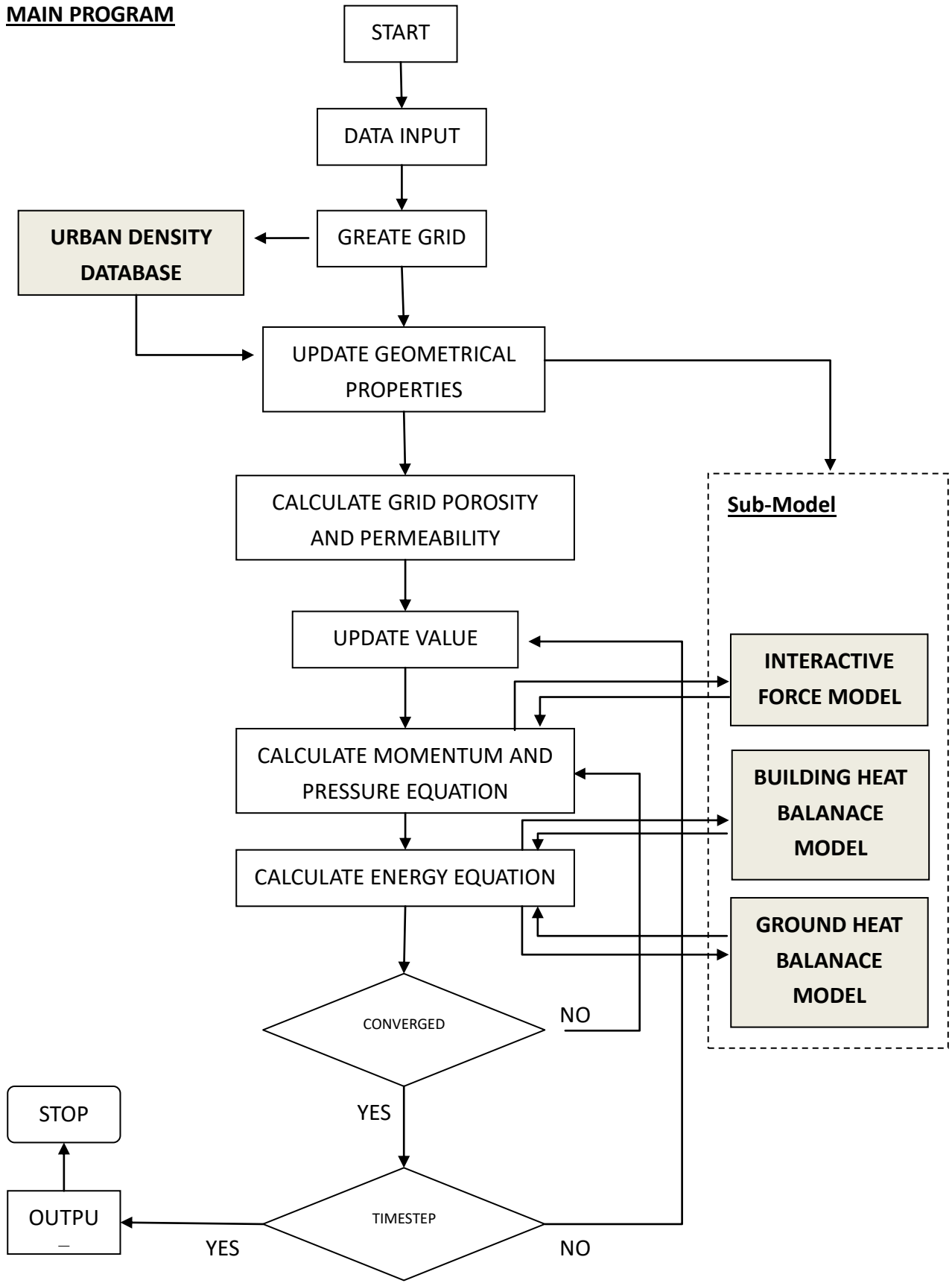

Figure C5. 2 Flow chart of the Main Program

URBAN DENSITY DATABASE

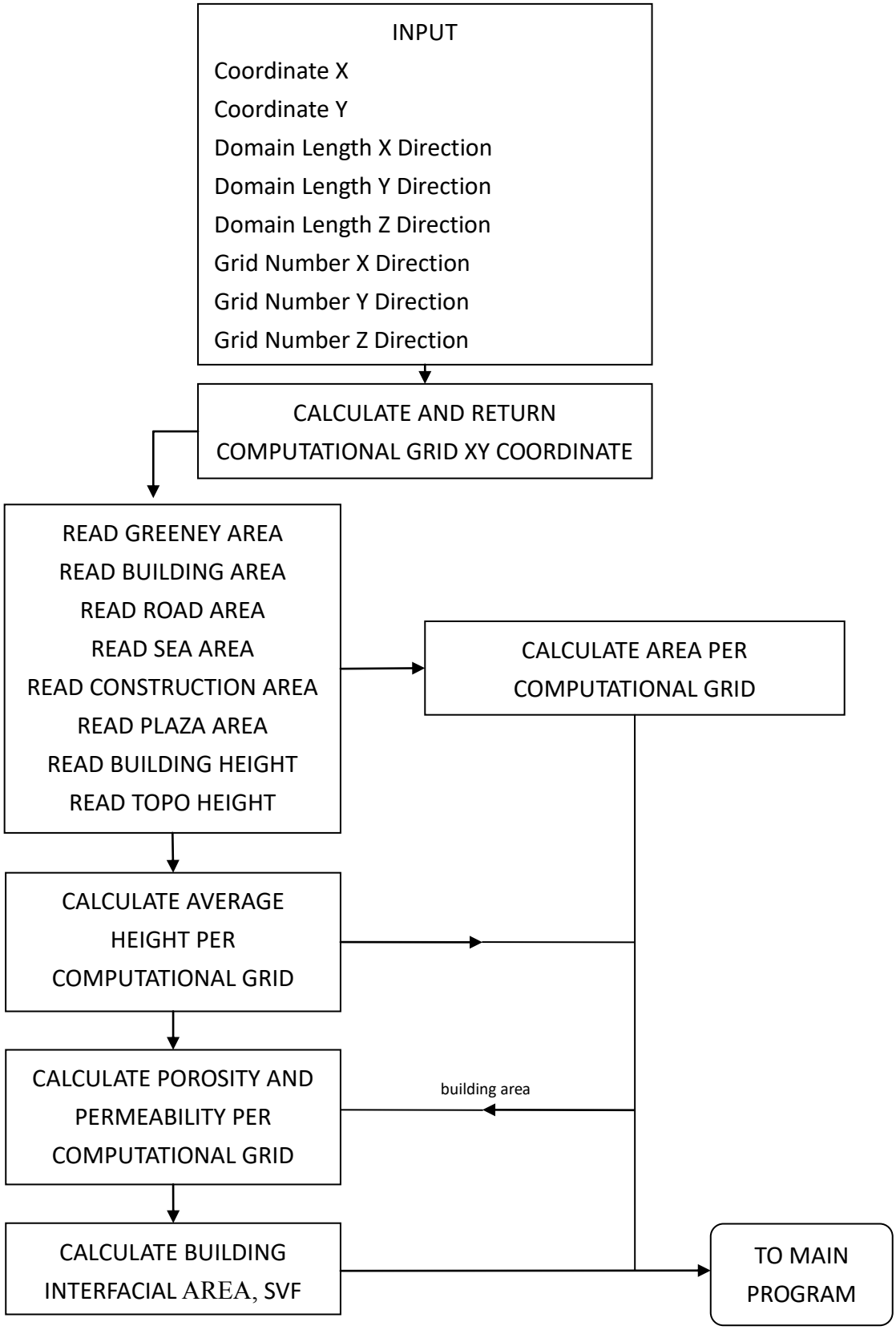

Figure C5. 3 Flow chart of Urban Density Database

CALCULATE MOMENTUM EQUATION

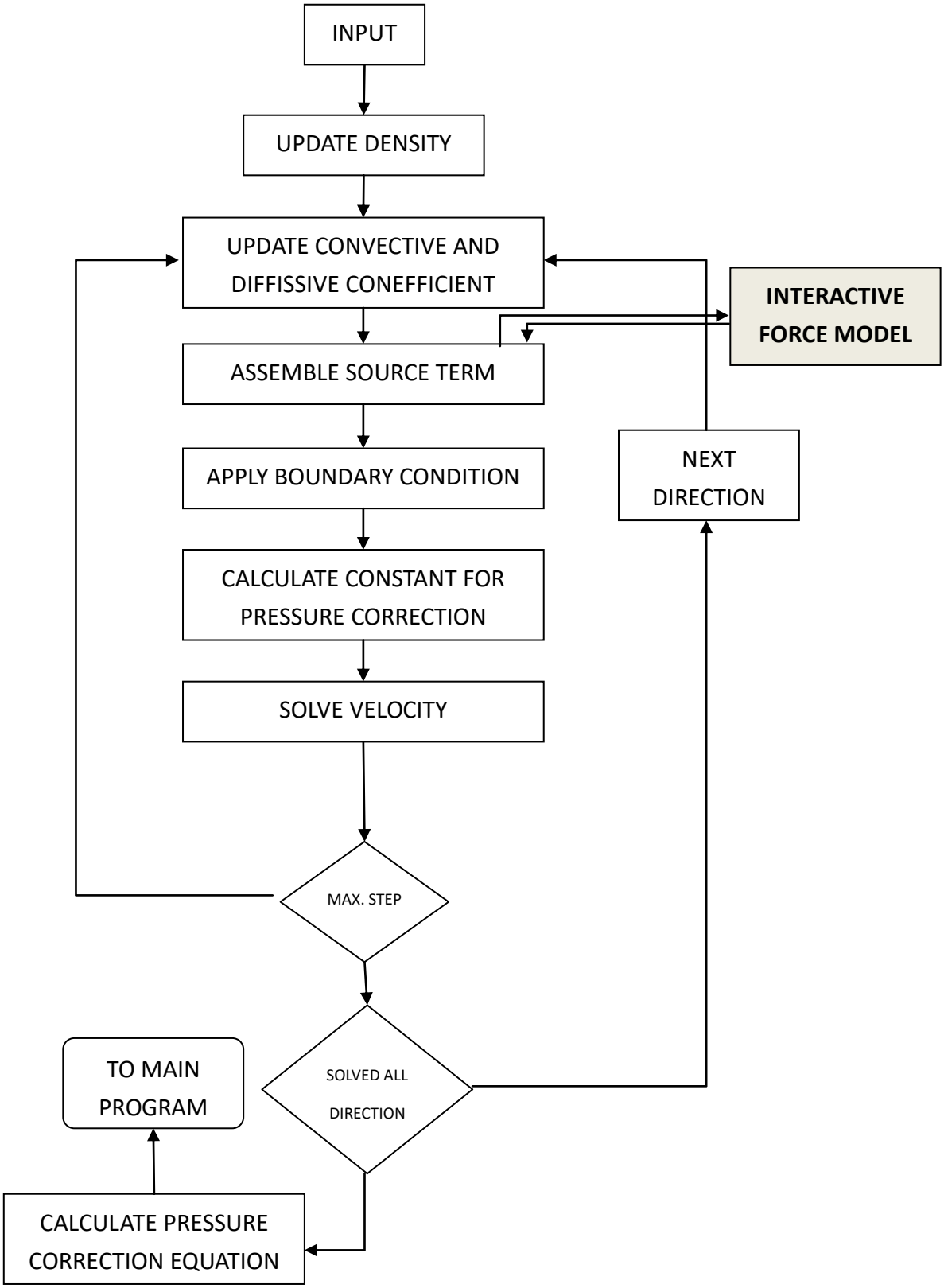

Figure C5. 4 Flow chart of Momentum Equation

CALCULATE PRESSURE CORRECTION EQUATION

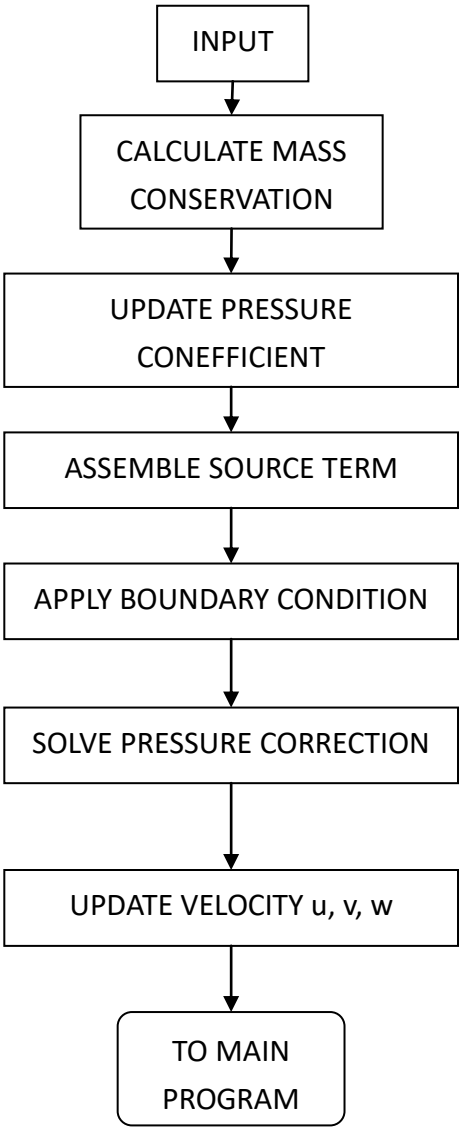

Figure C5. 5 Flow chart of pressure correction equation

CALCULATE ENERGY EQUATION

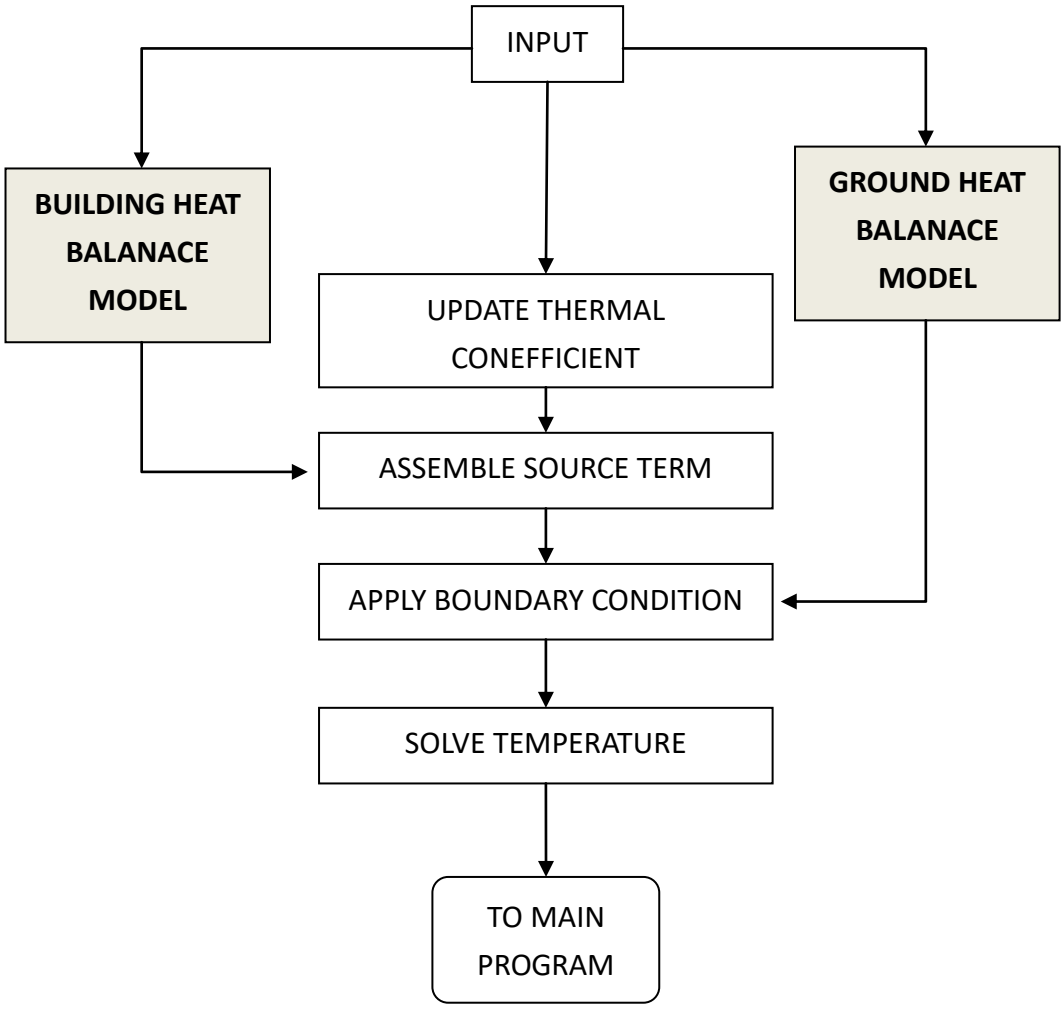

Figure C5. 6 Flow chart of energy equation

CALCULATE GROUND HEAT BALANACE EQUATION

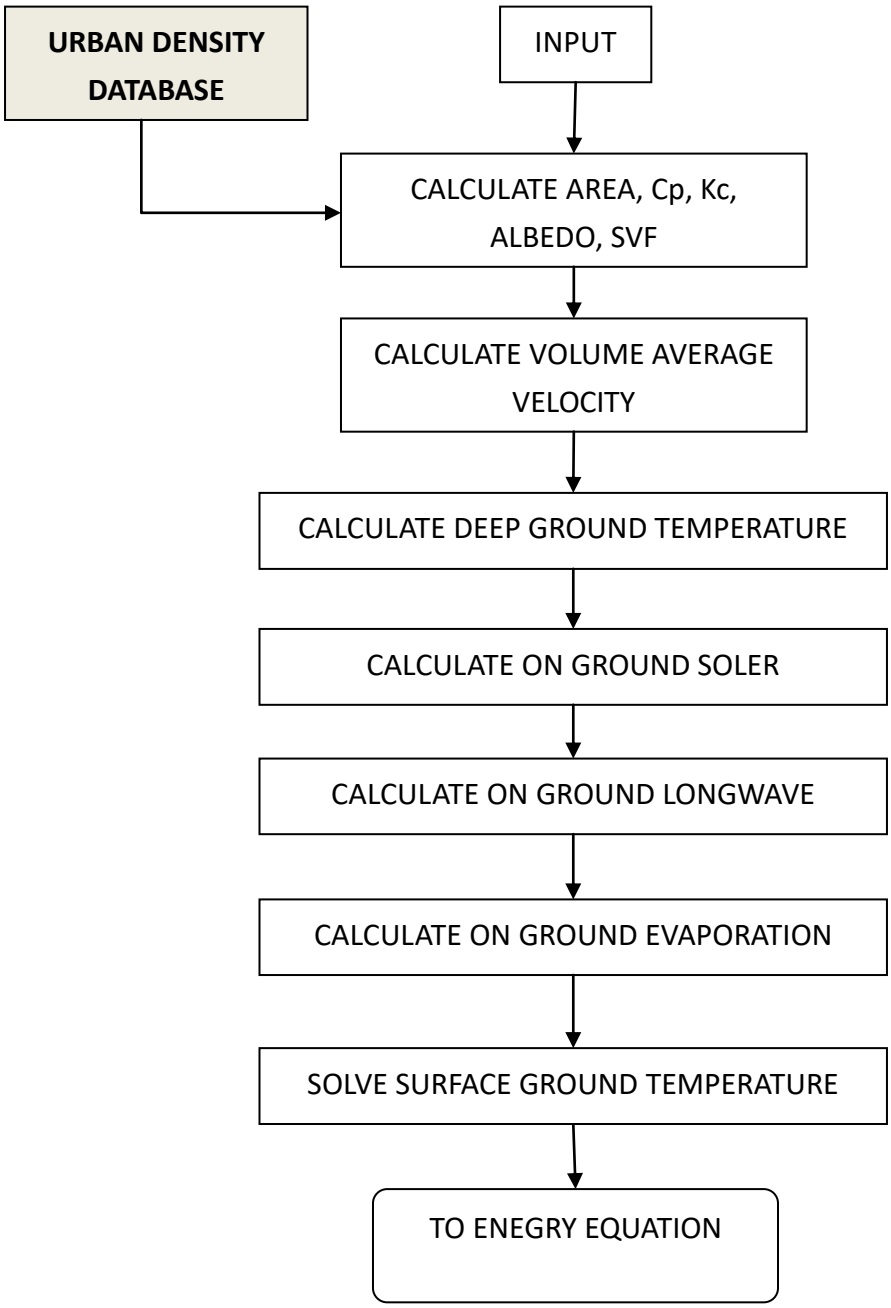

Figure C5. 7 Flow chart of ground heat balance equation

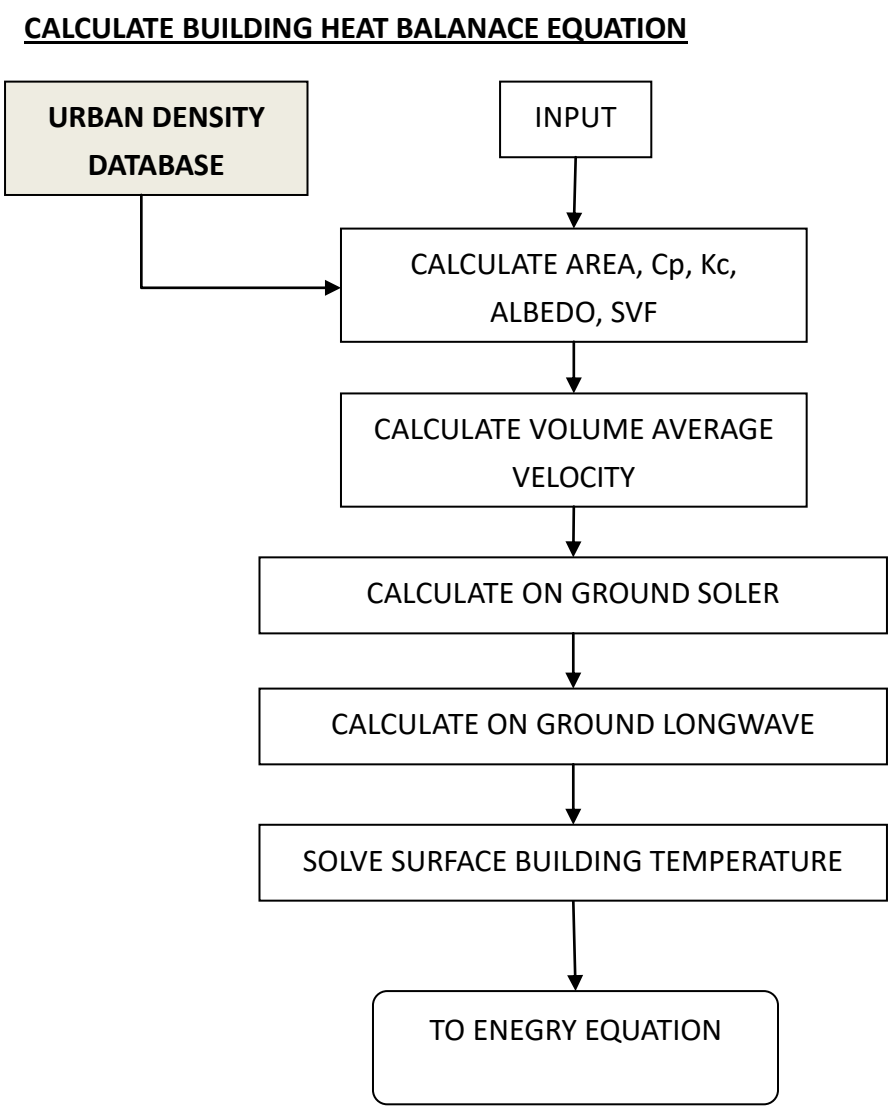

Figure C5. 8 Flow chart of building heat balance equation

5. 7 Summary

This Chapter has discussed the discretization form of the volume averaged Momentum Equation, volume averaged Energy Equations as well as the sub-models of Ground Energy Balance Model, Building Energy Balance Model. The details of the discretization form are given in Section 5.2 to 5.6.

During the discretization process, Fully Implicit Scheme is used for the discretization of the equation for the new model. This method would provide extra stability for the iteration step and allows larger time step in solving the PDE.

Furthermore, Cartesian grids method is used for computational grid in the new UHI Model. The Volume Averaging Approach allows the new model does not require to create the actual physical geometry. The geometry effect is replaced by the porosity and permeability of each control volume. Since the actual physical geometry is not require in the UHI model, and it also minimize the requirement of fine grid size at specific locations and allowing new UHI model can simply apply Cartesian grids method. Thus, this approach reduces the complicity of grid generation and iteration time.

A new computational code and control work flow has been developed for UHI Model and presented in Appendix B and Figure C5.2 to Figure C5.8. Unlike traditional CFD approach program, this new UHI model requires to connect to Urban Density Database and three sub-model, i.e. (1) the interactive force model, (2) building heat balance model and (3) ground heat balance model.

The development of the Urban Density Database has been introduced in order to capture the essential information from the GIS data, such as the average building height, average topo height, average building area, average greenery area, average water bodies area, average road area and average plaza area. However, since there are no researchers has developed the UHI

model using the volume averaging method, the standard CFD program is not able to connect the Urban Density Database as well as Interactive Force Model, Ground Energy Balance Model, Building Energy Balance Model together with the volume averaged governing equation. Therefore, as part of the thesis development it is requires to develop a unique program for the UHI Model that able to connect the database, volume averaged governing equation and the sub-models.

Chapter 6 Weather Data Analysis

Input boundary condition is essential to CFD modelling. There is different type of information can be input in boundary including air temperature profile, wind profile, pressure profile, turbulence intensity profile and etc. For UHI modelling, one of the essential input boundary information is the air temperature profile. This information can usually obtain from the weather station nearby the domain boundary location.

However, there may not be a reference weather station near the boundary location due to the large domain size requirement of the urban heat island model. For example, the Tsim Sha Tsui case study given in Chapter 7, the boundary location at ocean area at east, south and west directions, whereas the incoming wind is from the west boundary. Thus, there is no air temperature can be obtained since there are no weather station from near the west boundary location.

It is necessary to select a rural weather station for this UHI model, whereas the air temperature profile have no significant impact from the urban content of Hong Kong. The temperature profile at the boundary will be assumed same as the rural weather station, while the new UHI model will simulate the heat transfer as the air enter the domain.

In this Chapter, Section 6.1 to Section 6.4 introduce the method of collecting and analysing of measurement weather data from different Hong Kong areas. The sections also present the findings of the weather data among in 2015 from public weather stations and private weather stations. Fung Wing Yee (2009) suggest using Ta Kwu Ling (TKL) weather station as the reference rural area for urban heat island study based on the weather data between 1994 to 2004. Section 6.4 further present using Urban Density Database to classification the weather measurement locations to rural and urban area based on the “area classification criteria” from

Fung Wing Yee (2010). The weather data from 9 selected stations during summer period are used to compare with TKL weather data to formulae the UHI intensity (UHII) to check whether the data is suitable to be used as reference of rural area.

In Section 6.5 onward, the chapter presents the UHI intensity (UHII) using the Ta Kwu Ling (TKL) weather station as reference rural weather and compare with other UHI study of Hong Kong. The UHII variation of both studies has shown a strong similarity and indicating that using TKL weather data is suitable reference rural station and shall be used as the reference air temperature profile for the UHI modelling.

This is essential for this thesis, the Ta Kwu Ling temperature profile would be used as the temperature input boundary of the all urban area UHI simulation. The difference between the Ta Kwu Ling temperature profile and the simulated urban area temperature profile would be used to calculate the UHI intensity (UHII). A case study in Chapter 7 has further analysed the UHI intensity of Tsim Sha Tsui used the Ta Kwu Ling temperature profile as the reference rural weather for compassion.

6. 1 Urban Heat Island Intensity

Urban Heat Island effects the urban temperature throughout the day. Due to the presence of heat emission and thermal inertia in roads, buildings, and other structures that prevent the urban space from cooling down, Oke (1987) has recorded the maximum intensity of heat island occurs 3 to 5 hours after sunset. The urban heat island intensity (UHII) is used to quantify the urban heat island impact. It generally defined as temperature differences between urban areas and reference areas.

$$UHII = T_u - T_r \qquad \text{(Equation C6. 1)}$$

where T_u is the air temperature (°C) in urban area and T_r is the air temperature (°C) in the reference area.

Using fixed station to analysis Urban Heat Island Effect is a common approach. Many researchers have used this approach to study the heat island intensity. Tso (1996) has measured the heat island intensity is around 3℃ in Singapore. A study[6] of the Hong Kong Polytechnic University has measured the temperature differences between rural areas and city downtown of Hong Kong has a range of 1.5 to 4°C in summer daytime and 2 to 6.5°C in winter daytime. Giridharan (2005) has studied the maximum nocturnal UHI intensity was ranging from 0.4℃ to 1.3℃.

6. 2 HKO Public Weather Stations

It has been a long debate whether which public weather is urban or rural. HKO Headquarters (HKOH) and King's Park weather stations are located in Kowloon districts which are a high-density populated areas. Fung Wing Yee (2009) suggested that HKO Headquarters and King's Park weather stations could be defined as urban areas, while all other HKO stations would be defined as a suburban or rural area. In this study, HKOH is one of the key urban stations for fixed station data analysis.

Fung Wing Yee also suggested that the weather station in Hong Kong International Airport (HKA) is located in a reclamation area and therefore air temperature is highly dominated by its large concreted area natural. Thus, HKA station is not a suitable representative rural reference point in Hong Kong.

Fung Wing Yee suggests Ta Kwu Ling (TKL) as another reference station. It is located in the northern region of Hong Kong with generally low-density building and population environment. The station is one of the most undeveloped regions in Hong Kong.

[6] http://www.mypolyuweb.hk/lswong/homepage/UHI/index.html

6. 3 Community Weather Station

Since the public weather stations are mainly located in suburban and rural areas. Several near-surface air temperatures can be collected from private weather station website called Hong Kong Community Weather Information Network[7].

6. 4 Recorded Weather Data

Currently, there is not many UHII measurement has been conducted for Hong Kong except the work of Fung Wing Yee (2010). Fung Wing Yee analysed the air temperature and UHII from HKOH and TKL for 11 years (1994 - 2004). Fung Wing Yee also classified HKOH is an urban station and TKL is a suburban station and concluded that the HKOH has the highest monthly air temperature among all other selected stations.

This thesis has further analysed the air temperature and UHII condition during 2015 and compares to the previously 11 years measured data (1994 - 2004). A total of 5 HKO stations and 4 community stations were selected. The locations of the selected stations are marked in Table C6. 2 below.

Fung Wing Yee (2010) has also suggested criteria for station type classification to separate out the rural and urban condition, as shown in Table C6. 1. This thesis applied the Urban Density Database to classify the weather station for urban station, suburban station and rural station using a grid resolution range of 100m × 100m. Based on the analysis, Hong Kong Observatory, Ling Liang Church M H Lau Secondary School, Discovery College, China Holiness Church Living Spirit College and Chiu Chow Association Secondary School were grouped as urban station and other are rural stations.

[7] http://www.hko.gov.hk/education/edu04other/edu04_public0803_e.htm

Table C6. 1 Area classification criteria suggested from Fung Wing Yee (2010)

Criteria	**Urban**	**Suburban**	**Rural**
Built-up area (%)	>26	11 – 25	<10
Building type	>10 storey	3 – 10 storey	1-2 storey

Table C6. 2 Area classification criteria for the selected weather station

Station	x-axis	y-axis	using the built-up area consists of building, road and plaza areas. [8] (m)	Area Category
Hong Kong Observatory	835987	818113	36.6%	Urban
Lau Fau Shan	816375	836609	5.3%	Rural
Cheung Chau	862134	845230	0.0%	Rural
Ta Kwu Ling	834191	843209	4.8%	Rural
Waglan Island	849310	804859	10.0%	Rural
Ling Liang Church M H Lau Secondary School	836336	833433	35.2%	Urban
Discovery College	819517	818335	68.8%	Urban
China Holiness Church Living Spirit College	835949	835240	40.6%	Urban
Chiu Chow Association Secondary School	841735	830782	34.8%	Urban

[8] Built-up area consists of building, road and plaza areas.

6. 5 Annual Trend Analysis

HKOH is selected as an urban station to compare with the other stations. Annual heat island intensity between the urban station (HKOH) and four other stations (CCH, LFS, TKL, and WGL) was analysed. HKOH-CCH and HKOH-TKL have observed a significant trend, while HKOH-WGL had decreased to the 1.6 ℃ difference. For HKOH-LFS, it has a weak decreasing trend. The data from 1994 to 2004 is made referenced to Fung Wing Yee (2010) Study. The results finding is similar as compared to the works of Fung Wing Yee. However, at that time he indicated that there is no consistent observation can be drawn from the annual trend analysis. However, in 2015, it is observed that the temperature difference of HKOH-CCH and HKOH-TKL has observed significantly increased, while the temperature difference of HKOH-WGL is significantly reduced. The average UHII for 1994 to 2004 and 2015 is showed in Figure C6. 1 and Table C6. 3. It can be concluded that the UHI has significantly increased around HKOH.

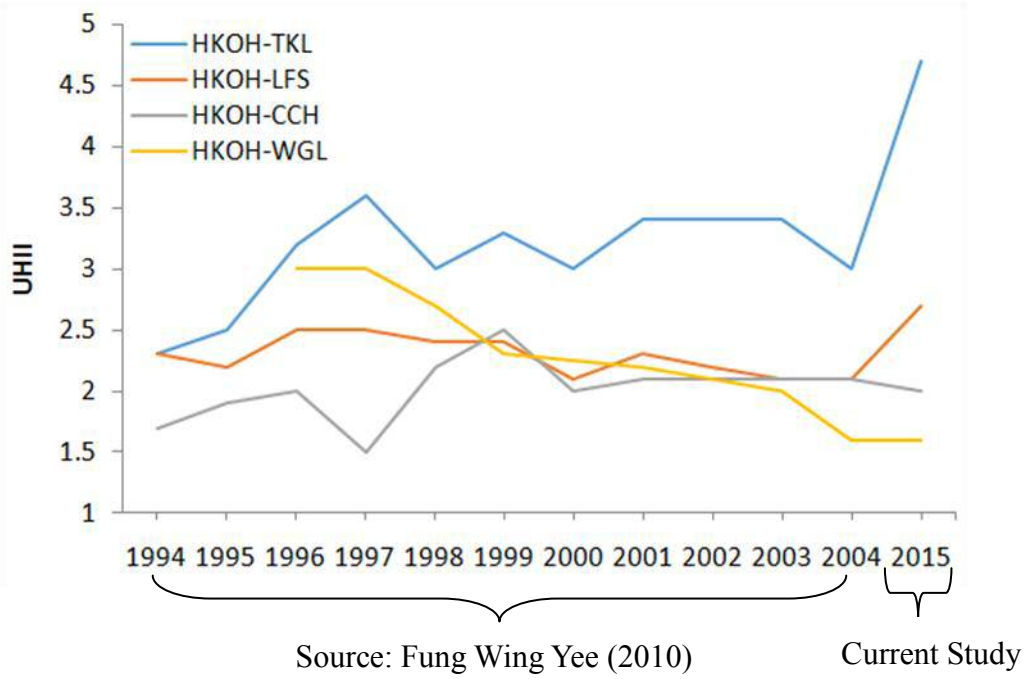

Figure C6. 1 Urban Heat Island Intensity 1994 to 2004 and 2015

Table C6. 3 Urban Heat Island Intensity 1994 to 2004 and 2015

Stations	Average of $UHII_{max}$ from 1994 to 2004 (℃)	Average of $UHII_{max}$ of 2015 (℃)
HKOH- CCH	2.0	2
HKOH- WGL	2.3	1.6
HKOH- LFS	1.8	2.7
HKOH- TKL	3.4	4.7

6. 6 Diurnal Trend Analysis

Diurnal variation of the heat island intensity among the stations was further investigated. Average diurnal variation of the heat island intensity is plot against each hour in Figure C6. 2. The mean hourly UHII was calculated by averaging hourly temperature difference between urban and suburban or rural station at 2015. In general, the maximum heat island intensity usually occurs at night and the minimum UHII usually the daytime.

The positive UHII indicated that the urban station – HKOH has a higher temperature than the rural station, while negative UHII indicated the urban station – HKOH has a lower temperature. Taken HKOH–LFS as an example, the positive UHII is from 18:00-8:00, while the negative UHII happened during daytime around 9:00 – 17:00. The results find indicated that the heat island effects occur after the sunset and can last until next day. That is inconsistent as compared with the Oke (1987) findings, which the heat island effects occur 3-4 hours after the sunset.

The negative UHII indicated that the urban weather station has a lower air temperature as compared to the suburban weather station. Fung Wing Yee (2009), suggest this phenomenon could be due to “Cool Island Effect”.

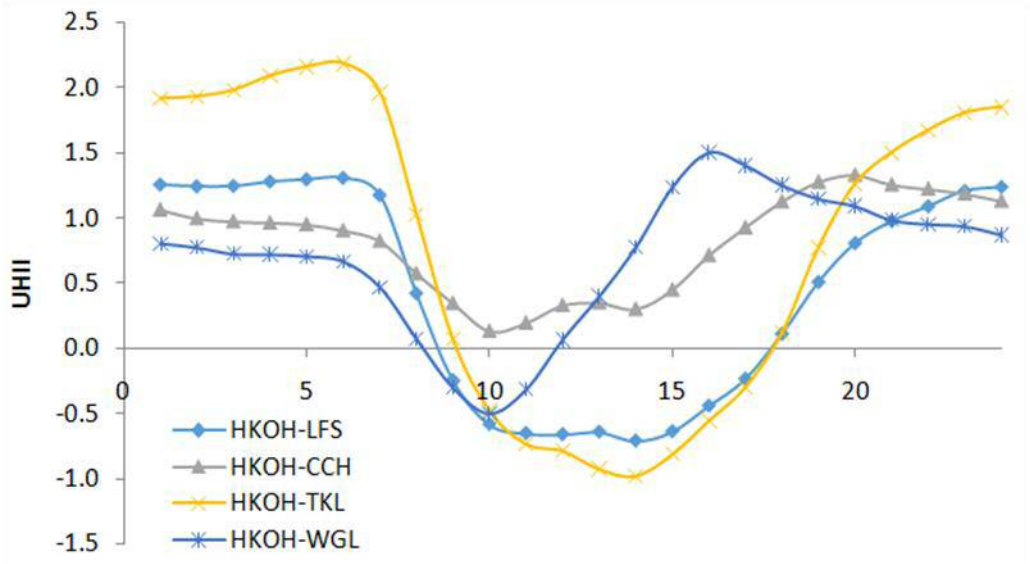

Figure C6. 2 Diurnal variation of the heat island intensity

The frequency distribution of the daily maximum heat island intensity is shown in below. The average maximum UHII was 2.7℃ and ranging from -1.9℃ and 11.5℃

6. 7 Further Analysis among Other Stations

Average the UHII among June (summer) 2015 and January (winter) 2015 is divided into the morning (6AM to 12NOON), afternoon (12NOON to 6PM) and evening (6PM to 12AM) periods for further analysis. The UHII is calculated by the hourly air temperature from each selected station and subtract the air temperature from the referenced rural station. In this study, Ta Kwu Ling (TKL) is selected for the referenced rural station as suggested by Fung Wing Yee (2009). TKL is a public weather station operated by HKO. It is located in a northern region of Hong Kong and the surrounding building environment is generally village type. This station is also recommended by Fung Wing Yee Study as a referenced. Through our density analysis, it surrounding built environment (within 100m × 100m) is digitizing into the density analysis parameters. Figure C6. 3 shows the aerial photo and density information of Ta Kwu Ling Station.

Ta Kwu Ling	Rural Area
X: 834191 Y: 843209 Built-up Area: 4.8% Non Built-up Area: 95.2% Average Terrain Elevation: 12.5mPD Average Building Height: 5.6m	Building: 2.0% Road: 0.0% Construction: 2.8% Tree: 57.0% Greenery: 38% Plaza: 0.0% Sea / water body: 0.2%

Figure C6. 3 Aerial photo and density information of Ta Kwu Ling station (Source: Lands Department GeoInfo Map)

For summer period, there is total of 9 weather stations to compare with the TKL rural station. They are Cheung Chau (CCH), Hong Kong Observatory Headquarter (HKO), Cheung Chuk Shan College (CCSC), Discovery College (Dis), Ling Liang Church M H Lau Secondary School (Ling), The Hong Kong Polytechnic University (PolyU), HKFYG Lee Shau Kee College (HKFYG), Lai Chack Middle School (LCMS) and The Chinese Foundation Secondary School (CFSS). Similar, their surrounding built environment (within 100m × 100m) is digitizing into the density analysis parameters through our density analysis.

Cheung Chau (CCH) Weather Station

Cheung Chau (CCH) is a public weather station operated by HKO. Cheung Chau is an island and located in a southern region of Hong Kong. The weather station is situated at a high ground at 18.6 mPD. The nearby surrounding building environment is generally a non-building area with villages at the downhill region. Thus, it is expected the site is quite high wind speed from the sea breeze. Figure C6. 4 shows the aerial photo and density information of Cheung Chau Station.

Cheung Chau (CCH)	Rural Area ~ Windy
X: 862134 Y: 845230 Built-up Area: 0.0% Non Built-up Area: 100.0% Average Terrain Elevation: 18.6mPD Average Building Height: 18.2m	Building: 0.0% Road: 0.0% Construction: 0.0% Tree: 50.4% Greenery: 49.6% Plaza: 0.0% Sea / water body: 0.0%

Figure C6. 4 Aerial photo and density information of Cheung Chau Station (Source: Lands Department GeoInfo Map)

Hong Kong Observatory Headquarter (HKO) Weather Station

Hong Kong Observatory Headquarter (HKO) station is located in the center of Kowloon at the Tsim Sha Tsui Area. It is one of the highest density regions in Hong Kong. It is also a city center and expected to have a high level of human activity during night time. There is a public park surrounding the weather station. Our analysis shows that it consists of around 36.6% build up area. Figure C6. 5 shows the aerial photo and density information of Hong Kong Observatory Headquarter Station.

Hong Kong Observatory Headquarter (HKO)	Urban Area
X: 835987 Y: 818113 Built-up Area: 36.6% Non Built-up Area: 63.4% Average Terrain Elevation: 11.0mPD Average Building Height: 35.1m	Building: 18.4% Road: 10.6% Construction: 7.4% Tree: 29.4% Greenery: 30.6% Plaza: 0.0% Sea / water body: 3.4%

Figure C6. 5 Aerial photo and density information of Hong Kong Observatory Headquarter Station (Source: Lands Department GeoInfo Map)

Cheung Chuk Shan College (CCSC) Weather Station

Cheung Chuk Shan College (CCSC) is located on the Hong Kong Island in North Point District. It is a private weather station and measurement sensor is located on the rooftop. At the northern, eastern and western region, it is generally high-rise and mid-rise buildings, while the southern region is generally greenery area. Even though the area is surrounded by building clusters, the site is actually situated on a high ground. Thus, the site can still enjoy the sea breeze from victory harbour. Figure C6. 6 shows the aerial photo and density information of Cheung Chuk Shan College (CCSC) Station.

Cheung Chuk Shan College (CCSC)	Urban Area ~ Windy
X: 838233 Y: 816336 Built-up Area: 65.6% Non Built-up Area: 34.4% Average Terrain Elevation: 86.2mPD Average Building Height: 51.6mPD	Building: 28.8% Road: 28.6% Construction: 8.2% Tree: 14.4% Greenery: 16.6% Plaza: 0.0% Sea / water body: 3.4%

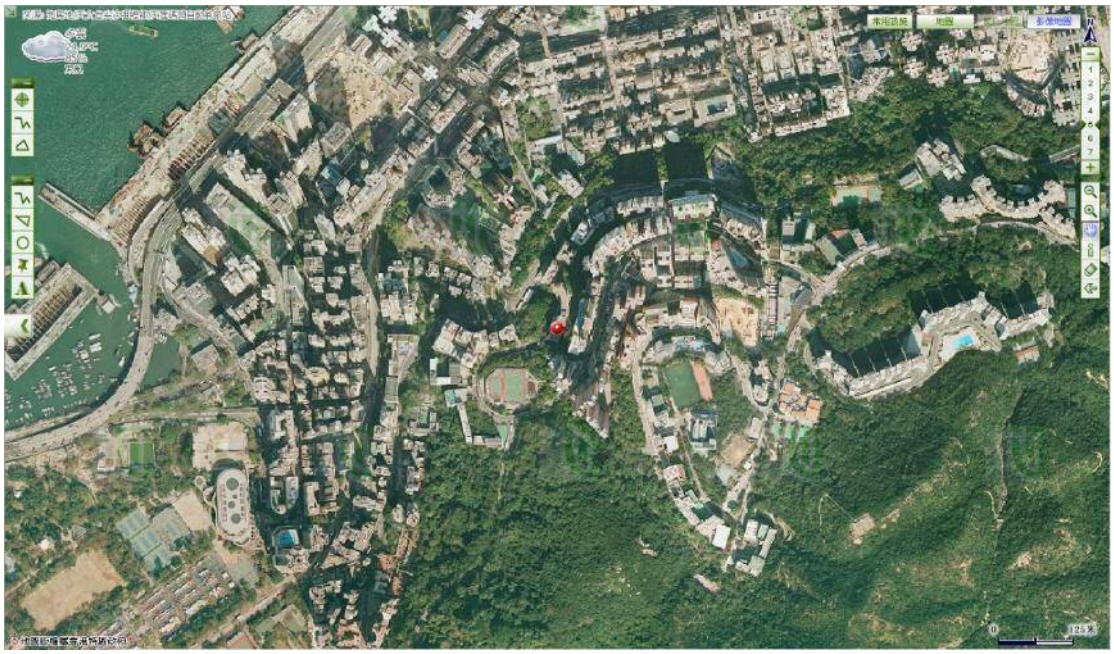

Figure C6. 6 Aerial photo and density information of Cheung Chuk Shan College (CCSC) Station (Source: Lands Department GeoInfo Map)

Discovery College (Dis) Weather Station

Discovery College (Dis) is located at the east of Lantau Island. It is a private weather station and measurement sensor is located on the rooftop. In general, the area mainly consists of high-density low rise building clusters. Due to the large building structure of the college, our analysis shows that it consists of around 68.8% builds up area. According to the Area Classification Criteria, it's area category belonged to an urban area. Figure C6. 7 show the aerial photo and density information of Discovery College (Dis) Station.

Discovery College (Dis)	Urban Area ~ Low Rise
X: 838233 Y: 816336 Built-up Area: 68.8% Non Built-up Area: 31.2% Average Terrain Elevation: 18.4mPD Average Building Height: 25.2m	Building: 58.8% Road: 7.2% Construction: 2.4% Tree: 14.4% Greenery: 20.8% Plaza: 8.0% Sea / water body: 0.6%

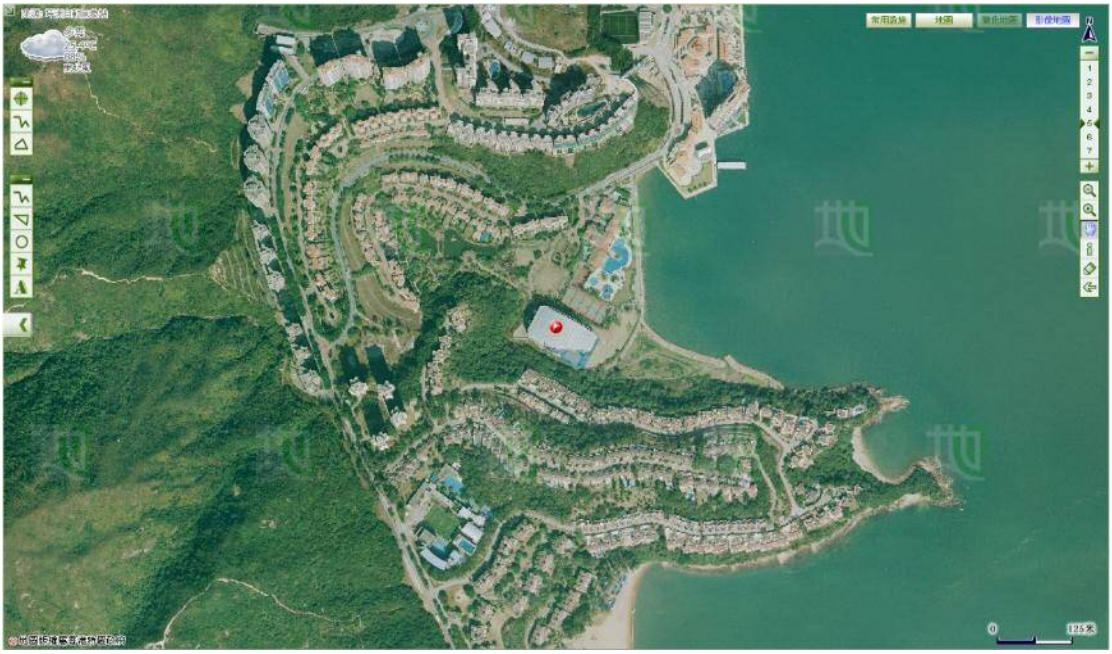

Figure C6. 7 Aerial photo and density information of Discovery College (Dis) Station (Source: Lands Department GeoInfo Map)

Ling Liang Church M H Lau Secondary School Weather Station

Ling Liang Church M H Lau Secondary School is located a northern part of Hong Kong within the Ta Po Area. It is situated on a small hill along the coastline which is expected to enjoy the good amount of land breeze and sea breeze throughout the year. Our analysis shows that the area consists of around 47.6% and 17% of tree and greenery area, respectively. Figure C6. 8 the aerial photo and density information of Ling Liang Church M H Lau Secondary School (Ling) Station.

Ling Liang Church M H Lau Secondary School (Ling)	Urban Area
X: 836336 Y: 833433 Built-up Area: 35.2% Non Built-up Area: 64.8% Average Terrain Elevation: 47.5mPD Average Building Height: 50.5m	Building: 32.2% Road: 0.4% Construction: 2.6% Tree: 47.6% Greenery: 17.0% Plaza: 0.0% Sea / water body: 0.2%

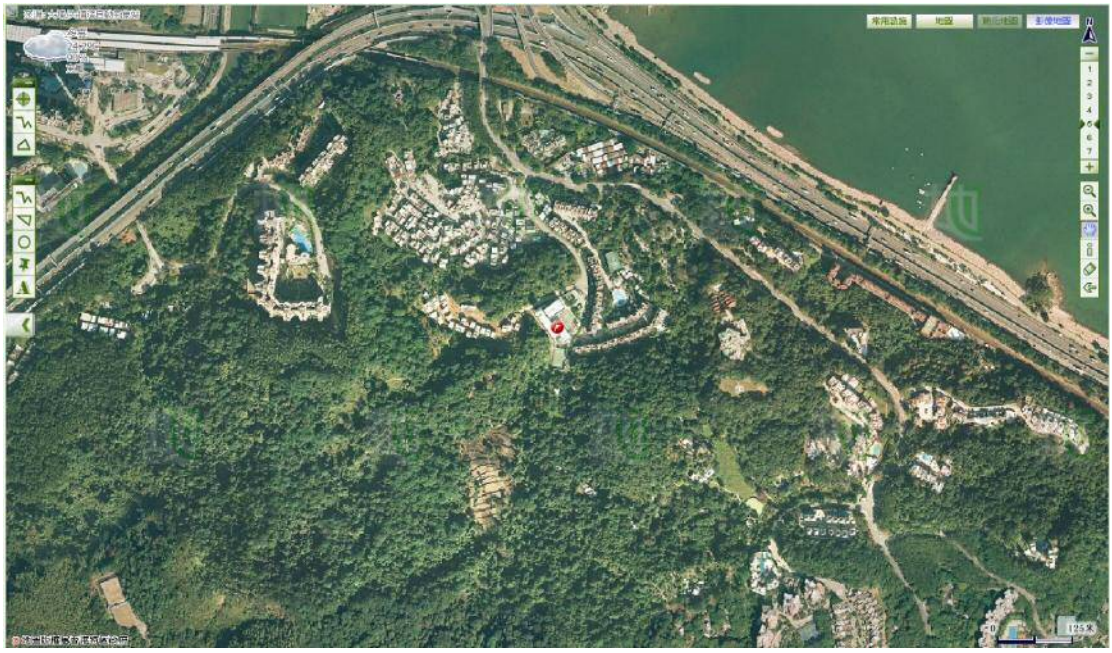

Figure C6. 8 Aerial photo and density information of Ling Liang Church M H Lau Secondary School (Ling) Station (Source: Lands Department GeoInfo Map)

The Hong Kong Polytechnic University (PolyU) Weather Station

The Hong Kong Polytechnic University (PolyU) is located in Tsim Sha Tsui Area, which is one of the highest density regions in Hong Kong. Our analysis shows that the building area is 86.2%, road area is 3.6%, construction area is 2.0% and plaza area is 7.8%, which makes the total build-up area over 90%. The area is expected to experience significantly urban heat island effect. Figure C6. 9 shows the aerial photo and density information of The Hong Kong Polytechnic University (PolyU) Station.

The Hong Kong Polytechnic University (PolyU)	Urban Area
X: 836578	Building: 86.2%
Y: 818267	Road: 3.6%
Built-up Area: 91.8%	Construction: 2.0%
Non Built-up Area: 8.2%	Tree: 0.2%
Average Terrain Elevation: 4.5mPD	Greenery: 0.0%
Average Building Height: 31.6m	Plaza: 7.8%
	Sea / water body: 0.2%

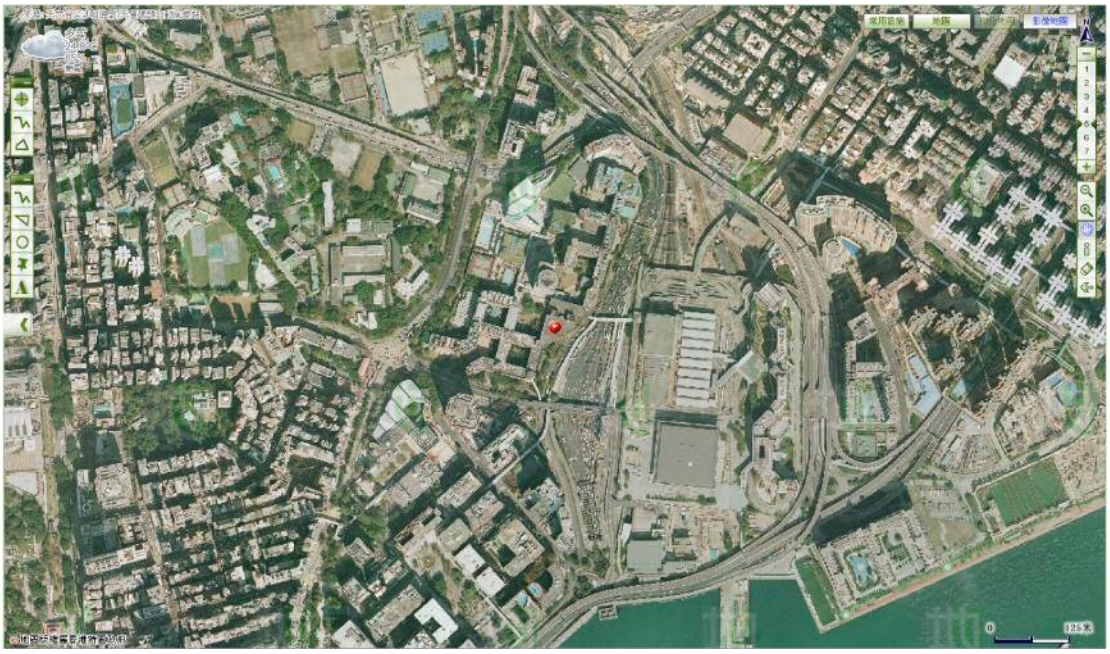

Figure C6. 9 Aerial photo and density information of The Hong Kong Polytechnic University (PolyU) Station (Source: Lands Department GeoInfo Map)

HKFYG Lee Shau Kee College (HKFYG) Weather Station

HKFYG Lee Shau Kee College (HKFYG) is located at the Tin Shui Wai in the northwest region of Hong Kong. Even through, the Tin Shui Wai is a remote area from the commercial center of Hong Kong. The area still has a quite high density of population and high-rise residential building. The measurement station is located in the urban fringe area between the Tin Shui Wai Town center and the wetland park of Hong Kong. Figure C6. 10 shows the aerial photo and density information of HKFYG Lee Shau Kee College (HKFYG) Station.

HKFYG Lee Shau Kee College (HKFYG)	Urban Area
X: 818520 Y: 835946 Built-up Area: 71.0% Non Built-up Area: 29.0% Average Terrain Elevation: 6.2mPD Average Building Height: 87.3m	Building: 59.8% Road: 5.0% Construction: 5.5% Tree: 4.0% Greenery: 0.0% Plaza: 23.5% Sea / water body: 1.2%

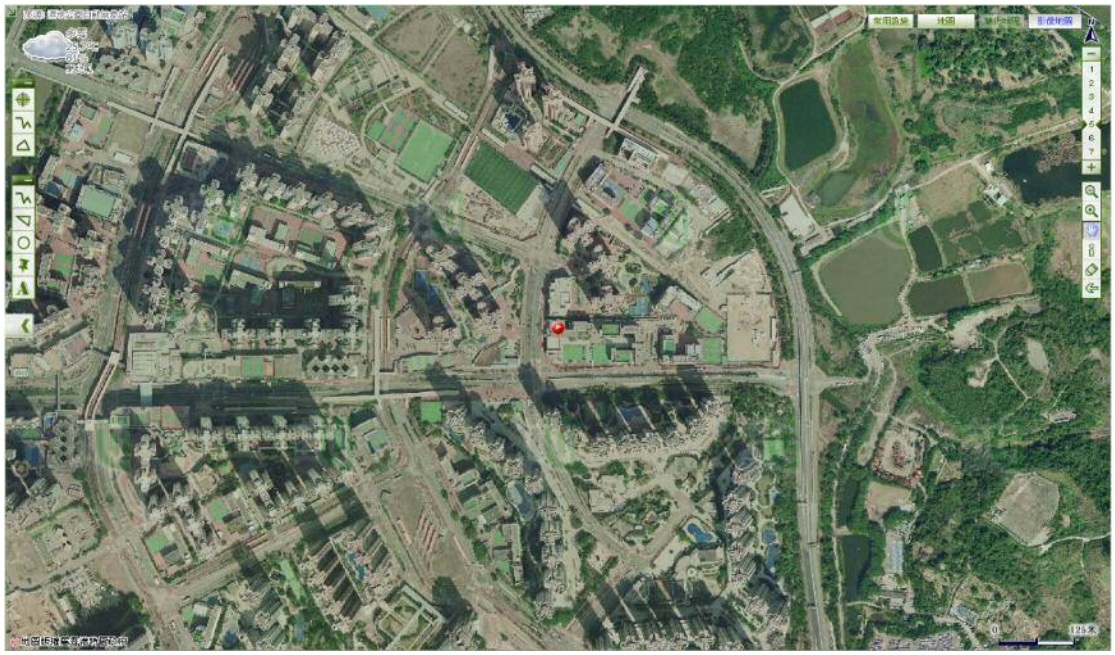

Figure C6. 10 Aerial photo and density information of HKFYG Lee Shau Kee College (HKFYG) Station (Source: Lands Department GeoInfo Map)

Lai Chack Middle School (LCMS) Weather Station

Similar to The Hong Kong Polytechnic University (PolyU), Lai Chack Middle School (LCMS) is also located in Tsim Sha Tsui Area. It is situated just beside the Kowloon Park. Kowloon Park is one of the largest urban parks in Hong Kong. Our analysis shows that the area consists of around 11.5% and 28.5% of tree and greenery area, respectively. It is expected the Kowloon Park and the sea breeze would induce some cooling effect to the area. Figure C6. 11 shows the aerial photo and density information of Lai Chack Middle School (LCMS) Station.

Lai Chack Middle School (LCMS)	Urban Area
X: 835394 Y: 818064 Built-up Area: 59.8% Non Built-up Area: 40.3% Average Terrain Elevation: 9.6mPD Average Building Height: 46.1m	Building: 52.3% Road: 0.0% Construction: 7.5% Tree: 11.5% Greenery: 28.5% Plaza: 0.0% Sea / water body: 0.5%

Figure C6. 11 Aerial photo and density information of Lai Chack Middle School (LCMS) Station (Source: Lands Department GeoInfo Map)

The Chinese Foundation Secondary School (CFSS) Weather Station

The Chinese Foundation Secondary School (CFSS) is also located in an urban fringe area with consists of around 32.5% and 26.8% of tree and greenery area, respectively. Figure C6. 12 shows the aerial photo and density information of The Chinese Foundation Secondary School (CFSS) Station.

The Chinese Foundation Secondary School (CFSS)	Urban Area
X: 833957 Y: 821933 Built-up Area: 40.6% Non-Built-up Area: 59.4% Average Terrain Elevation: 5.3mPD Average Building Height: 36.9	Building: 27.8% Road: 23.2% Construction: 5.1% Tree: 19.6% Greenery: 20.7% Plaza: 0.0% Sea / water body: 1.8%

Figure C6. 12 Aerial photo and density information of The Chinese Foundation Secondary School (CFSS) Station (Source: Lands Department GeoInfo Map)

6. 8 Summer June 2015 Morning (6AM to 12NOON)

According to HKO weather data, June 2015 was the hottest June in Hong Kong since records began in 1884. Since the TKL is a rural area, it has less shading and thermal massing, it can quickly receive direct sunlight and release back to the environment. According to Fung Wing Yee (2009), TKL also has low wind conditions and less affected by the sea breeze, thus it is expected the temperature variation is dominated by the solar irradiation.

The June morning mean temperature of TKL is 30.0℃, June mean morning minimum temperature of TKL is 25.3℃ and the June morning mean maximum temperature of TKL is 34.8 ℃. At 6AM, the mean air temperature is around 26.1℃ and quickly rises up to around 30.4℃ at 9AM. At 11AM, the temperature trend to rise slowly and reach 30.9℃. The hourly June morning mean temperature of TKL (6AM – 12NOON) is given in Figure C6. 13.

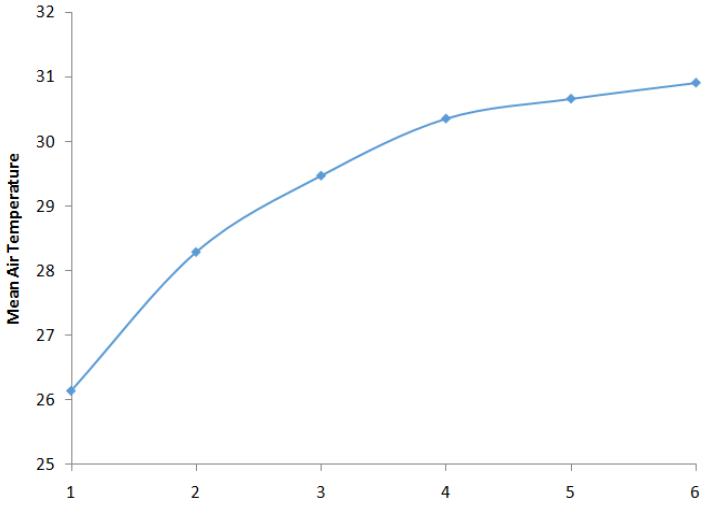

Figure C6. 13 Hourly June morning mean temperature of TKL (6AM – 12NOON)

The mean air temperature distribution during 2015 June morning (6AM – 12NOON) is shown in Figure C6. 14. The results showed that all stations had recorded a negative UHII during the summer morning period from 7AM onward. From a statistical point of view, the air temperature in TKL (rural station) is generally higher than the other stations. The recorded air temperature findings are also in-line with Fung Wing Yee data analysis from 1994 to 2004

weather data.

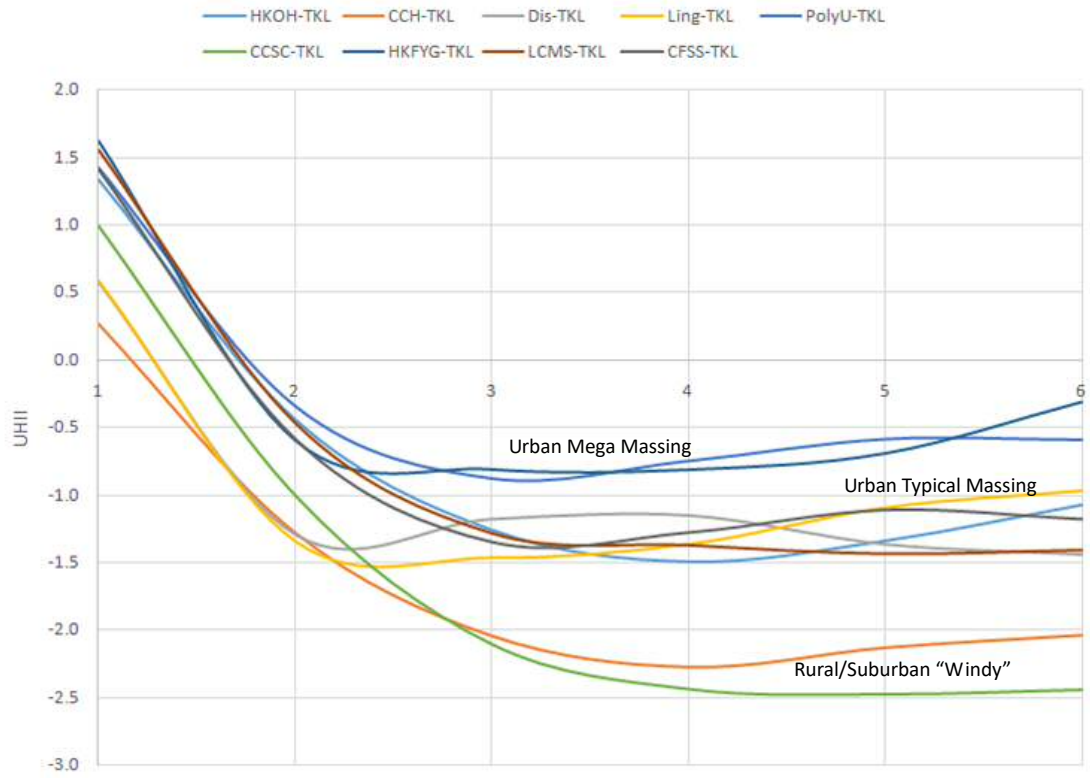

Figure C6. 14 Air temperature distribution during 2015 June morning (6AM – 12NOON)

The first group has the smallest negative UHII with a value from 1.4℃ to -0.9℃. The results indicated that the areas fall within this group would have a temperature generally rise along with TKL. In our selected weather stations, HKFYG and PolyU belong to this group. Based on our analysis, both stations are classified as an urban area. Compares to other urban stations, HKFYG and PolyU have the largest amount of built up areas as well as buildings area density.

The second group has an average UHII value ranging from 1.5 ℃ to -1.5℃. The results indicated that the air temperature within this group would not rise up as fast as TKL. The stations within this group are all belonged to urban stations with "Typical Massing", including Dis, Ling, CCSC, LCMS and CFSS.

The last group has the highest negative UHII with a value ranging from -1.0℃ to -2.5℃. The results indicated that the air temperature within this group would rise much less than TKL. The stations within this group are CCH and CCSC. The built environment of CCH and CCSC are belonged to rural and suburban areas, respectively. Their built up areas are close to TKL. However, both areas are located at high ground and close to the waterfront, the windy condition has greatly reduced the temperature rise of the areas.

In general, CCH and CCSC stations had received the lowest $UHII_{ave}$. Their $UHII_{max}$ and $UHII_{min}$ value is at the low-end region as compare to other stations. It suggested that the air temperature rise at the morning is slow throughout June. It is mainly beneficial by the sea breeze effect, which it could effectively remove the heat gain from the solar irradiation.

For the urban area with mega massing, the $UHII_{ave}$ is the highest, while there is no clear trend for the $UHII_{max}$ and $UHII_{min}$ value as compared with other urban stations. Table C6. 4 shows the average UHII of each station in 2015 June morning.

Table C6. 4 Average UHII of each station in 2015 June morning

Station	$UHII_{max}$	$UHII_{min}$	$UHII_{ave}$	Area Cat.
CCH	1.7	-4.1	-1.6	Rural
CCSC	2.8	-4.1	-1.6	Suburban
HKO	3.1	-2.7	-0.7	Urban
Dis	1.9	-4.7	-1.0	Urban
Ling	2.1	-4.2	-1.0	Urban
PolyU	3.7	-3.6	-0.3	Urban
HKFYG	2.7	-3.0	-0.3	Urban
LCMS	3.3	-3.8	-0.7	Urban
TCFSS	3.1	-3.3	-0.7	Urban

6. 9 Summer June 2015 Afternoon (12NOON to 6PM)

The June afternoon mean temperature of TKL is 31.8℃, June afternoon mean minimum temperature of TKL is 26.0℃ and the June afternoon mean maximum temperature of TKL is 35.8 ℃. The air temperature of TKL would reach the peak at 12NOON with a value of 31.5℃. Unlike morning, the air temperature of TKL in the afternoon is generally in a slow decreasing trend dropping from 31.5℃ and reaches 29.8℃at around 5PM. The hourly June afternoon mean temperature of TKL (12NOON – 6PM) is given in Figure C6. 15.

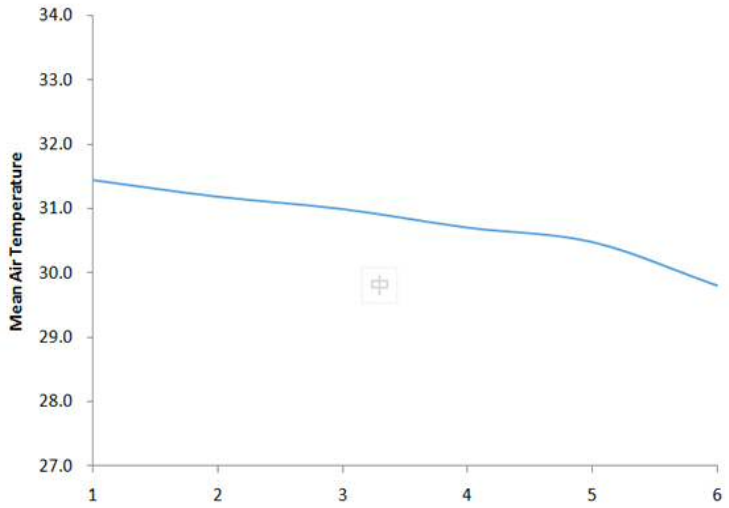

Figure C6. 15 Hourly June afternoon mean temperature of TKL (12NOON – 6PM)

The average air temperature distribution during 2015 June afternoon (12NOON-6PM) is given in Figure C6.16. The results generally showed that all stations had a negative UHII during the afternoon period from 7AM onward. From a statistical point of view, the air temperature in TKL (rural station) is generally higher than the other stations. The recorded air temperature findings are also in-line with Fung Wing Yee data analysis from 1994 to 2004 weather data.

The first group has the smallest negative UHII with a value ranging from -0.1℃ to -0.6℃. The results indicated that the areas fall within this group would have a temperature generally

rise along with TKL. In our selected weather stations, HKFYG and PolyU belong to this group. Based on our analysis, both stations are classified as an urban area. Compares to other urban stations, HKFYG and PolyU have the largest amount of built up areas as well as buildings area density.

The second group has the average UHII with a value ranging from -1℃ to -1.5℃. The results indicated that the air temperature within this group would not rise up as fast as TKL. The stations within this group are all belonged to urban stations with "Typical Massing", including Dis, Ling, CCSC, LCMS and CFSS.

The last group has the highest negative UHII with a value ranging from -1.9℃ to -2.5℃. The results indicated that the air temperature within this group would rise much less than TKL. The stations within this group are CCH and CCSC. The built environment of CCH and CCSC are belonged to rural and suburban areas, respectively. Their built up areas are close to TKL. However, both areas are located at high ground and close to the waterfront, the windy condition has greatly reduced the temperature rise of the areas.

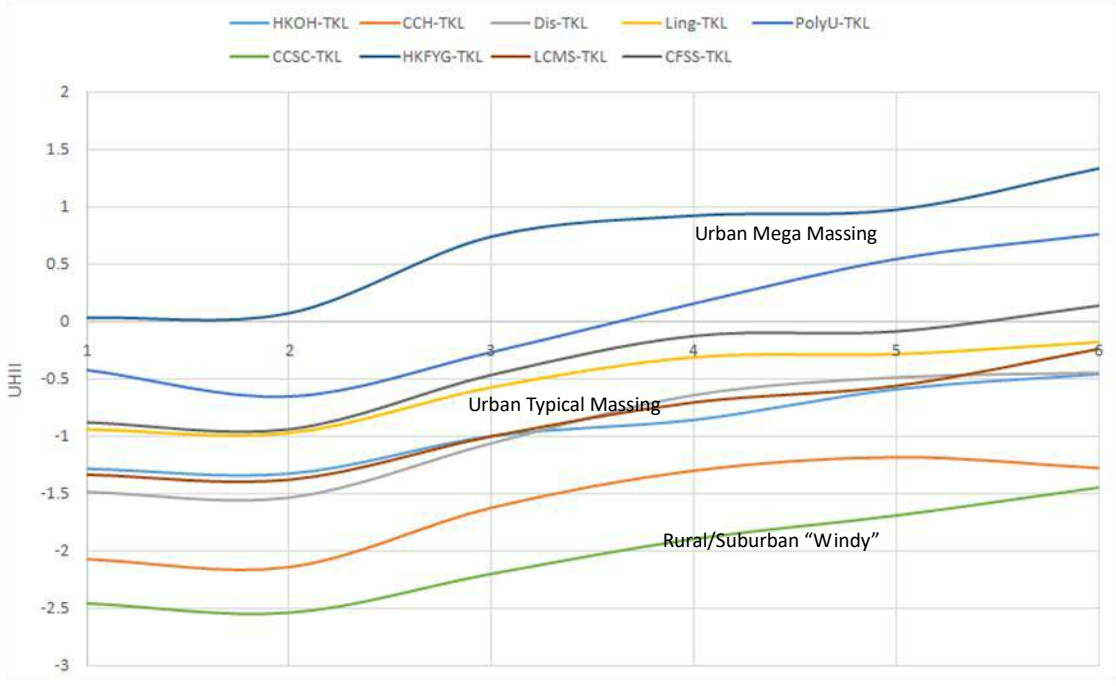

Figure C6. 16 Air temperature distribution during 2015 June afternoon (12NOON-6PM)

Similar to morning, CCH and CCSC stations had received the lowest $UHII_{ave}$. Their $UHII_{max}$ and $UHII_{min}$ value is at the low-end region as compare to other stations. The sea breeze effect is proved to able effectively remove the hot air from the solar irradiation.

For the urban area with mega massing, the $UHII_{ave}$ is the lowest, while there is no clear trend for the $UHII_{max}$ and $UHII_{min}$ value as compared with other urban stations. The average UHII of each station in 2015 June afternoon is given in Table C6. 5.

Table C6. 5 Average UHII of each station in 2015 June afternoon

Station	UHI_{max}	UHI_{min}	UHI_{ave}	Area Cat.
CCH	3.7	-5.0	-1.6	Rural
CCSC	3.8	-4.7	-1.8	Suburban
HKO	4.3	-4.1	-0.8	Urban
Dis	5.2	-4.5	-0.7	Urban
Ling	5.3	-3.4	-0.3	Urban
PolyU	3.5	-2.8	0.3	Urban
HKFYG	6.0	-2.2	1.1	Urban
LCMS	4.7	-3.3	-0.6	Urban
TCFSS	5.1	-4.8	-0.2	Urban

6. 10 Summer June 2015 Evening (6PM to 12AM)

The June evening mean temperature of TKL is 28.1℃, June evening mean minimum temperature of TKL is 24.7℃ and the June evening mean maximum temperature of TKL is 32.0 ℃. The air temperature of TKL would reach the peak at 6PM with a value of 29.7℃. Unlike morning, the air temperature of TKL in the afternoon is generally in a slow decreasing trend dropping from 29.7℃ and reaches 27.0℃ at 12AM, due to no solar radiation heat gain. The hourly June evening mean temperature of TKL (6PM – 12AM) is given in Figure C6. 17.

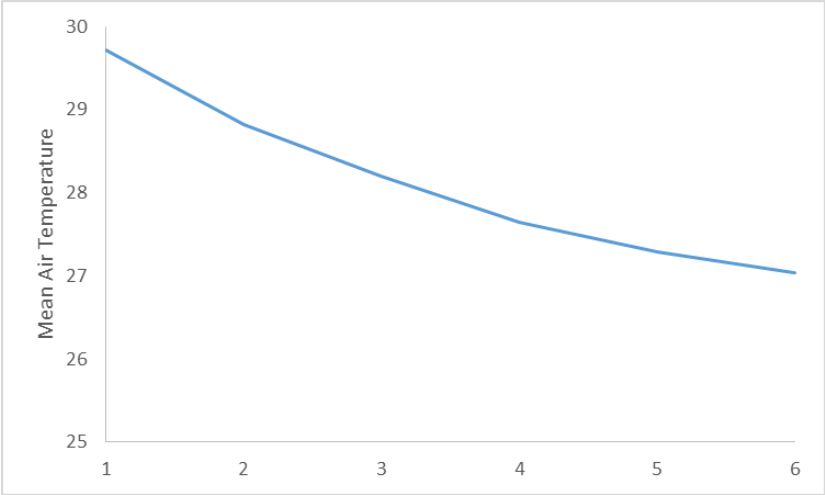

Figure C6. 17 Hourly June evening mean temperature of TKL (6PM – 12AM)

The mean air temperature distribution during 2015 June evening (6PM-12AM) is shown in Figure C6. 18. The results generally showed that all stations had a similar increase trend on the UHII with a positive UHII during the evening period from 6PM onward. From statistical point of view, the air temperature in TKL (rural station) is generally lower than the other stations except CCH. CCH would have a positive UHII from 9PM onward, indicating that the air temperature is lower in TKL during 6PM to 9PM, while similar to the TKL during 9PM to 12AM. Compares to other stations, CCH has less density-built environment and allow more wind to effectively cool down the land during night time.

Unlike morning and afternoon period, the UHII magnitude is quite similar in urban area. It is mainly due to the fact that there is no solar radiation load due the evening time. The dominated factor for the air temperature variation is the wind environment and outgoing long wave radiation. The urban areas would all experience calm wind environment and similar sky view factor, would induce similar cool down ability. Therefore, the temperature trend increases similarly among the urban area. There is slight difference of the air temperature. It is mainly related to the amount heat load that adopted during the daytime. As the air temperature decreased, the energy from the building mass and road would release back to the

space through convection, conduction and radiation effect. This thermal delay reflects the magnitude of urban heat island effect.

The first group has the highest negative UHII with a value ranging from 0.4℃ to -1.3℃. The results indicated that the air temperature within this group would rise much less than TKL. The stations within this group are CCH. The built environment of CCH and CCSC are belonged to rural areas. Their built up areas are close to TKL. However, the area is located at high ground and close to the waterfront, the windy condition has greatly reduced the temperature rise of the areas. The last group has the smallest negative UHII with a value ranging from 0℃ to 2.5℃. The results indicated that the areas fall within this group would have a temperature generally rise along with TKL. All the rest of the weather stations belong to this group. Based on our analysis, all stations are classified as an urban area.

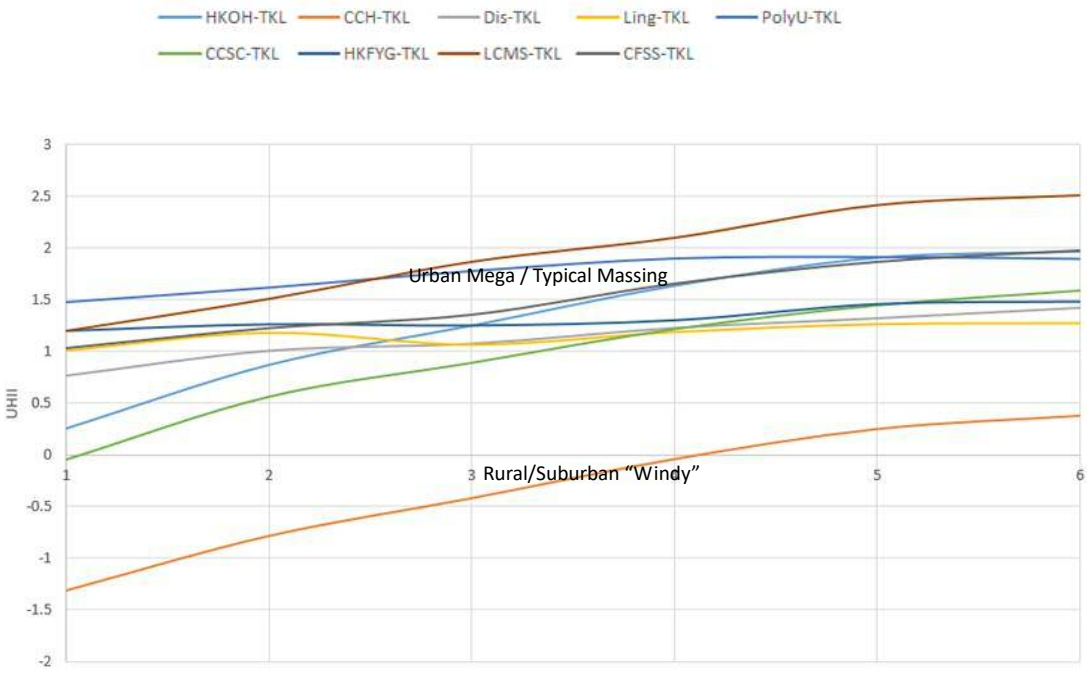

Figure C6. 18 Air temperature distribution during 2015 June evening (6PM-12AM)

Similar to morning, CCH stations had received the lowest $UHII_{ave}$. Their $UHII_{max}$ and $UHII_{min}$ value is at the low-end region as compare to other stations. The sea breeze effect is proved to able effectively remove the heat stored during daytime. For the urban area, the $UHII_{ave}$, $UHII_{max}$ and $UHII_{min}$ value as similar. The average UHII of each station in 2015 June evening is given in Table C6. 6.

Table C6. 6 Average UHII of each station in 2015 June evening

Station	UHI_{max}	UHI_{min}	UHI_{ave}	Area Cat.
CCH	3.0	-3.4	-0.3	Rural
CCSC	4.4	-1.2	1.0	Suburban
HKO	4.3	-1.6	1.4	Urban
Dis	4.2	-1.7	1.2	Urban
Ling	4.2	-0.7	1.2	Urban
PolyU	4.4	0.2	2.6	Urban
HKFYG	4.7	1.1	2.7	Urban
LCMS	4.6	0.1	2.0	Urban
TCFSS	4.5	-1.2	1.6	Urban

6. 11 Compare with other UHI Study

E. Ng (2007) has identified the Hong Kong UHI characteristic in his study. The UHII are often reached at the highest at about 11 o'clock at night and 3 o'clock in the morning with a range of 3 deg to 8 deg. And it is the reason that the urban heat island is other referred as a nighttime phenomenon. E. Ng (2007) has recorded the UHII variation for Hong Kong over 24 hours at 2006, as shown in Figure C6. 19. The following UHI phenomenon can be observed through E. Ng (2007) study.

1. High UHII during nighttime (12AM to 6AM)

2. Significant UHII drop during morning period (6AM to 12NOON)

3. Change from significant UHII drop to UHII increase during the afternoon period (12NOON to 6PM)

4. Significant UHII increase during evening period (6PM to 12AM)

Refers to the measured UHII data in Section 6.8 to 6.10 that used TKL weather station as rural reference weather data, similar UHI phenomenon can be also observed as compared with E. Ng (2007) recorded the UHII data. For example, (1) the measured UHII data in Section 6.8 also showed significant UHII drop during morning period, (2) the measured UHII data in Section 6.9 also showed the UHII change from decrease trend to increase trend during the afternoon period and (3) the measured UHII data in Section 6.10 also showed the UHII increase during evening period. The results indicated the TKL weather station is suitable used for rural reference weather data to calculate the UHII and act as the temperature boundary condition of the UHI model.

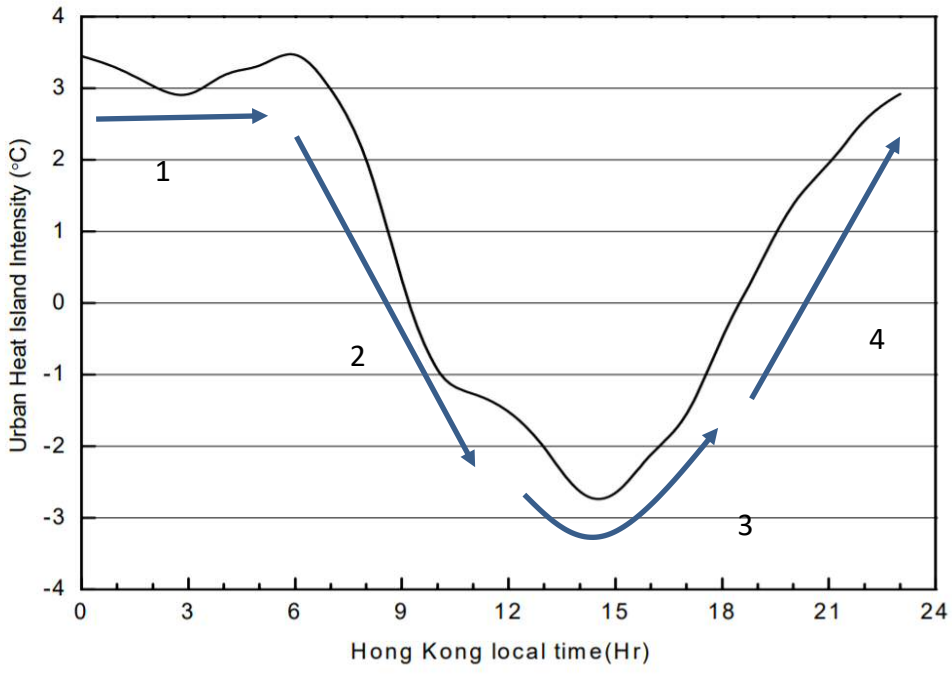

Figure C6. 19 The variation in UHII for Hong Kong over 24 hours in 2006 (Source: E. Ng (2007))

6. 12 Summary

Area classification for weather stations

Using the self-developed Urban Density Database and the area classification criteria from Fung Wing Yee (2009), the 9 selected weather stations have divided into 3 Area Categories, including rural, sub-urban and urban condition. The Area Categories is based on the built-up area condition and building types which is analysed in the Urban Density Database. The analysis suggests that Ta Kwu Ling (TKL) weather station can be classified as rural built environment. Thus, the Ta Kwu Ling (TKL) weather station is possible to be used as the reference weather station in the UHI model to calculate the UHII.

Reference rural weather station - Ta Kwu Ling (TKL)

The air temperature of the 9 weather stations has further analysed with the Ta Kwu Ling (TKL) weather station during June 2015 (summer period). The UHII of the 9 selected stations is calculated based on the Ta Kwu Ling (TKL) weather station as the reference rural weather station. The calculated UHII of the weather stations are divided in the morning period (6AM to 12NOON), afternoon period (12NOON to 6PM) and evening period (6PM to 12AM). The findings are summered in below:

Morning period (6AM to 12NOON) at Section 6.8

- Highest built up areas - smallest negative UHII with a value from 1.4℃ to -0.9℃
- Typical built up areas - average UHII value ranging from 1.5 ℃ to -1.5℃
- Lowest built up area - highest negative UHII with a value ranging from -1.0℃ to -2.5℃

Afternoon period (12NOON to 6PM) at Section 6.9

- Highest built up areas - smallest negative UHII with a value ranging from -0.1℃ to -0.6℃
- Typical built up areas - average UHII with a value ranging from -1℃ to -1.5℃
- Lowest built up area - highest negative UHII with a value ranging from -1.9℃ to -2.5℃

Evening period (6PM to 12AM) at Section 6.10

- Highest built up areas and Typical built up areas – similar UHII
- Highest built up areas and Typical built up areas – smallest negative UHII with a value ranging from 0℃ to 2.5℃.
- Lowest built up area - highest UHII with a value ranging from 0.4℃ to -1.3℃.

The UHI phenomenon during the morning, afternoon and evening period are further compared with the E. Ng study (2007) that recorded the UHII variation for Hong Kong over 24 hours at 2006. The UHII variation of both studies has shown a strong similarity. The results indicating that using TKL weather data is suitable reference rural station and shall be also used as the reference air temperature profile for the UHI modelling. The TKL air temperature profile will use as the temperature input boundary UHI simulation in Chapter 7.

Chapter 7 Case Study and Model Validation

This chapter discuss the model validation of the UHI model. Firstly, the chapter introduct using Lid-Driven Cavity flow measurement data to evaluate the flow field performance of the UHI model. The results show that the simulated data and the measurement data is in-line together indcated that the flow field performance of the UHI model is acceptable. Then the chapter presents a case study at Tsim Sha Tsui area in Hong Kong. An UHI simulation has been conducted using the new UHI model and the Urban Density Database. 3 sets of measurement has been carried out during 11 Jun 2015 to 14 Jun 2015. The simulated data is compared with the measurement data. The results also show that both data set is in good agreement and indcated that the performance of the UHI model is acceptable. Finally, the chapter also discussed the grid number reduction and the simulation time reduction of the Tsim Sha Tsui case study using the new UHI model method.

The volume averaging governing equation and procedures have been successfully implemented into the computer code to create the UHI Model. However, the validation of the volume averaging governing equation for modelling a large-scale environment is still remind a problem in the current research field. Christie (1996) and other researchers point of that the Volume Averaging Appoach has become an increasingly important tool in recent years for converting highly detailed geological models of reservoir to simulation grid, but there are no measure of quality available for any upscaling routine.

The difficulties to valid Volume Averaging Appoach is that the value of the dependent variable is the averaged in a 3 dimension space, but there is no technology available that can measure the dependent variable in 3 dimension evnrionment simultaneously, especially in a large scale. Using UHI model as an example, it is not possible to measure the volume averaged air temperature or air temperature in every 3-dimension spaces simultaneously in

the actural evnrionment to compare with the simulation results. Thus, The method to qualify the upscaling results is still one of the outstanding problems remained in this research field.

In this thesis, it is proposed to use the single point air temperature (measurement data) to compare with the simulated volume averaged air temperature data to valid the model performance. Thus, it is expected there would be an reasonable error between the simulation data and the measurement data. The error can be due to the simulation error or measurment error or the spatial variation of measurment, which cannot be idenitied under the current technologhy avalible. However, comparing the measurement air temperature and the simulated air temperature is still the most reliable approach to quantify the performance of the UHI model.

7. 1 Lid-Driven Cavity Flow – Validation on Flow Field of UHI Model

Ghia and Shin (1982) has carried out an experimental and numerical studies for fluid flow for a simple case. The standard case is fluid contained in a square domain with Dirichlet boundary conditions on all sides, with three stationary sides and one moving side (with velocity tangent to the side). Figure C7. 1 shows the general setting of the experimental and numerical studies in Ghia and Shin (1982) paper.

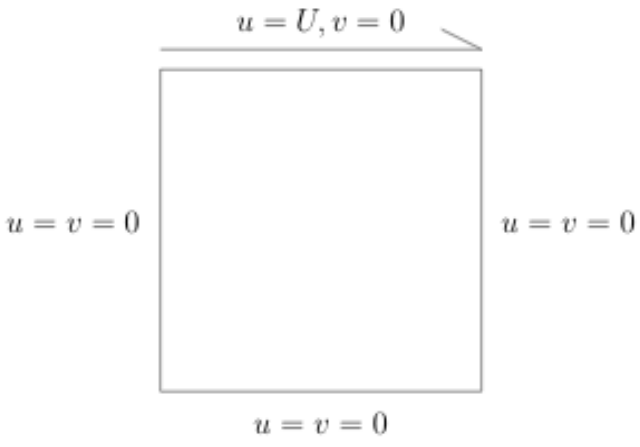

Figure C7. 1 Lid-Driven Cavity Flow setting

Both experiment data and numerical data has been published under different grid number and Reynold number conditions. Since then, the data published data become a well-known benchmark problem for the validation of new numerical methods and techniques. The published data for u-velocity along the vertical centerline at Re = 1000 is shown in Figure C7.2.

y	33×33
1.0000	1.00000
0.9766	0.63025
0.9688	0.55464
0.9609	0.49769
0.9531	0.45744
0.8516	0.34253
0.7344	0.19718
0.6172	0.06368
0.5000	−0.05594
0.4531	−0.10207
0.2813	−0.27793
0.1719	−0.37878
0.1016	−0.28356
0.0703	−0.20935
0.0625	−0.18884
0.0547	−0.16653
0.0000	0.00000

Figure C7. 2 Results for u-velocity along the vertical centerline at Re = 1000 with grid 33 × 33 (1m × 1m) (source: Ghia and Shin (1982))

Table C7. 1 Boundary condition of Lid-Driven Cavity Flow setting in UHI Model

	UHI Model
Model Scale	1:1 scale
Model Details	1m × 1m × 1m
Grid Type	Cartesian grids
Number of Grid	33 × 33 × 33
Reynolds numbers	1000
Inflow Boundary Condition	Velocity inlet condition at top wall with velocity equal 1m/s at u-direction
Wall Boundary Condition	Logarithmic law boundary at Bottom, East and West wall
Wall Boundary Condition	Symmetric boundary at North and South wall
Solving Algorithms	*Rhie* and *Chow* SIMPLE for momentum equation
Convergence Criteria	Below 0.5×10^{-3}

For UHI Model, it is tested based on domain length 1m x 1m x 1m, with grid number of 33(H) × 33(L) × 33(W) and Reynolds numbers of 1000. The UHI model setting is listed in Table C7. 1. The simulation results are compared with the data of Ghia and Shin (1982) under Reynolds numbers equal to 1000, as shown in Figure C7.3. The comparison shows that the simulated data from the UHI model and the Ghia and Shin (1982) data are are strongly comparable. The result indicating the UHI model can recreate the experimental data of Ghia and Shin (1982) and the UHI model is valid for flow simulation.

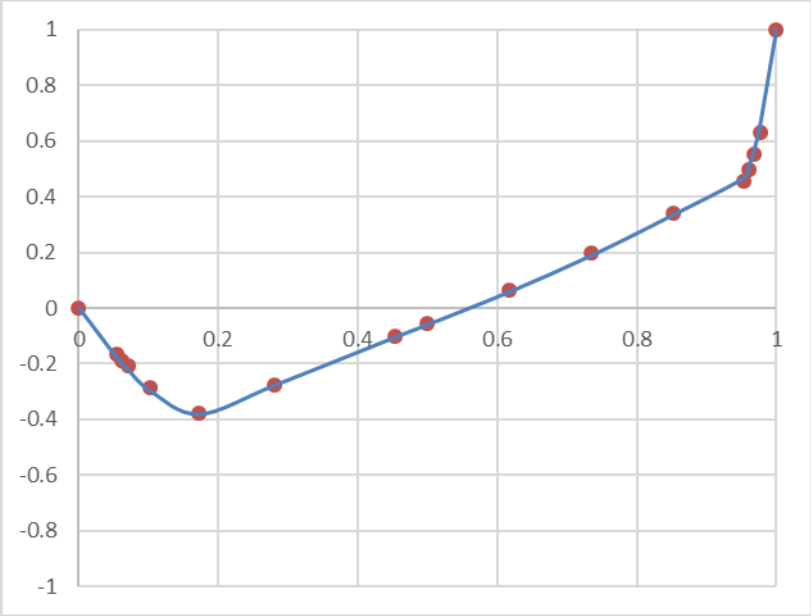

Figure C7. 3 U-velocity Results Companion: Simulation Results (Orange Dot) v.s. Ghia, Ghia, and Shin (1982) (Blue Line)

7. 2 Case Study - Tsim Sha Tsui – Validation on UHI Model

A case study has been carried out in Tsim Sha Tsui area to further valid the UHI Model to simulation the UHI intensity. The study area is around 2640m x 2640m, as shown in Figure C7. 4. The Urban Density Database has analysed the urban density of the study area in $10m^2$ resolution and recreating the area in the UHI Model with $80m^2$ resolution and grid number of 33 × 33 × 33. The 3D mesh and 3D terrain in the UHI model are shown in Figure C7.5. The density distribution of building, construction, greenery, road, sea and tree are given in

Figure C7. 8 to Figure C7. 13. The UHI model setting is listed in Table C7. 2 and the simulation contour and streamline plot are given in Figure C7 .14 and Figure C7. 15.

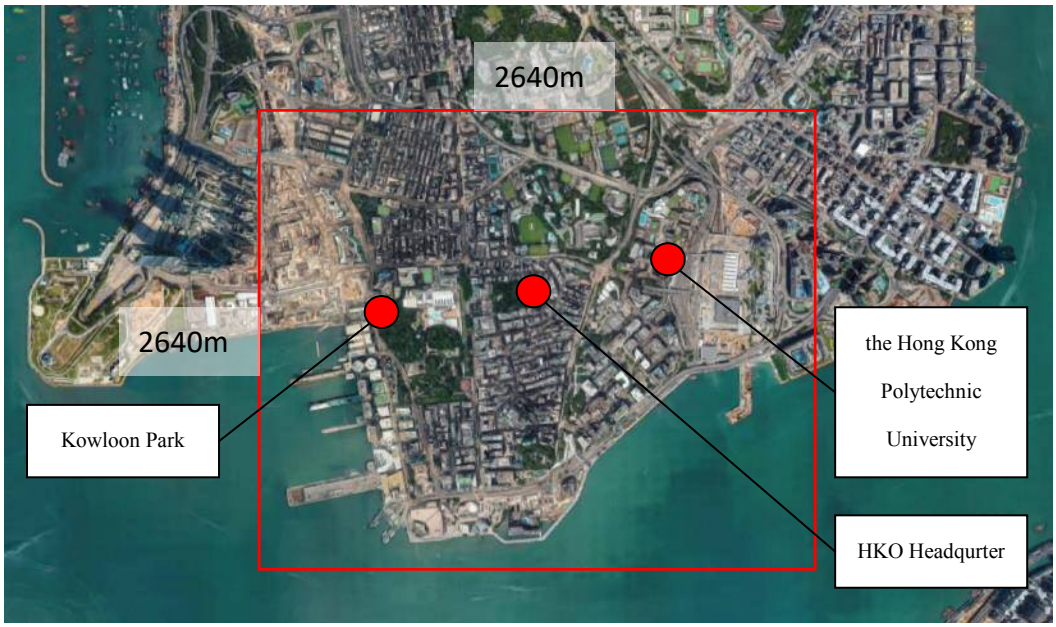

Figure C7. 4 Modelling location

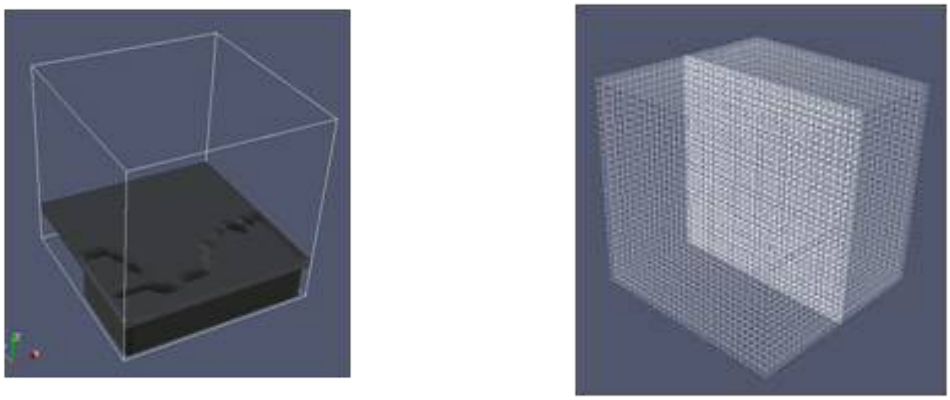

Figure C7. 5 Terrain of the area in the model (Left) and 3D mesh of the area in the model (right)

Table C7. 2 Boundary condition setting in UHI Model

	UHI Model
Model Scale	1:1 scale
Model Details	2640m × 2640m × 2640m
Grid Type	Cartesian grids
Number of Grid	33 × 33 × 33
Reynolds numbers	1000
Inflow Boundary Condition	Velocity inlet condition at west wall with power law velocity profile
Thermal Boundary Condition	temperature condition at west wall with TKL station temperature profile
Outflow Boundary Condition	Pressure boundary condition with dynamic pressure equal to zero at east wall
Wall Boundary Condition	Logarithmic law boundary at Bottom
Wall Boundary Condition	Symmetric boundary at top, north and south wall
Solving Algorithms	*Rhie* and *Chow* SIMPLE for momentum equation
Convergence Criteria	Below 0.5×10^{-3}

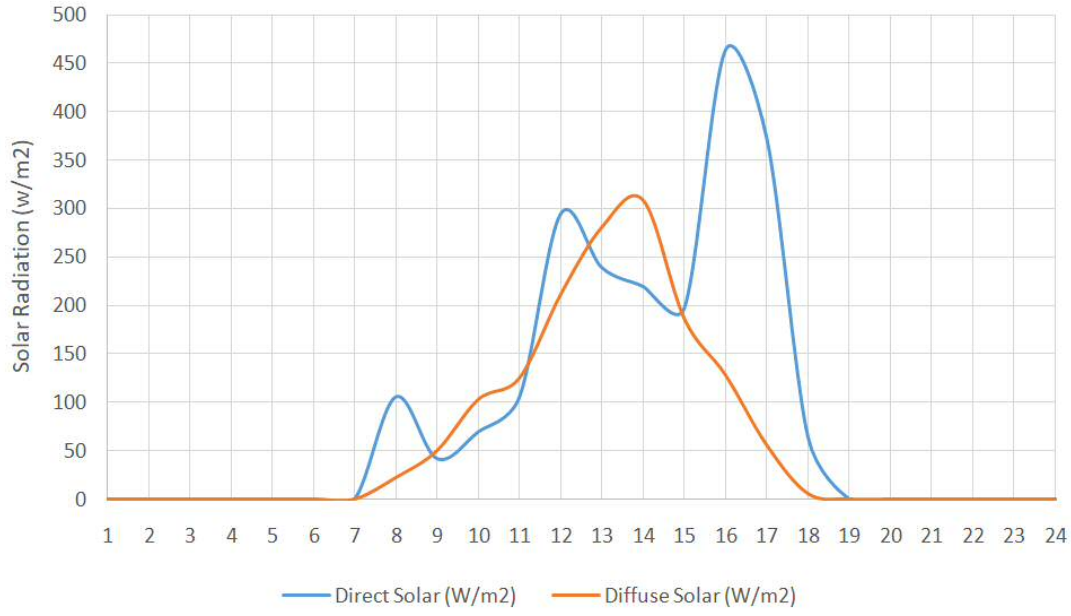

Figure C7. 6 Recorded solar radiation load (w/m^2) in King's Park Station during 11th June 2015

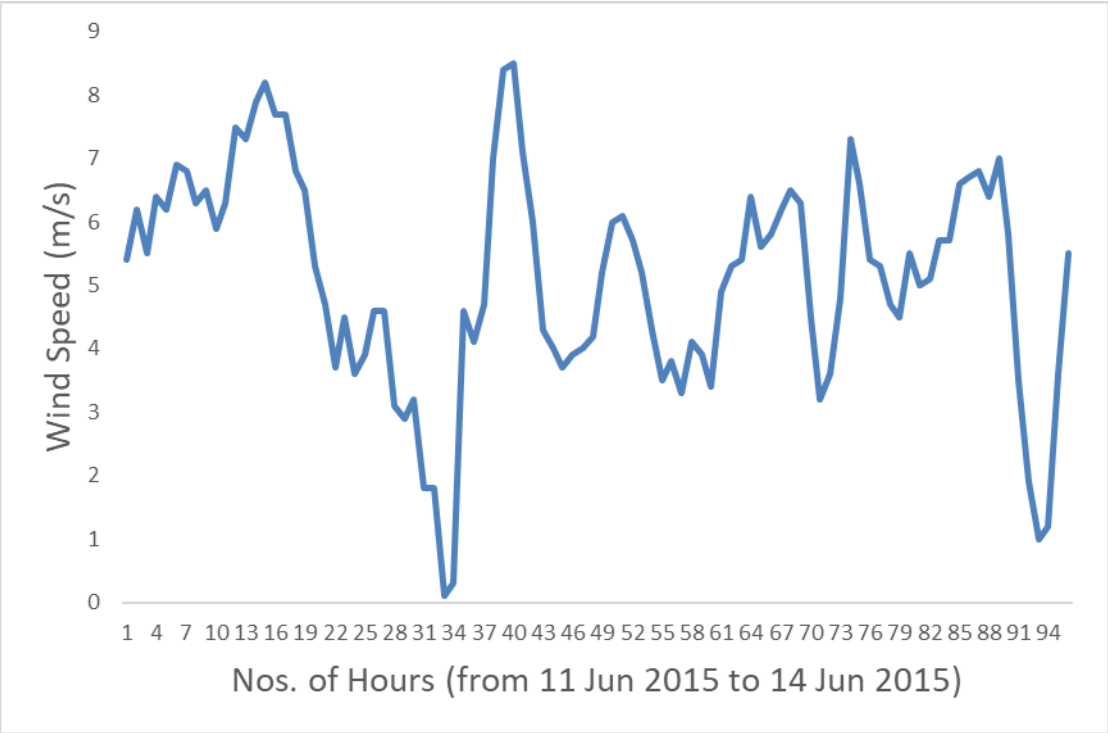

Figure C7. 7 Recorded wind speed in Wagland Island Station during 11 Jun 2015 to 14 Jun 2015

0	0	0	0	0	0	0	0	0	0	0	0	0	0	0	0	0	0	0	0	0	0	0	0	0	0	0	0	0	0	0	0	0
0	0	0	0	0	0	0	0	0	0	0	0	0	0	0	0	0	0	0	0	0	0	0	0	0	0	0	0	0	0	0	0	0
0	0	6.1	7.2	11	3.1	1.7	29	26	34	44	46	12	3	0.6	1.3	4.1	17	25	9.9	20	32	69	10	34	75	6.3	1.4	0	33	0	0	0
0	0	1.6	2.2	2.2	0.3	1.5	55	45	38	44	30	31	10	1.1	31	47	53	62	70	0.3	25	14	10	1	14	0	3.8	12	7.8	0	0	0
0	0	2.8	0.8	42	14	1.1	24	48	36	13	26	19	16	10	23	28	39	58	54	0.1	0	18	9.5	1.4	2.7	1.4	27	32	0.2	0	0	0
0	0	1.6	5.8	39	22	1.9	17	29	21	44	26	22	42	16	44	69	95	34	1.4	4.9	1.4	4.9	5.1	2.1	1.9	0.6	11	13	15	0	0	0
0	0	1.7	4.7	15	6.4	0.7	36	38	49	38	35	19	42	41	13	59	16	25	1.9	3.4	0.3	3.5	4.9	5.4	5.9	12	39	30	17	0	0	0
0	0	2.7	3.9	38	43	33	39	31	38	51	42	57	27	20	12	32	0	9.6	12	54	48	3.4	3.3	6.3	14	49	46	40	36	0	0	0
0	0	3.5	3.8	24	33	40	52	48	39	44	47	62	79	41	5.7	16	15	29	6.9	12	25	40	3.2	2.3	30	50	49	34	61	0	0	0
0	0	0	1.1	1.9	0.2	28	48	41	49	36	41	46	49	8.2	32	16	4.7	2.6	7.2	4.1	21	35	16	7.7	31	61	28	61	59	0	0	0
0	0	0	0	26	45	0.2	6.1	43	32	39	48	34	59	25	27	21	15	4.5	20	14	7.3	26	52	45	3.7	19	16	16	26	0	0	0
0	0	0	0	2.8	33	7.5	15	26	60	48	67	48	63	53	22	19	28	31	33	9.4	44	64	98	29	5.2	27	12	40	23	0	0	0
0	0	1.6	0	0	24	40	17	50	53	48	59	43	60	28	0	7.9	26	35	29	7.9	77	96	84	11	7.4	11	15	19	32	0	0	0
0	0	3.2	0	0	14	58	16	44	40	37	36	37	43	34	32	41	30	21	1.7	48	89	96	22	33	74	32	76	27	35	0	0	0
0	0	2.9	0	2	5.2	6.1	13	60	65	0.5	23	25	44	41	32	54	48	32	17	23	39	33	0.6	50	99	23	68	23	60	0	0	0
0	0	4.2	4.6	2.2	0.4	6.9	20	42	44	79	65	19	28	5.4	22	58	46	33	68	52	57	8.2	7.7	32	75	53	57	14	56	0	0	0
0	0	2.5	3.4	1.6	0.7	31	31	15	7	11	9.9	27	53	33	52	39	56	17	29	27	41	11	0.1	74	88	66	58	2	11	0	0	0
0	0	7.3	10	4	1.4	61	45	1.2	0.9	0	0	30	75	55	47	56	53	1.5	35	59	48	48	2.1	31	38	56	39	1.1	18	0	0	0
0	0	0	0	2.2	3.1	36	54	9.6	0.5	2	2.5	35	75	50	61	71	42	26	36	28	76	48	3.4	5	7.2	6.2	4.3	36	26	0	0	0
0	0	0	6.5	22	21	39	74	34	26	8.4	0	29	62	50	64	70	24	33	64	33	18	45	3.2	16	6.4	1.6	5.9	40	4.4	0	0	0
0	0	0	2.6	4.7	16	26	77	53	4.2	6.4	16	20	62	48	62	64	18	46	44	44	20	2.6	7.2	6	0	0	0	1.4	0	0	0	0
0	0	0	0	17	16	12	63	69	61	70	64	53	64	71	62	80	6.9	44	28	38	1.1	1.2	7.2	11	2	2.3	0	0	0	0	0	0
0	0	0	0	0.1	3.4	2.9	49	65	89	38	65	55	63	49	49	57	30	61	29	2.9	0.2	0	3.5	18	0.5	0.2	0	0	0	0	0	0
0	0	0	0	0	0	0	24	78	61	26	58	45	77	65	13	8.9	64	16	2.2	0.5	0	0	0	0	0	0	0	0	0	0	0	0
0	0	0	0	1.1	6.4	27	58	68	70	51	50	61	54	15	42	15	4.7	7.6	0.3	0	0	0	0	0	0	0	0	0	0	0	0	0
0	0	0	6	61	72	52	30	71	43	14	29	18	23	14	1.3	1.6	0.7	2.1	0	0	0	0	0	0	0	0	0	0	0	0	0	0
0	0	0	2.6	2.9	0.5	0	14	13	25	82	53	42	2.1	23	21	0.5	2.6	0.1	0	0	0	0	0	0	0	0	0	0	0	0	0	0
0	0	0	0	0	0	0	18	30	2.9	36	25	47	26	45	70	20	3.1	0	0	0	0	0	0	0	0	0	0	0	0	0	0	0
0	0	0	0	0	0	0	0	0.7	0.6	2.4	0.6	0	0.1	2	2.9	1	0	0	0	0	0	0	0	0	0	0	0	0	0	0	0	0
0	0	0	0	0	0	0	0	0	0	0	0	0	0	0	0	0	0	0	0	0	0	0	0	0	0	0	0	0	0	0	0	0
0	0	0	0	0	0	0	0	0	0	0	0	0	0	0	0	0	0	0	0	0	0	0	0	0	0	0	0	0	0	0	0	0
0	0	0	0	0	0	0	0	0	0	0	0	0	0	0	0	0	0	0	0	0	0	0	0	0	0	0	0	0	0	0	0	0
0	0	0	0	0	0	0	0	0	0	0	0	0	0	0	0	0	0	0	0	0	0	0	0	0	0	0	0	0	0	0	0	0

Figure C7. 8 Building Density per 80m × 80m computational grid

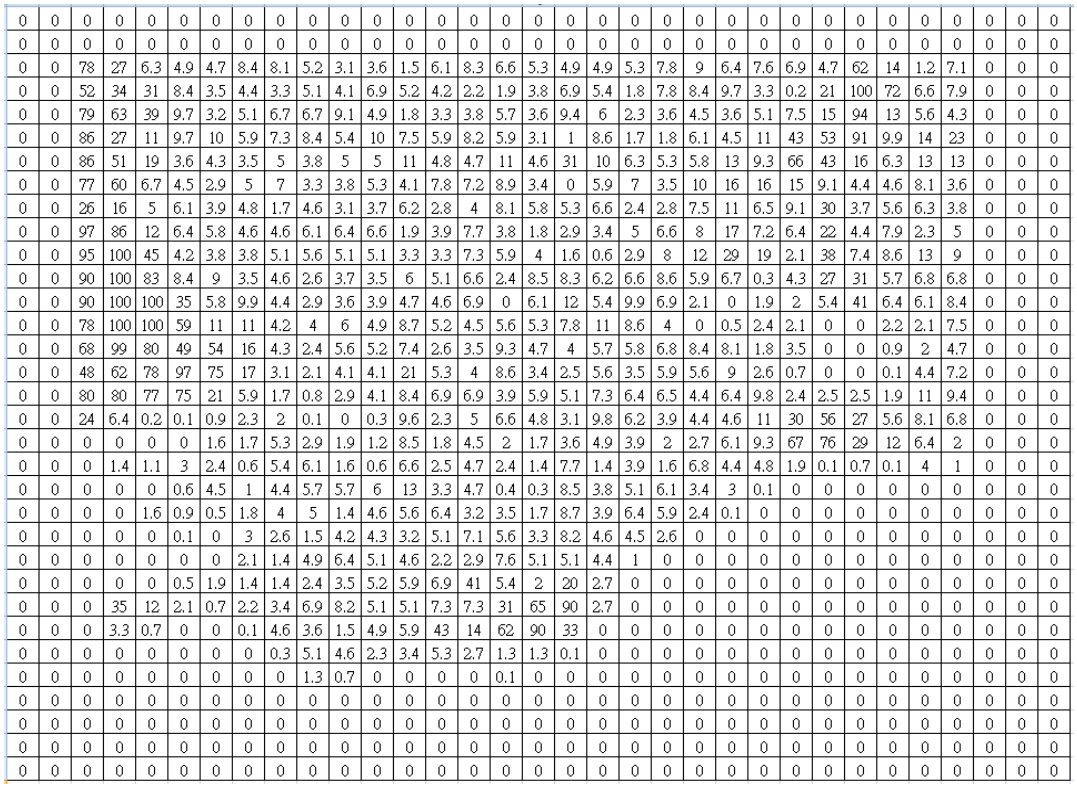

Figure C7. 9 Construction Density per 80m × 80m computational grid

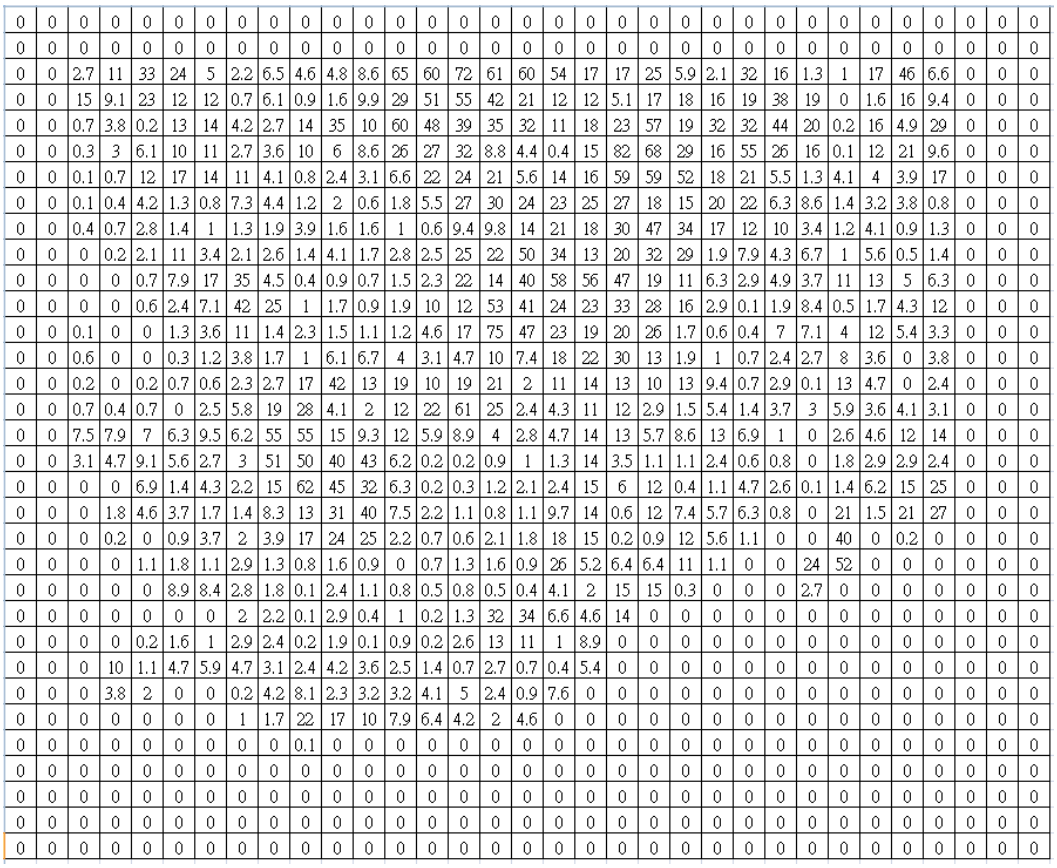

Figure C7. 10 Greenery Density per 80m × 80m computational grid

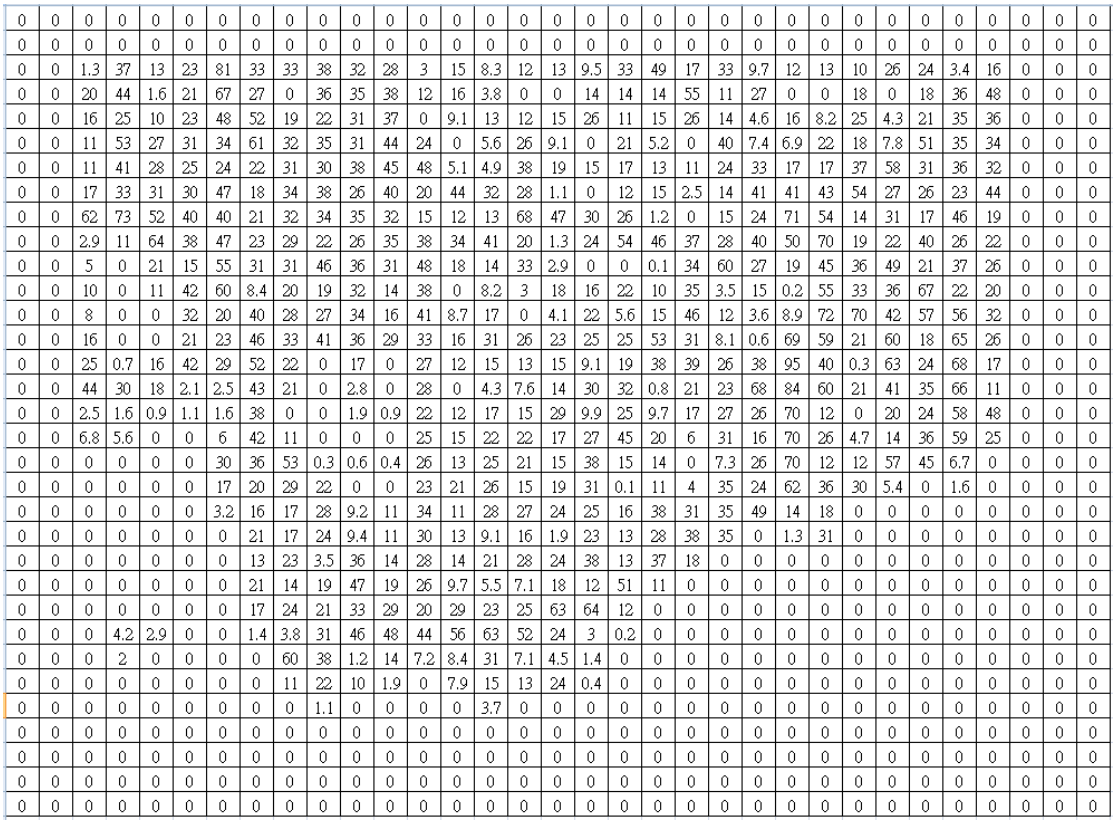

Figure C7. 11 Road Density per 80m × 80m computational grid

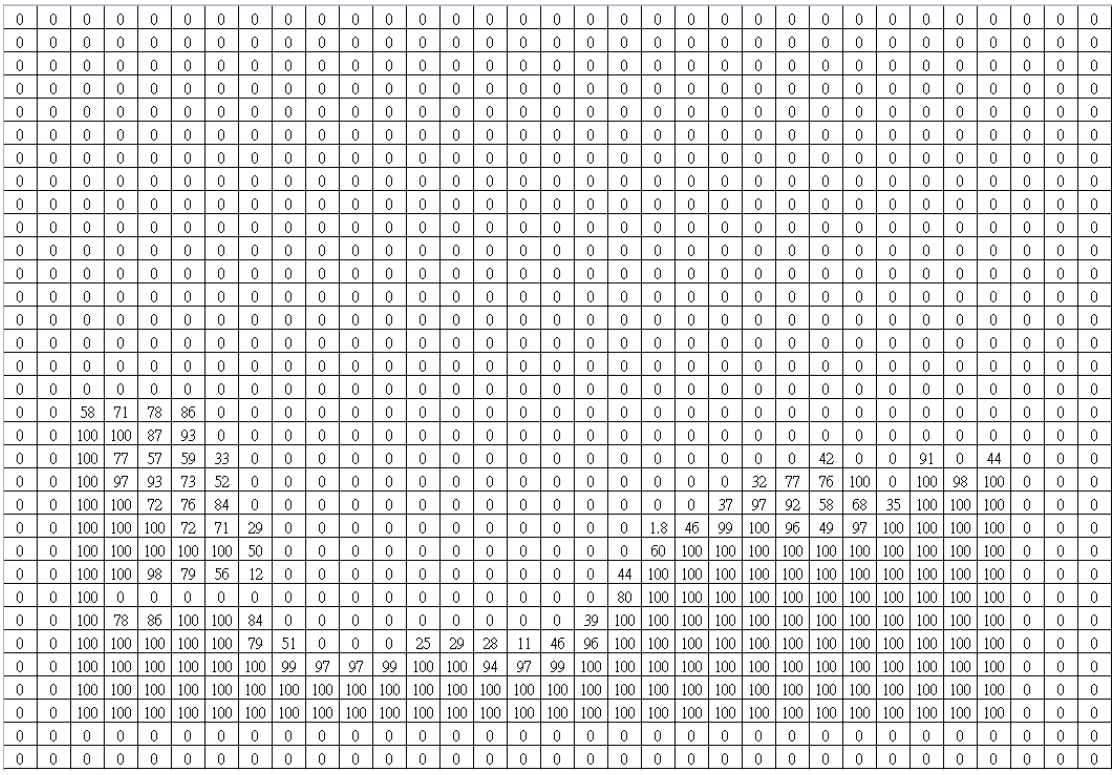

Figure C7. 12 Sea Density per 80m × 80m computational grid

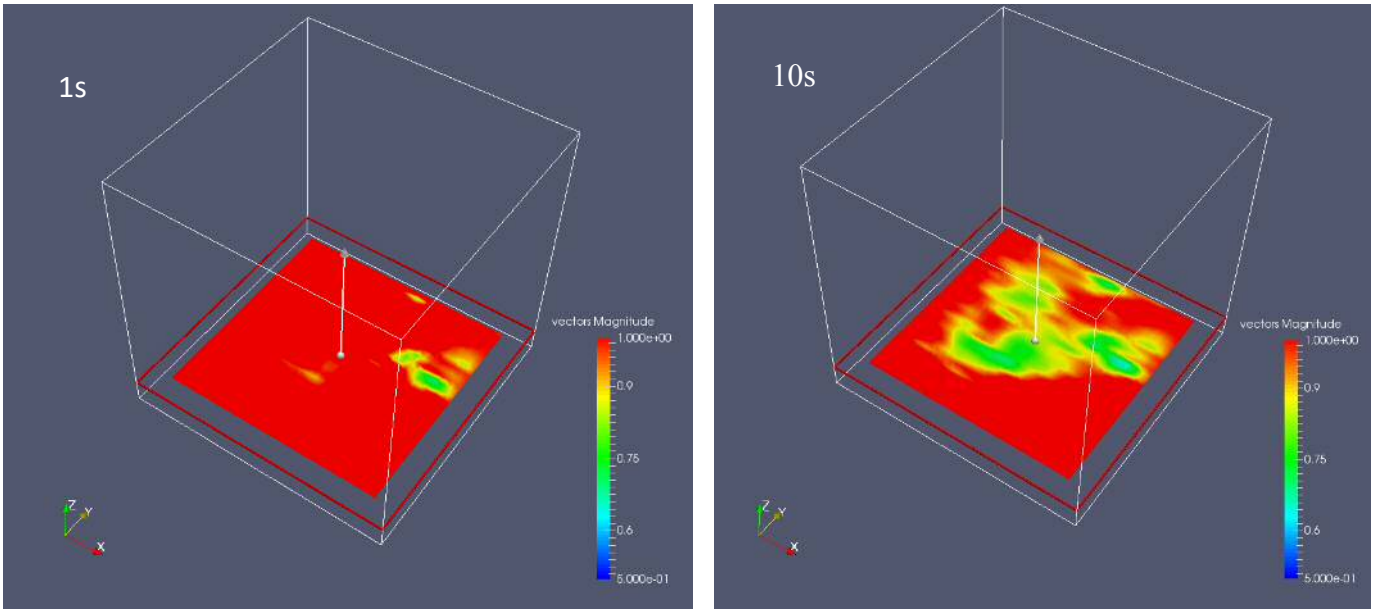

0	0	0	0	0	0	0	0	0	0	0	0	0	0	0	0	0	0	0	0	0	0	0	0	0	0	0	0	0	0	0	0	0
0	0	0	0	0	0	0	0	0	0	0	0	0	0	0	0	0	0	0	0	0	0	0	0	0	0	0	0	0	0	0	0	0
0	0	12	18	36	45	7	26	26	18	16	12	18	15	10	18	18	13	21	19	31	20	13	38	30	9	4	44	49	37	0	0	0
0	0	11	10	42	58	16	13	44	19	15	15	22	18	37	25	26	14	6	9	20	38	33	67	61	28	0	4	30	27	0	0	0
0	0	1	7	9	40	34	14	24	21	12	22	19	22	32	24	21	15	8	5	14	63	42	37	38	38	0	22	23	30	0	0	0
0	0	0	11	16	27	42	12	27	25	12	11	20	24	38	15	15	3	22	10	25	23	67	21	7	10	0	15	18	17	0	0	0
0	0	0	2	26	46	55	26	20	15	16	11	16	26	25	17	11	24	32	20	21	19	33	48	6	13	10	19	17	22	0	0	0
0	0	3	2	20	20	15	31	23	19	14	10	17	16	13	21	40	77	48	40	21	13	20	16	30	14	17	20	25	16	0	0	0
0	0	8	5	16	19	15	21	16	18	15	15	15	5	33	8	17	28	21	59	39	17	6	7	24	23	14	24	13	15	0	0	0
0	0	0	0	19	45	16	21	22	21	26	16	11	11	17	21	30	33	27	21	20	14	6	18	11	21	11	18	10	13	0	0	0
0	0	0	0	6	28	23	22	15	15	18	14	12	18	31	20	31	25	38	30	25	9	7	3	0	17	13	41	29	32	0	0	0
0	0	0	0	1	15	16	30	22	17	15	15	5	21	19	20	13	23	18	16	19	31	10	0	3	23	5	13	27	38	0	0	0
0	0	0	0	0	8	30	22	16	14	12	19	9	22	30	25	35	18	35	25	13	7	0	4	0	6	2	10	13	24	0	0	0
0	0	2	0	0	4	2	24	17	13	15	22	17	33	25	23	22	19	21	6	4	1	0	3	0	0	0	0	6	28	0	0	0
0	0	4	0	1	3	11	16	10	16	35	58	20	30	21	25	24	27	29	25	21	13	11	2	3	0	1	2	7	16	0	0	0
0	0	2	3	1	0	13	15	14	26	10	29	20	44	25	35	23	17	19	16	18	14	8	4	1	0	1	4	11	23	0	0	0
0	0	8	7	10	15	37	18	29	37	69	76	29	21	32	24	22	24	37	42	44	19	44	13	9	10	8	12	17	17	0	0	0
0	0	0	2	8	6	29	7	35	49	59	55	28	7	17	23	20	15	29	35	30	15	30	16	12	1	2	17	29	47	0	0	0
0	0	0	0	4	0	27	6	16	35	50	64	24	8	19	15	11	14	40	39	58	14	19	12	13	5	7	33	36	47	0	0	0
0	0	0	13	15	11	7	4	21	32	59	59	34	11	18	18	9	28	51	21	49	33	21	24	4	64	71	1	34	24	0	0	0
0	0	0	0	2	9	10	3	20	44	54	42	31	22	18	9	9	31	19	12	19	29	7	0	0	0	0	0	0	0	0	0	0
0	0	0	0	8	3	1	11	8	9	17	19	11	15	16	16	16	36	34	30	12	15	1	0	0	0	0	0	0	0	0	0	0
0	0	0	0	0	14	15	4	8	6	19	16	12	16	21	18	16	19	20	12	16	0	0	0	0	0	0	0	0	0	0	0	0
0	0	0	0	0	0	0	1	5	15	18	18	23	11	25	40	34	12	24	12	0	0	0	0	0	0	0	0	0	0	0	0	0
0	0	0	0	1	13	14	9	3	6	10	16	10	10	18	14	9	11	25	0	0	0	0	0	0	0	0	0	0	0	0	0	0
0	0	0	45	23	21	41	62	19	17	27	14	31	13	15	13	8	6	10	0	0	0	0	0	0	0	0	0	0	0	0	0	0
0	0	0	10	8	0	0	2	18	26	13	26	41	42	27	7	4	17	0	0	0	0	0	0	0	0	0	0	0	0	0	0	0
0	0	0	0	0	0	0	2	5	48	32	60	17	25	5	3	3	0	0	0	0	0	0	0	0	0	0	0	0	0	0	0	0
0	0	0	0	0	0	0	0	0	0	0	0	0	0	0	0	0	0	0	0	0	0	0	0	0	0	0	0	0	0	0	0	0
0	0	0	0	0	0	0	0	0	0	0	0	0	0	0	0	0	0	0	0	0	0	0	0	0	0	0	0	0	0	0	0	0
0	0	0	0	0	0	0	0	0	0	0	0	0	0	0	0	0	0	0	0	0	0	0	0	0	0	0	0	0	0	0	0	0
0	0	0	0	0	0	0	0	0	0	0	0	0	0	0	0	0	0	0	0	0	0	0	0	0	0	0	0	0	0	0	0	0
0	0	0	0	0	0	0	0	0	0	0	0	0	0	0	0	0	0	0	0	0	0	0	0	0	0	0	0	0	0	0	0	0

Figure C7. 13 Tree Density per 80m × 80m computational grid

Figure C7. 14 Velocity contour plot of the area at 10m above ground

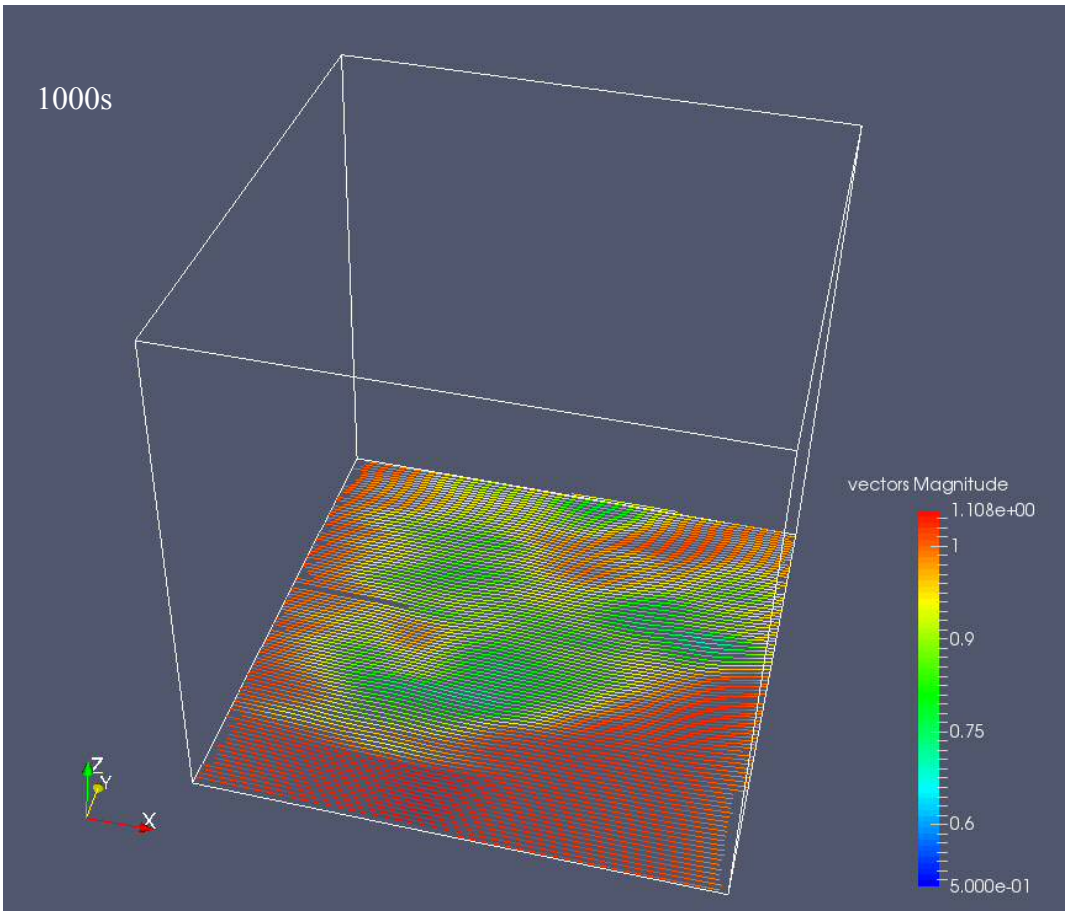

Figure C7. 15 Streamline plot of the area at 10m above ground

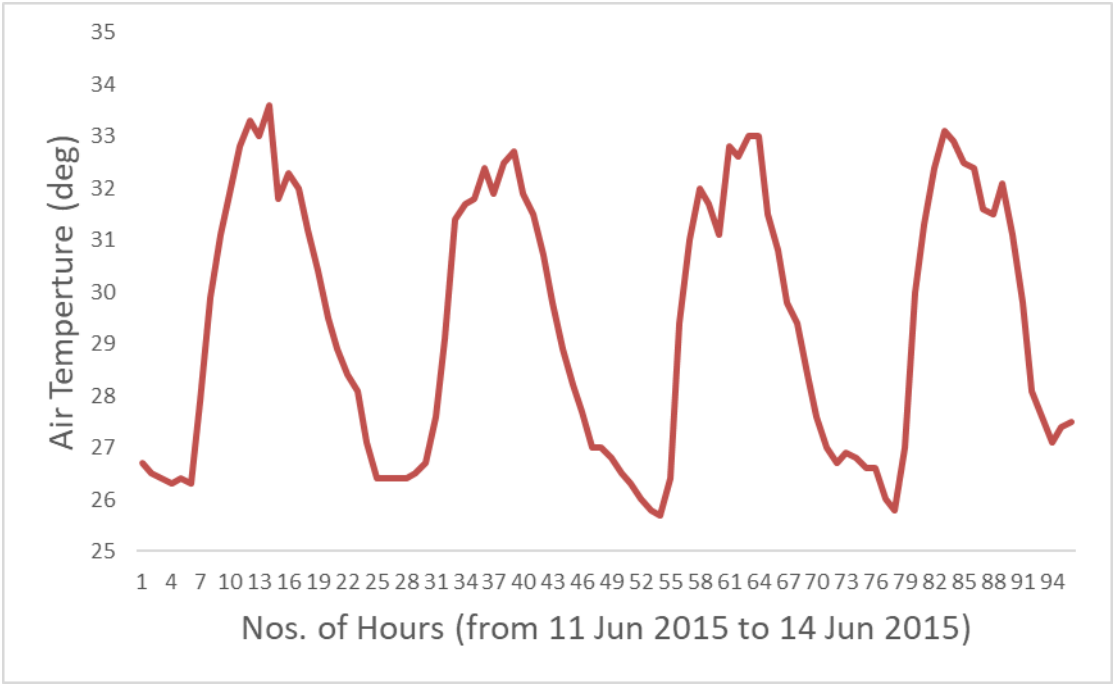

Figure C7. 16 Recorded air temperature in TKL Station during 11 Jun 2015 to 14 Jun 2015

There are 3 measurement locations in Tsim Sha Tsui area for results compensation, namely, HKO Headquarter, Kowloon Park and the Hong Kong Polytechnic University. The location is shown in Figure C7.4. The built environment are generally high-rise and high density condition for HKO Headquarter, low denisty and high greenary condition for Kowloon Park and mega denity condition for Hong Kong Polytechnic University.

TKL station shall be used as rural reference temperature, as suggested in Chatper 7. The air temperature profile of TKL station is used at the temperature boundary condition for the UHI simulation. The Wagland Island wind data and King's Park solar radiation data are also used at the boundary condition for the UHI simulation. The weather data of the solar radiation, velocity and temperature are shown in Figure C7. 6, Figure C7. 7 and Figure C7. 16, respectively. The UHII of the 3 weather stations are calculated by subtracking the simulated air temperature with the TKL measured air temperature. The air temperature comparisions of the measured and simulated data during 11 Jun 2015 to 14 Jun 2015 are shown in Figure C7. 17, Figure C7. 19 and Figure C7. 21.

R-squared (R^2) of the between the measured air temperature and the simulation air temperature is used for assessing the performance of models. R^2 is the squared correlation between the measured air temperature and the simulation air temperature by the model. The R^2 value is always between zero and one, while higher the R^2 value, the better the model. Eva Ostertagová (2012) resarch has classisficed the performance of prediction model by R^2 value mathematically. Accordingly to Eva Ostertagová (2012), an R^2 value of 0.9 or above is very good, a value above 0.8 is good, and a value of 0.6 or above could still satisfactory. However, for R^2 value is 0.5 or below the regression explains only 50 % or less of the variation in the data; therefore, prediction would be less satisfactory.

Figure C7.17, Figure C7.19 and Figure C7.21 shows the simulated air temperature profile and

the measured air temperature profile at Kowloon Park, HKO and PolyU, respectively. While Figure C7.18, Figure C7.20 and Figure C7.22 shows the R^2 value for the simulated air temperature profile and the measured air temperature profile at Kowloon Park, HKO and PolyU, respectively.

Accoring to Figure C7.17, Figure C7.19 and Figure C7.21, the simulated data and the measured data shows a strong similarity. The results shows that the simulated data closely follows the increasing and decreasing trend of the measured air temperature with the maximum 2°C of air temperature difference between simulated and measured data. It is noted that the simulated air temperature represented the volume averaging temperature of the computational grid, while the measured data only presented a point source air temperature. Thus, error between the simulated value and the measured value is expected.

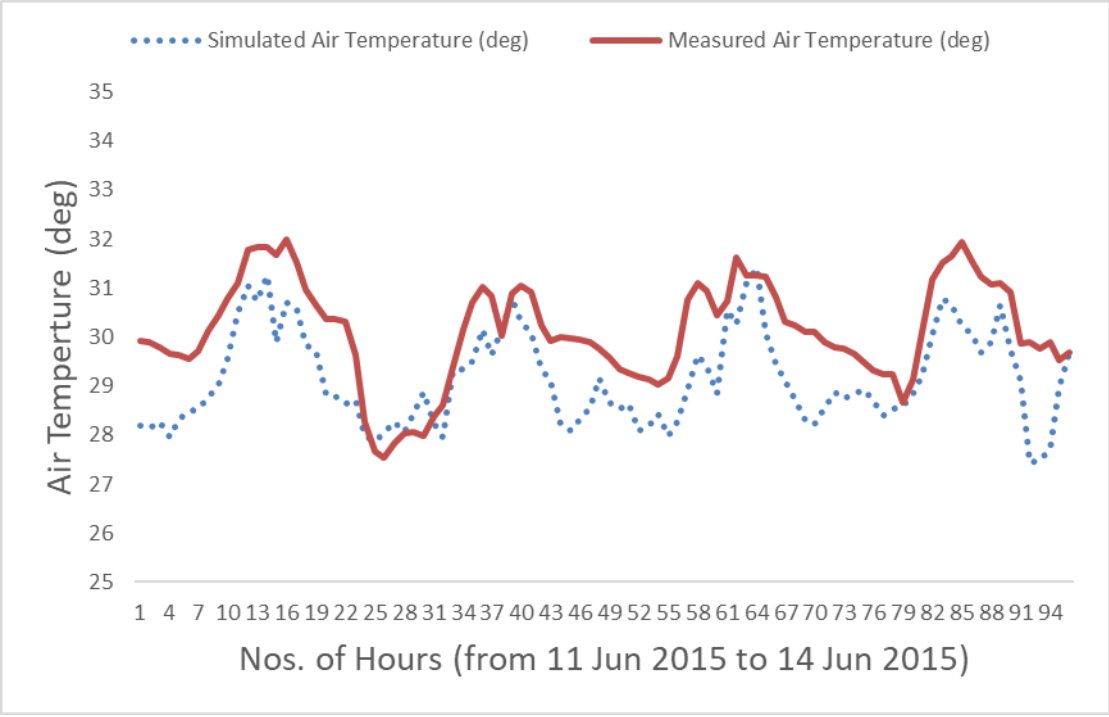

Figure C7. 17 Simulated v.s. measured air temperature at Kowloon Park during 11 Jun 2015 to 14 Jun 2015

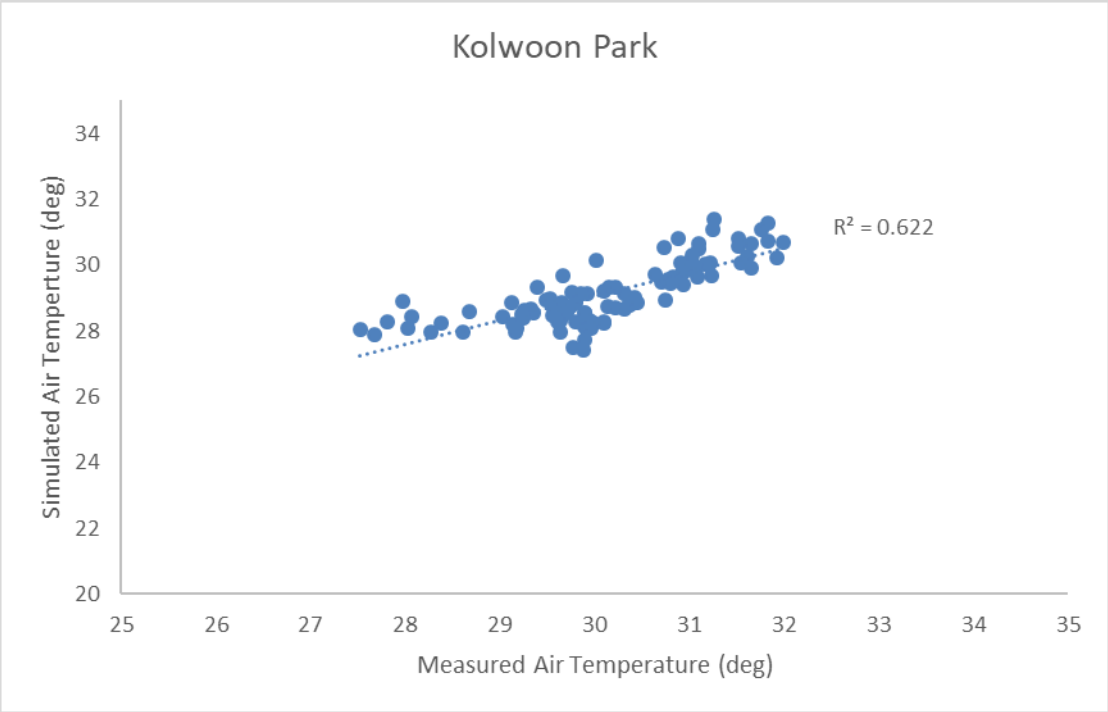

Figure C7. 18 Simulated v.s. measured air temperature at Kowloon Park during 11 Jun 2015 to 14 Jun 2015

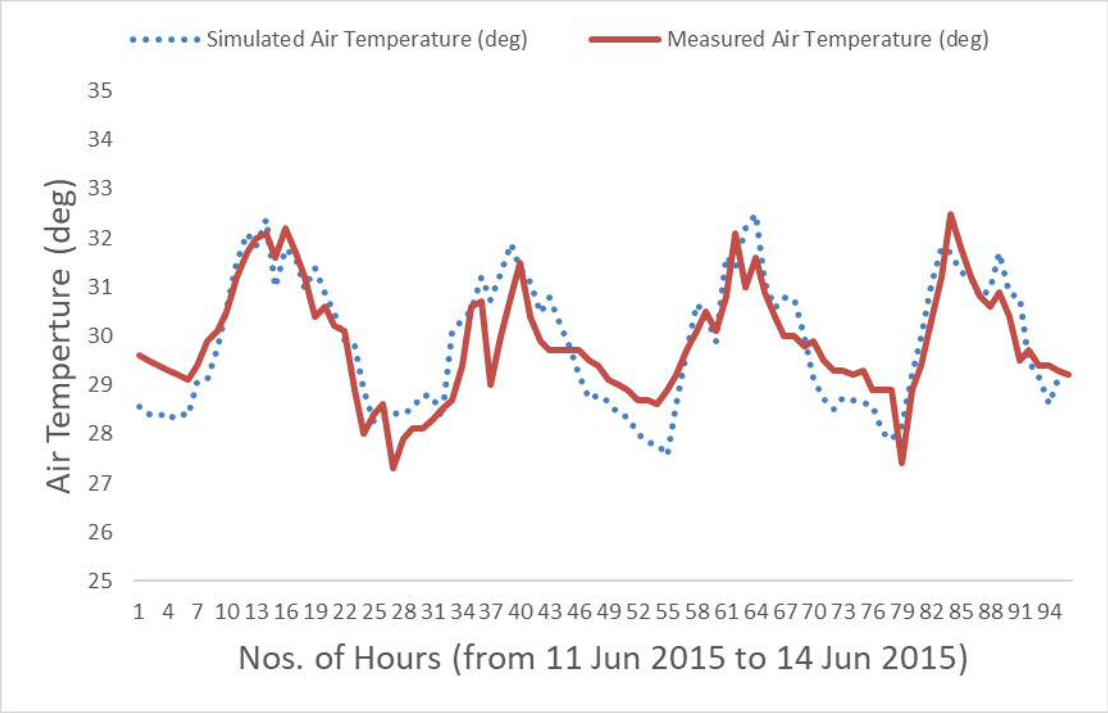

Figure C7. 19 Simulated v.s. measured air temperature at HKO during 11 Jun 2015 to 14 Jun 2015

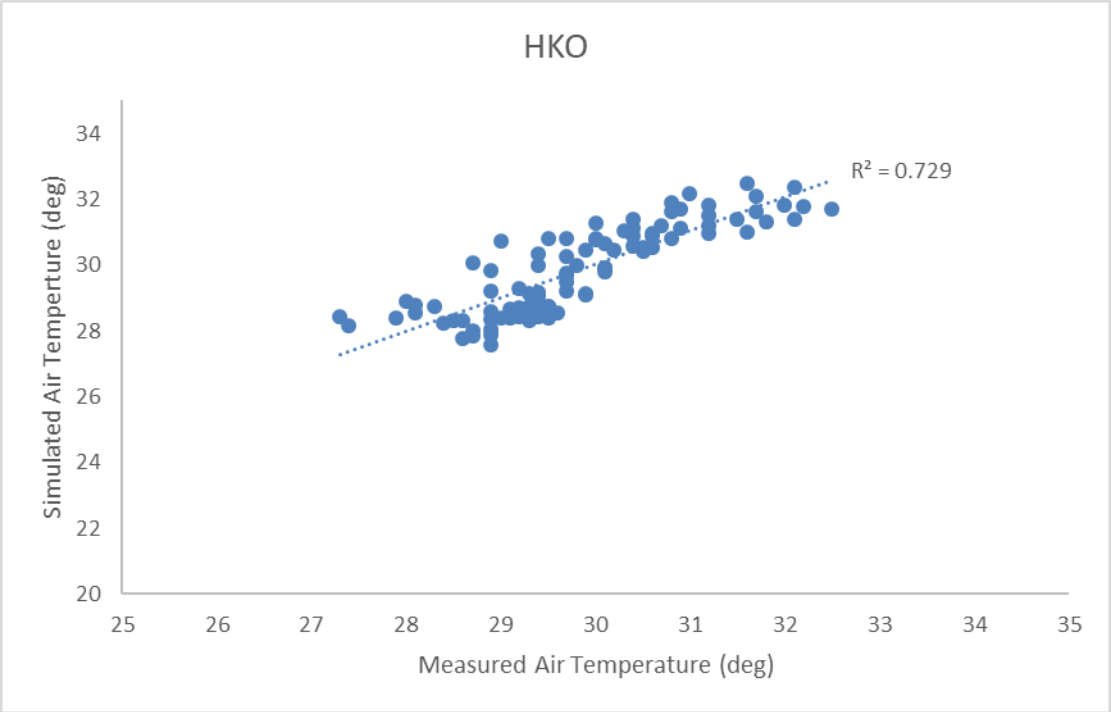

Figure C7. 20 Simulated v.s. measured air temperature at HKO during 11 Jun 2015 to 14 Jun 2015

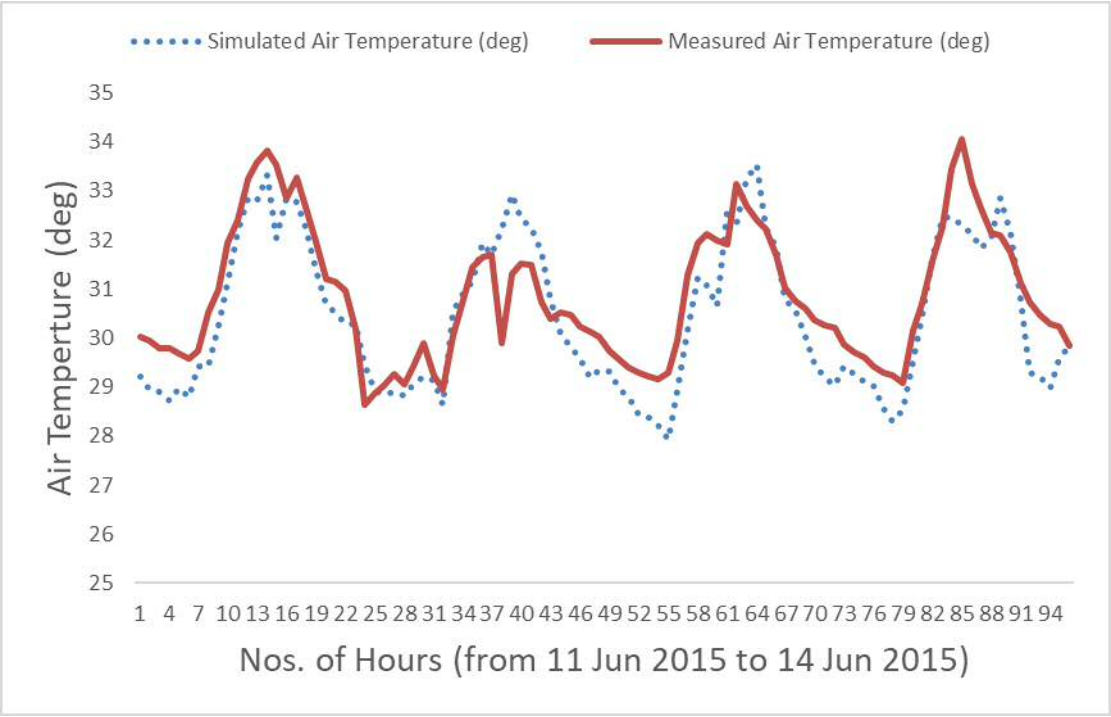

Figure C7. 21 Simulated v.s. measured air temperature at PolyU during 11 Jun 2015 to 14 Jun 2015

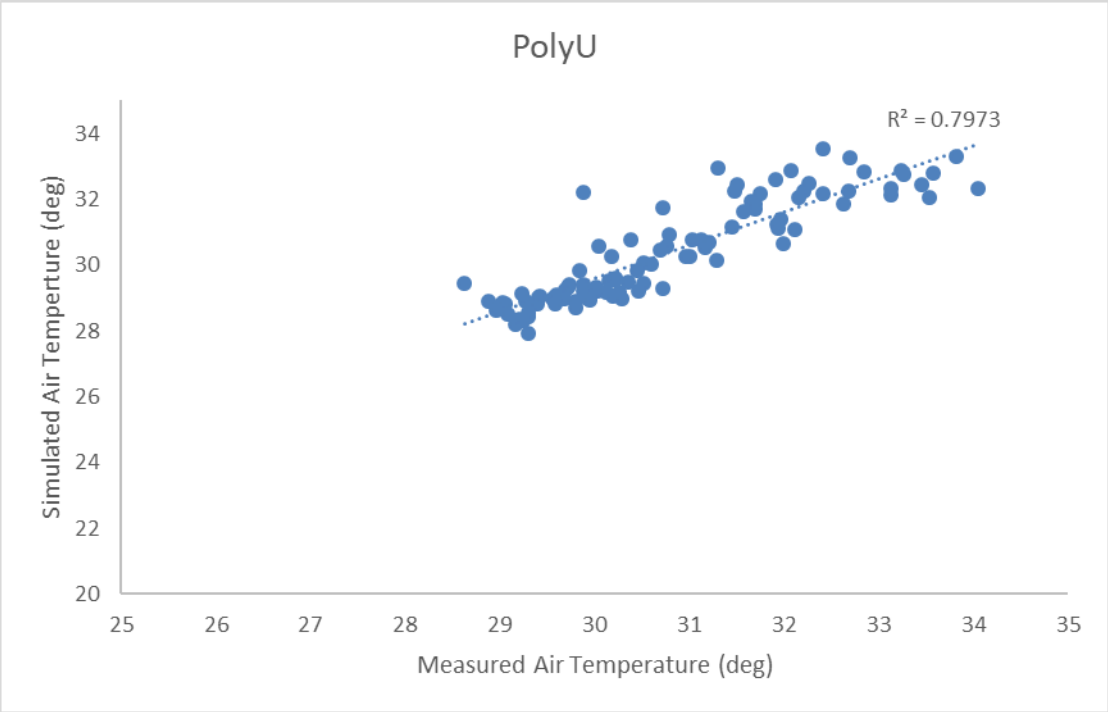

Figure C7. 22 Simulated v.s. measured air temperature at PolyU during 11 Jun 2015 to 14 Jun 2015

The R^2 value of the simulation data during 11 Jun 2015 to 14 Jun 2015 has been assessed. The results show that simulated air temperature for Kowloon Park, HKO and PolyU all shows a reasonably high R^2 value ranging from 0.622 to 0.793. According to Eva Ostertagová (2012) resarch, the performance of the UHI model is satisfactory. The results indicating that the UHI model can well predict the air temperature at the 3 measurement locaions. Table C7. 3 shows the table of the R^2 value.

Table C7. 3 R^2 value for Simulated v.s. measured air temperature during 11 Jun 2015 to 14 Jun 2015

Location	R^2
Kowloon Park	0.622
HKO	0.729
PolyU	0.793

7. 3 Compared UHII variation

The simulated UHII of Kowloon Park, HKO and PolyU during 11 Jun 2015 has been further studied. Figure C7. 23 shows the hourly UHII profile plot. According to the built environment analysis using the Urban Density Database in Chapter 6, the PolyU would has the highest built-up area, while the Kowloon Park would have the lowest built-up area and HKO's built-up area is in between Kowloon Park and PolyU. Based on the Urban Density Database the built-up area for the simulated area is:

- PolyU (highest built-up area)
- HKO (typical built-up area)
- Kowloon Park (lowest built-up area)

The simulated UHII of Kowloon Park, HKO and PolyU is further compared with the measured weather data of the 9 selected weather stations in Chapter 6.

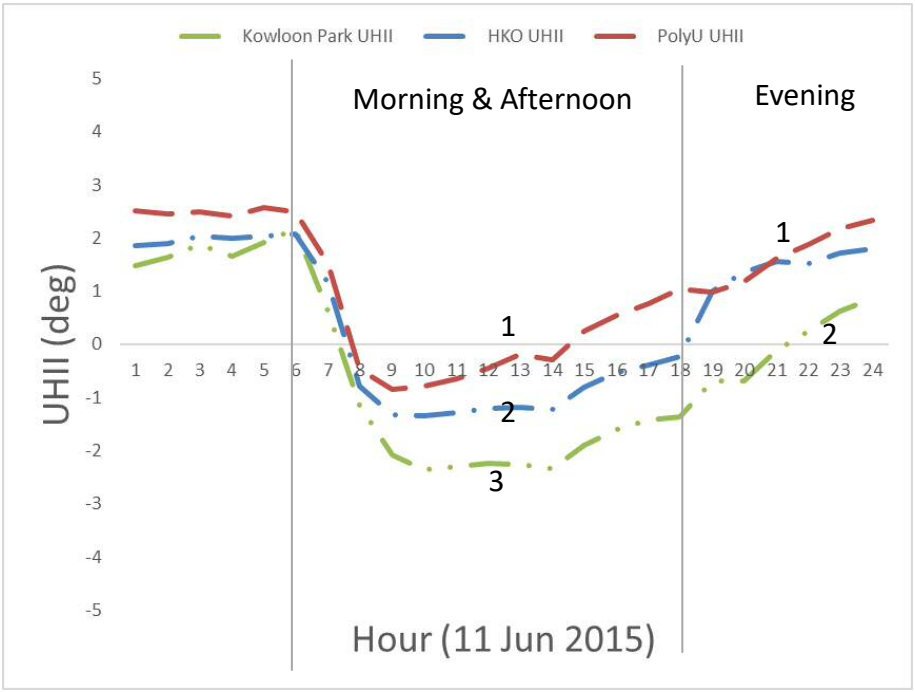

Figure C7. 23 Measured v.s. simlated UHII at 11 Jun 2015 at Kowloon Park, HKO and PolyU

Compare with June 2015 evening period UHII (6AM-12NOON)

Comparing with the measurement data in Section 6.8 the UHII during morning period 6AM to 12NOON, the simulated UHII during 11 Jun 2015 has the similar UHI phenomenon. For example, (1) PolyU (highest built-up area) has the smallest negative UHII, (2) HKO (typical built-up area) has the average UHII, and (3) Kowloon Park (lowest built-up area) has the highest negative UHII, as shown in Figure C7. 23.

Compare with June 2015 evening period UHII (12NOON-6PM)

Comparing with the measurement data in Section 6.9 the UHII during afternoon period 12NOON to 6PM, the simulated UHII also has the similar UHI phenomenon during 11 Jun 2015. For example, (1) PolyU (highest built-up area) has the smallest negative UHII, (2) HKO (typical built-up area) has the average UHII, and (3) Kowloon Park (lowest built-up area) has the highest negative UHII, as shown in Figure C7. 23.

Compare with June 2015 evening period UHII (6PM-12AM)

Comparing with the measurement data in Section 6.10 the UHII during evening period 6PM-12AM, the simulated UHII also has the similar UHI phenomenon. For example, both PolyU (highest built-up area) and HKO (typical built-up area) has similar UHII and the UHII are the lowest and Kowloon Park (lowest built-up area) has the highest negative UHII, as shown in Figure C7. 23.

Compare with E. Ng (2007) Data

Comparing with the E. Ng (2007) hourly UHII profile at 2006 in Figure C6. 19, the simulated UHII also shows a strong similarity between the two sets of data. For example, the simulated UHII is observed with the highest during the nighttime (12AM to 6AM), there is significant

UHII drop during morning period (6AM to 12NOON), UHII generally increased during the afternoon period (12NOON to 6PM) and the UHII significant increase during evening period (6PM to 12AM).

The UHII variation of the simulated data shows a strong similarity to Jun 2015 measurement data from 9 weather station as well as the data from E. Ng (2007) UHII data. The results indicate that the UHI model can truly predict the UHI intensity and suitable to simulate the UHI phenomenon in Hong Kong.

7. 4 Improvement of new UHI modelling approach

The new UHI modelling approach has shown a significant improvement in terms of grid cells reduction and CPU time reduction and requirement during the case study of Tsim Sha Tsui. The case study of modelling 2640m(D) × 2640m(W) × 2640m(H) area only require using 35,937 grid cells. Compared with the recommended grid resolution of 0.1m to 5m (say taken max. of 5m) given in Green Mark NRB (2015), using the new UHI modelling approach the number of Grid Cells can reduce 4000 times and CPU time can reduce from 50,000 hours (CPU × 1) to 0.1 hour (CPU × 1).

Table C7. 4 Improvement of new UHI modelling approach

	Traditional CFD Approach	Volume Averaging Approach	**Improvement**
Domain Size	2640m(D) × 2640m(W) × 2640m(H)	2640m(D) × 2640m(W) × 2640m(H)	-
Number of Grid Cells (5m per cell)	528(D) × 528(W) × 528(H) = 147,197,952 cells	33(D) × 33(W) × 33 (H) = 35,937 cells	**4,000 times reduction**
Estimated CPU time (refers to Figure C1. 3)	Approx. 50,000 hours for 1 CPU	Approx. 0.1 hour for 1 CPU	**500,000 times reduction**

7. 5 Summary

Flow Field Validation - Lid-Driven Cavity Flow

Validation studies have been conducted for the UHI model. In the first validation study, the UHI model conducted a Lid-Driven Cavity Flow simulation. The simlated results are compared with the experimental data from Ghia and Shin (1982). The Lid-Driven Cavity Flow problem is one of the most common validation process for new CFD code and has long been used as a test case for new codes or new solution methods. The problem geometry is simply a 2-dimensional. The boundary conditions is fluid contained in a square domain with Dirichlet boundary conditions on all sides, with three stationary sides and one moving side (with velocity tangent to the side). The UHI model setting follows experiment setup with a square domain of 1m × 1m × 1m, grid number of 33(H) × 33(L) × 33(W) and under Reynolds numbers of 1000. The simulation results are compared with the data of Ghia and Shin (1982) shows that the simulated velocity and the experiment data are comparable and indicating the performance of flow field of the UHI model is satisfactory.

Temperature Field Validation – Tsim Sha Tsui Case Study

In the second validation study, a field measurement has been setup in Tsim Sha Tsui area during 11 Jun to 14 Jun 2015. There are 3 measurement points to measure the air temperature within the Tsim Sha Tsui area simultaneously, including HKO Headquarter (HKO), Kowloon Park and the Hong Kong Polytechnic University (PolyU). The UHI model setting follows experiment setup with a square domain of 2640m × 2640m × 2640m and grid number of 33(H) × 33(L) × 33(W). The boundary conditions is fluid contained with velocity inlet condition at west wall using Wagland Island Station velocity profile, pressure boundary condition with dynamic pressure equal to zero at east wall and symmetric boundary at top, north and south wall. For the Thermal Boundary Condition, the TKL station temperature

profile is applied at top, north, east, south, west wall.

The simulated air temperature has been compared with the measured air temperature at Kowloon Park, HKO and PolyU. The results show the simulated data and the measured data has a strong similarity. The results shows that the simulated data closely follows the increasing and decreasing trend of the measured air temperature with the maximum 2℃ of air temperature difference between simulated and measured data.

Furthermore, the results show a reasonably high R^2 value ranging from 0.622 to 0.793 of the simulated data. According to Eva Ostertagová (2012) resarch, the performance of the UHI model is satisfactory. The results indicate that the UHI model can well predict the air temperature at 3 measurement locations.

Compares with Jun 2015 UHII data and E. Ng (2007) UHII data

The simulated results in Tsim Sha Tsui case study are further compared with the UHII variation among the 9 weather stations and E. Ng (2007) UHII data the discussed in Chapter 6. Using the Urban Density Database to analyse the built environment of the 3 measurement location, PolyU has the highest built-up area, HKO has the typical built-up area and Kowloon Park has the lowest built-up area.

The results findings shows the the simulated UHII variation and the UIHII data in Chapter 6 data has a strong similarity. For example, all data shows the highest built-up area has the smallest negative UHII, while the lowest built-up area has the highest negative UHII during morning period and afternoon period. For the UHII during evening period, the all temperature data has also shown the highest and typical built-up area has the lowest UHII, while lowest built-up area has the highest negative UHII. The results indicate the UHI model can truly predict the UHI intensity and suitable to simulate the UHI phenomenon in Hong Kong.

Improvement of the New UHI Model

Tsim Sha Tsui case study has demonstrated the significant improvement of using new UHI model to reduce the grid cells and CPU time. Comparing with the recommended grid resolution given by Green Mark NRB (2015), using the new UHI modelling approach, the number of Grid Cells can reduce 4000 times and CPU time (4000 times reduction) can reduce from 50,000 hours (CPU $\times$ 1) to 0.1 hour (CPU $\times$ 1) (500,000 times reduction).

Chapter 8 Conclusion

The Chief Executive's 2018 Policy Address has pointed out that Hong Kong must develop land resources to tackle the long-existing housing problem. The development of brownfield sites at Kwu Tung North / Fanling North, Hung Shui Kiu, Yuen Long South, the development of artificial islands and urban renewal development in old districts would inevitably induce greater urban heat island impacts to our living environment. This leads to poorer living quality and health problems. There is an urgent need to introduce a comprehensive urban heat island assessment in our existing town planning town system to ensure the new developments would be planning for a high-density but also a liveable city.

Key Findings

One of the main objectives of this study is to develop a simplified model for UHI study. In order to develop the new UHI, this study has developed Volume Averaging Governing Equations, the sub-modelling equations, urban density database. This study also carried out a case study in Tsim Sha Tsui areas to valid the UHI model. The result findings show that the measurement results and simulation results are in good agreement with high R^2 value ranging from 0.622 to 0.793. The Tsim Sha Tsui case study also proved the new UHI model performance improved significantly as compared to the traditional CFD approach. The number of Grid Cells has reduced 4000 times and CPU time has reduced 500,000 times reduction in the Tsim Sha Tsui case study.

Technical difficulties on modelling UHI study in Hong Kong

The large, highly irregular and complex built environment of Hong Kong induces technical difficulties for the UHI modelling, including, large computational power, long simulation time and complex setting.

Volume Averaging Approach for modelling the heterogeneities condition

Volume Averaging Approach has been identified as the solution to resolve the technical difficulties arise from modelling the heterogeneities condition. The essence of upscaling is to replace a heterogeneous unit with an equivalent homogeneous one, such that the fluid behaviour in the two systems is similar. This approach is suitable to simplify the UHI modelling and to reduce computational limitation.

Volume Averaging Approach is proposed in 1967 by Anderson and Jackson. This approach is further developed by Slattery (1967) and S. Whitaker (1967 & 1977) to study the viscoelastic fluids flow and fluids flow in porous media. Volume Averaging Approach to reduce the computational requirement has been widely applied in hydrology, solute transport, reservoir engineering, oil or gas flow simulation, geotechnical analysis and etc. This thesis applied the same principle for modelling Hong Kong urban content, which is also highly irregular, complex and covers large areas, i.e. heterogeneities condition. Currently, there is still no research applied Volume Averaging Approach to model UHI.

In this study, the concept and general equation of Volume Averaging Approach refers to the work of Amir Faghri (2010). Porosity or void fraction, intrinsic phase average, extrinsic phase average and general transport theorem has been discussed. Volume Averaging Approach has two levels, i.e. Microscopic and Macroscopic Level.

Volume averaging governing equations development

Macroscopic level contains the volume averaged governing equations using REV to solve macroscopic information, such as air velocity field, air temperature field, pressure field, buoyancy force and etc. The following volume averaging governing equations (Macroscopic level) has been developed:

- Volume Averaging Continuity Equation [equation C3. 10 to C3. 16]
- Volume Averaging Momentum Equation [equation C3. 17 to C3. 23]
- Volume Averaging Energy Equation [equation C3. 26 to C3. 31]

Sub-modelling development

Dasheng Qi (2000) has pointed out that the volume averaging of the governing equations would cause information loss at microscopic level, such as the spatial variation value of temperature, velocity and pressure. Sets of sub-models have developed additional terms or sub-models to approximate the lost information in the macroscopic level, such as geometrical effect, solar radiation, greenery evaporation effect etc. The following sub-model has been developed in this thesis:

- Interactive Momentum Force Model [equation C3. 24 to C3. 25]
- Ground / Building Energy Balance Model [equation C3. 32 to C3. 34]
- Net Shortwave Solar Radiation Model [equation C3. 35 to C3. 39]
- Surface Convective Heat Transfer Model [equation C3. 40 to C3. 41]
- Net Longwave Radiation Model [equation C3. 42 to C3. 46]
- Latent Heat Transfer Model [equation C3. 47 to C3. 49]
- Shading Model [equation C3. 50 to C3. 51]
- Deep Ground Temperature Model [equation C3. 52]

Urban density database development

Urban Density Database is developed to transform the GIS data to UHI model input, such as porosity, greenery area, building area, sea area, road area, terrain and building height. The GIS data collected from Hong Kong Lands Department including 3D Spatial Data, Digital Orthophoto DOP5000 and Digital Topographic Map iB5000. The Urban Density Database transforms the GIS to area data through the followings step:

- Step 1: Colouring
- Step 2: Overlaying
- Step 3: Pixel Analysis

The Urban Density Database transforms the GIS to building Height and terrain height data through the followings step:

- Input the 3D Spatial Data into Rhino.
- Using Grasshopper to place a set of control points in 10m separation and projected on to the building or terrain surface. The XYZ coordinate of each test point is then extracted and stored in the database.

Computational grid development

Since the UHI model adopted Volume Averaging Approach, the physical geometry information is replaced by porosity and permeability. The UHI model does not require to define different grid size at specific locations and can applies Cartesian grids approach. The advantage of Cartesian grids approach is that it allows a simple and flexible grid generation and an easy discretization of the solved PDE.

Discretization development

The discretization form of volume averaged equation and the sub-models (Ground / Building Energy Balance Model) have been developed. Fully Implicit Scheme is used for the discretization of the equation for the new model. This method would provide extra stability for the iteration step and allows larger time step in solving the PDE. A computational code and control work flow has developed based on the discretization equations. Unlike traditional CFD approach program, this new UHI model requires to connect to Urban Density Database and three sub-models, i.e. (1) the Interactive Force Model, (2) building heat balance model and (3) ground heat balance model.

Reference rural weather station selection - Ta Kwu Ling (TKL)

Air temperature of the 9 weather stations has further analysed during June 2015 (summer period). The 9 weather stations includes Hong Kong Observatory, Lau Fau Shan, Cheung Chau, Ta Kwu Ling, Waglan Island, Ling Liang Church M H Lau Secondary School, Discovery College, China Holiness Church Living Spirit College and Chiu Chow Association Secondary School. Ta Kwu Ling (TKL) is used as a reference rural weather station to calculated UHII of other weather stations and compared with the E. Ng study (2007). Both studies have shown a strong similarity in terms of UHII. The results indicating that using TKL weather data is suitable reference rural station.

Flow Field Validation - Lid-Driven Cavity Flow

UHI model conducted a Lid-Driven Cavity Flow simulation and compared with the experimental data from Ghia and Shin (1982). The simulation results are compared with the data of Ghia and Shin (1982) shows that the simulated velocity and the experiment data are comparable and indicating the performance of flow field of the UHI model is satisfactory.

Temperature Field Validation – Tsim Sha Tsui Case Study

A field measurement has been setup in Tsim Sha Tsui area during 11 Jun to 14 Jun 2015. There are 3 measurement points to measure the air temperature within the Tsim Sha Tsui area simultaneously, including HKO Headquarter (HKO), Kowloon Park and the Hong Kong Polytechnic University (PolyU). The results show the simulated data and the measured data has a strong similarity. The results shows that the simulated data closely follows the increasing and decreasing trend of the measured air temperature with the maximum 2℃ of air temperature difference between simulated and measured data. The results show a reasonably high R^2 value ranging from 0.622 to 0.793 of the simulated data. According to Eva Ostertagová (2012) research, the performance of the UHI model is satisfactory. The results indicate that the UHI model can well predict the air temperature at 3 measurement locations.

Compares with Jun 2015 UHII data and E. Ng (2007) UHII data

The simulated results in Tsim Sha Tsui case study are further compared with the UHII variation among the 9 weather stations and E. Ng (2007) UHII data. The results findings show the simulated UHII variation and the UIHII data in Jun 2015 and E. Ng (2007) has a strong similarity. For example, all data shows the highest built-up area has the smallest negative UHII, while the lowest built-up area has the highest negative UHII during morning period and afternoon period. For the UHII during evening period, the all temperature data has also shown the highest and typical built-up area has the lowest UHII, while lowest built-up area has the highest negative UHII. The results indicate that the UHI model can truly predict the UHI intensity and suitable to simulate the UHI phenomenon in Hong Kong.

Improvement of the New UHI Model

Tsim Sha Tsui case study has demonstrated the significant improvement of using new UHI model to reduce the grid cells and CPU time. Using the new UHI modelling approach, the number of Grid Cells can reduce 4000 times and CPU time can reduce 500,000 times as compared to traditional CFD approach.

A complete UHI model has been successfully developed to predict the complex process of mass and heat transfer such as convection and conduction effect, advective effect from sea and land breeze, solar radiation, long wave radiation, evaporation effect and buoyancy effect and etc. The concept and mathematics equation of the UHI model has been discussed and presented in this dissertation. The simulated air temperature has been further compared with the measurement results at three locations and showing a high degree of R^2 value and a strong similarity in term of UHI phenomenon.

Future Works

The urban heat island effect is a complex phenomenon mass and heat transfer such as convection and conduction effect, advective effect from sea and land breeze, solar radiation, long wave radiation, evaporation effect and buoyancy effect. And the high density of the building structure which make thermal delay effect significant. Thus, the simulation also needs to consider the transient effect. Since, these complex phenomenons occur in a city scale (10 km^2) urban space, using the traditional CFD approach is impractical due to the high computational power required. This research focus on reducing the complexly of UHI modelling and would to sacrifice some of the microscopic information and accuracy. Therefore, it is important to investigate to ways to increase the accuracy of the model and recapture of the microscopic information but without greatly increase the simulation time and computational power.

Also, the model is validated by field measurement only, while the measurement results would distorted by many uncontrollable affects, such as human load, traffic load and etc. Further experimental validations in a control environment are required to further validate the UHI model.

Reference

[1] Anderson T. B., Jackson R., Fluid Mechanical Description of Fluidized Beds. Equations of Motion, Ind. Eng. Chem. Fund.196764527-539, 1967

[2] Andre Bakker, The future of CFD in Engineering design, the Design Engineering Conference, The 16th National Manufacturing Week Rosemont, IL, USA, March 20-23, 2006

[3] Anita Coulter Flowe, Ashok Kumar, Analysis of velocity fields and dispersive cavity parameters as a function of building width to building height ratio using a 3-D computer model for squat buildings. Journal of Wind Engineering and Industrial Aerodynamics, Volume 86, Issues 2–3, June 2000, 87-12

[4] Ariane Middel, Sky View Factor footprints for urban climate modelling, Urban Climate, 25, 120-134, 2018

[5] Arnfield, A.J., Two decades of urban climate research: a review of turbulence, exchanges of energy and water, and the urban heat island. Int. J. Climatol. 23 (1), 1–26, 2003

[6] Atsushi Yamaguchi, A generalized canopy model for the wind prediction in the forest and the urban area, The Seventh Asia-Pacific Conference on Wind Engineering, 8-12, November 2009

[7] Bass B., Krayenhoff E.S., Mesoscale simulation of urban heat mitigation strategies in Toronto, Canada, Department of Geography, University of Western Ontario, 2002

[8] Best, M., 1998, A model to predict surface temperatures, Boundary-Layer Meteorol, 88, 279–306, 1998

[9] Bo-rong Lin, Studies of greening's effects on outdoor thermal environment, Tsinghua University, 2004

[10] Building and Construction Authority, Green Mark for NRB: 2015 Technical Guide and Requirements, 2015

[11] Burke, S.P, Plummer, W.B., Gas Flow through Packed Columns, Industrial and engineering chemistry, vol.20, No.11, p.p.1196-1200, 1928.11.

[12] Chan, E. Y.., A study of intracity variation of temperature-related mortality and socioeconomic status among the Chinese population in Hong Kong. Journal of Epidemiology and Community Health, 66(4): 322–327, 2012

[13] Chandler, T., 1961. Surface breeze effects of Leicester's heat island. East Midland Geogr. 15, 32–38

[14] Chow, T.T., Estimation of soil temperature profile in Hong Kong from climatic variables, Energy and Buildings, 43, 3568–3575, 2011

[15] Coirier W.J., Sura Kim, CFD Modelling for Urban Area Contaminant Transport and Dispersion: Model Description and Data Requirements, CFD Research Corporation, Alabama, JP2.11, 2006

[16] Critchfield, General Climatology, Prentice Hall, 1983

[17] Dasheng Qi, Upscaling in Reservoir Simulation, School of Petroleum Engineering, August, The University of New South of Wales Sydney, 2000

[18] Dimoudi and M. Nikolopoulou, Vegetation in the urban environment: microclimate analysis and benefits, Energy and Buildings, vol. 35, 2003, pp. 69 – 76, 2003

[19] Eva Ostertagová, Modelling Using Polynomial Regression, Procedia Engineering 48:500–506, 2012

[20] Fabio Murena, Giuseppe Favale, Sotiris Vardoulakis, Efisio Solazzo, Modelling dispersion of traffic pollution in a deep street canyon: Application of CFD and operational models, Atmospheric Environment, Volume 43, Issue 14, 2303-2311, May 2009

[21] Faghri A., Advanced Heat and Mass Transfer, 2009

[22] Fung W. Y., Lam, K. S., Nichol J. E. and Wong M. S., Heat Island Study - Satellite Derived Air Temperature, Journal of Applied Meteorology and Climatology, 48(4), 863-872, 2009

[23] Gallagher J., Gill L.W., McNabola A., Numerical modelling of the passive control of air pollution in asymmetrical urban street canyons using refined mesh discretization schemes, Building and Environment, 2012

[24] Ghia U., and Shin C.T., High-Re Solutions for Incompressible Flow Using the Navier-Stokes Equations and a Multigrid Method. Journal of Computational Physics, 48, 387-411, 1982

[25] Giridharan R., Nocturnal heat island effect in urban residential developments of Hong Kong, Energy And Buildings, v. 37 n. 9, p. 964-971, 2005

[26] Golany G., Urban design morphology and thermal performance, Atmospheric Environment 30(3), 455-465, February 1996

[27] Gomez F., Vegetation and climatic changes in a city, Ecological Engineering 10(4), 1998

[28] Green Power, Mitigate Urban Heat Island in Hong Kong, 2013

[29] Grimmond, An objective urban heatstorage model and its comparison with other schemes, Atmos. Environ. 25B, 311–326, 1991

[30] HKO, Mesoscale Model, https://www.hko.gov.hk/nhm/mesomodel_e.htm

[31] Hajra B., Stathopoulos T., A wind tunnel study of the effect of downstream buildings on near-field pollutant dispersion, Building and Environment, Volume 52, June 2012, 19-31

[32] Hangyu Li, Global upscaling for compositional flow simulation

[33] Hangyu Li, Upscaling for Compositional Reservoir Simulation, SPE Journal, 21 (3), pp. 873-887, 2016

[34] Harman, I. N., Radiative exchange in an urban street canyon. Bound.-Layer Meteor., 110,301–316, 2004

[35] Hartmut Eichel, Upscaling of Two-Phase Flow Processes in Porous Media, Kluwer Academic Publisher, 2004

[36] Hauge V.L., Flow-based grid coarsening for transport simulation, 12th European Conference on the Mathematicss of Oil Recovery, At Oxford, United Kingdom, September 2014

[37] Heat budget and thermodynamics at a free surface: Some theory and numerical implementation (revision 1.0c) ED 1300 BH, The University of Western Australia, Centre for Water Research, June 9, 1998

[38] Honjo, Simulation of thermal effects of urban green areas on their surrounding area, Energy and Buildings, vol. 35, pp. 358-367, 1990

[39] Hui Liu, An equivalent continuum multiscale formulation for 2D geometrical nonlinear analysis of lattice truss structure, Composite Structures, 160, 2017, 335-348

[40] Huizhi Liu, Baoming Wang, Jianguo Sang, Xiaoyun Wang, Numerical Model of Flow Field in Urban Canopy Layer, International Congress on Environmental Modelling and Software. 151, 2002

[41] Ian Nicholas Harman, The energy balance of urban areas, the University of Reading, Department of Meteorology, October 2003

[42] Jian Hang, Yuguo Li, Mats Sandberg, Experimental and numerical studies of flows through and within high-rise building arrays and their link to ventilation strategy, Journal of Wind Engineering and Industrial Aerodynamics, Volume 99, Issue 10, Pages 1036-1055, October 2011

[43] Kam Shing Leung, Estimating Average Sky View Factors of Urban Surfaces with Simple Geometric Parameters, PLEA 2008 – 25th Conference on Passive and Low Energy Architecture, Dublin, 22nd to 24th October 2008

[44] King M.J., MacDonald D.G., Todd S.P., Application of Novel Upscaling Approaches to the Magnus and Andrew Reservoirs. Presented at the European Petroleum Conference, The Hague, 20–22 October, 1998

[45] Kristóf G., Rácz N., Balogh, M., Adaptation of pressure based CFD solvers for mesoscale atmospheric problems. Bound-Lay Meteorol 131, 85-103, 2009

[46] Landsberg H. E., In: The Urban Climate, vol. 28. Academic Press,1981

[47] Liang Wang, Volume-averaged macroscopic equation for fluid flow in moving porous media, International Journal of Heat and Mass Transfer, International Journal of Heat and Mass Transfer 82, 357–368, 2015

[48] Limor Shashua-Bar, Milo E. Hoffman, Geometry and orientation aspects in passive cooling of canyon streets with trees, 2003

[49] Limor Shashua-Bar, Milo E. Hoffman, Vegetation as a climatic component in the design of an urban street, 2002

[50] Limor Shashua-Bara, Milo E. Hoffman, (2002) The Green CTTC model for predicting the air temperature in small urban wooded sites, Building and Environment 37, 1279–1288, 2002

[51] Losada I. J., Modelling the Interaction of Water Waves with Porous Coastal Structures, Journal of Waterway, Port, Coastal, and Ocean Engineering, Vol. 142, Issue 6, November 2016

[52] Marsh A., why shading calculations take so long, ISSN 1833-7570, issue 004, 05 Nov 2007

[53] Martilli A., An urban surface exchange parameterization for mesoscale models. Boundary-Layer Meteorol. 104, 261–304, 2002

[54] Maruyama, Optimization of roughness parameters for staggered arrayed cubic blocks using experimental data, J. of Wind Engineering, No.52, pp.424-429, 1992.

[55] Masson, A physically-based scheme for the urban energy budget in atmospheric models, Boundary-Layer Meteorol. 94(3), 357–397, 2000

[56] Matzarakis, Mapping of Urban Air Paths for Planning in Munich, Planning Applications of Urban and Building Climatology, Wiss. Ber. Inst. Meteor, Klimaforsch. Univ. Karlsruhe 16; 13 – 22, 1992

[57] Matzarakis, Urban Climate Analysis of Freiburg – An Integral Assessment Approach. Paper Presented at the 4th Japanese– German Meeting on Urban Climatology, 2005

[58] Miklós Balogh, Fine scale simulation of turbulent flows in urban canopy layers, Quarterly Journal of the Hungarian Meteorological Service, Vol. 114, No. 1–2, pp 135–148, January – June 2010

[59] Mohamed F. Yassin, Impact of height and shape of building roof on air quality in urban street canyons, Atmospheric Environment, Volume 45, Issue 29, 5220-5229, September 2011

[60] Ng E., Urban Heat Island in Hong Kong, A Position Paper, Department of Architecture, Chinese University of Hong Kong, 2007

[61] Ng E., Ren, C., China's adaptation to climate & urban climatic changes: A critical review, Urban Climate, 2017

[62] Ng E., Urban climatic map studies: a review, international journal of climatology, Int. J. Climatol., 2010

[63] Oke T., Classifying urban climate ?eld sites by local climate zones: the case of Nagano, Japan," in The Seventh International Conference on Urban Climate (Yokohama), 2009

[64] Oke T., The urban energy balance, SAGE Journals, Progress in Physical Geography: Earth and Environment, 1988

[65] Oke T., Boundary layer climates. Routledge, New York, 1987

[66] Oke T., The energetic basis of the urban heat island, Quarterly Journal of the Royal Meteorological Society, https://doi.org/10.1002/qj.49710845502, January 1982

[67] Oke T., The urban boundary layer in Montreal Boundary Layer Meteorology, 411–437, 1971

[68] P. A. Mirzaei, Approaches to study Urban Heat Island Abilities and limitations, Building and Environment 45, 2192-2201, 2010

[69] R. Giridharan, Daytime urban heat island effect in high-rise and high-density residential developments in Hong Kong, Energy and Building, Vol. 36, pp 525-534, 2004

[70] Rajagopalan P, Lim KC, Jamei E: Urban heat island and wind flow characteristics of a tropical city, Sol Energy, 107:159-170, 2014

[71] Roth M., Handbook of Environmental Fluid Dynamics, Volume Two, edited by Harindra Joseph Shermal Fernando

[72] Saitoh T. S., Modelling and simulation of the Tokyo urban heat island, Atmospheric Environment Vol. 30, No. 20, pp. 3431-3442, 1996

[73] Santamouris, M., Georgakis, C., Energy and indoor climate in urban environments: recent trends. Build. Ser. Eng. Res. Technol. 24 (2), 69–81, 2003

[74] Santamouris, M., Heat island research in Europe: the state of the art. Adv Build. Energy Res. 1 (1), 123–150, 2007

[75] Santamouris, M., Papanikolaou, N., Livada, I., Koronakis, I., Georgakis, C., Argiriou, A., Assimakopoulos, D., On the impact of urban climate on the energy consumption of buildings, Sol. Energy 70 (3), 201–216, 2001

[76] Scherer D., Improved concepts and methods in analysis and evaluation of the urban climate for optimizing urban planning process, Atmospheric Environment 33, 4185–4193, 1999

[77] Sergey Chaynikov, Theoretical and numerical upscaling of solute transport in porous media.

[78] Shinji Yoshida, Development of three Dimensional Plant Canopy Model for Numerical Simulation of Outdoor Thermal Environment, 6th International Conference on Urban Climate, 2006

[79] Slattery J. C., Flow of viscoelastic fluids through porous media, AIChE Journal Volume 13, Issue 6, 1967

[80] Suhas V. Patankar [58], Numerical Heat Transfer and Fluid Flow, 1980.

[81] Swaid H., Hoffman M. E., Prediction of urban air temperature variations using the analytical CTTC model, Energy and Buildings, 14, 313-324, 1990a

[82] Thom J., 3-D Grid Types in Geomodelling and Simulation – How the Choice of the Model Container Determines Modelling Results, Search and Discovery Article #40477, December 23, 2009

[83] Tso C. P., A survey of urban heat island studies in two tropical cities. Atmospheric Environment, 30, 507–19, 1996

[84] Versteeg and Malalasekera, An Introduction to Computational Fluid Dynamics the Finite Volume Method. Longman Scientific and Technical, England, 1995

[85] Wang X., McNamara K.F., Effects of street orientation on dispersion at or near urban street intersections, Journal of Wind Engineering and Industrial Aerodynamics, Volume 95, Issues 9–11, 1526-1540, October 2007

[86] Whitaker S., Diffusion and dispersion in porous media, AIChE Journal, Volume 13, Issue 31967, 1967

[87] Whitaker S., Fundamental principles of heat transfer, AIChE JournalVolume 23, Issue 5, 1977

[88] Whitaker, S., The Method of Volume Averaging, 1999

[89] Wienert U., Kuttler W., The dependence of the urban heat island intensity on latitude - A statistical approach, Meteorologische Zeitschrift 14(5), 677-686, October 2005

[90] Wong JKW, Lau LS-K, From the ‘urban heat island’ to the ‘green island’? A preliminary investigation into the potential of retrofitting green roofs in Mong kok district of Hong Kong, Habitat Int 2013, 39:25-35, 2013

[91] Wong N.H., Performance of Greenery Systems in Zero Energy Building of Singapore, International Conference on Sustainable Design and Construction (ICSDC), 2011

[92] Wong N.H, Urban heat island research: Challenges and potential, Frontiers of Architectural Research, Volume 5, Issue 2, Pages 276–278, June 2016

[93] Woolum, Notes from a study of the microclimatology of the Washington, DC area for the winter and spring seasons. Weatherwise, 17, No. 6, 1964

[94] Xiaomin Xie, Zhen Huang, Jia-song Wang, Impact of building configuration on air quality in street canyon, Atmospheric Environment, Volume 39, Issue 25, 4519-4530, August 2005

[95] Zhao-Lin Gu, Effect of uneven building layout on air floor and pollutant dispersion in non-uniform street canyons, Building and Environment, Volume 46, 2657-2665, 2011

Appendix A - Program Code – Urban Density Database

Calculate Density from GIS

```
import csv
def make_grid(source,Input1):
    wf = open("Density_OUTPUT.csv",'w',encoding='utf8',newline='')
    writer=csv.writer(wf)
    file = open(Input1, 'r', encoding="utf8")
    txt2 = file.readlines()
    for line in txt2:
        xy = line.split(",")
        x = int(xy[0])
        y = int(xy[1])
        file=open(source,'r',encoding="utf8") # not use csv lib. have "/n" at each
next line
        txt=file.readlines()
        average_value= []
        outList=[]
        total=0
        count= 0
        count_0 = 1
        for line in txt:
            new = line.split(",") # split the txt with ","
            print(new[2])
```

```
        Gridx = float(new[0])
        Gridy = float(new[1])
        height = float(new[2].strip()) # .strip is to remove the "/n"
        if Gridx >=x and Gridx <x+500 and Gridy >=y-500 and Gridy <y:
            print("right")
            total+=height # sum up total height
            count = count + 1
if count == 0 or total == 0:
        average_value = 0
        result=[x,y,average_value] # type: #LIST
elif count == 0 and total == 0:
        average_value = 0
        result=[x,y,average_value] # type: #LIST
else:
        average_value = total / count
        result=[x,y,average_value] # type: #LIST
print(result)
outList.append(result)
writer.writerow(result) # write out to csv
total=0
print(outList)
```

```
import pandas as pd
import csv
import os
class main():
    def __init__(self,folder):
        wf = open("height_sdf.csv",'w',encoding='utf8',newline='')
        self.writer=csv.writer(wf)
        self.set_folder(folder)
        wf.close()
    def set_folder(self,folder):
        folders = os.listdir(folder)
        for fd in folders:
            self.id=fd
            files = os.listdir(folder+fd)
            for file in files:
                #print (file)
                if file.endswith("sdf"):
                    path=folder+fd+"/"+file
                    #print (path)
                    self.read_sdf(path)
    def read_sdf(self,path):
        #df=pd.read_csv(path)
        #with open(path,'r') as f:
        #    reader =csv.reader(f)
```

```
            #       for row in reader:
            #               print (row)
            file=open(path,'r',encoding="utf8",errors='ignore')
            txt=file.readlines()
            for line in txt:
                str=line.strip()
                list=str.split(",")
                self.write_csv(list)
                #print (line)
        def write_csv(self,list):
            #print (type(list),list[1])
            x,y=self.get_location(list[1])
            print (list[9])
listData=[self.id,list[0],x,y,list[2][1:-1],list[4],list[6],list[8],list[9][1:-1],list[-2]]
            #print (listData)
            self.writer.writerow(listData)
        def get_location(self,string):
            y=str(8)+string[6:-1]
            x=str(8)+string[1:6]
            return x,y
```

```
import pandas as pd
import csv
import os
class main():
    def __init__(self,folder):
```

```
        wf = open("height_sdf.csv",'w',encoding='utf8',newline='')
        self.writer=csv.writer(wf)
        self.set_folder(folder)
        wf.close()
    def set_folder(self,folder):
        folders = os.listdir(folder)
        for fd in folders:
            self.id=fd
            files = os.listdir(folder+fd)
            for file in files:
                #print (file)
                if file.endswith("sdf"):
                    path=folder+fd+"/"+file
                    #print (path)
                    self.read_sdf(path)
    def read_sdf(self,path):
        #df=pd.read_csv(path)
        #with open(path,'r') as f:
        #       reader =csv.reader(f)
        #       for row in reader:
        #           print (row)
        file=open(path,'r',encoding="utf8",errors='ignore')
        txt=file.readlines()
        for line in txt:
            str=line.strip()
            list=str.split(",")
```

```
                self.write_csv(list)
                #print (line)
        def write_csv(self,list):
                #print (type(list),list[1])
                x,y=self.get_location(list[1])
                print (list[9])

listData=[self.id,list[0],x,y,list[2][1:-1],list[4],list[6],list[8],list[9][1:-1],list[12]]
                #print (listData)
                self.writer.writerow(listData)
        def get_location(self,string):
                y=str(8)+string[6:-1]
                x=str(8)+string[1:6]
                return x,y
def make_grid(source,source2):
        wf = open("height_grid.csv",'w',encoding='utf8',newline='')
        writer=csv.writer(wf)
        file = open(source2, 'r', encoding="utf8")
        txt2 = file.readlines()
        for line in txt2:
                xy = line.split(",")
                x = int(xy[0])
                y = int(xy[1])
                print (x,y)

                file=open(source,'r',encoding="utf8") # not use csv lib. have "/n" at each
```

```
next line
            txt=file.readlines()
            average_value= []
            outList=[]
            total=0
            count= 0
            count_0 = 1
            for line in txt:
                new = line.split(",") # split the txt with ","
                Gridx = int(new[0])
                Gridy = int(new[1])
                print( Gridx, Gridy)
                height = float(new[2].strip()) # .strip is to remove the "/n"
                if Gridx >=x and Gridx <x+500 and Gridy >=y-500 and Gridy <y:
                    print("right")
                    total+=height # sum up total height
                    count = count + 1
            if count == 0 or total == 0:
                average_value = 0
                result=[x,y,average_value] # type: #LIST
            elif count == 0 and total == 0:
                average_value = 0
                result=[x,y,average_value] # type: #LIST
            else:
                average_value = total / count
                result=[x,y,average_value] # type: #LIST
```

```
print(result)
outList.append(result)
writer.writerow(result) # write out to csv
total=0
print(outList)
```

```
import os
import rhinoscriptsyntax as rs
import shutil
import math


class main():
    def __init__(self):
        rs.UnitSystem(unit_system=4)
        rs.EnableRedraw(False)
        self.root="D:\Reference\Programming\Python\MapAnalysis\data\gis"
        """
        a:addition
        w:overwrite
        """
        f=open(self.root+"\\"+'height.csv','a')
        self.open_files(f)
        #self.export(self.hList)
        print("finish!!!")


    def open_files(self,f):
        folder = rs.BrowseForFolder(self.root,message=None)
        files=os.listdir(folder)
        hList=[]
        print("total file:"+str(len(files)))
```

```
        finish=0
        for file in files:
            if file.startswith("B"):
                #need to add logic to select latest topo file
                openfile=self.root+"\\"+file+"\\"+file+".3ds"
                #strOptions = " _SetUnWeldAngle=_Yes _UnWeldAngle=22.5 "
                rs.Command('_Open ' + openfile,0)
                rs.Command("_Enter",0)
                obj=rs.AllObjects(select=True)
                #rs.ViewTarget(view="Front",target=obj)
                height=self.get_height(obj)
                hList.append(height)
                rs.DocumentModified(modified=False)
                finish+=1
                print("finish:"+str(finish))
                row=file+","+str(height)
                f.write(row+"\n")
                shutil.move(self.root+"\\"+file,self.root+"\\finish")
        self.hList=hList

def get_height(self,obj):
        line=rs.MeshOutline(obj,view="Front")
        points=rs.PolylineVertices(line)
        #print (len(points))
        zList=[]
        for pt in points:
```

```
            zList.append(pt[2])
        height=max(zList)-min(zList)
        #print (height)
        return height

    def write_file(self,num):
        f=open(self.root+"\\"+'height.csv','w')
        f.write("\n"+num)
        f.close()

    def export(list):
        f=open(self.root+"\\"+'height.csv','w')
        for num in list:
            f.writeline(num)
        f.close()


class topo():
    def __init__(self):
        rs.UnitSystem(unit_system=4)
        rs.EnableRedraw(False)

self.root="D:\\Reference\\Programming\\Python\\MapAnalysis\\data\\gis\\all\\"

self.move="D:\\Reference\\Programming\\Python\\MapAnalysis\\data\\gis\\finish"
```

```
self.fail="D:\\Reference\\Programming\\Python\\MapAnalysis\\data\\gis\\fail"
        self.open_files()

    def open_files(self):

        cfolder = os.listdir(self.root)
        hList=[]
        print("total folder:"+str(len(cfolder)))
        finish=0
        for folder in cfolder:
            print (folder)
            #print(self.root+"\\"+folder)
            files = os.listdir(self.root+folder)
            """
            a:addition
            w:overwrite
            """
            f=open(self.root+folder+"\\"+'topo.csv','w')

            tFile=self.getLatest(files)
            #print (tFile)
            openfile=self.root+"\\"+folder+"\\"+tFile+"\\"+tFile+".3ds"
            #print("open file:"+openfile)
            rs.Command('_Open ' + openfile,0)
            rs.Command("_Enter",0)
            result,ptList=self.topo(f)
```

```
                if result:
                    self.write_file(ptList,f)
                    rs.DocumentModified(modified=False)
                    f.close()
                    shutil.move(self.root+"\\"+folder,self.move)
                else:
                    rs.DocumentModified(modified=False)
                    shutil.move(self.root+"\\"+folder,self.fail)
                """
                for file in tFiles:
                    openfile=self.root+"\\"+folder+"\\"+file+"\\"+file+".3ds"
                    print("open file:"+openfile)
                        #strOptions = " _SetUnWeldAngle=_Yes
_UnWeldAngle=22.5 "
                        rs.Command('_Open ' + openfile,0)
                        rs.Command("_Enter",0)
                        ptList=self.topo(f)
                        self.write_file(ptList,f)
                        rs.DocumentModified(modified=False)
                """


    def getLatest(self,files):
        vList=[]
        tList=[]
        for file in files:
```

```
            if file.startswith("T"):
                #print (file)
                try:
                    ver=int(file[-2:])
                    vList.append(ver)
                    tList.append(file)
                except:
                    pass
        #print (vList)
        key=max(vList)
        vtDict=dict(zip(vList,tList))
        tFile=vtDict[key]
        return tFile

def topo(self,f):
        #rs.ViewDisplayMode(view="Top")
        #rs.CurrentView(view="Top")
        obj=rs.AllObjects(select=True)
        line=rs.MeshOutline(obj,view="Top")
        rs.SimplifyCurve(line)
        #can change by ObjectsByType
        #topo=rs.LastObject(select=True)
        #rs.HideObject(topo)
        #curve=rs.AllObjects(select=True)
        curve=rs.ObjectsByType(4)
        center=rs.CurveAreaCentroid(curve[0])
```

```
        offset=rs.OffsetCurve(curve[0],center[0],16)
        points=rs.CurvePoints(curve[0])
        pt1 = self.get_end(points)
        pt2 = self.get_diagonal(points,pt1)
        rs.AddPoint(pt1)
        rs.AddPoint(pt2)
        #rs.ShowObject(topo)
        result,drape_srf=self.drape(pt1,pt2)
        if result:
            ctrlpts=self.get_ctrlpt(drape_srf,offset)
        else:
            ctrlpts=""
            #avgZ=get_avgZ(ctrlpts)
            #print (pt1,pt2,avgZ)
        return result,ctrlpts


def get_end(self,points):
        """
        extract end point which is closest to origin point
        """
        pt1=points[0]
        base = rs.Distance([0,0,0],pt1)
        for pt in points:
            dis=rs.Distance([0,0,0],pt)
            if dis < base:
                base = dis
```

```
                pt1=pt
        return pt1


def get_diagonal(self,points,pt1):
        #pt1=points[0]
        base = rs.Distance(points[1],pt1)
        for pt in points:
                dis=rs.Distance(pt,pt1)
                if dis > base:
                        base = dis
                        pt2=pt


        return pt2


def drape(self,pt1,pt2):
        a = "AutoSpacing=Yes"
        b = "Spacing=10"
        c = "AutoDetectMaxDepth=No"
        cmd="_Drape {0} {1} {2} {3} {4}".format(a,b,c,pt1,pt2)
        rs.CurrentView(view="Top")
        result = rs.Command(cmd, True)
        if result:
                drape_srf = rs.LastCreatedObjects(select=True)[0]
        else:
                print ("No result")
                drape_srf=""
```

```
        return result, drape_srf


def get_ctrlpt(self,surface,region):
        points=rs.SurfaceEditPoints(surface)
        endpts=rs.CurvePoints(region)
        pt1 = self.get_end(endpts)
        pt2 = self.get_diagonal(endpts,pt1)
        ctrlpts=[]
        if pt1[0]<pt2[0]:
                sx=pt1[0]
                lx=pt2[0]
        elif pt2[0]<pt1[0]:
                sx=pt2[0]
                lx=pt1[0]
        if pt1[1]<pt2[1]:
                sy=pt1[1]
                ly=pt2[1]
        elif pt2[1]<pt1[1]:
                sy=pt2[1]
                ly=pt1[1]
        for pt in points:
                if pt[0]>sx and pt[0]<lx:
                        if pt[1]>sy and pt[1]<ly:
                                ctrlpts.append(pt)
        return ctrlpts
```

```
    def get_avgZ(self,points):
        zList=[]
        for pt in points:
            #print (pt[0],pt[1],pt[2])
            zList.append(pt[2])
        rs.AddPoints(points)
        avg=sum(zList)/len(zList)
        return zList,avg

    def write_file(self,list,f):
        for pt in list:
            row = str(pt[0])+","+str(pt[1])+","+str(pt[2])
            f.write(row+"\n")
```

```
import csv

def
make_grid(Database1,Database2,Database3,Database4,Database5,Database6,Input1):
    wf = open("TopoElev_grid.csv",'w',encoding='utf8',newline='')
    writer=csv.writer(wf)

    file = open(Input1, 'r', encoding="utf8")
    txt2 = file.readlines()
```

```
for line in txt2:
    xy = line.split(",")
    x = int(xy[0])
    y = int(xy[1])

    if y >= 835999 and y < 848000:
        source = Database1

    elif y >= 823999 and y < 835999 and x >= 830000 and x < 860000:
        source = Database2

    elif y >= 823999 and y < 835999 and x >= 800000 and x < 830000:
        source = Database3

    elif y >= 811999 and y < 823999 and x >= 830000 and x < 860000:
        source = Database4

    elif y >= 811999 and y < 823999 and x >= 800000 and x < 830000:
        source = Database5

    else:
        source = Database6

    print(source)
    file=open(source,'r',encoding="utf8") # not use csv lib. have "/n" at each
```

```
next line
        txt=file.readlines()


        average_value= []
        outList=[]
        total=0
        count= 0
        count_0 = 1


        for line in txt:
            new = line.split(",") # split the txt with ","
            print(new[0])
            Gridx = float(new[0])
            Gridy = float(new[1])
            print(Gridx, Gridy)
            height = float(new[2].strip()) # .strip is to remove the "/n"
            if Gridx >=x and Gridx <x+500 and Gridy >=y-500 and Gridy <y:
                print("right")
                total+=height # sum up total height
                count = count + 1
        if count == 0 or total == 0:
            average_value = 0
            result=[x,y,average_value] # type: #LIST
        elif count == 0 and total == 0:
            average_value = 0
            result=[x,y,average_value] # type: #LIST
```

```
            else:
                average_value = total / count
                result=[x,y,average_value] # type: #LIST
            print(result)
            outList.append(result)
            writer.writerow(result) # write out to csv
            total=0
            print(outList)


if __name__=='__main__':
    Database1 =
"D:\\RESEARCH_UrbanHeatIsland\\DENSITY\\topo\\Database\\84800to835999.csv
"
    Database2 =
"D:\\RESEARCH_UrbanHeatIsland\\DENSITY\\topo\\Database\\835999to823999_8
30000to860000.csv"
    Database3 =
"D:\\RESEARCH_UrbanHeatIsland\\DENSITY\\topo\\Database\\835999to823999_8
00000to830000.csv"
    Database4 =
"D:\\RESEARCH_UrbanHeatIsland\\DENSITY\\topo\\Database\\823999to811999_8
30000to860000.csv"
    Database5 =
"D:\\RESEARCH_UrbanHeatIsland\\DENSITY\\topo\\Database\\823999to811999_8
00000to830000.csv"
    Database6 =
```

"D:\\RESEARCH_UrbanHeatIsland\\DENSITY\\topo\\Database\\823999to811999_800000to830000.csv"

make_grid(Database1,Database2,Database3,Database4,Database5,Database6,Input1)

Appendix B - Program Code – Urban Heat Island Model

Momentum Equation

```
Sub UMomentum()

For I = 2 To NIMM
For J = 2 To NJMM
For K = 2 To NKMM
    souC(I, J, K) = 0
    souP(I, J, K) = 0
Next K
Next J
Next I

For I = 2 To NIMM
For J = 2 To NJMM
For K = 2 To NKMM

If gdiffe(I, J, K) = 0 Then
    AE1(I, J, K) = dmax1(-gconve(I, J, K), 0#)
Else
    AE1(I, J, K) = gdiffe(I, J, K) * (dmax1(0#, 1# - 0.5 * Abs(gconve(I, J, K) /
    gdiffe(I, J, K)))) + dmax1(-gconve(I, J, K), 0#)
End If
```

```
If gdiffe(I - 1, J, K) = 0 Then
    AW1(I, J, K) = dmax1(gconve(I - 1, J, K), 0#)
Else
    AW1(I, J, K) = gdiffe(I - 1, J, K) * (dmax1(0#, 1# - 0.5 * Abs(gconve(I - 1, J, K)
    / gdiffe(I - 1, J, K)))) + dmax1(gconve(I - 1, J, K), 0#)
End If

If gdiffn(I, J, K) = 0 Then
    AN1(I, J, K) = dmax1(-gconvn(I, J, K), 0#)
Else
    AN1(I, J, K) = gdiffn(I, J, K) * (dmax1(0#, 1# - 0.5 * Abs(gconvn(I, J, K) /
    gdiffn(I, J, K)))) + dmax1(-gconvn(I, J, K), 0#)
End If

If gdiffn(I, J - 1, K) = 0 Then
    AS1(I, J, K) = dmax1(gconvn(I, J - 1, K), 0#)
Else
    AS1(I, J, K) = gdiffn(I, J - 1, K) * (dmax1(0#, 1# - 0.5 * Abs(gconvn(I, J - 1, K) /
    gdiffn(I, J - 1, K)))) + dmax1(gconvn(I, J - 1, K), 0#)
End If

If gdifft(I, J, K) = 0 Then
    AT1(I, J, K) = dmax1(-gconvt(I, J, K), 0#)
Else
    AT1(I, J, K) = gdifft(I, J, K) * (dmax1(0#, 1# - 0.5 * Abs(gconvt(I, J, K) / gdifft(I,
```

```
        J, K)))) + dmax1(-gconvt(I, J, K), 0#)
End If

If gdifft(I, J, K - 1) = 0 Then
        AB1(I, J, K) = dmax1(gconvt(I, J, K - 1), 0#)
Else
        AB1(I, J, K) = gdifft(I, J, K - 1) * (dmax1(0#, 1# - 0.5 * Abs(gconvt(I, J, K - 1) /
        gdifft(I, J, K - 1)))) + dmax1(gconvt(I, J, K - 1), 0#)
End If

Next K
Next J
Next I

For K = 2 To NKMM
For J = 2 To NJMM
For I = 2 To NIMM
        gpe = (gp(I, J, K) + gp(I + 1, J, K)) / 2#
        gpw = (gp(I, J, K) + gp(I - 1, J, K)) / 2#
        souC(I, J, K) = -gpor(I, J, K) * (gpe - gpw) / dx(I, J, K)
Next I
Next J
Next K

Call souC_shear_u(gdudy, gdwdy, souC)
```

```
For K = 2 To NKMM
For J = 2 To NJMM
For I = 2 To NIMM
    gpore(I, J, K) = (gpor(I, J, K) + gpor(I + 1, J, K)) / 2#
    gporw(I, J, K) = (gpor(I, J, K) + gpor(I - 1, J, K)) / 2#
    gporn(I, J, K) = (gpor(I, J, K) + gpor(I, J + 1, K)) / 2#
    gpors(I, J, K) = (gpor(I, J, K) + gpor(I, J - 1, K)) / 2#
    gport(I, J, K) = (gpor(I, J, K) + gpor(I, J, K + 1)) / 2#
    gporb(I, J, K) = (gpor(I, J, K) + gpor(I, J, K - 1)) / 2#
    varpore(I, J, K) = (gu(I, J, K) / gpor(I, J, K) + gu(I + 1, J, K) / gpor(I + 1, J, K)) /
    2#
    varporw(I, J, K) = (gu(I, J, K) / gpor(I, J, K) + gu(I - 1, J, K) / gpor(I - 1, J, K)) /
    2#
    varporn(I, J, K) = (gu(I, J, K) / gpor(I, J, K) + gu(I, J + 1, K) / gpor(I, J + 1, K)) /
    2#
    varpors(I, J, K) = (gu(I, J, K) / gpor(I, J, K) + gu(I, J - 1, K) / gpor(I, J - 1, K)) /
    2#
    varport(I, J, K) = (gu(I, J, K) / gpor(I, J, K) + gu(I, J, K + 1) / gpor(I, J, K + 1)) /
    2#
    varporb(I, J, K) = (gu(I, J, K) / gpor(I, J, K) + gu(I, J, K - 1) / gpor(I, J, K - 1)) /
    2#
Next I
Next J
Next K

For K = 2 To NKMM
```

```
For J = 2 To NJMM
    If (gvboundtype1(J, K) = "w") Then '            (Neumann)
        gpore(NIMM, J, K) = gpor(NIMM, J, K)
    End If
    If (gvboundtype2(J, K) = "w") Then '            (Neumann)
        gporw(2, J, K) = gpor(2, J, K)
    End If
Next J
Next K
For K = 2 To NKMM
For I = 2 To NIMM
    If (gvboundtype3(I, K) = "w") Then '            (Neumann)
        gporn(I, NJMM, K) = gpor(I, NJMM, K)
    End If
    If (gvboundtype4(I, K) = "w") Then '            (Neumann)
        gpors(I, 2, K) = gpor(I, 2, K)
    End If
Next I
Next K
For J = 2 To NJMM
For I = 2 To NIMM
    If (gvboundtype5(I, J) = "w") Then '            (Neumann)
        gport(I, J, NKMM) = gpor(I, J, NKMM)
    End If
    If (gvboundtype6(I, J) = "w") Then '            (Neumann)
        gporb(I, J, 2) = gpor(I, J, 2)
```

```
        End If
Next I
Next J
For K = 2 To NKMM
For J = 2 To NJMM
For I = 2 To NIMM
            dpordx = (gpore(I, J, K) - gporw(I, J, K)) / dx(I, J, K)
            dpordy = (gporn(I, J, K) - gpors(I, J, K)) / dy(I, J, K)
            dpordz = (gport(I, J, K) - gporb(I, J, K)) / dz(I, J, K)
            dvardx = (varpore(I, J, K) - varporw(I, J, K)) / dx(I, J, K)
            dvardy = (varporn(I, J, K) - varpors(I, J, K)) / dy(I, J, K)
            dvardz = (varport(I, J, K) - varporb(I, J, K)) / dz(I, J, K)
        If (spor(I, J, K) > 1E-20) Then
                souC(I, J, K) = souC(I, J, K) - gvis(I, J, K) * (dpordx * dvardx +
                dpordy * dvardy + dpordz * dvardz)
        End If
Next I
Next J
Next K

If Energy = "ON" Then
            For K = 2 To NKMM
            For J = 2 To NJMM
            For I = 2 To NIMM
                gravterm = gravx
                souC(I, J, K) = souC(I, J, K) + gpor(I, J, K) * (gden(I, J, K) - gdenamb)
```

```
                * gravterm
            Next I
            Next J
            Next K
End If
For K = 2 To NKMM
For J = 2 To NJMM
For I = 2 To NIMM
    souC(I, J, K) = souC(I, J, K) + gdenold(I, J, K) * guold(I, J, K) / dt
Next I
Next J
Next K

If Porosity = "ON" Then
            For K = 2 To NKMM
            For J = 2 To NJMM
            For I = 2 To NIMM
                temp = gpor(I, J, K) * PermX(I, J, K)
                souP(I, J, K) = ((1.8 * gden(I, J, K) * gu(I, J, K) / (180# * temp) ^ 0.5),
                0)
            Next I
            Next J
            Next K
End If

For K = 2 To NKMM
```

```
For J = 2 To NJMM
For I = 2 To NIMM
    souC(I, J, K) = souC(I, J, K) * vol(I, J, K)
    souP(I, J, K) = souP(I, J, K) * vol(I, J, K)
Next I
Next J
Next K

For K = 2 To NKMM
For J = 2 To NJMM
For I = 2 To NIMM
    AP1(I, J, K) = AE1(I, J, K) + AW1(I, J, K) + AN1(I, J, K) + AS1(I, J, K) + AT1(I,
    J, K) + AB1(I, J, K) + gdenold(I, J, K) * vol(I, J, K) / (dt) - souP(I, J, K)
Next I
Next J
Next K

For K = 2 To NKMM
For J = 2 To NJMM
Select Case (gvboundtype1(J, K))
    Case "n", "p" 'Pressure and Outlet
    AP1(NIMM, J, K) = AP1(NIMM, J, K) - AE1(NIMM, J, K)
    AE1(NIMM, J, K) = 0#
  Case "d"        'Inlet
    AP1(NIMM, J, K) = AP1(NIMM, J, K) + AE1(NIMM, J, K)
    souC(NIMM, J, K) = souC(NIMM, J, K) + 2# * gvboundvalue1(1, J, K) *
```

```
        AE1(NIMM, J, K)
        AE1(NIMM, J, K) = 0#
    Case "w", "s"        'Wall and symmetric
        AP1(NIMM, J, K) = AP1(NIMM, J, K) + AE1(NIMM, J, K)
        AE1(NIMM, J, K) = 0#
End Select

Select Case (gvboundtype2(J, K))
    Case "n", "p" 'Pressure and Outlet
        AP1(2, J, K) = AP1(2, J, K) - AW1(2, J, K)
        AW1(2, J, K) = 0#
    Case "d"          'Inlet
        AP1(2, J, K) = AP1(2, J, K) + AW1(2, J, K)
        souC(2, J, K) = souC(2, J, K) + 2# * gvboundvalue2(1, J, K) * AW1(2, J, K)
        AW1(2, J, K) = 0#
    Case "w", "s"        'Wall and symmetric
        AP1(2, J, K) = AP1(2, J, K) + AW1(2, J, K)
        AW1(2, J, K) = 0#
End Select
Next J
Next K
For K = 2 To NKMM
For I = 2 To NIMM
Select Case (gvboundtype3(I, K))
    Case "n", "p", "s" 'Pressure symmetric and Outlet
        AP1(I, NJMM, K) = AP1(I, NJMM, K) - AN1(I, NJMM, K)
```

```
        AN1(I, NJMM, K) = 0#
    Case "d"          'inlet
        AP1(I, NJMM, K) = AP1(I, NJMM, K) + AN1(I, NJMM, K)
        souC(I, NJMM, K) = souC(I, NJMM, K) + 2# * gvboundvalue3(1, I, K) * AN1(I,
        NJMM, K)
        AN1(I, NJMM, K) = 0#
    Case "w"        'Wall
        AP1(I, NJMM, K) = AP1(I, NJMM, K) + AN1(I, NJMM, K)
        AN1(I, NJMM, K) = 0#
    End Select
    Select Case (gvboundtype4(I, K))
    Case "n", "p", "s" 'Pressure symmetric and Outlet
        AP1(I, 2, K) = AP1(I, 2, K) - AS1(I, 2, K)
        AS1(I, 2, K) = 0#
    Case "d"          'inlet
    AP1(I, 2, K) = AP1(I, 2, K) + AS1(I, 2, K)
        souC(I, 2, K) = souC(I, 2, K) + 2# * gvboundvalue4(1, I, K) * AS1(I, 2, K)
        AS1(I, 2, K) = 0#
    Case "w"          'Wall
        AP1(I, 2, K) = AP1(I, 2, K) + AS1(I, 2, K)
        AS1(I, 2, K) = 0#
End Select
Next I
Next K

For J = 2 To NJMM
```

```
For I = 2 To NIMM
Select Case (gvboundtype5(I, J))
   Case "n", "p", "s" 'Pressure symmetric and Outlet
      AP1(I, J, NKMM) = AP1(I, J, NKMM) - AT1(I, J, NKMM)
      AT1(I, J, NKMM) = 0#
   Case "d"          'inlet
      AP1(I, J, NKMM) = AP1(I, J, NKMM) + AT1(I, J, NKMM)
      souC(I, J, NKMM) = souC(I, J, NKMM) + 2# * gvboundvalue5(1, I, J) * AT1(I,
      J, NKMM)
      AT1(I, J, NKMM) = 0#
   Case "w"        'Wall
      AP1(I, J, NKMM) = AP1(I, J, NKMM) + AT1(I, J, NKMM)
      AT1(I, J, NKMM) = 0#
End Select
Select Case (gvboundtype6(I, J))
   Case "n", "p", "s" 'Pressure symmetric and Outlet
      AP1(I, J, 2) = AP1(I, J, 2) - AB1(I, J, 2)
      AB1(I, J, 2) = 0#
   Case "d"        'inlet
      AP1(I, J, 2) = AP1(I, J, 2) + AB1(I, J, 2)
      souC(I, J, 2) = souC(I, J, 2) + 2# * gvboundvalue6(1, I, J) * AB1(I, J, 2)
      AB1(I, J, 2) = 0#
   Case "w"        'Wall
      AP1(I, J, 2) = AP1(I, J, 2) + AB1(I, J, 2)
      AB1(I, J, 2) = 0#
End Select
```

```
Next I
Next J
If gvelurf <> 1# Then
    For K = 2 To NKMM
    For J = 2 To NJMM
    For I = 2 To NIMM
        AP1(I, J, K) = AP1(I, J, K) / gvelurf
        souC(I, J, K) = souC(I, J, K) + (1# - gvelurf) * AP1(I, J, K) * gu(I, J, K)
    Next I
    Next J
    Next K
End If

For K = 2 To NKMM
For J = 2 To NJMM
For I = 2 To NIMM
    apU(I, J, K) = gpor(I, J, K) / (AP1(I, J, K) - (AE1(I, J, K) + AW1(I, J, K) +
    AN1(I, J, K) + AS1(I, J, K) + AT1(I, J, K) + AB1(I, J, K)))
Next I
Next J
Next K

Call stone_(gu, AE1, AW1, AN1, AS1, AT1, AB1, AP1, souC, nsweep, stopcr, ptestcr)
End Sub
Function dmax1(var1, var2)
```

End sub

Energy Equation

```
Sub Energy_()


For K = 2 To NKMM
For J = 2 To NJMM
For I = 2 To NIMM
    FE(I, J, K) = gufacee(I, J, K) * (gden(I, J, K) + gden(I + 1, J, K)) / 2# * areaE(I, J,
    K) * gcp(I, J, K)
    FW(I, J, K) = gufacee(I - 1, J, K) * (gden(I - 1, J, K) + gden(I, J, K)) / 2# *
    areaE(I - 1, J, K) * gcp(I, J, K)
    FN(I, J, K) = gvfacen(I, J, K) * (gden(I, J, K) + gden(I, J + 1, K)) / 2# * areaN(I,
    J, K) * gcp(I, J, K)
    FS(I, J, K) = gvfacen(I, J - 1, K) * (gden(I, J - 1, K) + gden(I, J, K)) / 2# *
    areaN(I, J - 1, K) * gcp(I, J, K)
    FT(I, J, K) = gwfacet(I, J, K) * (gden(I, J, K) + gden(I, J, K + 1)) / 2# * areaT(I, J,
    K) * gcp(I, J, K)
    FB(I, J, K) = gwfacet(I, J, K - 1) * (gden(I, J, K - 1) + gden(I, J, K)) / 2# *
    areaT(I, J, K - 1) * gcp(I, J, K)
    gtdiffe(I, J, K) = gk(I, J, K) / dxe(I, J, K) * areaE(I, J, K)
    gtdiffw(I, J, K) = gk(I, J, K) / dxe(I - 1, J, K) * areaE(I - 1, J, K)
    gtdiffn(I, J, K) = gk(I, J, K) / dyn(I, J, K) * areaN(I, J, K)
    gtdiffs(I, J, K) = gk(I, J, K) / dyn(I, J - 1, K) * areaN(I, J - 1, K)
    gtdifft(I, J, K) = gk(I, J, K) / dzt(I, J, K) * areaT(I, J, K)
```

```
        gtdiffb(I, J, K) = gk(I, J, K) / dzt(I, J, K - 1) * areaT(I, J, K - 1)
Next I
Next J
Next K


For I = 2 To NIMM
For J = 2 To NJMM
For K = 2 To NKMM
If gtdiffe(I, J, K) = 0 Then
        AE1(I, J, K) = gtdiffe(I, J, K) * (0#) + dmax1(-FE(I, J, K), 0#)
Else
        AE1(I, J, K) = gtdiffe(I, J, K) * (dmax1(0#, 1# - 0.5 * Abs(FE(I, J, K) / gtdiffe(I,
        J, K)))) + dmax1(-FE(I, J, K), 0#)
End If
If gtdiffw(I, J, K) = 0 Then
        AW1(I, J, K) = gtdiffw(I, J, K) * (0#) + dmax1(FW(I, J, K), 0#)
Else
        AW1(I, J, K) = gtdiffw(I, J, K) * (dmax1(0#, 1# - 0.5 * Abs(FW(I, J, K) /
        gtdiffw(I, J, K)))) + dmax1(FW(I, J, K), 0#)
End If
        If gtdiffn(I, J, K) = 0 Then
        AN1(I, J, K) = gtdiffn(I, J, K) * (0#) + dmax1(-FN(I, J, K), 0#)
Else
        AN1(I, J, K) = gtdiffn(I, J, K) * (dmax1(0#, 1# - 0.5 * Abs(FN(I, J, K) / gtdiffn(I,
        J, K)))) + dmax1(-FN(I, J, K), 0#)
End If
```

```
If gtdiffs(I, J, K) = 0 Then
    AS1(I, J, K) = gtdiffs(I, J, K) * (0#) + dmax1(FS(I, J, K), 0#)
Else
    AS1(I, J, K) = gtdiffs(I, J, K) * (dmax1(0#, 1# - 0.5 * Abs(FS(I, J, K) / gtdiffs(I,
    J, K)))) + dmax1(FS(I, J, K), 0#)
End If
If gtdifft(I, J, K) = 0 Then
    AT1(I, J, K) = gtdifft(I, J, K) * (0#) + dmax1(-FT(I, J, K), 0#)
Else
    AT1(I, J, K) = gtdifft(I, J, K) * (dmax1(0#, 1# - 0.5 * Abs(FT(I, J, K) / gtdifft(I, J,
    K)))) + dmax1(-FT(I, J, K), 0#)
End If
If gtdiffb(I, J, K) = 0 Then
    AB1(I, J, K) = gtdiffb(I, J, K) * (0#) + dmax1(FB(I, J, K), 0#)
Else
    AB1(I, J, K) = gtdiffb(I, J, K) * (dmax1(0#, 1# - 0.5 * Abs(FB(I, J, K) / gtdiffb(I,
    J, K)))) + dmax1(FB(I, J, K), 0#)
End If
gtempoldap = gpor(I, J, K) * gcp (I, J, K) * gden (I, J, K) * vol(I, J, K) / dt

va = (gu(I, J, K) ^ 2 + gv(I, J, K) ^ 2 + gw(I, J, K) ^ 2) ^ 0.5
hsg(I, J, K) = 10.9 + 4 * va

    AP1(I, J, K) = (AE1(I, J, K) + AW1(I, J, K) + AN1(I, J, K) + AS1(I, J, K) +
    AT1(I, J, K) + AB1(I, J, K) + gtempoldap + (hsg(I, J, K) * asg(I, J, K)) * vol(I, J,
    K))
```

```
        B(I, J, K) = gtempoldap * gtempold(I, J, K) + hsg(I, J, K) * asg(I, J, K) * stemp(I,
        J, K) * vol(I, J, K)
Next K
Next J
Next I

Call SetupBoundary_GasTemperature_(gk, gk, gk, AE1, AW1, AN1, AS1, AT1, AB1,
AP1, B)

If gtempurf < 1# Then
For K = 2 To NKMM
For J = 2 To NJMM
For I = 2 To NIMM
   AP1(I, J, K) = AP1(I, J, K) / gtempurf
   B (I, J, K) = B(I, J, K) + (1# - gtempurf) * AP1(I, J, K) * gtemp(I, J, K)
Next I
Next J
Next K
        End If
Call stone_(gtemp, AE1, AW1, AN1, AS1, AT1, AB1, AP1, B, ngtempsweep,
gtempstopcr, gtempres)
End Sub
```

Ground Energy Balance

```
Function EnergyBalance()

Dim Tg() As Double

layers = 5
Depth = 3
Fo = 0.5

ReDim Tg(layers)

    dg = Depth / layers
    gArea = dx(x, y, 2) * dy(x, y, 2)
    gVol = dx(x, y, 2) * dy(x, y, 2) * dg

Tg_HK = (0.4041 * Exp(-1.4284 * Depth) * Tsky) _
    + (4.687 * Exp(-0.2223 * Depth) * Sin(2 * 3.14 / 365 * day_ - 0.3465 * Depth -
    2.0866)) _
    + (15.3297 * (-2 / 3.14) * Atn(-2.7204 * Depth)) + 11.4603

    BH = typeHeight 'BuildingHeight
    SC = typeDen(2) * 100
    If BH <> 0 Then
        SVF = dmin1(Abs(1.342 * (gArea ^ 0.5 / (gArea ^ 0.5 + BH))), 1)
    Else
        SVF = 1
    End If

Erate_ = Erate(count)
Idir_ = Idir(count)
Idif_ = Idif(count)

Ido = Idif_ * (1 - typeDen(2)) * gArea * albedo_ * SVF + Idir_ * gArea * (typeDen(1)
* 0.5 + typeDen(3) + typeDen(4)) * albedo_ * SVF
bolt = 5.6 * 10 ^ -8
Iwave_in = Abs(bolt * e_sky * (Tsky + 273) ^ 4 * SVF) * gArea * (typeDen(1) +
typeDen(3) + typeDen(4))
```

```
e_sky = 0.92 * 10 ^ -5 * (Tsky + 273) ^ 2
Iwave_out = -Abs(bolt * e_sky * (Tsky + 273) ^ 4 * SVF) * gArea * (typeDen(1) +
typeDen(3) + typeDen(4))
L = 2491.146 - 2.302 * Tsky
Ilat = L * 1 / 3.6 * Erate_ * gArea * typeDen(1)

Tss = Ts_old(x, y) - 273.1
aPP = Cp_ * gVol / dt_in
aT = 10.9 + 4.1 * va
aB = kc_ / dg

A1 = Ido / aPP
A2 = Iwave_in / aPP
A3 = Iwave_out / aPP
A4 = Ilat / aPP

For I = 1 To sweep
    For J = 1 To layers
    If J = 1 Then

    Tss = ENERGYBAL(gArea, aT, aPP, aB, Tsky, Tss, Tg(1)) _
        + (A1) + (A2) + (A3) + (A4)
    Tg(1) = ENERGYBAL(gArea, kc_ / (dg / 2), Cp_ * gVol / dt_in, kc_ / dg, Tss,
    Tg(1), Tg(J + 1))
ElseIf J = layers Then
    Tg(layers) = ENERGYBAL(gArea, kc_ / dg, Cp_ * gVol / dt_in, kc_ / (dg / 2),
    Tg(J - 1), Tg(layers), Tg_HK)
Else
    Tg(J) = ENERGYBAL(gArea, kc_ / dg, Cp_ * gVol / dt_in, kc_ / dg, Tg(J - 1),
    Tg(J), Tg(J + 1))
End If

Next J
Next I
Ts(x, y) = Tss

End Function
```

```
Sub BuildingEnergyModel()


If BuildHeight(I, J) <= zn(I, J, K) Then
    bArea = BuildDen(I, J) / 100 * areaE
End If
    bVol = dx(I, J, K) * dy(I, J, K) * dx(I, J, K)
    va = (gu(I, J, K) ^ 2 + gv(I, J, K) ^ 2 + gw(I, J, K)) ^ 0.5
    Tsky = gtemp(I, J, K)


    Idir_ = Idir(count)
    Idif_ = Idif(count)


    BH = BuildHeight(I, J) 'typeHeight 'BuildingHeight
    SC = BuildDen(I, J)
    If BH <> 0 Then
        SVF = Abs(1.342 * (bArea / (bArea + BH)))
    Else
        SVF = 1
    End If


    Ido = (Idif_ + dir_) * bArea * albedo_ * SVF
    stemp_ = stempold_ - 273.15
    aPP = Cp_ * gVol / dt_in
    aT = 10.9 + 4.1 * va
```

```
    aB = kc_ / dgz
    A1 = Ido / aPP

For I = 1 To sweep
    stemp_(I, J, K) = ENERGYBAL(gArea, aT, aPP, aB, Tsky, stemp_(I, J, K),
    stemp_1) + (A1)
    stemp__1 = ENERGYBAL(gArea, kc_ / (dgz / 2), Cp_ * gVol / dt_in, kc_ / dgz,
    stemp_, stemp__1, stemp__2)
    stemp__2 = ENERGYBAL(gArea, kc_ / dgz, Cp_ * gVol / dt_in, kc_ / (dgz / 2),
    stemp__1, stemp__2, 25.5)
    stemp_old = stemp_(I, J, K)
    If Abs(stemp_old - stemp_(I, J, K)) < 0.01 Then flag3
Next I
flag3:
End Sub
```

```
Function ENERGYBAL(Area, aT, aPP, aB, T1, T2, T3) As Double
ENERGYBAL = 1 / aPP * ((aB * Area * (T3 - T2) _
                     + aT * Area * (T1 - T2) _
                     + aPP * T2))
End Function
```

Appendix C - Pixel Analysis

The urban density data such as amount of greenery, road, plaza, construction, building, sea as well as building and terrain height can be obtained from the GIS data using the self-developed Pixel Analysis technique. Below show an example of using Pixel Analysis at the northwest region of Hong Kong to calculate the different areas in each grid.

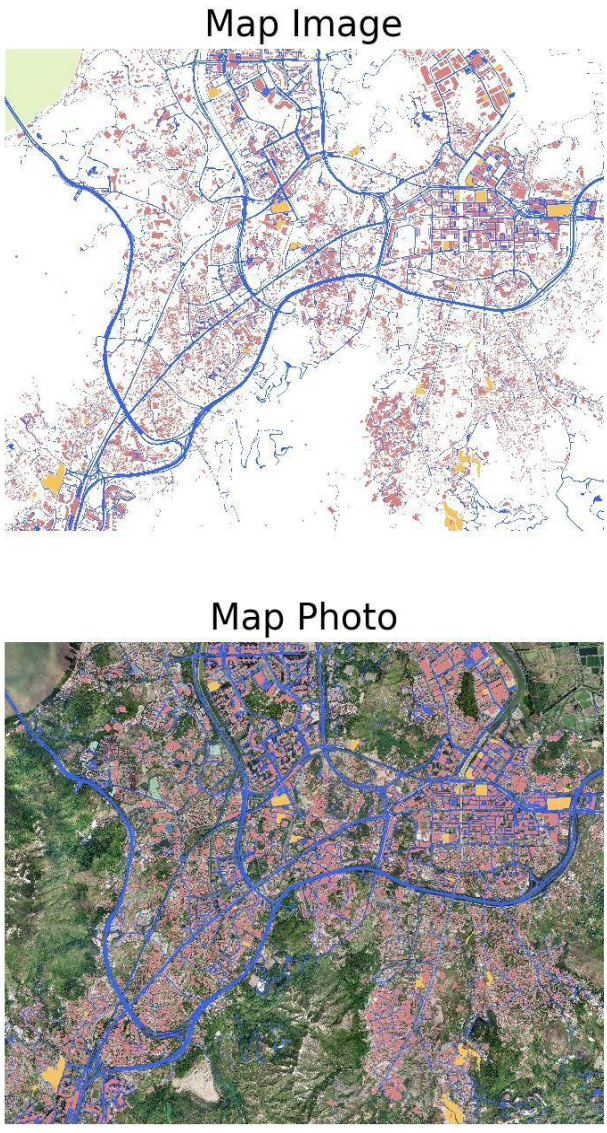

Figure A1 Digital Map iB1000 (above) and Digital Orthophoto DOP5000 (below)

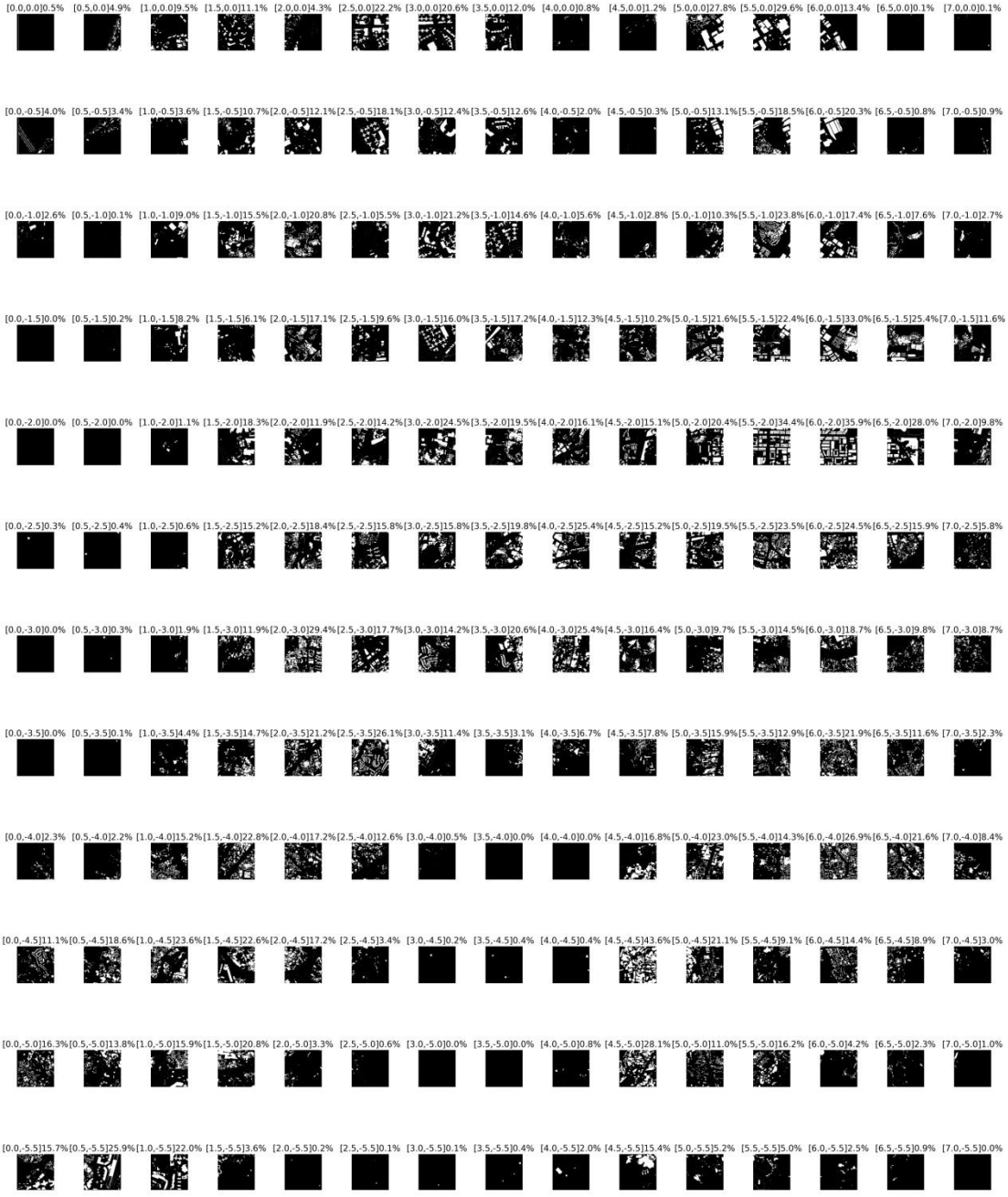

Figure A2 Building density under 500m x 500m grid

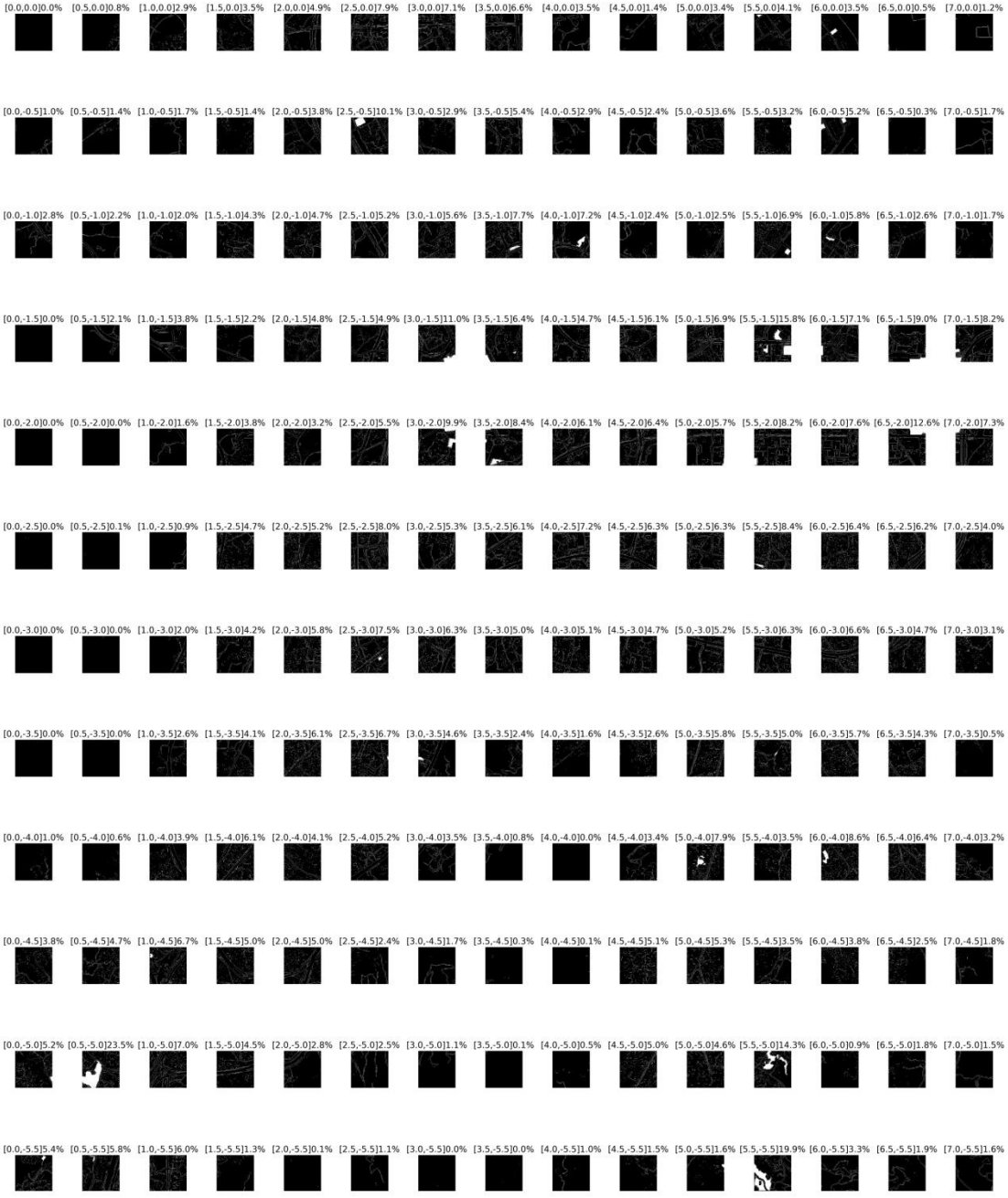

Figure A3 Construction density under 500m x 500m grid

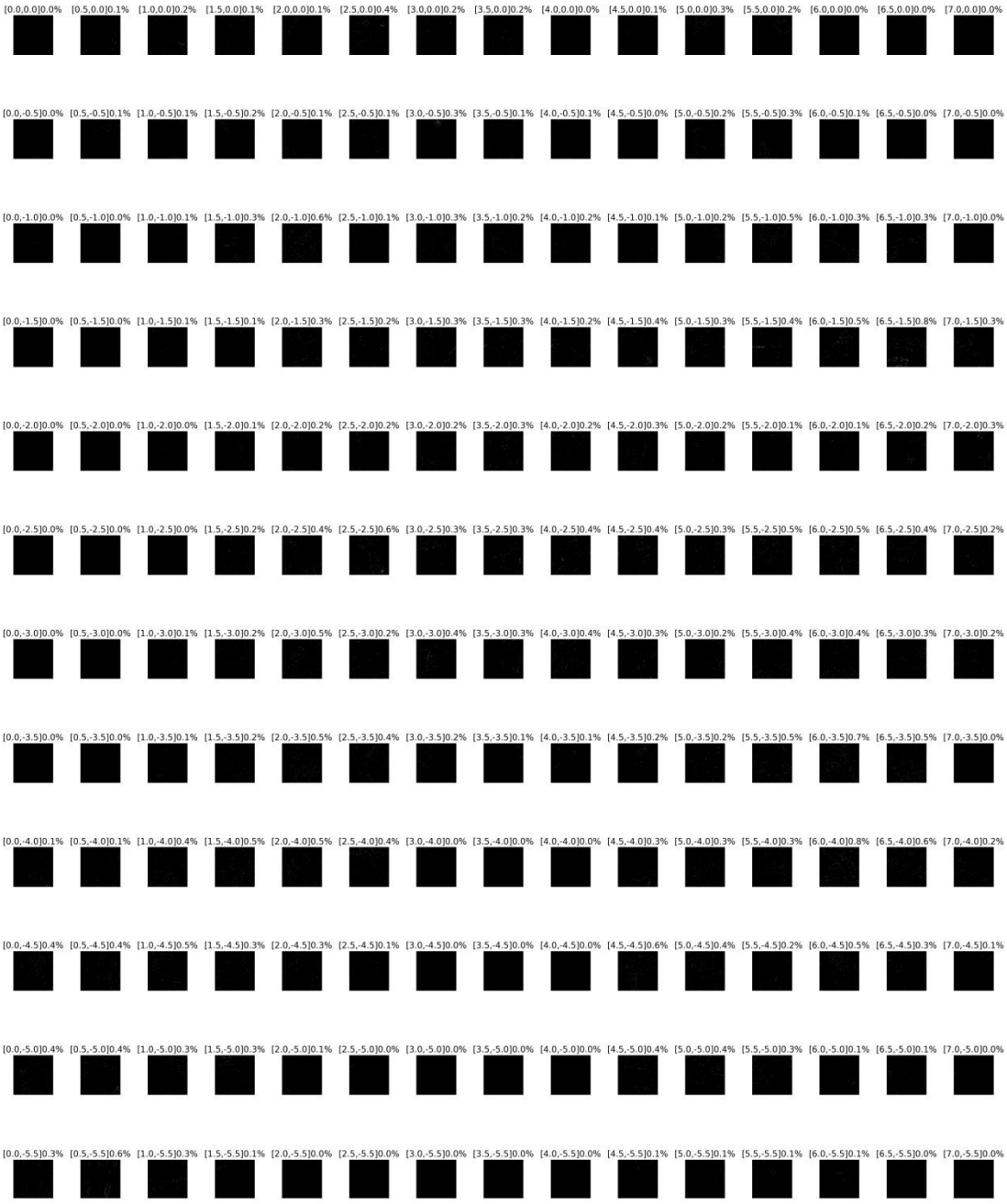

Figure A4 Plaza density under 500m x 500m grid

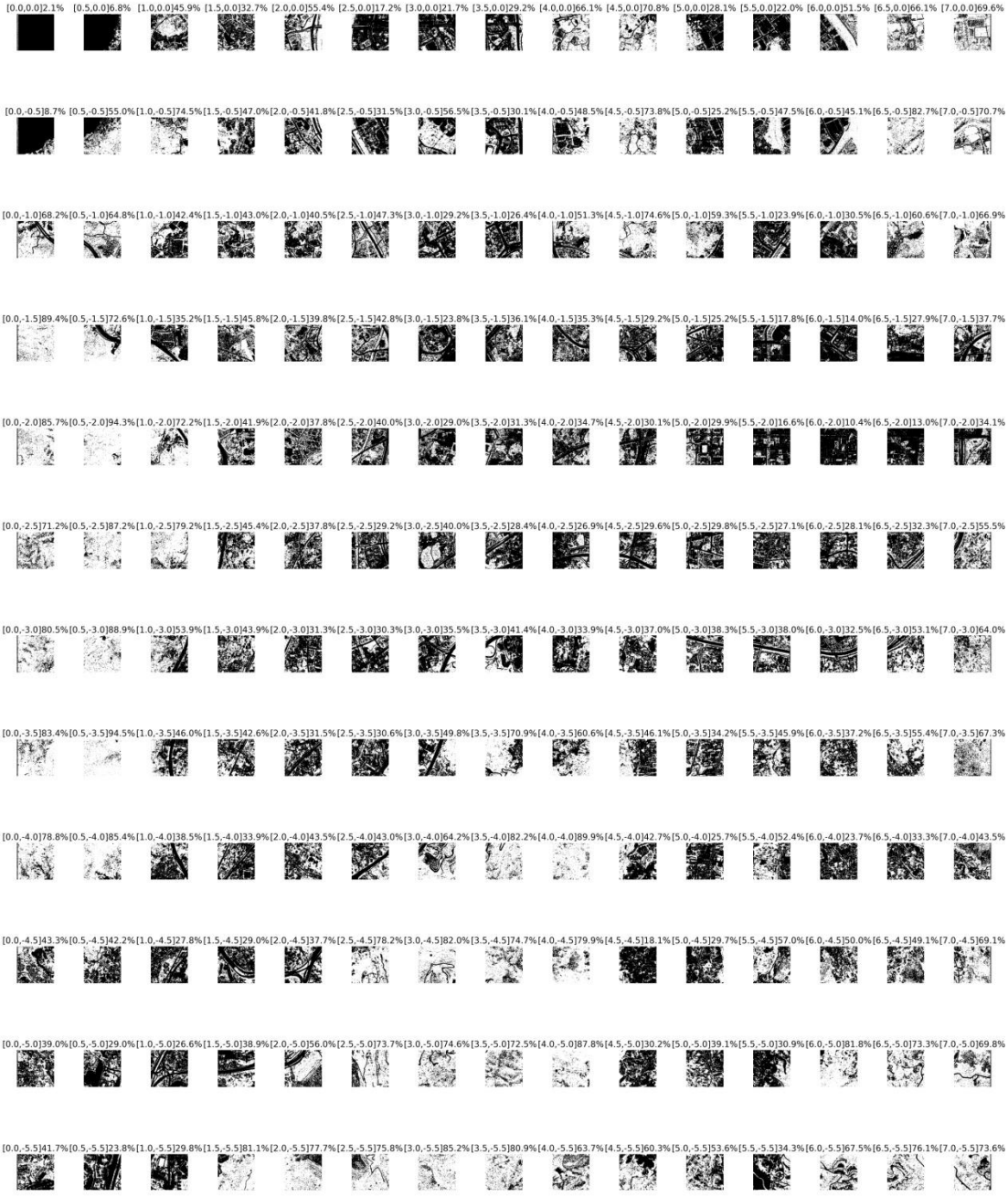

Figure A5 Tree density under 500m x 500m grid

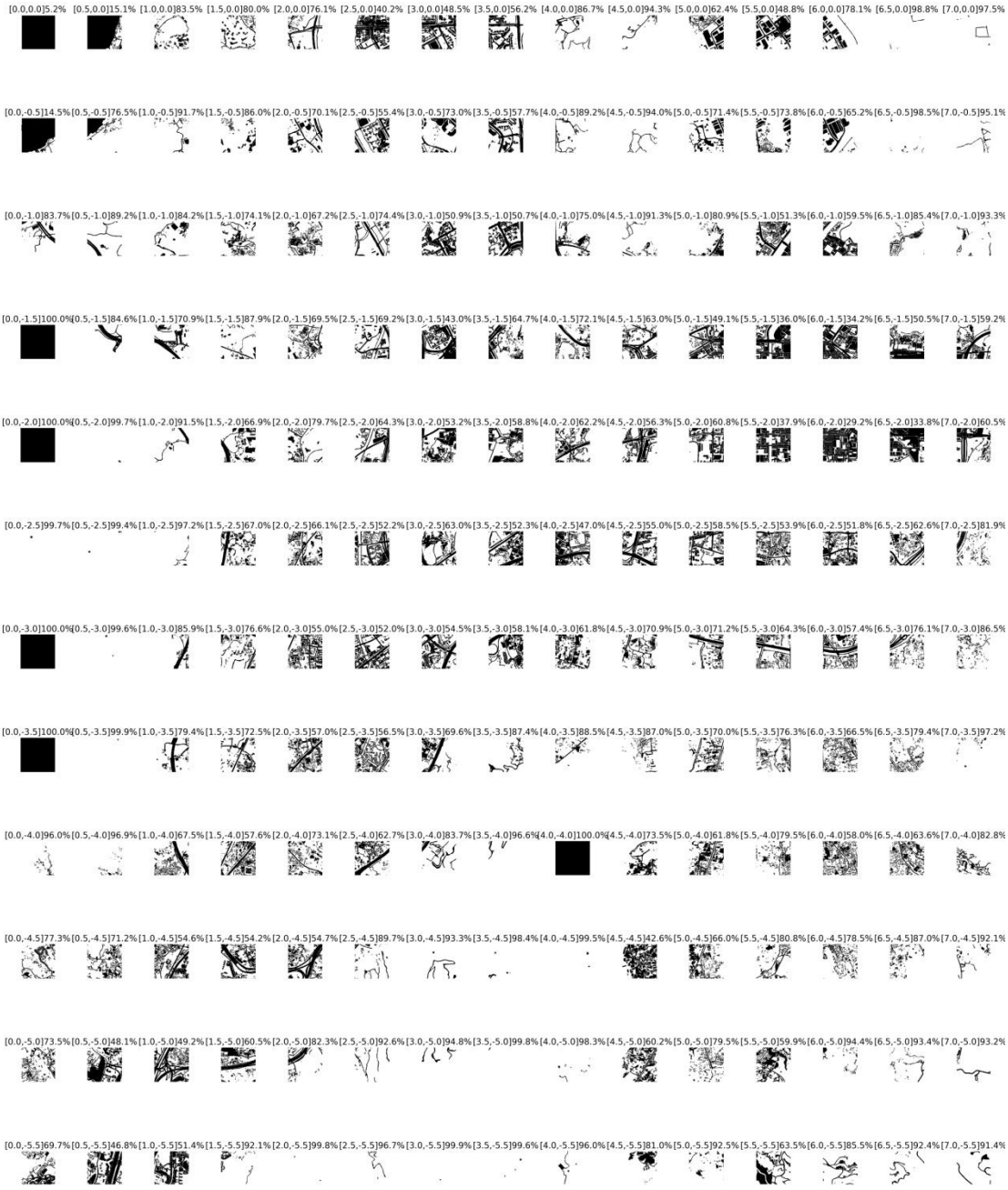

Figure A6 Greenery density under 500m x 500m grid

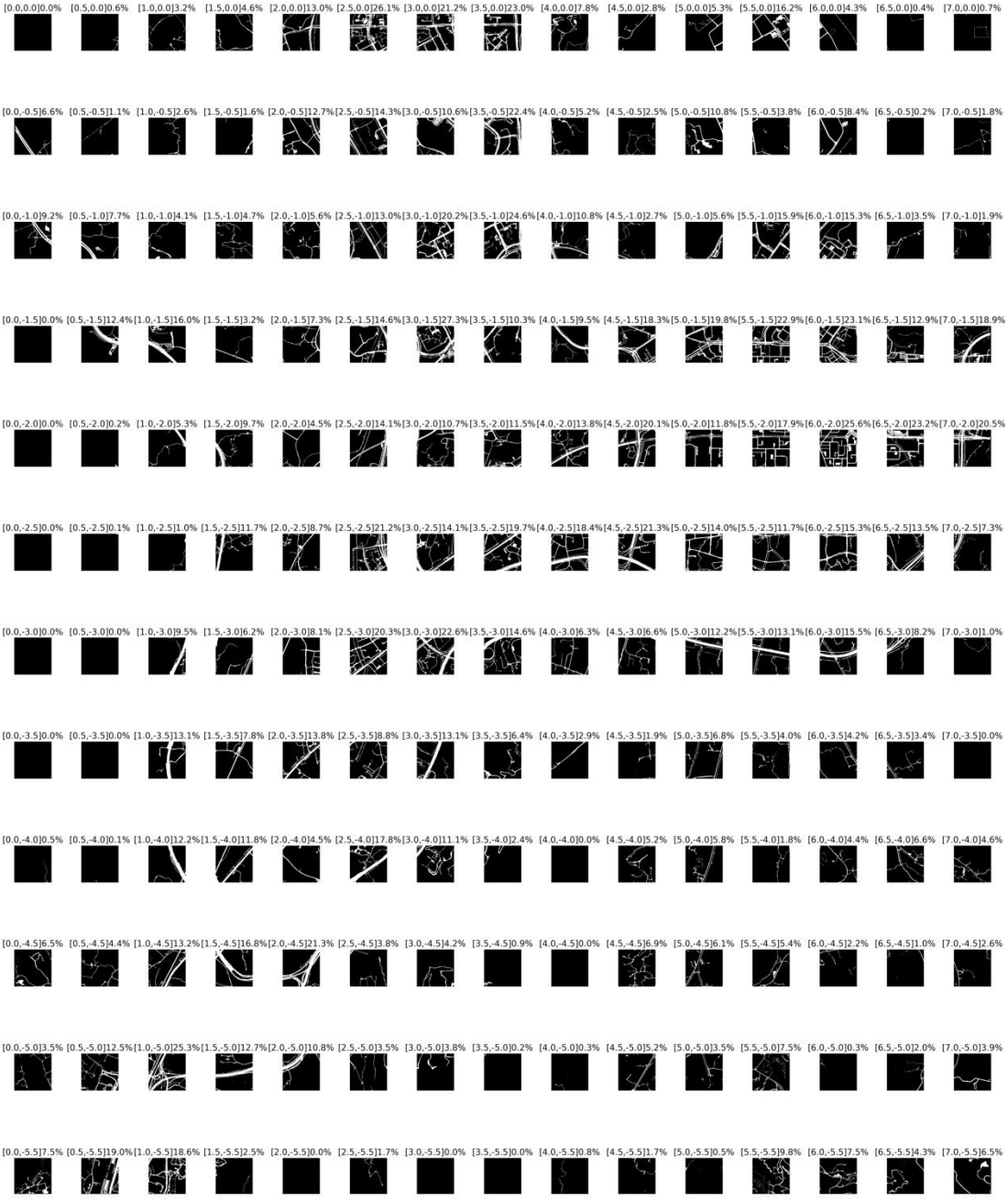

Figure A7 Road density under 500m x 500m grid

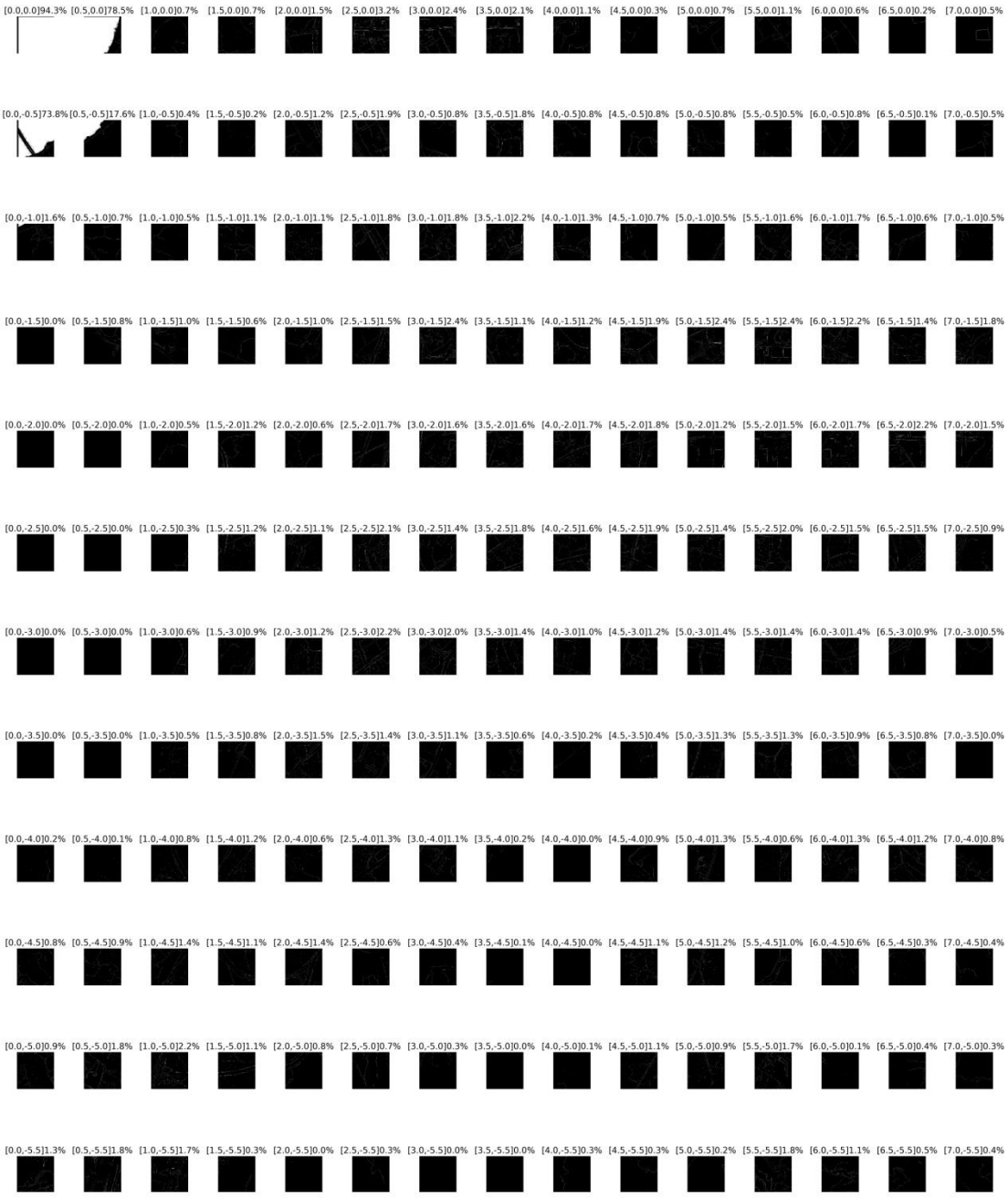

Figure A8 Sea density under 500m x 500m grid

Below figures summarized the density data of building area, greenery area, sea area, road area and construction area under 500m x 500m grid of Hong Kong. It is noted that the Urban Density Database is created based on 10m x 10m due to accuracy, however, due to computational power limitation it cannot be visualized.

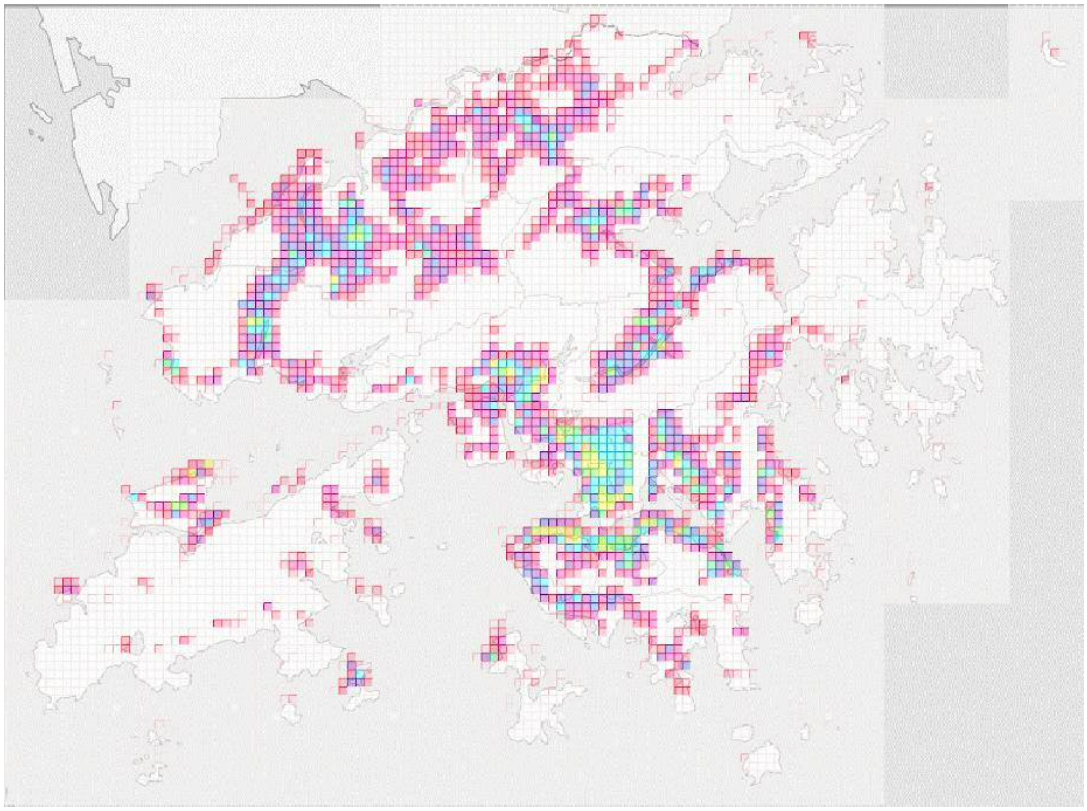

Figure A9 Building Area Density Map (under 500m x 500m grid)

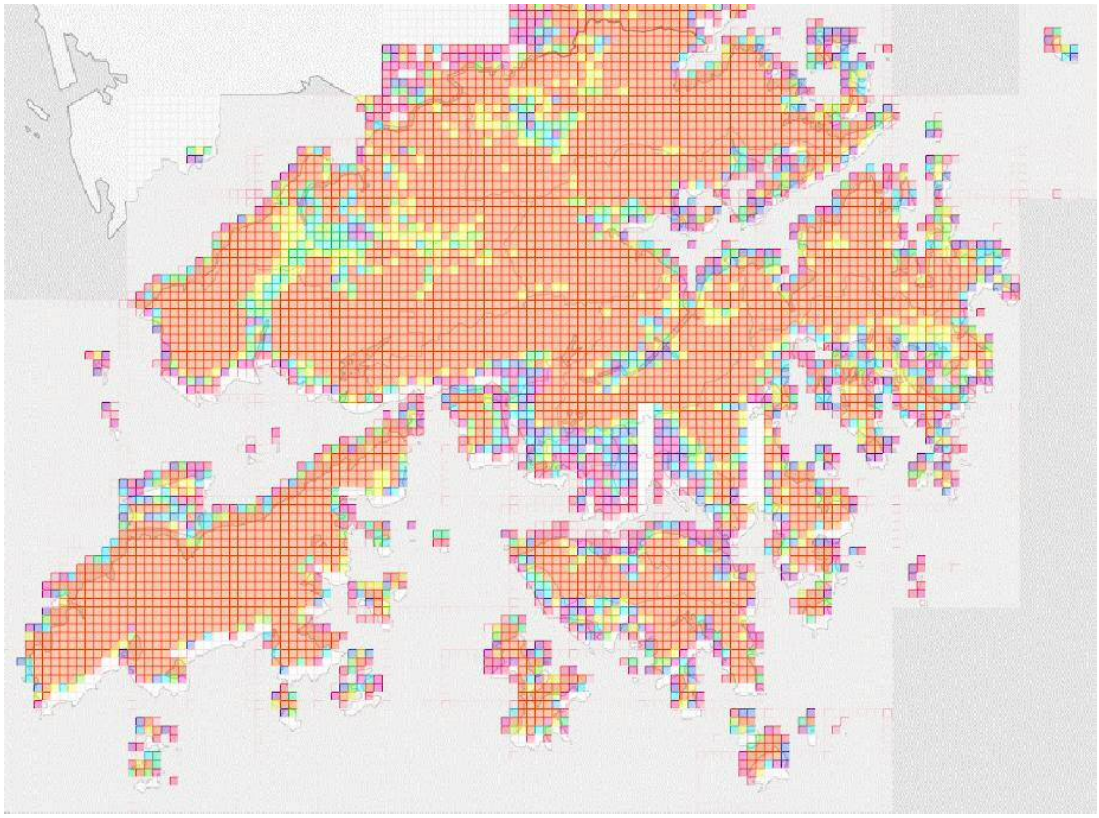

Figure A10 Greenery Density under 500 x 500m grid

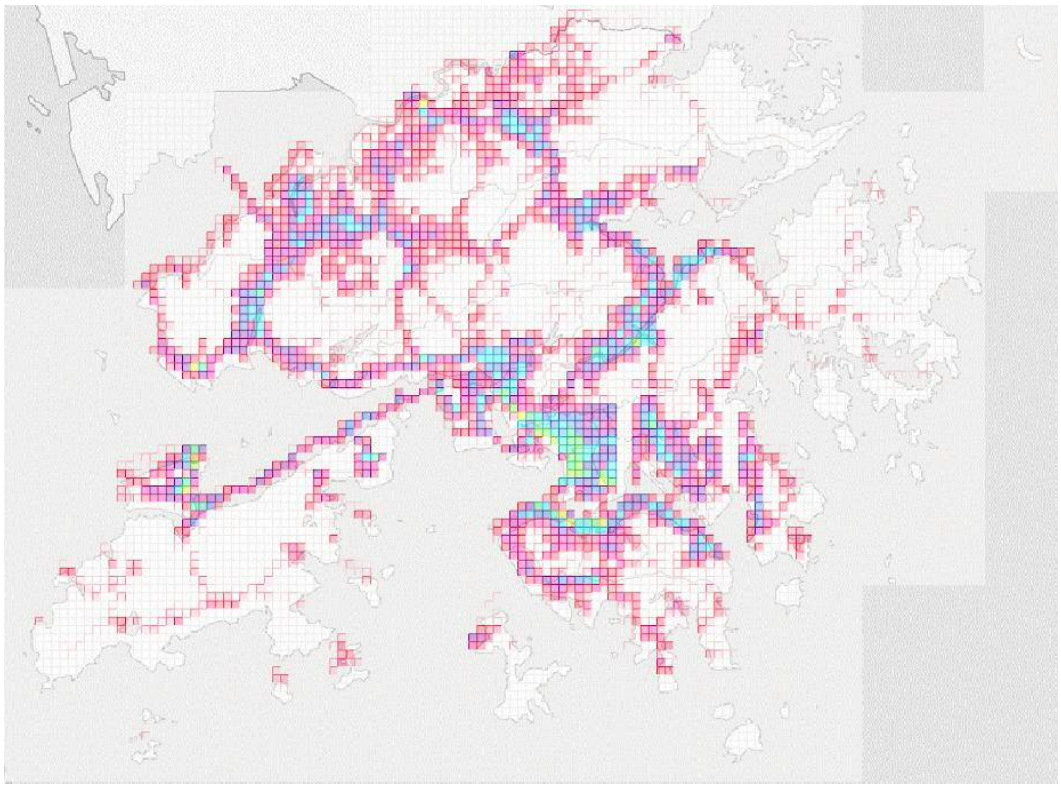

Figure A11 Road Density under 500 x 500m grid

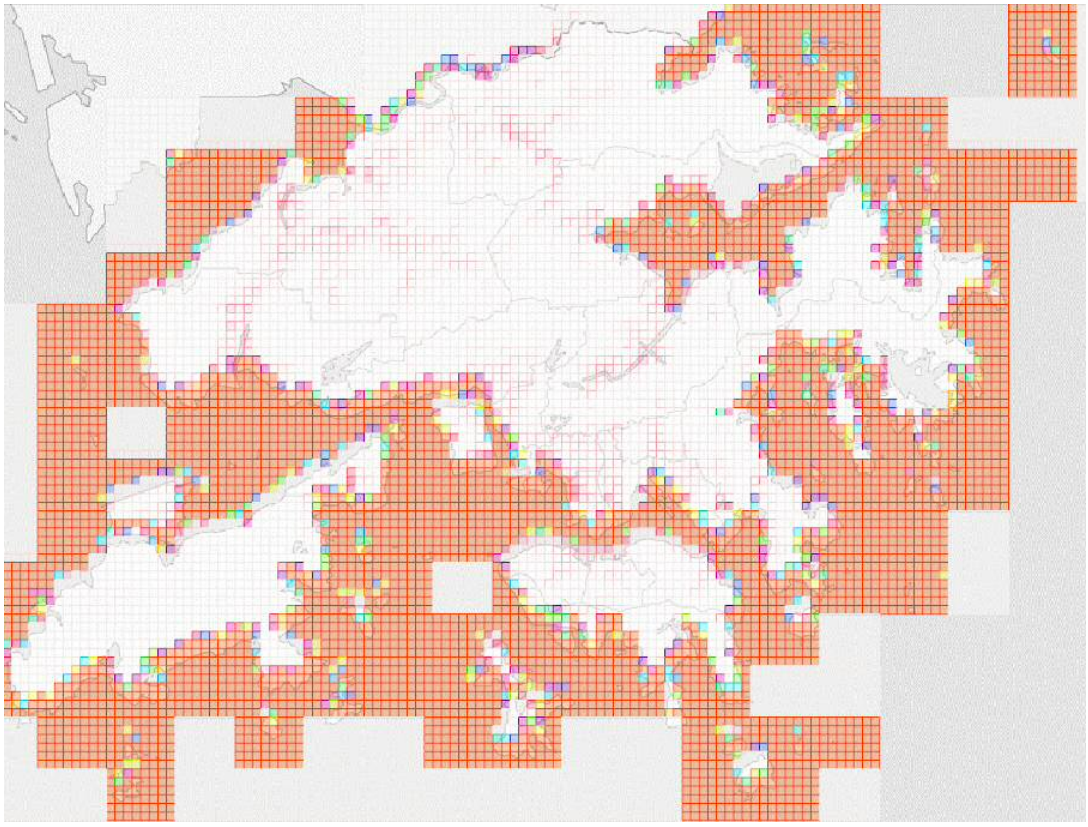

Figure A12 Sea Density under 500 x 500m grid